



Provided by the author(s) and University of Galway in accordance with publisher policies. Please cite the published version when available.

Title	Site-directed mapping of nucleosome structure and dynamics in vitro
Author(s)	Doran, Jonathan
Publication Date	2013-03-04
Item record	http://hdl.handle.net/10379/3608

Downloaded 2024-03-13T07:59:50Z

Some rights reserved. For more information, please see the item record link above.





NUI Galway
OÉ Gaillimh

Site-directed mapping of nucleosome structure and dynamics *in vitro*

Jonathan Doran

Centre for Chromosome Biology,
Biochemistry Department,
School of Natural Sciences,
National University of Ireland, Galway

A thesis submitted to the National University of Ireland, Galway for a
degree of Doctor of Philosophy

March 2013

Supervisor: Dr. Andrew Flaus

<i>Contents</i>	<i>i</i>
<i>Figures</i>	<i>vii</i>
<i>Tables</i>	<i>x</i>
<i>Abbreviations</i>	<i>xii</i>
<i>Acknowledgements</i>	<i>xiv</i>
<i>Abstract</i>	<i>xv</i>
<i>Chapter 1 Introduction</i>	<i>1</i>
<i>Chapter 2 Materials and methods</i>	<i>27</i>
<i>Chapter 3 Site-directed nucleosome mapping</i>	<i>53</i>
<i>Chapter 4 Nucleosome sliding</i>	<i>113</i>
<i>Chapter 5 Conclusion</i>	<i>188</i>
<i>References</i>	<i>190</i>
<i>Appendix</i>	<i>198</i>

Chapter 1	Introduction	1
1.1	Role of chromatin in organising the genome	1
1.2	Hierarchical structure of chromatin	1
1.3	Nucleosome structure	2
1.3.1	Octamer structure	2
1.3.2	DNA structure	6
1.4	Histones	9
1.5	Nucleosome positioning	10
1.5.1	Types of positioning	10
1.5.2	<i>In vitro</i> nucleosome positioning sequences	11
1.5.3	5S rDNA sequence	12
1.5.4	Alpha satellite sequence	12
1.5.5	MMTV LTR	12
1.5.6	Widom 601 sequences	13
1.5.7	Genomic encoding of organised nucleosomes	15
1.6	Dynamic nucleosomes	15
1.6.1	Passive nucleosome dynamics	16
Nucleosome breathing		16
Thermal nucleosome sliding		16
Twist defect diffusion		17
Loop/bulge diffusion		18
1.6.2	ATP-dependent chromatin remodeling	19
SWI/SNF family		19
ISWI family		20
CHD family		20
INO80 family		21
1.6.3	Histone chaperones	21
1.7	Methods for determining nucleosome positioning	22
1.7.1	Nucleases	22

Enzymatic nucleases	22
Chemical nucleases	22
1.7.2 Site directed nucleosome mapping	23
1.8 Current state of research for mapping nucleosome positions	24
1.9 Aims of the project	25
<i>Chapter 2 Materials and methods</i>	27
2.1 Materials	27
2.1.1 Source of chemicals	27
2.1.2 Source of enzymes	28
2.2 Equipment	28
2.3 DNA methods	29
2.3.1 PCR mutagenesis	29
2.3.2 Recombinant <i>Taq</i> polymerase preparation	30
2.3.3 Nucleosomal DNA amplification	32
2.3.4 Amplified nucleosomal DNA purification	33
2.3.5 G-Track preparation	34
2.4 Protein methods	35
2.4.1 Recombinant histone expression	35
2.4.2 Recombinant histone purification	36
2.4.3 Histone octamer refolding	39
2.4.4 Histone octamer gel filtration	41
2.4.5 Mapping reagent attachment	42
Attachment of N-[S-(2-pyridylthio)cysteaminy] ethylenediamine-N,N,N',N'-tetraacetic acid	43
Attachment of 1,10 Phenanthroline-5- maleimide	44
2.5 Nucleosome methods	45
2.5.1 Nucleosome formation	45
2.5.2 Native gel electrophoresis	47
2.5.3 Nucleosome mapping	48

2.5.4	Nucleosome thermal sliding	49
2.5.5	Denaturing gel electrophoresis	50
2.5.6	Image analysis using AIDA	51
2.6	Materials and methods workflow	52
<i>Chapter 3 Site-directed nucleosome mapping</i>		53
3.1	Introduction	53
3.2	Comparison of Cu^{2+} and Fe^{2+} on nucleosome mapping	58
3.2.1	Observations	58
3.2.2	Interpretation	58
3.3	Nucleosome mapping at SHL 0.5	62
3.3.1	Observations	62
3.3.2	Interpretation	67
3.4	Nucleosome mapping at SHL 1.5	69
3.4.1	Observations	69
3.4.2	Interpretation	72
3.5	Nucleosome mapping at SHL 2.5	73
3.5.1	Observations	73
3.5.2	Interpretation	76
3.6	Nucleosome mapping at SHL 3.5	77
3.6.1	Observations	77
3.6.2	Interpretation	80
3.7	Nucleosome mapping at SHL 4.5	81
3.7.1	Observations	81
3.7.2	Interpretation	87
3.8	Nucleosome mapping at SHL 5.5	89
3.8.1	Observations	89
3.8.2	Interpretation	95
3.9	Nucleosome mapping at SHL 6.5	97
3.9.1	Observations	97

	<i>Contents</i>
3.9.2 Interpretation	103
3.10 Compiled data from SHL 0.5 to SHL 6.5	105
3.10.1 Results	105
3.11 Discussion	108
3.11.1 Reagents and DNA cutting	109
3.11.2 NucA sequence nucleosome mapping	110
3.11.3 601 sequences nucleosome mapping	111
3.11.4 NucA versus 601	112
3.11.5 In solution nucleosomes versus crystal structures	112
<i>Chapter 4 Nucleosome sliding</i>	<i>113</i>
4.1 Introduction	113
4.2 Nucleosome sliding on 601.2	115
4.2.1 Observations	115
4.2.2 Interpretation	116
4.3 Nucleosome sliding on NucA	119
4.3.1 Observations	119
4.3.2 Interpretation	119
4.4 Nucleosome sliding on NucA-31	123
4.4.1 Observations	123
4.4.2 Interpretation	123
4.5 NucA-31 sliding at 37°C mapped at SHL 0.5	127
4.5.1 Observations	127
4.5.2 Interpretation	127
4.6 NucA-31 sliding at 45°C mapped at SHL 0.5	131
4.6.1 Observations	131
4.6.2 Interpretation	131
4.7 NucA-31 sliding at 37°C mapped at SHL 1.5	134
4.7.1 Observations	134
4.7.2 Interpretation	134

4.8	NucA-31 sliding at 45°C mapped at SHL 1.5	138
4.8.1	Observations	138
4.8.2	Interpretation	138
4.9	NucA-31 sliding at 37°C mapped at SHL 2.5	141
4.9.1	Observations	141
4.9.2	Interpretation	141
4.10	NucA-31 sliding at 45°C mapped at SHL 2.5	144
4.10.1	Observations	144
4.10.2	Interpretation	144
4.11	NucA-31 sliding at 37°C mapped at SHL 3.5	147
4.11.1	Observations	147
4.11.2	Interpretation	147
4.12	NucA-31 sliding at 45°C mapped at SHL 3.5	151
4.12.1	Observations	151
4.12.2	Interpretation	151
4.13	NucA-31 sliding at 37°C mapped at SHL 4.5	155
4.13.1	Observations	155
4.13.2	Interpretation	155
4.14	NucA-31 sliding at 45°C mapped at SHL 4.5	159
4.14.1	Observations	159
4.14.2	Interpretation	159
4.15	NucA-31 sliding at 37°C mapped at SHL 5.5	163
4.15.1	Observations	163
4.15.2	Interpretation	163
4.16	NucA-31 sliding at 45°C mapped at SHL 5.5	167
4.16.1	Observations	167
4.16.2	Interpretation	167
4.17	NucA-31 sliding at 37°C mapped at SHL 6.5	171
4.17.1	Observations	171
4.17.2	Interpretation	171

	<i>Contents</i>
4.18 NucA-31 sliding at 45°C mapped at SHL 6.5	175
4.18.1 Observations	175
4.18.2 Interpretation	175
4.19 Sliding of variant nucleosomes mapped at SHL 0.5	179
4.19.1 Observations	179
4.19.2 Interpretation	180
4.20 Discussion	182
4.20.1 Thermally induced nucleosome sliding	182
4.20.2 Similarities and differences in sliding	184
4.20.3 Nucleosome sliding patterns	186
4.20.4 Nucleosome sliding conclusions	187
4.20.5 <i>Xenopus</i> , human and human containing hH2AX nucleosome sliding	187
<i>Chapter 5 Conclusion</i>	<i>188</i>
5.1 Site-directed nucleosome mapping	188
5.2 Thermal nucleosome sliding	188
<i>References</i>	<i>190</i>
<i>Appendix</i>	<i>198</i>
Nucleosome positioning sequences	198
PCR primers	199

Figures

Figure 1.1	Chromatin compaction	2
Figure 1.2	Nucleosome core particle	3
Figure 1.3	Core histone secondary structure	4
Figure 1.4	Histone pairing handshake configuration	4
Figure 1.5	Four-Helix bundle binding sites	5
Figure 1.6	Nucleosomal super helical locations	7
Figure 1.7	Twist defect diffusion	18
Figure 1.8	Loop defect diffusion	19
Figure 2.1	Example of primer design for PCR mutagenesis of histone H4 S47C	30
Figure 2.2	Nucleosomal DNA purification chromatogram trace	34
Figure 2.3	Nucleosomal DNA purification	34
Figure 2.4	Histone purification chromatogram trace	39
Figure 2.5	SDS-PAGE of histone purification	39
Figure 2.6	Histone octamer gel filtration chromatogram trace	42
Figure 2.7	Histone octamer on SDS PAGE	42
Figure 2.8	Schematic representation of stepwise micro dialysis nucleosome formation	47
Figure 2.9	Native PAGE cell apparatus	48
Figure 2.10	Materials and methods workflow	52
Figure 3.1	Nucleosome core particle structure showing seven cysteine mutations	55
Figure 3.2	Enlarged view of the seven super helical location mapping sites	56
Figure 3.3	Positional terminology of nucleosomal DNA mapping with denaturing PAGE band migration	57
Figure 3.4	Comparison of Cu ²⁺ and Fe ²⁺ on nucleosome mapping with EDTA and phenanthroline reagents	60
Figure 3.5	Nucleosome mapping at SHL 0.5 with EDTA and phenanthroline on NucA, 601 and 601.2	64

Figure 3.6	Nucleosome mapping at SHL 1.5 with EDTA and phenanthroline on NucA, 601 and 601.2.....	70
Figure 3.7	Nucleosome mapping at SHL 2.5 with EDTA and phenanthroline on NucA, 601 and 601.2.....	74
Figure 3.8	Nucleosome mapping at SHL 3.5 with EDTA and phenanthroline on NucA, 601 and 601.2.....	78
Figure 3.9	Nucleosome mapping at SHL 4.5 with EDTA and phenanthroline on NucA, 601 and 601.2.....	83
Figure 3.10	Nucleosome mapping at SHL 5.5 with EDTA and phenanthroline on NucA, 601 and 601.2.....	91
Figure 3.11	Nucleosome mapping at SHL 6.5 with EDTA and phenanthroline on NucA, 601 and 601.2.....	99
Figure 3.12	Nucleosome mapping positions for NucA, 601 and 601.2 using EDTA and phenanthroline mapping reagents.....	107
Figure 3.13	Chemical structure of mapping reagents.....	109
Figure 4.1	Thermal sliding of the 601.2 nucleosome mapped at SHL 0.5.....	117
Figure 4.2	Thermal sliding of NucA on 252 bp mapped at SHL 0.5.....	121
Figure 4.3	Thermal sliding of NucA-31 on 221 bp DNA mapped at SHL 0.5.....	125
Figure 4.4	Thermal sliding of 105(NucA)-31 mapped at SHL 0.5 (37 °C).....	129
Figure 4.5	Thermal sliding of 105(NucA)-31 mapped at SHL 0.5 (45 °C).....	132
Figure 4.6	Thermal sliding of 105(NucA)-31 mapped at SHL 1.5 (37 °C).....	136
Figure 4.7	Thermal sliding of 105(NucA)-31 mapped at SHL 1.5 (45 °C).....	139
Figure 4.8	Thermal sliding of 105(NucA)-31 mapped at SHL 2.5 (37 °C).....	142
Figure 4.9	Thermal sliding of 105(NucA)-31 mapped at SHL 2.5 (45 °C).....	145
Figure 4.10	Thermal sliding of 105(NucA)-31 mapped at SHL 3.5 (37 °C).....	149
Figure 4.11	Thermal sliding of 105(NucA)-31 mapped at SHL 3.5 (45 °C).....	153
Figure 4.12	Thermal sliding of 105(NucA)-31 mapped at SHL 4.5 (37 °C).....	157

Figure 4.13	Thermal sliding of 105(NucA)-31 mapped at SHL 4.5 (45 °C).....	161
Figure 4.14	Thermal sliding of 105(NucA)-31 mapped at SHL 5.5 (37 °C).....	165
Figure 4.15	Thermal sliding of 105(NucA)-31 mapped at SHL 5.5 (45 °C).....	169
Figure 4.16	Thermal sliding of 105(NucA)-31 mapped at SHL 6.5 (37 °C).....	173
Figure 4.17	Thermal sliding of 105(NucA)-31 mapped at SHL 6.5 (45 °C).....	177
Figure 4.18	Thermal sliding of variant nucleosomes mapped at SHL 0.5.....	181

Tables

Table 2.1	A list of chemical reagents and their suppliers.....	27
Table 2.2	A list of enzymes and their suppliers.....	28
Table 2.3	Equipment types, makes and models used throughout the project.....	28
Table 2.4	PCR mutagenesis reactants, concentrations and volumes.....	30
Table 2.5	PCR mutagenesis cycle.....	30
Table 2.6	<i>Taq</i> pol purification buffers.....	31
Table 2.7	PCR amplification of nucleosomal DNA.....	32
Table 2.8	Purification buffers for amplified nucleosomal DNA.....	33
Table 2.9	FPLC program for nucleosomal DNA purification.....	33
Table 2.10	G-Track preparation buffers.....	35
Table 2.11	2YT medium.....	36
Table 2.12	Inclusion body preparation buffers.....	37
Table 2.13	Histone purification buffers.....	38
Table 2.14	FPLC histone purification program.....	38
Table 2.15	Histone octamer refolding buffers.....	40
Table 2.16	Typical concentrations and volumes observed in octamer refolding.....	40
Table 2.17	Octamer gel filtration buffer.....	41
Table 2.18	FPLC octamer gel filtration program.....	41
Table 2.19	Mapping locations and the corresponding cysteine mutant.....	43
Table 2.20	Steps and duration for EDTA reagent attachment to octamer.....	44
Table 2.21	Steps and duration for phenanthroline reagent attachment to octamer.....	45
Table 2.22	Typical volumes and concentrations for nucleosome formation.....	46
Table 2.23	Nucleosome stepwise dialysis buffers and durations.....	46
Table 2.24	Native PAGE buffers and gel constituents.....	47

Table 2.25	Summary of nucleosome mapping procedure.....	49
Table 2.26	Formamide sample buffer.....	50
Table 2.27	Fuji phosphor-imager setting.....	50
Table 3.1	Number of times mapping was performed for each nucleosome.....	108
Table 4.1	Number of times the nucleosome sliding assay was performed per SHL.....	182
Table 4.2	Summary of sliding observations from SHL 0.5 to SHL 6.5.....	183

Abbreviations

A	Adenine
Å	Angstrom
AFM	Atomic force microscopy
APS	Ammonium persulphate
Asf1	Anti-silencing function 1
ATP	Adenosine triphosphate
bp	Base-pair
C	Cytosine
CAF-1	Chromatin assembly factor 1
CENP-A	Centromere protein A
CHD	Chromodomain helicase DNA binding
Chz1	Chaperone for H2AZ-H2B
Cy	Cyanine
DMSO	Dimethyl sulphoxide
DNA	Deoxyribonucleic acid
DNase I	Deoxyribonuclease I
dNTP	Deoxyribonucleotide triphosphate
DSB	Double strand break
DTT	Dithiothreitol
EDTA	Ethylenediaminetetraacetic acid disodium salt dihydrate
EDTA Reagent	N-[S-(2-Pyridylthio)cysteaminy]ethylenediamine- N,N,N',N'-tetraacetic acid
EDTA/Fe²⁺	EDTA reagent in conjunction with iron
ExoIII	Exonuclease III
FPLC	Fast protein liquid chromatography
FRET	Förster resonance energy transfer
g	Gravity
G	Guanine
HEPES	4-(2-Hydroxyethyl)piperazine-1-ethanesulfonic acid
HPLC	High performance liquid chromatography
HRE	Hormone response element
INO80	Inositol requiring mutant 80
IPTG	Isopropyl-β-D-thiogalactopyranoside
ISWI	Imitation switch
L	Loop
LA	Lysogeny agar
LB	Lysogeny broth
LPG	Long pass green
LPR	Long pass red
LTR	Long terminal repeat
MES	2-(N-morpholino)ethanesulphonic acid

MMTV	Mouse mammary tumor virus
MNase	Micrococcal nuclease
mRNA	Messenger ribonucleic acid
ms	Millisecond
MWCO	Molecular weight cut off
Nap1	Nucleosome assembly protein 1
NFR	Nucleosome free region
NucA	Nucleosome position sequence A
NucB	Nucleosome position sequence B
PAGE	Poly acrylamide gel electrophoresis
PCR	Polymerase chain reaction
PDB	Protein data bank
Phen/Cu²⁺	Phenanthroline reagent in conjunction with copper
Phen/Fe²⁺	Phenanthroline reagent in conjunction with iron
PMSF	Phenylmethanesulphonyl fluoride
PTM	Post translational modification
rDNA	Ribosomal DNA
rRNA	Ribosomal ribonucleic acid
SANT	SWI3, ADA2, N-CoR and TFIIB
SDS	Sodium dodecyl sulfate
SHL	Super helical location
SLIDE	SANT like ISWI
Snf2	Sucrose non-fermenting 2 family
SWI/SNF	Switch/sucrose non-fermenting
T	Thymine
Taq Pol	<i>Taq</i> DNA polymerase from <i>Thermus aquaticus</i>
TBS	Tris buffered saline
TEMED	<i>N,N,N',N'</i> -tetramethylethylenediamine
Tris	2-Amino-2-(hydroxymethyl)-1,3-propanediol
tRNA	Transfer ribonucleic acid
TSS	Transcription start site
UV	Ultraviolet
φ	Dyad
•OH	Hydroxyl radical

Acknowledgements

I would like to express my sincere appreciation to my supervision Dr Andrew Flaus for all the opportunities, guidance and support he gave me throughout the years.

I would like to convey my immense gratitude to my parents and family for their constant support. I would also like to thank my girlfriend Clara for everything.

I would like to thank all the members of our lab, past and present, for their support throughout the years. Especially to David, Indu, Martin and Catherine to who my research is most related. I would like to extend my thanks to all members of the Centre for Chromosome Biology for their help and friendship throughout the PhD and also to the Comeragh College, Carrick on Suir.

Finally I would like to thank Profs. Tom Owen-Hughes and Song Tan for their gifts and correspondence.

Abstract

The nucleosome core particle is the most basic unit of chromatin packaging. It is composed of an octamer of two each of the histone proteins H2A, H2B, H3 and H4 wrapped in ~147 bp of DNA. Nucleosome positioning and sliding are distinct dynamic properties of nucleosomes pivotal for essential chromatin processes such as replication, transcription and repair.

To gain a better understanding of these properties site-directed mutagenesis was used to introduce a cysteine residue onto the surface of the octamer at each of the seven super helical location (SHL) points of contact on the pseudo dyad symmetric nucleosome. An EDTA/Fe²⁺ derivative or a 1,10-phenanthroline/Fe²⁺ derivative was then tethered to the cysteine adjacent to the SHL points of contact. When activated, these derivatives generate hydroxyl radicals, which break the DNA backbone adjacent to the point of contact. Denaturing PAGE can then be used to determine the size of these DNA fragments at base-pair resolution, which can be mapped back to the SHL points of contact.

Site-directed mapping was carried out on nucleosomes containing the well-characterised 147 bp MMTV NucA, 601 and 601.2 nucleosome positioning sequences. This showed that NucA, 601 and 601.2 were structurally equivalent, that EDTA and phenanthroline derivatives produced distinct mapping patterns, and that transient dynamics within the nucleosome could be interpreted.

EDTA/Fe²⁺ mapping at each of the SHL points of contact was used to investigate the mechanism of nucleosome sliding for thermally mobilised nucleosomes incubated at 37°C and 45°C. These results suggest nucleosome sliding along a 221 bp MMTV NucA DNA sequence proceeded in near single base-pair steps, without any large-scale metastable intermediate structures being observed.

Taken together, the results indicate that the nucleosome structure in solution is consistent with those of static crystal structures. It also indicates that nucleosome sliding occurs in near single base-pair steps characteristic of a twist defect diffusion mechanism. Finally, the mapping observed with the reagents used indicate that they occupy different positions within the minor groove and this high resolution characterisation of their behaviour provides the basis for expanding investigations of nucleosome properties *in vitro* and *in vivo*.

Chapter 1 Introduction

1.1 Role of chromatin in organising the genome

Genome organisation is a vast and complex process facilitated by chromatin. Genome organisation influences many processes including DNA packaging, replication, transcription, recombination and DNA repair for which the substrate is chromatin and is based on repeating nucleosome units. Direct *cis* acting factors or indirect *trans* acting factors regulate genome organisation.

1.2 Hierarchical structure of chromatin

The fundamental repeating unit of eukaryotic chromatin is the nucleosome, which is composed of a nucleosome core particle and flanking linker DNA. The nucleosome core particle is composed of an octamer of histone proteins wrapped in ~147 bp of DNA (Luger et al., 1997; Davey et al., 2002).

The linker DNA between core particles can vary in length and is usually between 40-60 bp depending on species and tissue, giving an overall nucleosome repeat length of ~200 bp. Linker histones are capable of binding the inter-nucleosomal linker DNA creating what is known as a chromatosome (Simpson, 1978; Widom, 1998).

Controversy surrounds the next level of chromatin compaction. Once it was generally accepted that repeating arrays of nucleosomes were further condensed into a 30 nm fibre in a one start or two start arrangement with or without linker histones respectively (Finch and Klug, 1976; Schalch et al., 2005; Robinson et al., 2006). However, more recent studies with cryo-electron microscopy and small angle X-ray scattering found no evidence of an ordered structure within human mitotic chromosomes, noting a fractal 10 nm fiber, irregular polymer-melt like arrangement, which allows for a more dynamic genome (Eltsov et al., 2008; Nishino et al., 2012). Schematic illustrations of both models are represented in Figure 1.1.

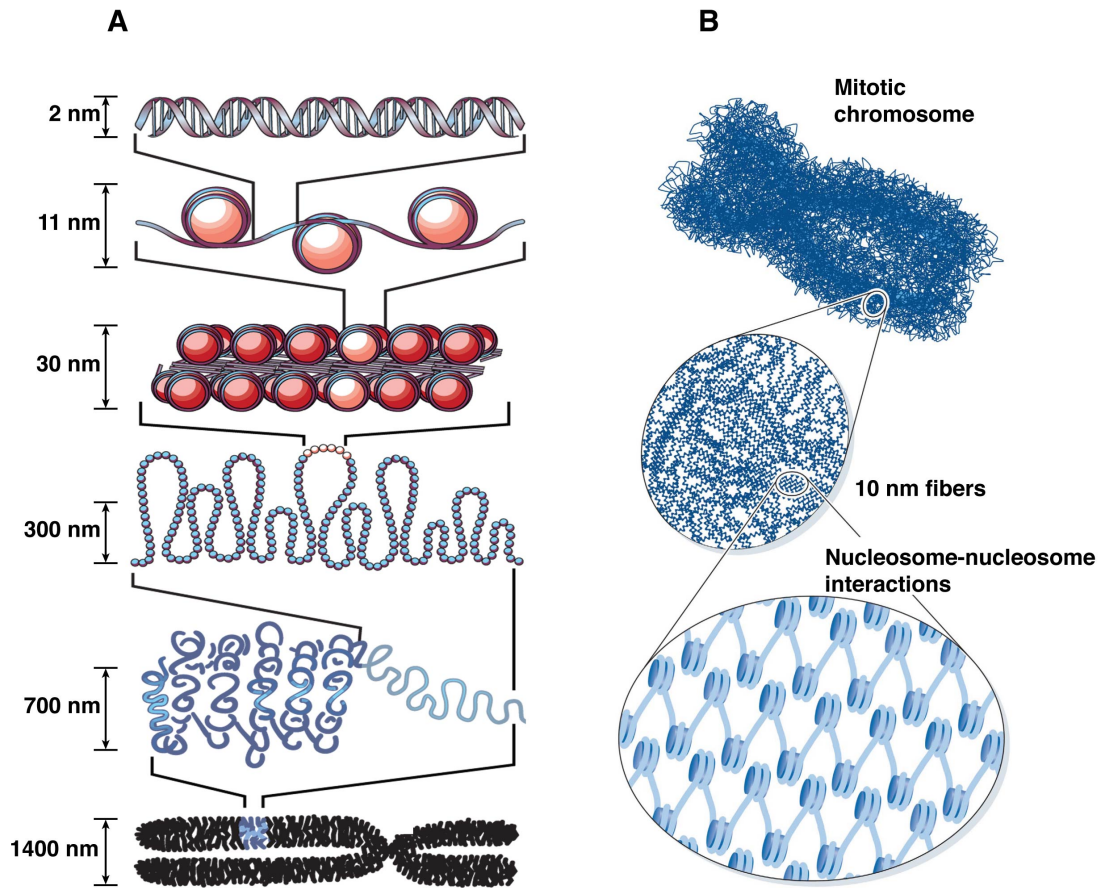


Figure 1.1 Chromatin compaction. **A.** Traditionally accepted schematic model for the higher order structure of chromatin. This model demonstrates regular levels of chromatin compaction from the most basic nucleosome through to a 30 nm fibre with further levels of compaction leading to the mitotic chromosome (Felsenfeld and Groudine, 2003). **B.** This represents the emerging viewpoint on chromatin compaction where nucleosomes are arranged in an irregular, fractal nature for a more dynamic genome (Hansen, 2012).

1.3 Nucleosome structure

1.3.1 Octamer structure

The nucleosome core particle consists of an octamer of two each of the histone proteins H2A, H2B, H3 and H4 wrapped in a left-handed spiral 1.67 times with ~147 bp of B-form DNA. Over the course of this wrapping DNA makes contact with the octamer surface every helical turn where the minor grooves face inward (Luger et al., 1997; Davey et al., 2002; Richmond and Davey, 2003). The crystal structure of the core nucleosome particle containing the 601 strong positioning sequence is represented in Figure 1.2, (Vasudevan et al., 2010). A list of some of the different nucleosome crystal structures solved to date along with their histone species composition and DNA sequence is given in Tan and Davey, 2011.

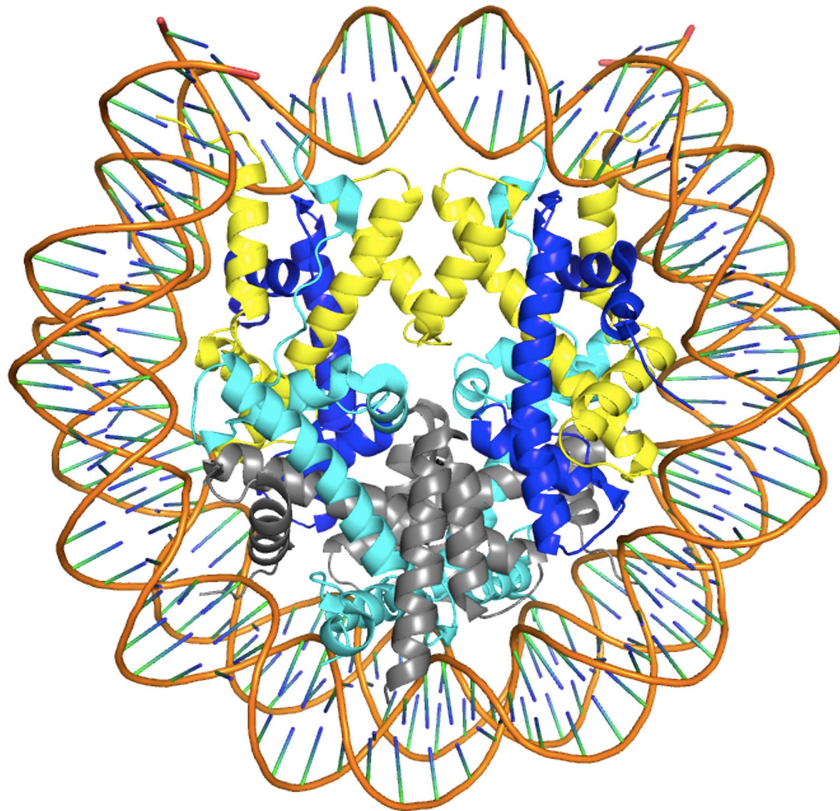


Figure 1.2 Nucleosome core particle. Crystal structure of the nucleosome core particle containing the 601 strong positioning sequence. Histones H2A, H2B, H3 and H4 are coloured cyan, grey, yellow and blue respectively, DNA is coloured brown. Structure from Protein Data Bank (PDB) entry 3LZ0 (Vasudevan et al., 2010).

The four core histones H2A, H2B, H3 and H4 form a tertiary protein structure known as a histone fold from three α -helices, $\alpha 1$ - $\alpha 3$, which are joined by two loops L1-L2 to form the histone fold domain $\alpha 1$ -L1- $\alpha 2$ -L2- $\alpha 3$. Histone fold extensions including α -helices, β strands and unstructured tail regions are located outside of the histone fold domain (Vasudevan et al., 2010). A schematic representation of the secondary structural arrangement for the core histones is represented in Figure 1.3.

The histones associate in a mainly hydrophobic, antiparallel binding to form a histone fold dimer or handshake motif. Histones H3 and H4 associate with each other to form one H3-H4 dimer, with subsequent H3-H4 dimer self-association forming the $(\text{H3-H4})_2$ tetramer. Histones H2A and H2B also associate in an antiparallel handshake motif configuration to form the H2A-H2B histone fold dimer (Arents et al., 1991). The pairing of partner histones is represented in Figure 1.4.

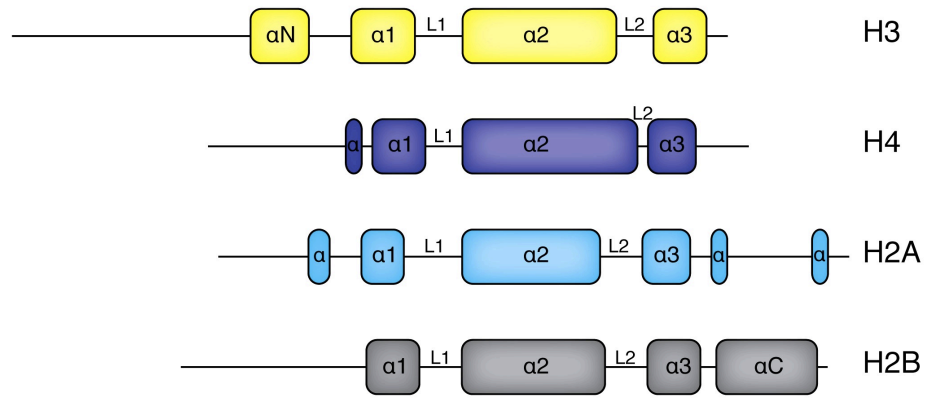


Figure 1.3 Core histone secondary structure. Secondary structure of the core histones H2A, H2B, H3 and H4 in cyan, grey, yellow and blue respectively. The α -helices (α) and loops (L) which make up the histone fold domain are labeled ($\alpha 1$ -L1- $\alpha 2$ -L2- $\alpha 3$). Also shown are the extra α -helices αN and αC of H3 and H2B respectively. The short α -helical runs outside the histone fold domain of H2A and H4 are denoted by α .

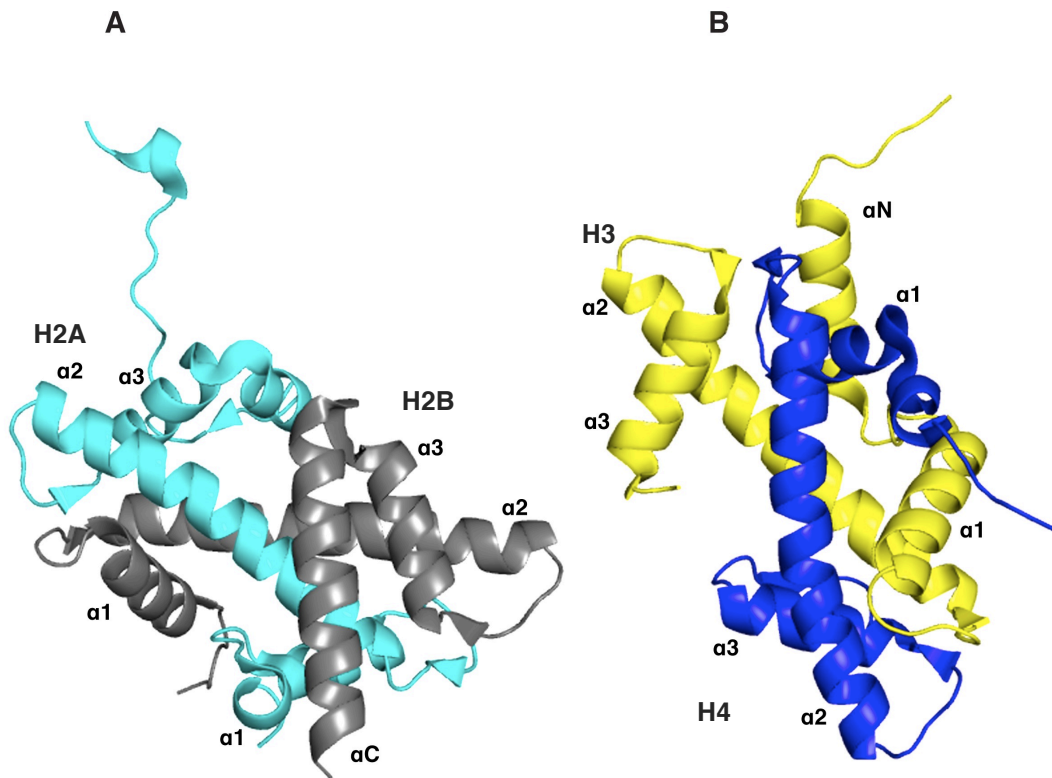


Figure 1.4 Histone pairing handshake configuration. A. H2A and H2B in cyan and grey respectively. B. H3 and H4 in yellow and blue respectively. Alpha-helical positions are represented. Structure from PDB entry 3LZ0 (Vasudevan et al., 2010).

The $(H3-H4)_2$ tetramer is formed from the binding of two H3-H4 dimers through a dyad symmetric four helix bundle from the C-terminal portions of the $\alpha 2$ and the $\alpha 3$ helices of H3. The $\alpha 2$ and $\alpha 3$ helices of the two H3 molecules are bound by hydrogen bonding and a series of hydrophobic interactions (Luger et al., 1997).

Subsequent binding of each H2A-H2B dimers to the (H3-H4)₂ tetramer via another four helix bundle between the $\alpha 2$ and $\alpha 3$ helices of H2B and H4 caps the octamer. The H2B-H4 four helix bundle assembly is similar to that of the H3-H3 four helix bundle occurring through hydrogen bonding and series of hydrophobic interactions (Arents et al., 1991; Luger et al., 1997) although it is relatively less stable. The position of the four helix bundles are represented in Figure 1.5.

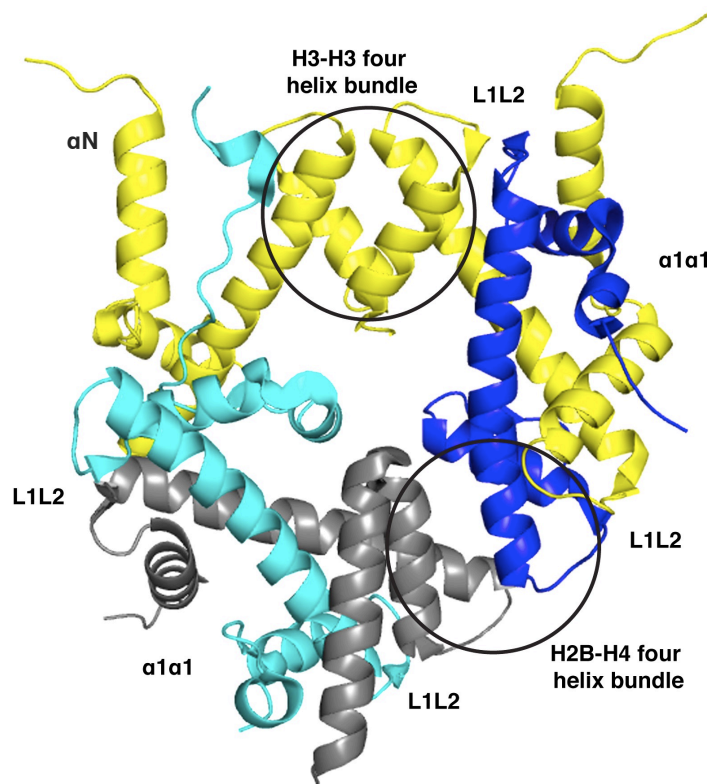


Figure 1.5 Four helix bundle binding sites. Schematic representation of one half of the histone octamer. Circled are two four helix bundles. Top circle is the tetrameric four helix bundle between the $\alpha 2$ and $\alpha 3$ helices of histones H3. The bottom circle shows the four helix bundle between tetrameric H4 $\alpha 2$ and $\alpha 3$ helices and dimeric H2B $\alpha 2$ and $\alpha 3$ helices. The schematic nomenclature represents the seven locations of histone/DNA contact for half the nucleosome core particle. Structure from PDB entry 3LZ0 (Vasudevan et al., 2010).

The combined arrangement of the folded histones produces a spiral scaffold for DNA binding. Each histone fold produces paired L1L2 loops between $\alpha 1$ and $\alpha 2$, (L1) and between $\alpha 2$ and $\alpha 3$, (L2). Antiparallel arrangement of the histones place L1 and L2 adjacent to create a histone-DNA interaction surface. Each histone pair has two L1L2 histone-DNA interaction surfaces allowing for 8 of the 14 DNA minor groove contact points. Each histone dimer also provides a second type of interaction surface for DNA to bind, formed by the $\alpha 1$ helices of each histone pair known as $\alpha 1\alpha 1$. There are four of these $\alpha 1\alpha 1$ interaction surfaces spread around the octamer. A

final two interaction surfaces come from the α N helices of each H3. This gives 14 interaction surfaces for octamer-DNA binding, and the arrangement of these 14 interaction surfaces is responsible for the left-handed wrapping of DNA around the nucleosome (Luger et al., 1997; Flaas, 2011). Figure 1.5 shows the arrangement of the DNA-protein interaction sites L1L2, α 1 α 2 and α N and the protein-protein four helix bundle interaction sites.

The two extra α -helical regions both of which are involved in stabilising the nucleosome are located on the H3 N-terminal tail (H3 α N) between residues 45-55 and on the H2B C-terminal tail (H2B α C) between residues 101-120 (Vasudevan et al., 2010). Other sites within the histone octamer also serve to increase structural stability, including a molecular cluster between H2A and H3-H4, a β -sheet docking between H2A-H4 and H4-H2B docking (Wood et al., 2005).

The histone tails which function in remodeling and epigenetics are the least structured part of the histone octamer. The highly basic tails comprise approximately 28% of the total core histone sequence and generally exit the nucleosome structure through the minor grooves (Luger and Richmond, 1998). The longest histone tail is the N-terminus tail of H3, which is 44 residues long with 38 residues external to the nucleosome core. Its functions include mediating the repulsion between the entry/exit DNA. The longest C-terminal tail is that of H2A and has 40 residues, the majority of which are contained within the nucleosome structure. The H2A C-terminal tail functions include nucleosome stability and the mediation of protein interactions involved in chromatin dynamics (Vogler et al., 2010; Flaas, 2011).

1.3.2 DNA structure

DNA can exist in three major forms: right-handed A-DNA and B-DNA, and the left-handed Z-DNA. In aqueous solution and *in vivo* DNA is essentially in B-form (Belmont et al., 2000).

Nucleosomal DNA in the core particle comprises ~147 bp of B-DNA wrapped 1.67 times round the histone octamer in a left-handed superhelix (Richmond and Davey, 2003). DNA contacts the surface of the histone octamer 14 times in the course of this wrapping where the minor grooves face the octamer surface. These contacts occur at seven locations on either half of the histone octamer creating a

pseudo dyad symmetric complex where the central dyad axis passes through a base-pair. Where the centrally positioned major groove faces the histone octamer, this location is designated Super Helical Location 0 (SHL 0). Each successive full helical turn at either side of SHL 0 where the major groove faces the octamer is given a integral value of $\pm 1-7$, Figure 1.6. Each successive half turn is denoted as $\pm 0.5-6.5$ where the minor grooves face the octamer surface (Luger et al., 1997).

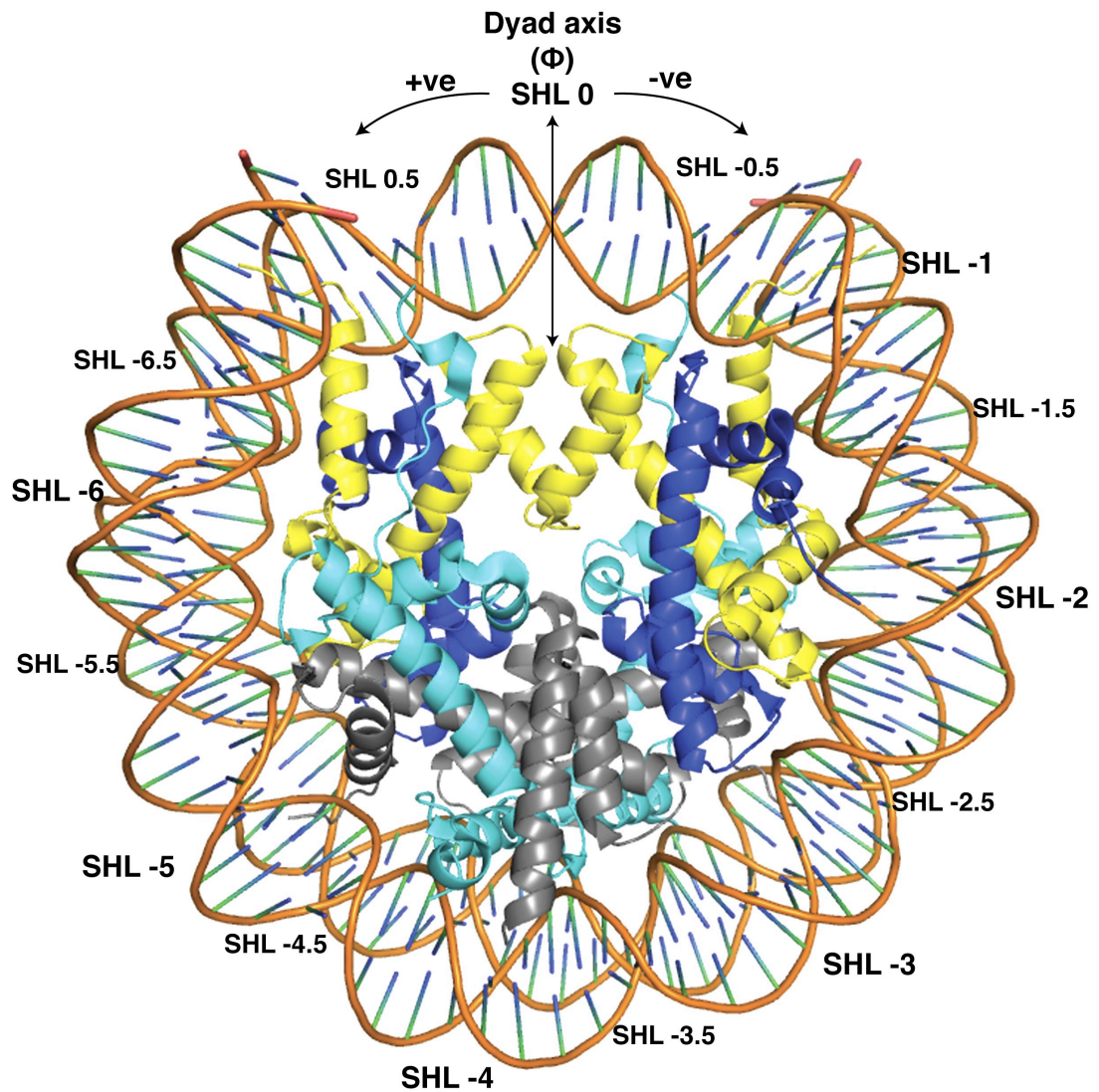


Figure 1.6 Nucleosomal super helical locations. Nucleosome structure showing the nomenclature for the super helical locations (SHL) around the nucleosome. SHL 0 is the centre of the nucleosome and is where the central major groove faces the octamer surface. The dyad axis passes through the central base-pair of SHL 0. Each full helical turn from SHL 0 has an integer value $\pm 1-7$ and each half turn from SHL 0 is denoted SHL $\pm 0.5-6.5$. Negative values are given for the first half of the nucleosome with the positive values given for the second half. Structure from PDB entry 3LZ0 (Vasudevan et al., 2010).

The direct interactions between DNA and histones at the 14 contact points are mediated by ~ 120 hydrogen bonds and various charge-charge interactions (Luger

and Richmond, 1998; Davey et al., 2002). These bonds occur between the protein backbone or amino acid side chains and the DNA phosphate backbone or the minor groove. The trend for the number of individual bonds per DNA contact site generally decreases from the centre of the nucleosome. This trend could explain the greater affinity observed by DNA for the tetramer over the dimer during the ionic gradient dialysis of *in vitro* nucleosome formation (Luger and Richmond, 1998; Davey et al., 2002; Flaas, 2011).

DNA stretching at SHL ± 2 or ± 5 has been observed in some crystal structures due to an over-twist or under-wind between nucleotides in the DNA at these locations. At these over-twist sites ~ 9 bp instead of ~ 10 bp per helical turn are observed. Common to both SHL ± 2 and SHL ± 5 is a preceding histone interaction with $\alpha 1 \alpha 1$ at SHL ± 1.5 and SHL ± 4.5 and a succeeding L1L2 histone interaction at SHL ± 2.5 and SHL ± 5.5 (Luger et al., 1997; Vasudevan et al., 2010; Tan and Davey, 2011). DNA stretching is not unique to specific crystal structures or one DNA sequence. It has been observed in α -satellite, and 601 sequences of 145, 146 and 147 bp in length. DNA stretching has also been observed using human and *Xenopus* octamers and in experiments on nucleosomes in solution (Edayathumangalam et al., 2005). Therefore, it would seem that localised DNA stretching within the nucleosome is not an artefactual anomaly of crystallisation but an intrinsic characteristic of nucleosomes.

The positioning of A/T and G/C bases along a DNA sequence plays an important role in its favourability to form nucleosomes. A/T bases are predominately found in the inward facing minor grooves where the DNA contacts the surface of the octamer, with G/C bases predominantly found in the outward facing minor grooves (Satchwell et al., 1986). The A/T bias associated with the minor grooves comes from the ability of A/T to form tight narrow grooves while G/C containing sequences form wider grooves. Tight narrow grooves are not solely composed of A/T nucleotides, so the more general term which includes the common minor groove dinucleotides TA and TG refers to pyrimidine-purine steps (Travers and Klug, 1987). However, this can only be interpreted as a general rule as the inward facing minor grooves are far from absent of G/C bases. For example, a palindromic derivative of the 601 strong positioning sequence contains a trinucleotide run GGG/CCC in 6 of the 8 minor grooves around the dyad of its nucleosome. However, this has markedly reduced

affinity compared to the parent 601 although it still demonstrates greater affinity for the nucleosome than α -satellite DNA (Chua et al., 2012). Also the addition of G/C bases in the minor groove breaks runs of A/T bases, which have been shown to form nucleosome free regions (NFR) around promoters and drive nucleosome positioning (Yuan et al., 2005). Due to the ability of G/C bases to occupy most locations around the nucleosome, G/C% has been rationalised as a means of predicting nucleosome occupancy (Chua et al., 2012).

1.4 Histones

Histone proteins can be divided into two main categories: replication dependent canonical histones and replication independent non-canonical histone variants.

Replication dependent canonical histones include the core histones H2A, H2B, H3 and H4, and the linker histone H1. Their mRNA is expressed at the beginning of S-phase to coincide with DNA replication and in contrast to the vast majority of mRNA in eukaryotes their mRNA is non-polyadenylated. However, histone mRNAs contain a unique 3' stem-loop structure crucial for their regulation (Marzluff et al., 2008).

The linker histone H1 is a lysine rich replication dependent histone involved in chromatin compaction. The secondary structure of H1 consists of a short amino terminus, 3 central alpha-helices and a beta-hairpin which form a tertiary globular structure which binds DNA, and a long unstructured carboxyl terminus. H1 binds nucleosomal DNA at the entry/exit region, creating the chromatosome, aiding DNA compaction and chromatin assembly. Histone H1, just like the core histones is also the target for many post-translational modifications (Cerf et al., 1994; Brown et al., 2006; Happel and Doenecke, 2009; Vogler et al., 2010; Xiao et al., 2012).

A number of related histone types or variants are incorporated into nucleosomes in place of the normal replication dependent histones. These replication independent non-canonical histone variants are expressed throughout the cell cycle and their mRNA includes a poly-adenylation. The function of these histone variants is diverse with roles in processes such as chromosome segregation, transcriptional

regulation, DNA repair and sex chromosome condensation (Marzluff et al., 2008; Talbert and Henikoff, 2010).

Some of the common histone variants include CENP-A, a H3 variant involved in assembly and function of the kinetochore (Sullivan, 2001). Histone H3.3 another H3 variant has been associated with transcriptionally active genes and is enriched with post-translational modifications (PTMs) associated with gene activation (Hake and Allis, 2006). H2AZ a variant of H2A has been mapped to the 5' end of genes and has been implicated in processes such as transcriptional control and the suppression of antisense RNAs (Draker and Cheung, 2009; Zofall et al., 2009). Another H2A variant H2AX plays a major role in DNA repair by initiating the DNA damage response to double strand breaks by the phosphorylation of H2AX S139 (γ H2AX) (Lowndes and Toh, 2005; Pinto and Flaus, 2010).

Processes such as condensation, replication, transcription, repair and recombination are regulated by a wide variety of histone post-translational modifications (PTM) such as acetylation, carbonylation glycosylation, methylation, phosphorylation, ribosylation, sumoylation and ubiquitylation (Peterson and Laniel, 2004; Fuchs et al., 2006; Bannister and Kouzarides, 2011).

1.5 Nucleosome positioning

Nucleosome positioning is defined as the location of nucleosomal DNA relative to the histone octamer and it can be influenced intrinsically and extrinsically. Intrinsic nucleosome positioning is influenced by a combination of DNA sequence, octamer composition and post-translational modification of histones. Extrinsic nucleosome positioning involves external factors such as chaperones and ATP dependent chromatin remodelers (Campos and Reinberg, 2009; Flaus, 2011).

1.5.1 Types of positioning

The position of the DNA molecule relative to the histone octamer can be explained as having two basic phases. Rotationally positioned nucleosomes expose the same DNA face to solution and are related by shifts of ~10 bp multiples due to the helical turn pitch of DNA. Translationally positioned nucleosomes occupy a

specific location within a sequence so positions can differ by a single base pair, ultimately exposing all nucleotides of the DNA to solution (Drew and Travers, 1985; Satchwell et al., 1986; Zhang et al., 2009).

The observation of phased nucleosome arrays led to the suggestion that nucleosomes can be statistically positioned starting from a barrier. The barrier could be an unfavourable sequence, or a DNA binding protein that prevents nucleosome positioning, therefore driving statistical positioning by biasing the position of adjacent nucleosomes (Kornberg and Stryer, 1988; Flaus, 2011). Statistical positioning would also legitimise the highly regular pattern of nucleosome positioning observed across the eukaryotic genome at the 5' end of genes (Yuan et al., 2005; Zhang et al., 2011).

1.5.2 *In vitro* nucleosome positioning sequences

Over 95% of genomic DNA has relatively the same affinity for histone octamers as randomly synthesised DNA (Lowary and Widom, 1997). This suggests that endogenous DNA sequences contribute relatively little to their own nucleosome formation. For this reason the use of nucleosome positioning sequences have become an essential tool for *in vitro* analysis of nucleosome structure and function (Lowary and Widom, 1997).

A number of different DNA sequences exist that demonstrate nucleosome positioning. These nucleosome positioning sequences have been used in a range of *in vitro* experiments from nucleosome reconstitution and base pair resolution mapping to X-ray crystallography. These positioning sequences have been discovered through biochemical interest in specific endogenous loci in the case of 5S rDNA, alpha satellite and MMTV sequences (Donehower et al., 1981; Hörz et al., 1983; Simpson and Stafford, 1983) and through screening of synthetic DNA fragment libraries as with the 601 sequences (Lowary and Widom, 1998).

1.5.3 5S rDNA sequence

The 260 bp *Lytechinus variegatus* DNA sequence is composed of a 120 bp sequence encoding the 5S ribosomal RNA, which is flanked by 90 bp on the 5' side and 50 bp on the downstream side. Association with chicken erythrocyte core histones and subsequent DNase I digestion revealed a ~145 bp region was protected from nuclease digestion (Simpson and Stafford, 1983). This led to the 5S rDNA sequence being used in numerous pivotal *in vitro* nucleosome studies from nucleosome tandem repeats (Simpson et al., 1985) to nucleosome sliding (Pennings et al., 1991).

1.5.4 Alpha satellite sequence

Alpha satellite DNA is a tandem repeat of a 171 bp sequence located in the centromere of primates (Alves et al., 1994). The ability of alpha satellite to reconstitute nucleosomes is probably aided by the presence of poly-A tracts and intrinsic curvature (Bussiek et al., 2007). The majority of nucleosome crystal structures to date are based on a palindromic 146 bp sequence isolated from a 73 bp region of human alpha satellite DNA originally used by Luger and colleagues in the 2.8 Å nucleosome crystal structure (Luger et al., 1997; Tan and Davey, 2011).

1.5.5 Mouse Mammary Tumor Virus Long Terminal Repeat (MMTV LTR)

MMTV in infected mouse milk is ingested into the gut where it is adsorbed via Peyers patches and taken in by lymphocytes with subsequent entry into the blood stream via the thoracic duct. From the blood the virus makes its way to mammary tissue where it lays dormant until the age of lactation is reached. During lactation expression of the MMTV is greatly increased under the influence of steroid hormones. However, tumour formation is as a result of viral enhancers acting on native proto-oncogenes and not due to virally encoded oncogenes (Matsuzawa et al., 1995).

The complex retroviral MMTV is 9 kb in length and like all retroviruses is flanked by LTRs. The 3' LTR is 1.3 kb in length which encodes a superantigen and contains a steroid-inducible promotor region (Ross, 2010). The 3' LTR contains at least 6 specifically positioned nucleosomes that span the LTR from 3' to 5' and are designated A-F (Richard-Foy and Hager, 1987).

The steroid-inducible promotor or hormone response element (HRE) is silent in the absence of hormone. However, binding of the glucocorticoid steroid hormone to its cytoplasmic receptor, with subsequent translocation of the hormone bound receptor to the nucleus allowing it to bind to the MMTV's HRE and initiate transcription. This induction involves the disruption of nucleosome B (NucB) which is in the region of the HRE (Belikov et al., 2001).

In vitro base pair resolution mapping of nucleosome A (NucA) and nucleosome B (NucB) show these nucleosomes to center at +70 and -127 bp respectively, relative to transcription start site (+1). The NucB DNA sequence demonstrated A/T richness along with G/C periodicity making this position relatively stable in contrast to the NucA sequences which demonstrates a G/C content more characteristic of regular genomic DNA. These contrasting sequence affinities for nucleosome positioning are observed during thermal sliding where NucA sliding is initiated at ~47°C while temperatures over 50°C are needed to initiate NucB sliding (Flaus and Richmond, 1998; Flaus, 2011). Other work using the MMTV NucA and NucB positioning sequences demonstrated that nucleosomes could invade the DNA territories occupied by their neighbours (Engelholm et al., 2009). The ATP-dependent chromatin remodelers ISWI and Chd1 have also been analysed on MMTV sequences (Stockdale et al., 2006).

1.5.6 Widom 601 sequences

Due to the strength of nucleosome positioning demonstrated by the 601 sequences they have become amongst the most popular sequences used for the study of nucleosomes *in vitro*. The 601 strong positioning sequence was isolated using Systematic Evolution of Ligands by Exponential Enrichment (SELEX) from a starting pool of 5×10^{12} individual 220 bp chemically synthesised DNA sequences. This pool went through 8 rounds of PCR amplification with subsequent HPLC

purification before undergoing competitive reconstitution on chicken erythrocyte histones by NaCl gradient from 2M to physiological concentrations from which the strongest 10% were selected and purified by 2 rounds of sucrose gradient centrifugation. The DNA was then extracted from the purified nucleosomes to re-enter the selection cycle at the PCR amplification stage. After 15 rounds of enrichment ~30-50 species remained of which 9 were ranked by competitive reconstitution with 601 demonstrating the highest affinity for nucleosome formation (Lowary and Widom, 1998).

Crystal structure analysis of the 601 nucleosome demonstrates that the fundamental aspects that give the 601 sequence its affinity for the histone octamer are the flexible pyrimidine-purine base pair steps that occur in 9 of the 12 minor groove blocks that face the octamer surface. The highly deformable TA dinucleotide is at the majority of these sites. The major grooves of the 601 nucleosome display GC richness, especially around the center of the nucleosome (Vasudevan et al., 2010). Stretch is also observed in both halves of the nucleosome at SHL ± 5 , which is due to an extreme kinking event at purine-purine or pyrimidine-pyrimidine steps (Makde et al., 2010; Vasudevan et al., 2010).

Alterations were subsequently made to the original 601 sequence to allow for restriction enzyme DNA cleavage in order to observe transient site exposure. A total of 12 nucleotide changes were made to one half of the 601 sequence using 2 rounds of PCR mutagenesis to create the 601.2 sequence (Anderson and Widom, 2000). The affinity the 601.2 sequence demonstrated for the nucleosome was less than the original 601 sequence. Nevertheless it demonstrated affinity ~10 times that of the 5S sequence (Lowary and Widom, 1998; Anderson and Widom, 2000).

The high stability and homogeneous nature of the 601 sequences make them ideal species for *in vitro* structure and functional studies. However, the high thermal stability of these nucleosomes probably renders them sub-optimal for the study of thermal nucleosome sliding (Flaus, 2011).

1.5.7 Genomic encoding of organised nucleosomes

Initially Lowary and Widom showed through competitive nucleosome reconstitution that 95% of bulk genomic DNA has an affinity for histone octamer that is similar to randomly synthesised DNA. This implied that the intrinsic formation of endogenous nucleosomes contributed relatively little to *in vivo* nucleosome organisation (Lowary and Widom, 1997). However, conflicting data has emerged on the issue of genomic encoding for *in vivo* nucleosome organisation.

It has been shown that DNA sequence has a central role in organising endogenous nucleosomes and that as much as 50% of nucleosome organisation can be attributed to intrinsic nucleosome positioning by genomic encoding (Segal et al., 2006; Kaplan et al., 2009). Others have argued against a genomic code for nucleosome positioning and instead supported the theory that the nucleosome organisation pattern around coding regions are due mainly to ATP utilising *trans* acting factors such as remodelers and transcriptional machinery (Zhang et al., 2009; Gkikopoulos et al., 2011; Zhang et al., 2011; Hughes et al., 2012).

Recent high resolution data from human cells has shown that almost half of the genome contains regularly spaced nucleosome arrays, much of which had some intrinsic nucleosome preference for their DNA sequences over others. Within some regions of the genome this intrinsic preference was outperformed by competing DNA binding proteins and that other intrinsically positioned nucleosomes were actively shifted (Gaffney et al., 2012).

The degree to which genomic nucleosome organisation relies on a positioning code is still uncertain and further research and debate is required. However, it is probable that the complexity of genome organisation and function will not rely on a single *cis* or *trans* acting factor but of combinations of both factors.

1.6 Dynamic nucleosomes

Nucleosomes are dynamic complexes that are capable of active and passive structural alterations that allow DNA access for processes such as replication, transcription and repair. Active nucleosome dynamics are performed extrinsically by ATP-dependent chromatin remodelers, while passive nucleosome dynamics include

activities such as nucleosome breathing and sliding (Luger, 2006; Blossey and Schiessel, 2011).

1.6.1 Passive nucleosome dynamics

Nucleosome breathing

Nucleosome breathing is a process whereby the entry/exit DNA transiently unwraps from the surface of the octamer. This behaviour has been shown using restriction enzymes, AFM and various FRET techniques (Polach and Widom, 1995; Li et al., 2004; Koopmans et al., 2009; Shlyakhtenko et al., 2009). It has been shown that the transient unwrapping of the entry/exit DNA occurs in a progressive manner from both DNA termini, where DNA on/off rates are greatest for the external-most parts of the nucleosome with progressively lower rates observed approaching the center of the nucleosome (Polach and Widom, 1995; Koopmans et al., 2009). The duration of the DNA on/off rates for the DNA termini have been shown to be ~50 ms for the off rate with a frequency of ~3-4 of these events occurring per second (Li et al., 2004). However, others have shown various different frequencies through varying experimental approaches, reviewed in Buning and van Noort, 2010. The spontaneous unwrapping of nucleosomal DNA allows sequence exposure to regulatory proteins that would otherwise be inhibited from binding due to the steric arrangement of bound nucleosomal DNA (Anderson et al., 2002).

Thermal nucleosome sliding

Nucleosome sliding is an ATP-independent process whereby the histone octamer slides relative to the DNA sequence resulting in a repositioning of the nucleosome. The newly translocated nucleosome can expose DNA that is available for DNA regulatory proteins involved in processes such as replication, transcription and repair. Spontaneous nucleosome sliding has been observed *in vitro* in a temperature dependent manner on nucleosome positioning sequences (Pennings et al., 1991; Flaus and Richmond, 1998; Miyagi et al., 2011), making endogenous nucleosome sliding at 37°C on genomic DNA quite plausible. Two main mechanisms of ATP-independent nucleosome sliding have been proposed: Twist

defect diffusion and loop/bulge defect diffusion (Flaus and Owen-Hughes, 2003; Blossey and Schiessel, 2011).

Twist defect diffusion

The proposed twist defect diffusion mechanism explains nucleosome mobilisation through single base pair steps. The single base pair defect originates at the DNA entry/exit site and comprises the loss or gain of a single base pair within the DNA between adjacent contact points. This twist defect causes a local conformational change within the DNA pitch that is under-twisted for the addition of a base pair or over-twisted for the loss of a base pair. Subsequent diffusion of these twist defects around the nucleosome, ultimately resolving in the linker DNA causes the nucleosome to shift by 1 bp (Flaus and Owen-Hughes, 2003; Blossey and Schiessel, 2011). A schematic illustration of twist defect diffusion is represented in Figure 1.7.

Twist defects at SHL ± 2 and ± 5 have been observed in crystal structures (Richmond and Davey, 2003; Ong et al., 2007; Vasudevan et al., 2010) while nucleosomes in solution have been shown to exist in multiple twist defect states (Edayathumangalam et al., 2005). It has also been shown for nucleosomes in solution that the periodicity of DNA around the central two to four turns is slightly greater 10.5-11 bp than the flanking DNA which is ~ 10 bp. This has not been observed in any of the nucleosome crystal structures solved to date and may be sequence dependent or come from a dynamic equilibrium of the nucleosomes in solution (Negri et al., 2001). These data would indicate that twist defect diffusion is a possible mechanism for nucleosome sliding *in vitro* and *in vivo*.

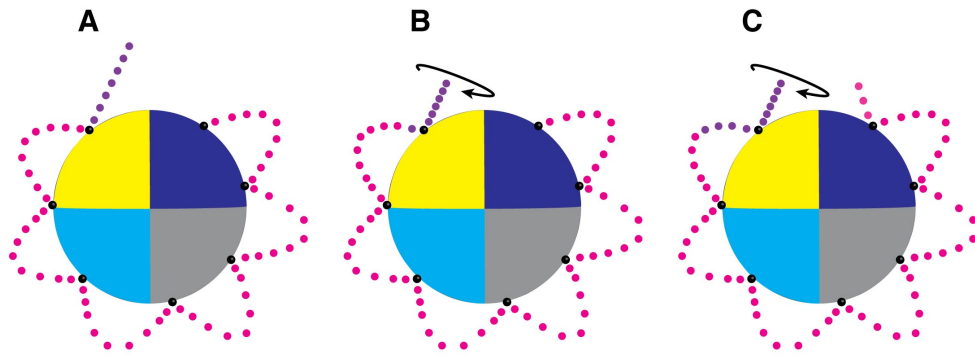


Figure 1.7 Twist defect diffusion. **A.** Nucleosome in an equilibrated energetic state. **B.** Twisting occurs in the linker region of DNA external to the nucleosome core particle. This causes under-twist/over-winding in the linker region, which causes a single base pair to enter the nucleosome core particle creating a DNA twist defect within the nucleosome core particle. **C.** Further under-twisting of the linker DNA causes more base pairs to enter the nucleosome core particle. To release this high energetic state base pairs are released off the far side of the nucleosome. Effectively shifting the nucleosome. Octamer represented by the large sphere, quadrants represent individual histones. Small black spheres represent the DNA/octamer points of contact. DNA is represented in magenta and purple.

Loop/Bulge diffusion

Loop diffusion, has a number of names including bulge diffusion or wave diffusion. In this mechanism, loops of ~ 10 bp or multiples of ~ 10 bp diffuse around the nucleosome resolving into the linker DNA, ultimately sliding the nucleosome in multiples of ~ 10 bp. In the simplest case the length of the loop is a multiple of the DNA helical pitch that occurs between the contact points of DNA and octamer. Nucleosome breathing at the DNA entry/exit causes an unbinding of the DNA from the histone octamer that can rebind further inside the nucleosome, creating a loop. If the loop diffuses back to its site of formation the nucleosome is not shifted. However, if the loop diffuses around the nucleosome and resolves at the opposite side of formation, the nucleosome will effectively slide by the length of the loop (Flaus and Owen-Hughes, 2003; Blossey and Schiessel, 2011). In contrast with twist diffusion, loop diffusion will keep the same rotational setting of DNA throughout its slide, which could aid some DNA binding proteins while perturbing others. Loop diffusion is illustrated in Figure 1.8.

Nucleosomal DNA loops in conjunction with ATP-dependent remodelers have been claimed to be observed in nucleosome sliding (Strohner et al., 2005; Liu et al., 2011). However, nucleosomal DNA loops have also been claimed in the absence of ATP-dependent remodelers (Bussiek et al., 2005). These data suggest that loop

formation is an ongoing process within the nucleosome and that the process of endogenous nucleosome sliding through loop diffusion is probable.

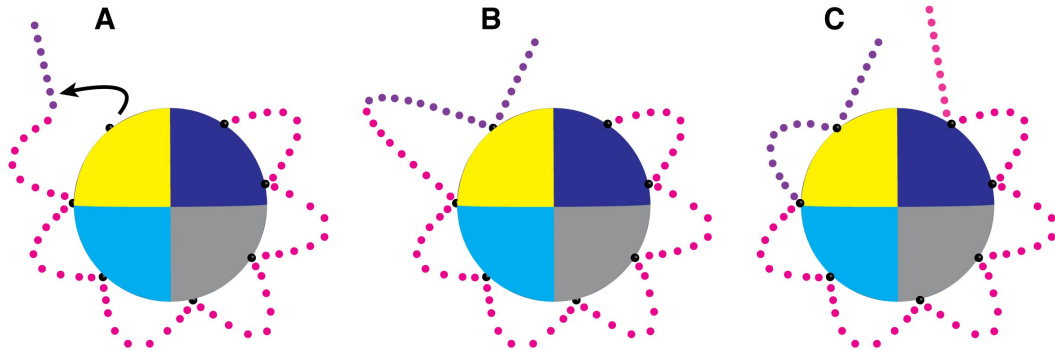


Figure 1.8 Loop defect diffusion. **A.** Nucleosome in the dynamic process of nucleosome breathing at the outer most part of the nucleosome. **B.** The original linker length of DNA has rebound inside the nucleosome core particle creating a loop or bulge within the structure. **C.** The loop travels around the surface of the octamer, resolving into the opposite linker DNA. This process effectively slides the nucleosome by the length of the loop that is greater than 1 DNA helical pitch. Octamer represented by the large sphere, quadrants represent individual histones. Small black spheres represent the DNA/octamer points of contact. DNA is represented in magenta and purple.

1.6.2 ATP-Dependent chromatin remodeling

ATP-dependent chromatin remodeling is a process whereby nucleosomes are actively altered to facilitate DNA regulatory processes, such as replication, transcription and repair. These nucleosome rearrangements are catalysed by the Sucrose non-fermenting 2 (Snf2) family of ATPases that are capable of driving nucleosome translocations, exchanging histones or completely removing the histone octamer from DNA. The main ATP-dependent chromatin remodeling families are SWItch/Sucrose Non-Fermenting (SWI/SNF), Imitation SWItch (ISWI), Chromodomain Helicase DNA binding (CHD) and INOsitol requiring mutant 80 (INO80) each of which belongs to the Snf 2 family of ATPases (Gangaraju and Bartholomew, 2007; Ho and Crabtree, 2010; Flauss and Owen-Hughes, 2011).

SWI/SNF family

It has been reported that the multi-protein complex SWI/SNF produces loop defects on the surface of nucleosomes enabling restriction enzyme digest of the unbound DNA (Zhang et al., 2006; Liu et al., 2011). It has also been shown that

SWI/SNF binds the nucleosome ~20 bp from the dyad at SHL 2 and shifts the nucleosome in ~50 bp increments presumably through the formation of loops on the nucleosome surface (Zofall et al., 2006). Therefore it is possible that these loop defects present sterically favourable DNA for binding proteins, while also aiding nucleosome sliding.

ISWI family

The ISWI family of ATP-dependent chromatin remodelers have been shown to slide nucleosomes along DNA, with different ISWI family members demonstrating their own directional preference (Stockdale et al., 2006). ISW2 like SWI/SNF also binds the nucleosome around SHL 2 and shifts the nucleosome in increments of 9-11 bp, suggesting that the mechanism behind nucleosome sliding appears again to be the formation of a loop structure (Zofall et al., 2006). However, recent single molecule FRET data has shown that ISWI initiates remodeling with a 7 bp step that translocates 7 bp of DNA to the exit linker in single base-pair steps. This places a strain of 7 bp on the nucleosome, which causes 3 bp to enter the nucleosome via the entry linker. With the strain on the nucleosome now at 4 bp this allows 3 bp to again leave the nucleosome via the exit linker bringing the strain back to 7 bp. This cycle of 3 bp steps continues for the total translocation (Deindl et al., 2013). ISWI catalysed nucleosome sliding has various functions including chromatin assembly, nucleosome spacing and transcriptional repression (Gangaraju and Bartholomew, 2007; Erdel and Rippe, 2011).

CHD family

The CHD family has been shown to be involved in the highly regular spacing of nucleosomes at the 5' end of genes following the transcription start site (TSS) (Pointner et al., 2012). Like ISWI, the Chd1 chromatin remodeler possesses DNA binding domain in SWI3, ADA2, N-CoR and TFIIB (SANT) and SANT Like ISWI (SLIDE) domains suggesting partial redundancy especially with regard to nucleosome spacing (Ryan et al., 2011). It has also been shown that the Chd1 DNA binding domains affinity for extra-nucleosomal DNA is the main factor determining the direction Chd1 slides the nucleosome (McKnight et al., 2011). Interestingly Chd1

has been shown to function in the deposition of the histone variant H3.3 onto chromatin *in vivo* (Konev et al., 2007) making Chd1 quite functionally diverse with regards to remodeling.

INO80 family

The INO80 family of chromatin remodelers regulate transcriptional activation and DNA repair. INO80 precisely spaces mononucleosomes towards the centre of DNA fragments and needs a minimum of 33-43 bp of extranucleosomal DNA to do so with 70 bp being the optimum required length. INO80 also showed that it can space nucleosome arrays, reducing an initial linker length of 50 and 79 bp down to ~30 bp for arrays of 2-3 nucleosomes (Udugama et al., 2011). It has been demonstrated that INO80 is involved in the repair of double strand breaks (DSBs) and is recruited to the damage site by H2A-S129 phosphorylation (van Attikum et al., 2004). The INO80 complex was also implicated in removal of UV lesions by the nucleotide excision repair pathway (Jiang et al., 2010).

1.6.3 Histone chaperones

The process of removing or assembling histone proteins from or to the DNA during processes such as transcription, replication and repair is mediated by histone chaperones. In general histone chaperones can be classified into H3-H4 or H2A-H2B chaperones based on their preferential histone binding (Burgess and Zhang, 2013).

The histone chaperone anti-silencing function 1 (Asf1) is a highly conserved acidic protein that binds the H3 carboxyl terminus of the H3-H4 dimer and prevents the formation of the H3-H4 tetramer, thereby preventing nucleosome formation (English et al., 2006). Another histone chaperone, nucleosome assembly protein 1 (Nap1) has been shown to promote nucleosome assembly by disfavours non-nucleosomal interactions between DNA and the H2A-H2B dimer (Andrews et al., 2010). Other histone chaperones include the chromatin assembly factor 1 (CAF-1), which binds H3.1-H4 and promotes tetramer formation. The histone chaperone for H2AZ-H2B (Chz1) binds the dimer and deposits it for nucleosome formation near the gene promoter (Burgess and Zhang, 2013).

1.7 Methods for determining nucleosome positioning

1.7.1 Nucleases

Enzymatic nucleases

Three commonly used nucleases in the study of nucleosome positioning are Micrococcal Nuclease (MNase), Deoxyribonuclease I (DNaseI) and Exonuclease III (ExoIII). These nucleases work on the principle that free DNA is cleaved more readily than nucleosomal bound DNA. Therefore, footprinting analysis where the linker DNA is more prone to cleavage than core DNA produces a footprint pattern on denaturing PAGE, and nucleosome positions can be deciphered (Flaus, 2011). Some of the earliest nucleosomal structural studies dating back almost four decades used MNase and DNaseI to look at nucleosome positioning (Noll, 1974; Finch and Klug, 1976; Ronald Morris, 1976; Prunell, 1983). Other studies introduced certain restriction enzyme cleavage sites into modified positioning sequences to observe dynamics and mobility (Pennings et al., 1991; Anderson and Widom, 2000).

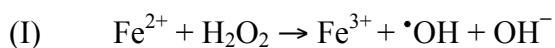
The most commonly used nuclease in the study of nucleosomes is the *Staphylococcus aureus* micrococcal nuclease. MNase preferentially cleaves at the 5' side of A or T over C or G with a 30 times greater cleavage rate for the former (Dingwall et al., 1981; Clark, 2010). This sequence preference for A/T nucleotides has raised questions about the suitability of MNase for nucleosome mapping (Chung et al., 2010). However, once properly controlled MNase sequence bias is not significant (Allan et al., 2012). Recently, much of the work involving MNase is centered around the high throughput sequencing of whole genome mononucleosomal DNA fragments from MNase digested chromatin (Yuan et al., 2005; Schones et al., 2008; Gaffney et al., 2012).

Chemical nucleases

Chemical nucleases are categorised into two main groups based on the reaction process: oxidative nucleases and hydrolytic nucleases. The oxidative nucleases use redox chemistry to cleave the deoxyribose ring of the DNA backbone and usually consist of a synthetic chemical ligand and metal ion complex. Two common chemical nucleases used in the study of chromatin structure are 1,10-

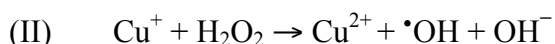
phenanthroline/copper (Phen/Cu²⁺) and EDTA/iron (EDTA/Fe²⁺) (Sigman, 1990). Potassium permanganate (KMnO₄) in conjunction with piperidine has also been used in the oxidative attack on DNA for use in footprinting studies, but KMnO₄ has a preference for oxidising thymidine residues (Spicuglia et al., 2004; Chua et al., 2012). Hydrolytic chemical nucleases hydrolyse the phosphodiester bond and usually consist of a large multinuclear ligand and metal cofactor that mimic the chemistry of natural restriction enzymes (Cowan, 2001; Liu and Wang, 2008).

The EDTA/Fe²⁺ reaction uses ferrous iron (Fe²⁺) and hydrogen peroxide (H₂O₂) to produce hydroxyl radicals (•OH). The simplest form of this reaction known as the Fenton reaction is shown in reaction I below (Fenton, 1894; Winterbourn, 1995).



The hydroxyl radicals produced by the Fenton reaction during DNA scission abstract the most accessible hydrogen from the deoxyribose carbons. This produces a carbon-based sugar radical which structurally rearranges, ultimately breaking the DNA backbone (Pogozelski and Tullius, 1998).

The mechanism of DNA scission by phenanthroline/copper is uncertain. It could be through a reaction similar to the Fenton reaction that uses copper instead of iron to produce hydroxyl radicals, as in reaction II below.



However, the identity of the oxidising species is more likely to be copper bound oxidant such as [CuO]⁺, [CuOH]²⁺ or CuO₂H. DNA scission is probably through abstraction of the 1' deoxyribose carbon, which produces a deoxyribose radical with subsequent structural rearrangement resulting in cleavage of the DNA backbone (Pogozelski and Tullius, 1998; Barnham et al., 2004).

1.7.2 Site directed nucleosome mapping

Site directed nucleosome mapping is a technique whereby a chemical nuclease is attached to a directed site on the octamer surface. Activation of the nuclease will cleave the adjacent DNA leaving behind separate DNA fragments,

from which the position of the DNA relative to the octamer surface can be mapped. This technique has been successfully used *in vitro* using a thiol-reactive EDTA derivative, which has been tethered to an engineered cysteine on the surface of the octamer (Flaus et al., 1996; Flaus and Richmond, 1999). Using the EDTA derivative as iron chelator, the Fenton reaction is initiated with the addition of ascorbate and hydrogen peroxide, producing hydroxy radical cleavage of the DNA.

The binding position of the linker histone H1 to the core nucleosome was also demonstrated by site-directed mapping. This technique used a similar EDTA derivative tethered to an engineered cysteine within the globular domain of H1 (Dumoulin et al., 1996). Site-directed mapping has also been used from sites within rRNA binding proteins for providing information into the structural organisation of rRNA and positions of their binding proteins (Heilek et al., 1995; Wilson and Noller, 1998). These techniques have also been used with 1,10-phenanthroline as the mapping reagent (Mazumder et al., 1993).

A similar technique has recently been used *in vivo* to develop a genome wide map of nucleosome positions in yeast. This technique used a phenanthroline derivative tethered to an engineered cysteine and produced hydroxyl radical DNA cleavage on the addition of copper, mercaptopropionic acid and hydrogen peroxide. This method produced a genome-wide map of unprecedented consistency and accuracy, and demonstrated stronger nucleosomal dinucleotide signals than that of MNase mapping (Brogaard et al., 2012).

The advantage of using site-directed mapping techniques for mapping nucleosomes and other nucleic acid complexes is that the position of the DNA/RNA relative to the position of the tethered reagent is mapped to base accuracy.

1.8 Current state of research for mapping nucleosome positions

Originally much of the work on nucleosome mapping was done using restriction enzymes. This was based on the principle that non-specific restriction enzymes cleave the free linker DNA more readily than nucleosomal bound DNA, therefore leaving behind DNA fragments that can be observed by electrophoresis.

The most commonly used restriction enzymes for mapping nucleosome position are MNase, DNase I and Exo III, (Flaus, 2011).

Another form of nucleosome mapping uses in solution hydroxyl radicals to cleave the most exposed DNA to produce a DNA footprint of the nucleosome. This is based on the principle that free DNA and DNA within the exposed major groove are more prone to DNA cleavage by hydroxyl radical attack than the inward facing minor grooves, (Hayes et al., 1990).

Later work by Flaus *et al* produced site-specific hydroxyl radical DNA cleavage within the nucleosome by tethering an EDTA derivative onto the thiol of a mutated cysteine residue on the octamer surface. This produced a nucleosome map that could be used to determine the position of a nucleosome to base-pair resolution (Flaus et al., 1996).

Nowadays genome wide nucleosome mapping techniques such as Chip-Seq are popular for determining nucleosome positioning. This technique uses native chromatin digested into mono-nucleosomes by MNase before being chromatin precipitated and sequenced. Recently the site-specific mechanism of nucleosome mapping developed by Flaus *et al* has been adapted to allow for *in vivo* mapping of the yeast genome. The resulting mononucleosome DNA fragments are then sequenced to produce a genome wide map of nucleosome positions at base-pair resolution, (Brogaard et al., 2012).

The key questions that still need to be answered on nucleosome structure and dynamics are: what are the exact positions of DNA relative to the octamer and do they differ between nucleosome species; are in-solution nucleosomes consistent with the crystal structure; and what are the mechanisms of nucleosome sliding.

1.9 Aims of the project

The original site-directed mapping of the nucleosome by Flaus et al., 1996 used SHL 0.5 as the mapping location. Our aim is to develop this technique across all of the seven SHL sites, effectively giving us a complete nucleosome footprint at all histone-DNA contact sites. Using this complete map we can interpret the position

of any nucleosome bound DNA relative to the histones to probe local structural variations in solution.

Using this approach we compare the mapping of popular nucleosome positioning sequences using separate EDTA and phenanthroline based mapping reagents. This allows us to compare the in solution nucleosome with known crystal structures. We also use the complete mapping approach to look for evidence supporting mechanism(s) involved in thermal nucleosome mobilisation. Finally, we compare the mapping of nucleosomes containing different histone species or variant composition.

Chapter 2 Materials and Methods

2.1 Materials

2.1.1 Source of chemicals

Chemicals	Source	Code
1,10 Phenanthroline-5-maleimide	Gift from Prof. Tom Owen-Hughes	-
2-(<i>N</i> -morpholino)ethanesulphonic acid (MES)	Melford	B2002
2-Mercaptoethanol	Sigma-Aldrich	63689
4-(2-Hydroxyethyl)piperazine-1-ethanesulfonic acid (HEPES)	Sigma	H7006
Agar	Sigma	A5306
Agarose	Fisher	10776644
Ammonium ferrous sulphate hexahydrate	Fluka	09719
Ammonium persulphate	Sigma	A3678
Ampicillin sodium salt	Melford	A0104
Ascorbic acid	Sigma	A5960
Benzamidine hydrochloride hydrate	Sigma-Aldrich	B6506
Boric acid	Sigma	B7901
Bromphenol blue	Sigma-Aldrich	B0126
Chelex 100 resin 200-400 mesh, sodium form	BIO-RAD	142-2842
Chloramphenicol	Duchefa Biochemie	C0113
Copper (II) sulphate	BHD	103733C
Dimethyl sulphate	Sigma-Aldrich	D186309
Dimethyl sulphoxide (DMSO)	Sigma	D8418
Dithiothreitol (DTT)	Melford	MB1015
Ethylenediaminetetraacetic acid disodium salt dihydrate	Sigma	E5134
Formamide	Sigma	F9037
Glacial acetic acid	Sigma-Aldrich	338826
Glycerol	Sigma-Aldrich	G6279
Guanidine hydrochloride	Melford	MB2002
Hydrochloric acid fuming 37%	Fluka	84415
Hydrogen peroxide 30%	Fluka	16911
Isopropyl- β -D-Thiogalactopyranoside (IPTG)	Melford	MB1008
LB Broth	Sigma	L3022
N-[S-(2-Pyridylthio)cysteaminy]ethylenediamine-N,N,N',N'-tetraacetic acid (EDTA reagent)	Toronto Research Chemicals Inc.	P996250
N,N,N',N'-Tetramethylethylenediamine (TEMED)	Sigma	T9281
Orange G	Sigma	O3756
Phenol Chloroform Isoamyl alcohol (25:24:1)	Sigma	P2069
Phenylmethanesulphonyl fluoride (PMSF)	Sigma	P7626
Piperidine	Aldrich	411027
Sigmacote	Sigma	SL2
Sodium acetate	Sigma-Aldrich	S8750
Sodium cacodylate hydrate	Fluka	31533
Sodium chloride	Sigma-Aldrich	S3014

Sodium dodecyl sulfate	Sigma	L4390
Sucrose	Sigma	S7903
Triton X-100	Sigma	T8787
Trizma base (2-Amino-2-(hydroxymethyl)-1,3-propanediol)	Sigma	T1503
tRNA, Carrier	Sigma	R4752
Tryptone	Melford	T1332
Tween 20	Sigma	P9416
Urea	Melford	U1363
SequaGel-8	Geneflow	A2-0028
Xylene cyanol FF	Sigma	X4126
Yeast extract	Melford	GY1333

Table 2.1 A list of chemical reagents and their suppliers

2.1.2 Source of enzymes

Enzyme	Source
KOD <i>Taq</i> Polymerase	Novagen
<i>Taq</i> Polymerase	See method 2.3.2
Lysozyme	Sigma

Table 2.2 A list of enzymes and their suppliers

2.2 Equipment

Type	Make	Model
Centrifuge	Hettich	Rotanta 460R
	Beckman Coulter	Avanti J-20 XPI
	Sigma	1-15K
Dialysis		
Micro Dialysis Block	Riteway Engineering Ltd	4X4 dialysis chambers (Flaus and Richmond, 1999)
Electrophoresis and Imaging		
Protein	BIO-RAD	Mini-Protean tetra cell
DNA	Owl	EasyCast Mini Gel

Native	Engineering & Design Plastics Ltd	Custom made for AFL
Gel imaging	Fujifilm	FLA-5100
FPLC and chromatography		
FPLC	GE Healthcare	ÄKTA Purifier
Chromatography columns		
Anion exchange	Pharmacia Biotech	Mono Q
Cation exchange	GE Healthcare	HiTrap SP FF 5ml
Gel Filtration	GE Healthcare	Superdex 200 10/300 GL
Incubator shaker	Labconco	Freezone 2.5
PCR	Eppendorf	Mastercycler epgradient S
Sonication	Branson	Digital Sonifier 250

Table 2.3 Equipment types, makes and models used throughout the project

2.3 DNA methods

2.3.1 PCR mutagenesis

Our method of PCR mutagenesis uses a complementary pair of 39 mer primers that flank each side of the mutated codon by 18 bases. The mutagenic three base codon involves the minimum change to encode the desired amino acid mutation. This can be seen in Figure 2.1 where a single base change in the wildtype coding strand from cytosine to guanine allows for a mutation from serine to cysteine.

Amplification of the mutated plasmid is KOD polymerase driven, requiring additional Mg_2SO_4 with manufacturers standard PCR reactants and a final concentration of 5% DMSO. Reaction conditions and cycle parameters are shown in Tables 2.4 and 2.5.

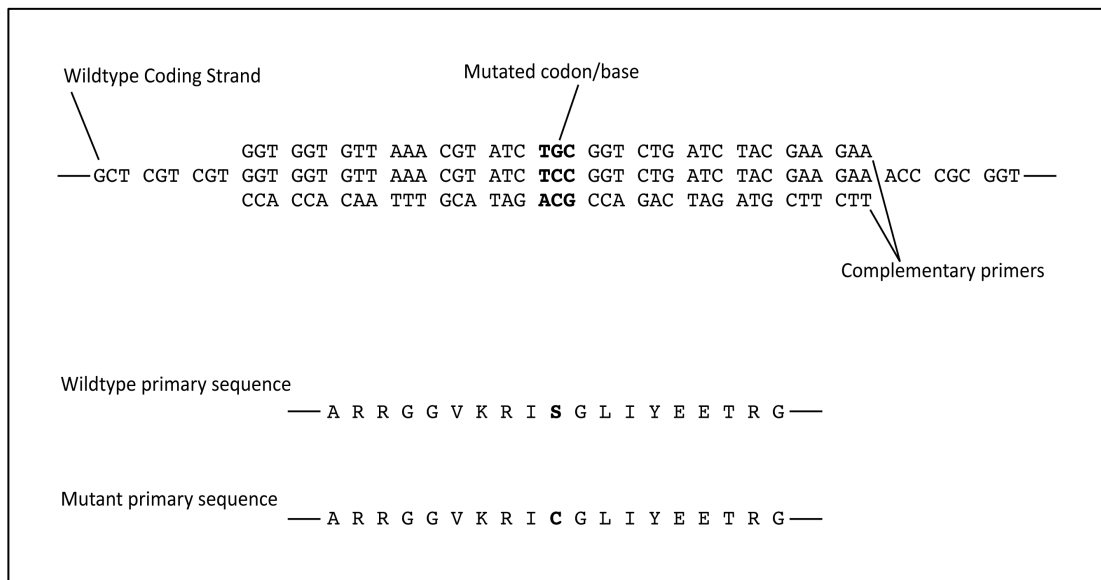


Figure 2.1 Example of primer design for PCR mutagenesis of histone H4 S47C.

	Stock concentration	Reaction concentration	Volume for 50 μ l reaction
Deionised H ₂ O	-	-	24.5 μ l
KOD Buffer	10 X	1 X	5 μ l
Mg ₂ SO ₄	25 mM	1.5 mM	3 μ l
Template	100 ng/ μ l	10 ng/ μ l	5 μ l
dNTPs	2 mM	200 μ M	5 μ l
Primers	10 μ M	400 nM	2+2 μ l
DMSO	100 %	5 %	2.5 μ l
KOD Polymerase	1 U/ μ l	0.02 U/ μ l	1 μ l

Table 2.4 PCR mutagenesis reactants, concentrations and volumes

Stage	Temperature (°C)	Duration (min:sec)	
Initialisation	95	02:00	
Denaturation	95	00:30	x16
Annealing	56	00:20	
Extension	68	00:30 /kb	
Final Extension	72	05:00	
4°C Hold	4	∞	

Table 2.5 PCR mutagenesis cycle

2.3.2 Recombinant *Taq* polymerase preparation

A *Taq* polymerase (*Taq* Pol) expression plasmid (a gift from Prof. Tom Owen-Hughes) was transformed into the Rosetta 2(DE3) pLysS strain of *E.coli* and

plated on Lysogeny Agar (LA) containing dual selection for ampicillin and chloramphenicol at concentrations of 50 µg/ml and 40 µg/ml respectively. From this a 100 ml overnight starter culture of Lysogeny Broth (LB) containing 50 µg/ml ampicillin and 40 µg/ml chloramphenicol antibiotics was inoculated and incubated at 37°C.

The following day 1 liter of LB containing the dual selection antibiotics was inoculated with 50 ml of the overnight starter culture and incubated at 37°C until an OD₆₀₀ of 0.3-0.4 was reached. Isopropyl-β-D-thiogalactopyranoside (IPTG) was then added to a final concentration of 0.5 mM and incubated for 16 hours at 37°C. The culture was harvested with a 15 minute centrifugation at 5,000 g. The pellet was resuspended in 100 ml of *Taq* wash buffer, then spun down and resuspended in 50 ml of pre-lysis buffer and incubated at room temperature for 15 minutes. Then 50 ml of lysis buffer was added prior to a 60 minute incubation at 80°C. The resulting lysate suspension was then centrifuged at 12,000 g for 10 minutes at 4°C. The supernatant which contains the *Taq* Pol was saved and added to an equal volume of *Taq* storage buffer and stored at -20°C for short term storage and at -80°C for long term storage. The *Taq* Pol purification buffers and their constituents are shown in Table 2.6.

***Taq* Pol purification buffers**

<i>Taq</i> wash buffer	<i>Taq</i> pre-lysis buffer
50 mM Tris-HCL pH 7.9	50 mM Tris-HCL pH 7.9
50 mM Glucose	50 mM Glucose
1 mM EDTA	1 mM EDTA
	Lysozyme (4 mg/ml)
<i>Taq</i> lysis buffer	<i>Taq</i> storage buffer
10 mM Tris-HCl pH 7.9	20 mM HEPES pH 7.9
50 mM KCl	100 mM KCl
1 mM EDTA	100 µM EDTA
1 mM PMSF	500 µM PMSF
0.5% Tween 20	1 mM DTT
0.5% Triton X100	75% Glycerol

Table 2.6 *Taq* Pol purification buffers

2.3.3 Nucleosomal DNA amplification

Nucleosomal DNA was PCR amplified in 50 µl reaction volumes in 96-well plates yielding ~5 µl of PCR product per run, all catalyzed by in-house purified *Taq* Pol. All DNA fragments were amplified using the same reaction conditions with only minor differences between yields. The PCR product from multiple reactions were pooled and stored at -20°C until purification. After purification typical yields from 5 µl of PCR product were approximately 300 pmols. Reaction conditions and PCR parameter are shown in Table 2.7.

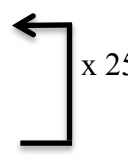
Nucleosomal DNA PCR amplification			
10 X Taq buffer			
100 mM Tris-HCl pH 9.0			
500 mM KCl			
15 mM MgCl ₂			
1% Triton X-100			
PCR reactants			
	Stock concentrations	Reaction concentration	Volume for 5 ml reaction
Deionised H₂O	-	-	4278 µl
10X <i>Taq</i> buffer	10X	1X	500 µl
Template	1 µg/ µl	400 pg/ µl	2 µl
dNTPs	25 mM	250 µM	10 µl
Primers	100 µM	200 nM	10 µl
<i>Taq</i> Pol	-	40 µl/ml	200 µl
PCR Cycle			
Stage	Temperature (°C)	Duration (min:sec)	
Initialisation	95	02:00	
Denaturation	95	00:30	
Annealing	48	00:35	
Extension	72	00:35	
Final extension	72	05:00	
4°C hold	4	∞	

Table 2.7 PCR amplification of nucleosomal DNA

2.3.4 Amplified nucleosomal DNA purification

The pooled PCR product was thawed, ethanol precipitated and the DNA pellet was dissolved in 10 ml of Tris-buffered saline (TBS). This DNA solution was then loaded onto a MonoQ column for purification using a NaCl gradient. Purification buffers and FPLC program breakpoints are shown in Tables 2.8 and 2.9 respectively.

A typical chromatogram trace from DNA purification is shown in Figure 2.2. Peak fractions were run on a 1% agarose gel to identify the pure fractions, which were pooled, ethanol precipitated, air dried and stored at -20°C until nucleosome formation. Figure 2.3 shows successive peak fractions from a typical DNA purification run on a 1% agarose gel.

Amplified nucleosomal DNA purification buffers

Tris-Buffered Saline (TBS)	Purification buffer A	Purification buffer B
50 mM Tris-HCl pH 7.5	50 mM Tris-HCl pH 7.5	50 mM Tris-HCl pH 7.5
100 mM NaCl	1 mM EDTA	1 mM EDTA
		2 M NaCl

Table 2.8 Purification buffers for amplified nucleosomal DNA

Breakpoint	Instructions
0.00	Base Volume
0.00	Alarm Pressure Enabled, 2.2 {MPa}, 0.00 {MPa}
0.00	Flow 0.75 {ml/min}
0.00	AutoZeroUV
2.00	Gradient 10 {%B}, 0.00 {base}
7.00	Gradient 45 {%B}, 75 {base}
28.43	Fractionation 96WellPlate, 0.500 {ml}, NextLine, Volume
71.20	FractionationStop
83.70	Gradient 100 {%B}, 0.00 {base}
88.70	Gradient 0 {%B}, 0.00 {base}
93.70	Flow 1.00 {ml/min}

Table 2.9 FPLC program for nucleosomal DNA purification

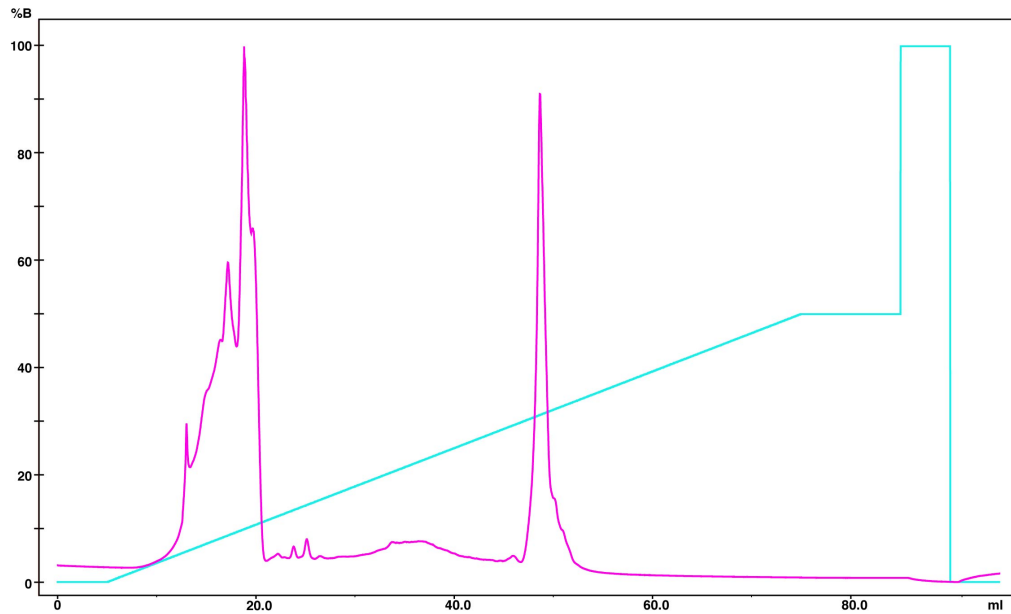


Figure 2.2 Nucleosomal DNA purification chromatogram trace. The magenta line represents the UV absorbance at 260 nm and the cyan line represents the percentage of purification buffer B. The large series of peaks to the left represent dNTPs, while the large central peak represents 147 bp nucleosomal DNA. A small broad peak between the large peaks represents primers.

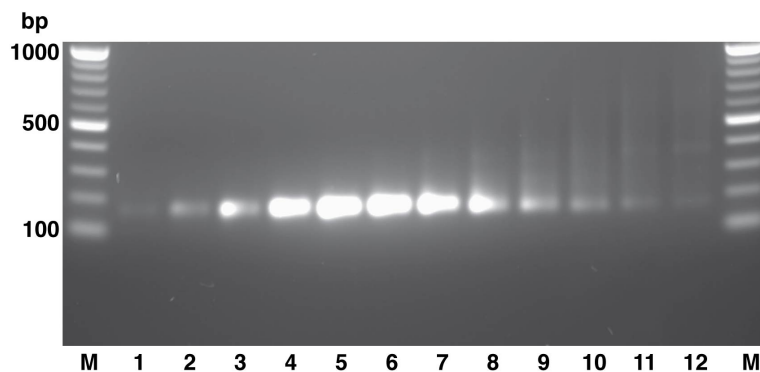


Figure 2.3 Nucleosomal DNA purification. Successive peak fractions were run on a 1% agarose gel to determine fraction purity. The purest fractions were lanes 1-7 with lanes 8-12 containing some degree of contamination.

2.3.5 G-Track preparation

G-Tracks are known DNA sequences that are chemically cleaved at guanine nucleotides. They can be used as a DNA ladder in denaturing gel electrophoresis to determine unknown DNA fragment size.

250 pmol of dried cyanine labeled DNA in a screw cap tube was resuspended in 200 µl of methylation buffer. 1 µl of dimethyl sulphate was then added and the reaction incubated at 25°C for 4 minutes.

The reaction was stopped with the addition of 50 µl of Stop buffer and 750 µl of 100% ethanol. This was then centrifuged at 18,000 g for 10 minutes to precipitate the DNA. The pellet was resuspended in 250 µl of 300 mM sodium acetate pH 5.5 and 750 µl of 100% ethanol then re-precipitated and air-dried.

The pellet was then resuspended in 100 µl of 10% piperidine and heated to 90°C for 30 minutes. Sodium acetate pH 5.5 and MgCl₂ were then added at a concentration of 300 mM and 10 mM respectively. 600 µl of ethanol was then added and incubated at -20°C for 15 minutes before a 15 minute centrifugation at 18,000 g. The supernatant was decanted, the pellet air-dried and resuspended in 100 µl of formamide loading buffer then stored at -20°C. G-Track buffers and their properties are shown in Table 2.10.

G-Track preparation buffers

Methylation buffer	Stop buffer	Formamide loading buffer
50 mM sodium cacodylate	1.5 M sodium acetate pH 5.5	Formamide
1 mM EDTA	10 % 2-mercaptoethanol	20 mM EDTA
	tRNA (100 µg / ml)	

Table 2.10 G-Track preparation buffers

2.4 Protein methods

2.4.1 Recombinant histone expression

The gene containing pET 3a vector was transformed into the Rosetta 2(DE3) pLysS strain of *E.coli* and spread plated onto LB agar containing 50 µg/ml ampicillin and 40 µg/ml chloramphenicol. A fresh colony was inoculated into a 200 ml starter culture of 2YT medium containing 50 µg/ml ampicillin and 40 µg/ml chloramphenicol and grown overnight at 37°C with 80 rpm for aeration.

The following morning 50 ml of starter culture was inoculated into 1 liter of 2YT media containing 50 µg/ml ampicillin and 40 µg/ml chloramphenicol and grown for 3-4 hours at 37°C with 180 rpm for aeration. Then the culture was induced with the addition of 0.5 mM IPTG and grown for another 4-6 hours before harvesting at 5,000 g for 15 minutes. The cell pellet was washed in 20-30 ml of TBS, further spun down, decanted and stored at -20°C awaiting further processing. The constituents of 2YT media are shown in Table 2.11.

2YT medium (1L)
16g Tryptone
10g Yeast Extract
5g NaCl

Table 2.11 2YT medium

2.4.2 Recombinant histone purification

The *E.coli* cell pellet containing the expressed protein in inclusion body form was allowed to thaw at room temperature for 1 hour to lyse before 20 ml of Wash buffer I was added. This was vortexed to homogeneity and sonicated for 1 minute using 20 second pulses with 10 second rest periods between pulses at 20% amplitude using a Branson sonifier. This suspension was then centrifuged at 30,000 g for 15 minutes and decanted. These steps were repeated once.

Then 20 ml of Wash buffer II was added, resuspended using a combination of vortexing and pipetting, centrifuged for 15 minutes at 30,000 g and decanted. This was repeated once.

Then 20 ml of Wash buffer I was added to the pellet, resuspended using a combination of vortexing and pipetting, centrifuged at 30,000 g for 15 minutes and decanted. This was repeated once.

This pellet contains the histone as an inclusion body and can be stored at -20 °C until further processing. Buffers used in the processing of histone inclusion bodies are shown in Table 2.12.

Inclusion body preparation buffers		
Wash buffer I	Wash buffer II	Unfolding buffer
50 mM Tris-HCl pH 7.5	50 mM Tris-HCl pH 7.5	7 M Guanidine HCl
100 mM NaCl	100 mM NaCl	20 mM Tris-HCl pH 7.5
5 mM 2-mercaptoethanol	5 mM 2-mercaptoethanol	10 mM DTT
1 mM benzamidine hydrochloride	1 mM benzamidine hydrochloride	
	1 % Triton X-100	

Table 2.12 Inclusion body preparation buffers

The inclusion body pellets are unfolded by the addition of 5 ml of a buffered 7M guanidine hydrochloride solution. This Unfolding buffer will dissolve most of the pellet when left to rotate at room temperature for 1-2 hours although occasional agitation with a transfer pipette may also be necessary.

After the pellet dissolved, Histone purification buffer A was added to bring the volume up to 20 ml. This suspension was then centrifuged at 35,000 g for 20 minutes to pellet any debris. The resulting supernatant was decanted into a clean centrifuge tube and re-centrifuged 2 more times under the same conditions. The 20 ml resulting supernatant was added to 55 ml of Histone purification buffer A to give a total 1:15 dilution of the guanidine hydrochloride. This 75 ml solution of buffered urea and unpurified histone was then filtered before loading onto a cation exchange column at 2.5 ml/min.

After the 75 ml had loaded onto the column the Histone purification program was started which elutes the purified histone by a gradient into Histone purification buffer B. Histone purification buffers are shown in Table 2.13 and the FPLC histone purification program is shown in Table 2.14. A typical example of a FPLC histone purification chromatogram trace is shown in Figure 2.4.

The purification was monitored by running on a 15% SDS-PAGE. Peak fractions were identified, pooled and dialysed in 5 litres of 3 mM 2-mercaptoethanol 3 times for at least 3 hours each at 4°C, usually the third time overnight. The dialysed histone was then aliquoted into 10 ml aliquots, frozen down at -80 °C and lyophilised for 24-48 hours at -50°C and 0.04 mBar for long-term storage. A typical example of histone purity is demonstrated in Figure 2.5.

Histone purification buffers

Histone purification buffer A	Histone purification buffer B
7M Urea	7M Urea
50mM Tris-HCl pH 7.5	50mM Tris-HCl pH 7.5
1mM EDTA	1mM EDTA
	2M NaCl

Table 2.13 Histone purification buffers

Breakpoint	Instructions
0.00	Base Volume
0.00	Alarm_Pressure Enabled, 0.3 {MPa}, 0.00 {MPa}
0.00	InjectionValve Load
0.00	Flow 2.5 {ml/min}
5.00	Gradient 15 {%B}, 0 {base}
5.00	Fractionation 96WellPlate, 2.000 {ml}, NextLine, Volume
15.00	Gradient 50 {%B}, 35 {base}
55.00	Gradient 100 {%B}, 0 {base}
65.00	Gradient 0 {%B}, 0.00 {base}
70.00	Flow 1.00 {ml/min}

Table 2.14 FPLC histone purification program

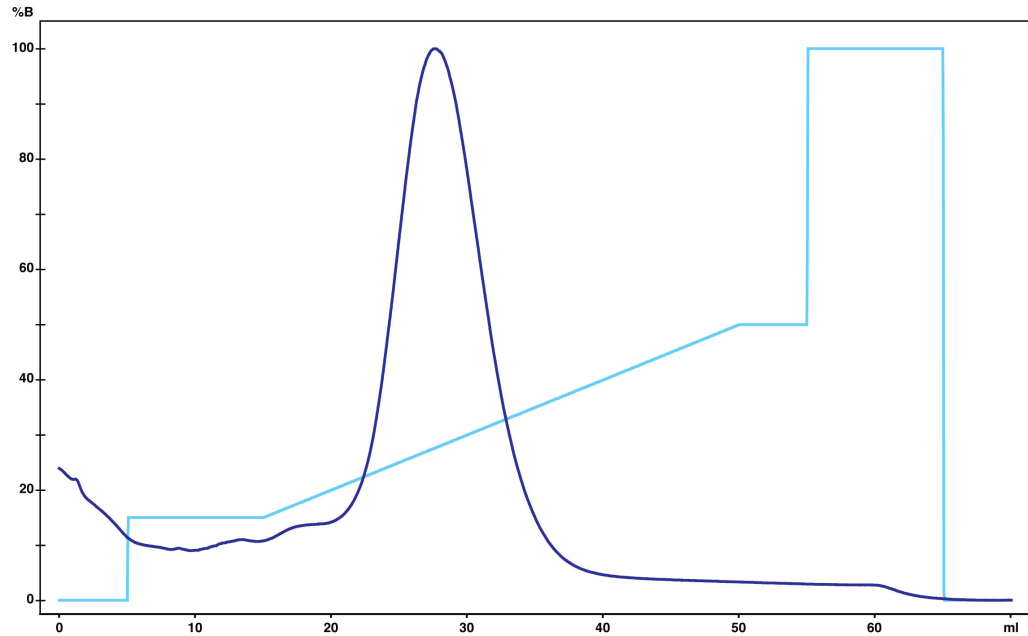


Figure 2.4 Histone purification chromatogram trace. A typical example of histone purification by cation exchange. The blue line represents the UV absorbance at 280 nm and the cyan line represents the percentage of Histone purification buffer B.

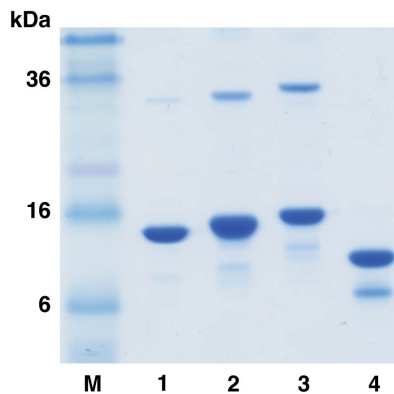


Figure 2.5 SDS-PAGE of histone purification. Lanes 1-4 are typical purifications of human histones H2A, H2B, H3 and H4 respectively.

2.4.3 Histone octamer refolding

Equal quantities (3-6 mg) of lyophilised histones H2A, H2B, H3 and H4 were placed in separate 1.5 ml tubes. Then 1-1.5 ml of Unfolding buffer was added to each tube and left to incubate at room temperature for 0.5-2 hours with occasional inversion. The unfolded histones were then centrifuged at 18,000 g for 10 minutes, the histone containing supernatant placed into new tubes and the UV absorbance was read at 276 nm. Histone Buffers are shown in Table 2.15.

The histone concentration was then calculated using the Beer-Lambert law from the known histone extinction coefficients and the UV absorbance at 276 nm. The 4 histones were then pooled together in an equimolar ratio and adjusted to a concentration of 1 mg/ml. This suspension was dialysed into 660 ml of Refolding buffer twice for 3 hours each and a third time overnight. Table 2.16 shows a typical calculation of refolding an octamer that gives a total volume of 20.83 ml made up of 386 nmol of each protein brought to a concentration 1 mg/ml.

Histone octamer refolding buffers

Histone unfolding buffer	Refolding buffer
7M Guanidine HCl	10mM Tris-HCl pH 7.5
20mM Tris-HCl pH 7.5	2M NaCl
10mM DTT	1mM EDTA
	5mM 2-mercaptoethanol

Table 2.15 Histone octamer refolding buffers

Beer-Lambert law $A = \epsilon cl$ or $c = A/\epsilon l$

A = Absorbance (276 nm) ϵ = Extinction coefficient (L/M/cm)

c = Concentration (mol/l) l = Path length (1 cm)

Histone	A_{276}	ϵ	μM	Molar Ratio	Ratio x 1.4	mg /ml	mg/ 1.4 ml
xH2A	1.3	4350	298.8	0.923	1.292	4.17	5.39
xH2B	2.0	7250	275.8	1.000	1.400	3.72	5.21
xH3	1.5	4640	323.3	0.853	1.194	4.94	5.90
xH4	1.7	5800	293.1	0.941	1.317	3.29	4.33
Total Protein					5.203ml		20.83mg

Table 2.16 Typical concentrations and volumes observed in octamer refolding

2.4.4 Histone octamer gel filtration

After the overnight dialysis the refolded octamer was concentrated to a volume of 500 μ l in 10k MWCO centrifugal filter tubes before being centrifuged at 18,000 g for 10 minutes to pellet any aggregate. The 500 μ l of supernatant was then loaded onto a Superdex 200 gel filtration column at a rate of 0.5 ml/min for octamer purification. Peak filtrates were then run on 15% SDS-PAGE to identify pure octamer fractions before being pooled and concentrated to 1 ml of 20-30 μ M in centrifugal filters. The concentrated octamer was then stored on ice until further processing. Tables 2.17 and 2.18 show the Octamer gel filtration buffer and the FPLC octamer gel filtration program respectively. Figures 2.6 and 2.7 show the FPLC octamer gel filtration chromatogram trace and the purified octamer on SDS-PAGE respectively.

Octamer gel filtration buffer
10 mM Tris-HCl pH 7.5
2M NaCl
1mM EDTA

Table 2.17 Octamer gel filtration buffer

Breakpoint	Instructions
0.00	Base Volume, {23.56 ml}, Superdex_200_HR_10/300
0.00	Alarm_Pressure Enabled, 1.0 {MPa}, 0.00 {MPa}
0.00	Flow 0.5 {ml/min}
0.00	AutoZeroUV
1.00	InjectionValve Inject
4.00	InjectionValve Load
7.00	Fractionation 96WellPlate, 1.000 {ml}, NextLine, Volume
10.00	Fractionation 96WellPlate, 0.5 {ml}, NextTube, Volume
21.00	Fractionation 96WellPlate, 1.000 {ml}, NextTube, Volume
38.00	FractionationStop
38.00	Flow 0.00 {ml/min}

Table 2.18 FPLC octamer gel filtration program

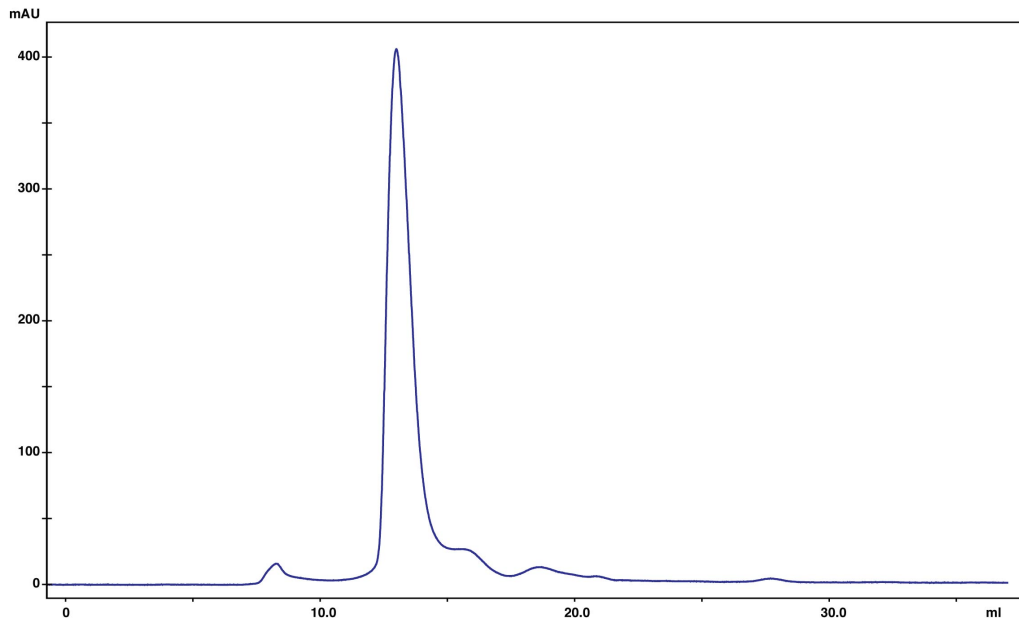


Figure 2.6 Histone octamer gel filtration chromatogram trace. The purple line represents the UV absorbance at 280 nm of the flow through from a Superdex 200 column of refolded histones. The large peak represents histone octamer with small peaks from left to right representing histone aggregates, histone dimers and monomeric histones.

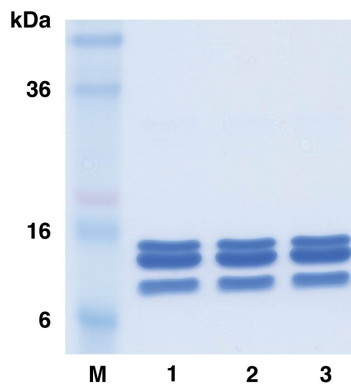


Figure 2.7 Histone octamer on SDS PAGE. SDS PAGE showing constituents of gel filtered histone octamer, lanes 1-3 are identical. From top to bottom the bands represent *Xenopus* histones H3, H2A+H2B and H4 respectively.

2.4.5 Mapping reagent attachment

Reagent attachment is via the sulphur of a site specific engineered cysteine placed near the interface between DNA and histone. To map at Super Helical Location (SHL) 0.5 an octamer of histones H2A, H2B, H3 C110A and H4 S47C was prepared to enable attachment on H4. Either an EDTA derivative N-[S-(2-Pyridylthio) cysteaminy]ethylenediamine-N,N,N',N'- tetraacetic acid or a phenanthroline derivative 1,10 Phenanthroline-5-maleimide can be used for site

directed nucleosome mapping via the production of hydroxyl radicals. The mapping locations and corresponding cysteine mutants are shown in Table 2.19.

Super Helical Location (SHL)	Cysteine point mutation
0.5	H4 S47C
1.5	H4 T30C
2.5	H3 D81C
3.5	H2B T85C
4.5	H2A T16C
5.5	H2B G50C
6.5	H3 T45C

Table 2.19 Mapping locations and the corresponding cysteine mutant

Attachment of N-[S-(2-Pyridylthio)cysteaminyl]ethylene- diamine - N,N,N',N'-tetraacetic acid (EDTA reagent)

500 µl of ~25 µM octamer was reduced using 10 mM DTT for 30 minutes on ice prior to four two-hour steps of dialysis in 500 ml of 5 mM MES pH 6.0, 2 M NaCl. After which the octamer concentration was recalculated. The EDTA reagent can now be attached to the free thiol of the cysteine via disulfide bond.

0.5 mg of EDTA reagent was added to 108 µl of 100 mM Tris pH 7.5 to give a ~10 mM EDTA solution. 400 µl of octamer was added to a new 1.5 ml tube, 20 µl of 1 M Tris pH 7.5 was then added before adding the molar excess volume of 100 µl of 10 mM EDTA solution. The reaction was allowed to progress overnight at room temperature after which the new octamer concentration was calculated allowing for the addition of the reagent and Tris buffer (~19.23 µM).

Finally, the unattached EDTA was dialysed out of solution through four steps of 500 ml of 20 mM Tris-Cl pH 7.5, 2 M NaCl for 3 hours with the fourth time overnight. The EDTA-attached octamer was then stored on ice for up to three weeks. Table 2.20 briefly summarises the steps involved for attachment of EDTA to histone octamer.

Step	Description	Temp (°C)	Duration (hh:mm)
1	400 µl of 25 µM Octamer reduced in 10mM	0	00:30
2	Octamer dialysis in 5mM MES pH 6.0, 2M NaCl	4	4 x 02:00
3	Calculate octamer concentration	-	-
4	100 µl of 10mM EDTA reagent added to 420 µl	20	12:00
5	Recalculate octamer concentration	-	-
6	Dialyse octamer into 500 ml of 20 mM Tris pH	4	3 x 03:00
7	Storage for <i>in-vitro</i> assays	0	< 500:00

Table 2.20 Steps and duration for EDTA reagent attachment to octamer

Attachment of 1,10 Phenanthroline-5-maleimide

After octamer gel filtration the purified octamer was concentrated to ~25 µM. Then 0.5 mg of 1,10 Phenanthroline-5-maleimide was dissolved in 40 µl of DMSO before the addition of 40 µl of 50 mM HEPES pH 7.0 in 10 µl increments forming a 20 mM 1,10 Phenanthroline-5-maleimide solution. Then 12.5 µl of the 20 mM phenanthroline solution was added to 400 µl of the ~25 µM octamer giving a 25 times molar excess of reagent to octamer in 412.5 µl. 0.05 times this volume of 1M HEPES pH 7.0 was then added giving a total reaction volume of ~433 µl. This was allowed to react at room temperature with occasional inversion. After 25 minutes the reaction was stopped by adding 1 M DTT to a final concentration 25 mM DTT which produced a final octamer volume of ~444 µl. The new octamer concentration was then ~22.52 µM. Finally, the unattached reagent was dialysed away with 4 changes of 500 ml 20 mM Tris-Cl pH 7.5, 2 M NaCl for 3 hours with the final step being overnight. The reagent-attached octamer was then stored on ice for up to 3 weeks. Table 2.21 briefly summarises the steps involved in attaching 1,10 phenanthroline-5-maleimide to a histone octamer.

Step	Description	Temp (°C)	Duration (hh:mm)
1	0.5 mg reagent is dissolved in 40 µl DMSO. 4 x 10 µl of 50 mM HEPES pH 7.0 is added to form 80 µl of a 20 mM solution of phenanthroline.	20	-
2	12.5 µl of reagent is added to 400 µl of ~25 µM octamer. Then add 0.05 volumes of 1M HEPES pH 7.0. Incubate with occasional inversion.	20	00:25
3	Stop reaction with 25 mM DTT	20	5
4	Calculate new octamer concentration	-	-
5	Dialyse octamer into 500 ml of 20 mM Tris pH 7.5, 2 M NaCl	4	3 x 03:00 1 x 12:00
7	Storage for <i>in-vitro</i> assays	0	< 500:00

Table 2.21 Steps and durations for phenanthroline reagent attachment to octamer

2.5 Nucleosome methods

2.5.1 Nucleosome formation

Octamer and DNA are added together in an equimolar ratio in a solution of 20 mM Tris pH 7.5, 2 M NaCl. The NaCl was dialysed away in 4 steps using buffers with 20 mM Tris pH 7.5 and successively 0.85 M, 0.65 M, 0.5 M and 0 M NaCl to reduce the ionic strength therefore increasing the affinity of DNA for octamer producing a nucleosome.

For the production of 250 pmol of nucleosome from ~20 µM octamer and ~10 µM DNA, the octamer was spun down at 10,000 g for 10 min at 4°C and the supernatant placed in a new tube. Deionized H₂O was then added to the purified DNA fragment to bring it to a concentration of ~10 µM. 9.25 µl of deionized H₂O was then added to a new 1.5 ml tube and 25 µl of DNA, 34.25 µl of 40 mM Tris pH 7.5 and 12.5 µl of octamer were subsequently added. This solution was incubated on ice for 30 minutes before being added to the micro dialysis units in 40 µl samples. The sample was dialysed for two hours each in 9 ml of Buffers A-D with an additional step in fresh Buffer D plus Chelex 100 resin for between 2-12 hours. The nucleosomes were then ready for *in vitro* assays. Tables 2.22 and 2.23 show a summary of the nucleosome formation procedure and the buffers used in stepwise dialysis of nucleosome formation respectively.

Nucleosome formation (250 pmol)			
Step	Description	Temp (°C)	Duration (hh:mm)
1	Add dH ₂ O to DNA for a concentration of ~ 10 µM. Calculate required volume for 250 pmol of DNA, e.g. 250 pmol / 10 µM = 25 µl.	0	-
2	Calculate volume of 20 µM octamer for required 250 pmol, e.g. 250 pmol / 20 µM = 12.5 µl.	0	-
3	For 250 pmol of nucleosome in 80 µl. First make 67.5 µl (80-12.5) of 250 pmol DNA in 2 M NaCl by adding 25 µl DNA, 8.75 µl of dH ₂ O and 33.75 µl of 40 mM Tris pH 7.5, 4 M NaCl.	0	-
4	Add 12.5 µl of octamer to the 67.5 µl of 250 pmol DNA in 20 mM Tris pH 7.5, 2 M NaCl	0	-
5	Incubate on ice for 30 minutes.	0	00:30
7	Add to micro dialysis chambers in 40 µl volumes for stepwise reduction of ionic strength.	4	10:00 to 20:00

Table 2.22 Typical volumes and concentrations for nucleosome formation

Nucleosome Stepwise dialysis			
Step	Buffer	Properties	Duration (Hours)
1	A	20mM Tris pH7.5 0.85 M NaCl	2
2	B	20mM Tris pH7.5 0.65 M NaCl	2
3	C	20mM Tris pH7.5 0.5 M NaCl	2
4	D	20mM Tris pH7.5	2
5	D + Chelex 100	20mM Tris pH7.5	2-12

Table 2.23 Nucleosome stepwise dialysis buffers and durations

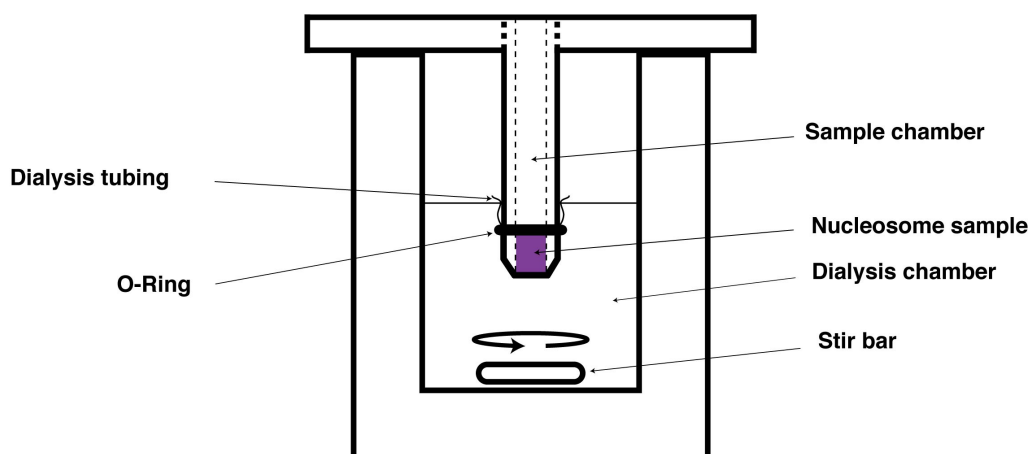


Figure 2.8 Schematic representation of stepwise micro dialysis nucleosome formation. This illustrates the stepwise micro dialysis nucleosome formation procedure. The unassembled nucleosome constituents are placed into the sample chamber in 40 μ l volumes. The sample chamber is then placed into the pre-chilled dialysis chamber which contains 9 ml of 4°C dialysis buffer. The assembled unit is then placed on a magnetic stirrer and left to dialyse in a 4°C cold room. Every two hours the dialysis buffer is changed with the final dialysis step usually overnight.

2.5.2 Native gel electrophoresis

A 5% native gel was cast and pre-run at 300 V for 180 minutes at 4°C in a custom made gel rig designed with pumped buffer recirculation and fan for increased heat dissipation. These innovations allowed for a low ionic strength running buffer and constant running temperatures, which collectively helped keep the nucleosomes stable during electrophoresis.

10-20 pmol of nucleosome in 10% sucrose was then loaded and the gel was run for 150-180 minutes at 300 V and 4°C. The gel was then scanned using the Fuji phosphor-imager at 400 V using the appropriate wavelength and filter, see Table 2.27. Table 2.24 shows the buffers and native gel constituents used in the native PAGE visualisation of nucleosomes.

Native PAGE preparation

10X TBE (1L)		5% Native gel (50 ml)		Native Running Buffer
Tris base	107.8 g	dH ₂ O	40.3 ml	0.2X TBE
Boric acid	55.03 g	10X TBE	1.0 ml	
Na ₂ -EDTA	7.446 g	30% Bis-Acrylamide	8.33 ml	
		10% APS	350 μ l	
		TEMED	20 μ l	

Table 2.24 Native PAGE buffers and gel constituents

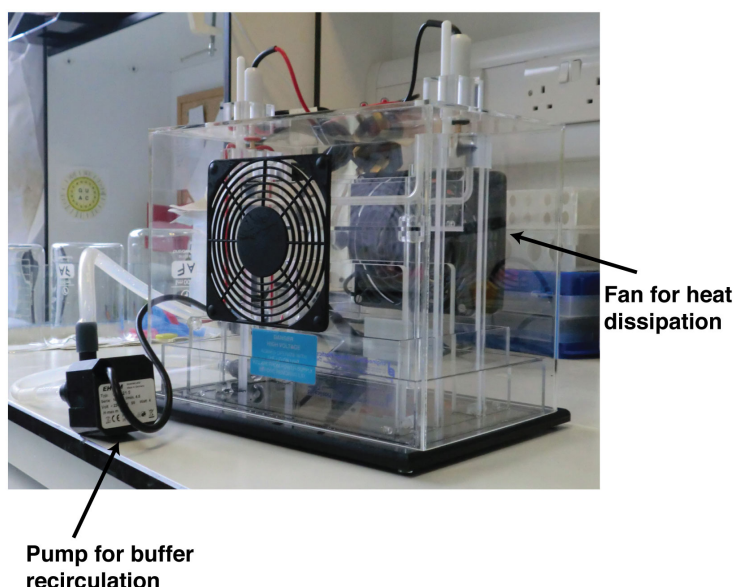


Figure 2.9 Native PAGE cell apparatus. Picture of the custom designed native PAGE cell apparatus. The pump allows use of a low ionic strength running buffer while the fan aids heat dissipation from system during electrophoresis.

2.5.3 Nucleosome mapping

A 2 mM solution of ammonium ferrous sulfate was prepared by adding 39 mg of NH_4FeSO_4 to 50 ml of degassed Milli Q H_2O . 20 μl of this solution was then added to 980 μl of Milli Q H_2O to make a 40 μM solution of NH_4FeSO_4 . Similarly, a 2 mM solution of copper (II) sulphate solution was prepared by adding 16 mg of CuSO_4 to 50 ml of degassed Milli Q H_2O . 20 μl of this solution was then added to 980 μl of Milli Q H_2O to produce a 40 μM solution of CuSO_4 . A 22.7 mM solution of ascorbic acid ($\text{C}_6\text{H}_8\text{O}_6$) was made by adding 200 mg of $\text{C}_6\text{H}_8\text{O}_6$ to 50 ml of degassed Milli Q H_2O . 400 μl of this solution was then added to 100 μl of 1M Tris pH 7.5 to make 18 mM solution of $\text{C}_6\text{H}_8\text{O}_6$. 330 μl of 30% hydrogen peroxide was then added to 50 ml of degassed Milli Q H_2O to produce a 0.2% solution H_2O_2 .

Traditionally Fe^{2+} was used in conjunction with EDTA and Cu^{2+} was used in conjunction with phenanthroline for the production of hydroxyl radicals used in footprinting.

For mapping, 20-30 pmol of fresh nucleosome was required per reaction in a volume of 10 μl . 1 μl of the 40 μM NH_4FeSO_4 solution or 1 μl of the 40 μM CuSO_4 solution was added to the fresh nucleosome and incubated on ice for 15 minutes. Then 5 μl of the 18 mM $\text{C}_6\text{H}_8\text{O}_6$ solution was added before adding 5 μl of the 0.2%

H₂O₂ solution, this was then left to incubate on ice for 60 minutes. For a negative control the metal solution and the hydrogen peroxide were replaced with Milli Q H₂O.

After the elapsed incubation, protein and DNA were separated by adding 20 µl of phenol chloroform isoamyl alcohol. The upper ~20 µl aqueous phase was carefully taken off and added to a new 0.5 ml centrifuge tube. 10 µg of a 2.5 µg/µl solution of carrier tRNA was added before 2 µl of 3 M sodium acetate pH 5.4 and 75 µl of -20°C absolute ethanol was added. This was then incubated at -20°C for 15-30 minutes and then spun down at 18,000 g, at 0°C for 15 minutes. The supernatant was removed and 100 µl of -20°C 70 % ethanol was added. This was then spun down for 10 min at 18,000 g, at 0°C and decanted and air dried before being stored at -20°C. A summary of the mapping procedure is shown in Table 2.25.

Nucleosome mapping

Step	Description	Temp (°C)	Duration (hh:mm)
1	1 µl of 40 µM NH ₄ FeSO ₄ or 1 µl of the 40 µM CuSO ₄ is added to 20-30 pmol of fresh nucleosome and incubated on ice for 15 minutes.	0	00:15
2	5 µl of the 18 mM C ₆ H ₈ O ₆ is then added immediately before 5 µl of the 0.2 % H ₂ O ₂ is added. This was left to incubate on ice for 60 minutes	0	01:00
3	DNA is then phenol/chloroform extracted and ethanol precipitated	0	00:45
4	DNA pellet is washed in 70% ethanol and re-centrifuged, decanted and air dried, before being stored at -20°C	0	00:30

Table 2.25 Summary of nucleosome mapping procedure

2.5.4 Nucleosome thermal sliding

Thermal nucleosome sliding was achieved by incubating 15 µl of 3 µM (45 pmol) freshly assembled nucleosome per reaction at the required temperature in a PCR-cycler heating block. Using the PCR cycler gives more accuracy over a standard heating block while also allowing a temperature gradient to be used. For nucleosome sliding we used a temperature gradient from 25-60°C for 60 minutes prior to mapping to screen for the energy required to slide various nucleosomes. For

a more detailed investigation of sliding on weak positioning sequences we kept the temperature constant (37°C or 45°C) while incubating over a time course from 1-128 minutes. After incubation ~15 pmol of each reaction was loaded in a final concentration of 10% sucrose onto a 5% native gel while the remaining ~30 pmol was used for nucleosome mapping.

2.5.5 Denaturing gel electrophoresis

An 8% denaturing gel was cast using commercially available ready made solution and pre-run in 1X TBE at 60 W using a temperature controlled powerpac until it reached 55°C. The samples were resuspended in 12 µl of Formamide sample buffer before being heated at 95°C for 5 minutes. 6 µl was then loaded onto the hot pre-run equilibrated gel (50-55°C) and the gel was run for the appropriate length of time at 60 W and 55°C constant. After the denaturing gel had run the appropriate length it was let cool to room temperature before disassembling the glass plates. Then the gel is scanned using a Fuji phosphor-imager at 750 V using the appropriate wavelength and filter, see Table 2.27. Table 2.26 shows the Formamide sample buffer constituents.

Formamide sample buffer (500 µl)
480 µl Formamide
20 µl 500 mM EDTA
Orange G / Bromphenol blue / Xylene cyanol as appropriate

Table 2.26 Formamide sample buffer

Fuji phosphor-imager settings				
	Fluorophore	Laser (nm)	Filter	Voltage (V)
Native PAGE	Cy3	532	LPG	400
	Cy5	635	LPR	400
Denaturing gel	Cy3	532	LPG	750
	Cy5	635	LPR	750

Table 2.27 Fuji phosphor-imager setting. A list of the Fuji phosphor-imager setting for the various gels and fluorophores used throughout the project.

2.5.6 Image analysis using AIDA

Denaturing gels were analysed using Advanced Image Data Analyzer (AIDA) software. Peak profiles were determined by running signal quantification down individual lanes using the lane determination settings under 1D Evaluation in AIDA. Signal profiles were then exported as a PICT image and assembled into figures using Adobe illustrator CS4.

2.6 Materials and methods workflow

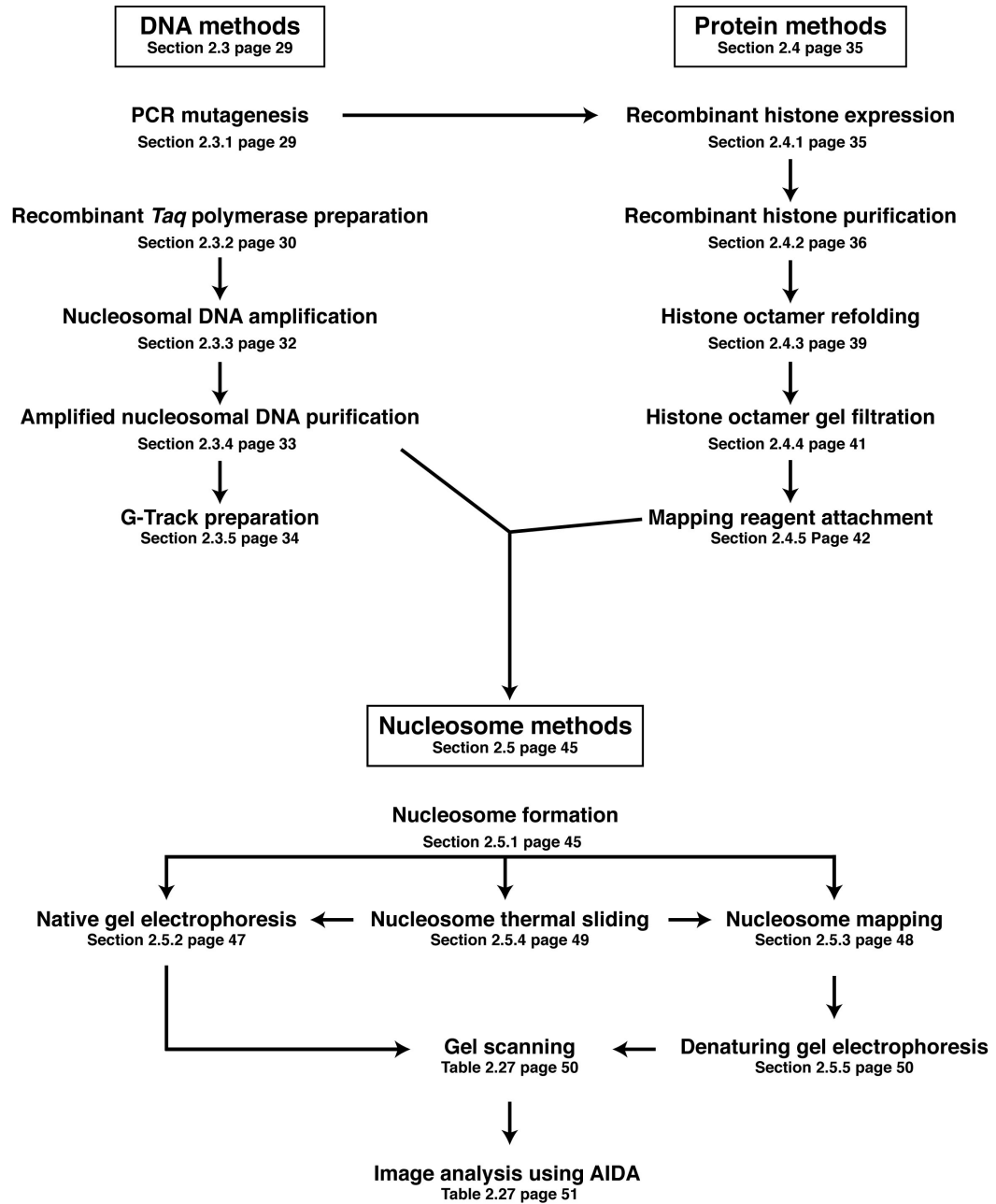


Figure 2.10 Materials and methods workflow. The workflow shows the steps through DNA, protein and nucleosome methods and how these methods are linked form the production of nucleosomal DNA and reagent attachment to nucleosome mapping and image analysis.

Chapter 3 Site-directed nucleosome mapping

3.1 Introduction

Site-directed nucleosome mapping is a technique whereby a chemical nuclease is tethered to a strategically chosen cysteine on the octamer surface of the nucleosome. In the case of reactions in this work the site-specific nuclease is a metal chelator tethered to a cysteine. This tethered metal chelator becomes the reaction center for hydroxyl radical production with the addition of a divalent metal and H₂O₂. Initiation of the hydroxyl radicals from the tethered reagent on the octamer surface will cleave the adjacent DNA backbone to generate DNA fragments allowing the exact cutting site to be determined by denaturing PAGE DNA sequencing, (Flaus et al., 1996).

For this mapping two different chemicals were compared which have the ability to act as hydroxyl radical producing site-specific chemical nucleases. The first is the original mapping chemical used by Flaus et al., 1996, N-[S-(2-pyridylthio)cysteaminy]ethylenediamine-N,N,N',N'-tetraacetic acid which is hereafter referred to as EDTA reagent. The second is a phenanthroline based chemical, 1,10 phenanthroline-5-maleimide similar to the reagent used by Brogaard et al., 2012.

To obtain a complete map of the nucleosome, all points of contact between DNA and protein were targeted. Seven sites were strategically chosen on one half of the nucleosome, effectively giving 14 mapping sites along the pseudo dyad-symmetric 147 bp length. A single non-basic residue was chosen adjacent to each one of the seven SHL positions and mutated to cysteine by site-directed mutagenesis. The mutated cysteine subsequently becomes the sole position of hydroxyl radical production for each half of the nucleosome. Therefore, creating seven different nucleosomes each with a separate cysteine mutation is enough to give an entire map or effectively an inverse footprint of the nucleosome.

The position of the seven mutated cysteines for half the nucleosome are represented in Figure 3.1 and a close-up view of each mutated cysteine is represented in Figure 3.2 A-G. Also Figure 3.2 H shows the known EDTA/Fe²⁺ cleavage pattern at SHL 0.5 S47C.

Due to the dyad symmetry of the nucleosome two cleavage sites exist that cut each DNA strand three times, these cuts are located two bases upstream of the dyad and 5 and 6 bases downstream of the dyad for the primary and secondary cuts respectively.

Three DNA sequences were chosen for mapping: the MMTV nucleosome A, (Richard-Foy and Hager, 1987), the synthetic 601, (Lowary and Widom, 1998) and the 601 derivative 601.2, (Anderson and Widom, 2000). These so-called nucleosome positioning sequences were chosen because they form large populations of stable nucleosomes at unique locations and are amongst the most well-studied positioning sequences in the chromatin field.

Due to the complexity of mapping each strand of the three DNA sequences using two different mapping reagents, a uniform system relating to specific locations within a DNA fragment was devised to aid with the description and visualisation of results. The published single strand sequence of each of NucA, 601 and 601.2 is referred to as the forward strand with its complimentary strand referred to as the reverse strand. The first 73 bases from the 5' end are referred to as upstream of the dyad with bases 75-147 referred to as downstream. DNA cleavage that occurs upstream is referred to as primary cleavage while DNA cleavage that occurs downstream is referred to as secondary cleavage. A schematic representation of this system showing EDTA and phenanthroline derivative cleavage sites at two SHL locations can be seen in Figure 3.3A. Figure 3.3B shows what these cleavage sites would look like on a denaturing PAGE.

Nucleosome structure showing DNA cleavage sites

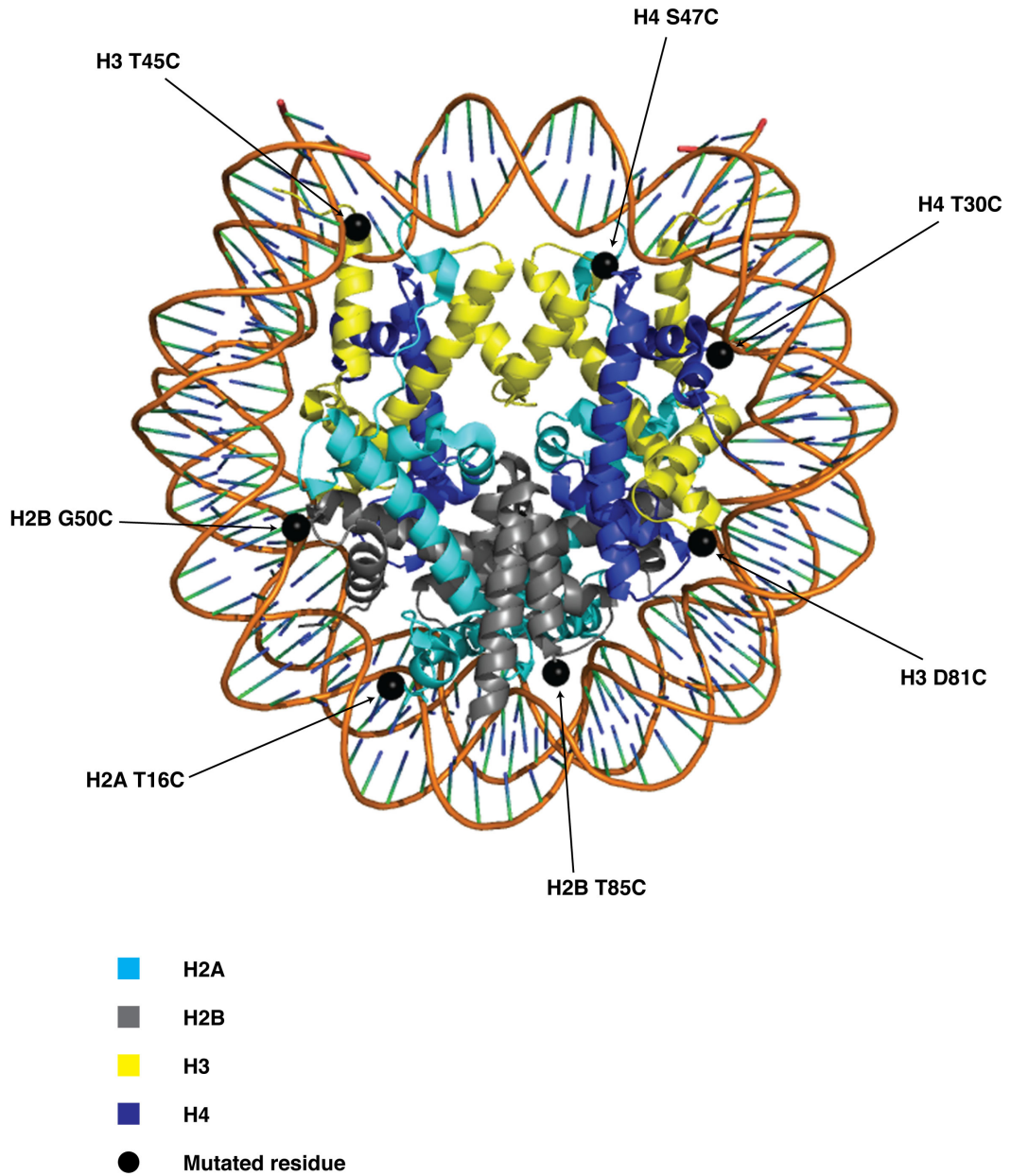


Figure 3.1 Nucleosome core particle structure showing seven cysteine mutations. Black spheres of 4 Å diameter located adjacent to the minor groove contact points and centered on the sulphur of the mutated cysteine are representative of the mapping positions for half the nucleosome. Structure from PDB entry 3LZ0 (Vasudevan et al., 2010).

Mapping Sites

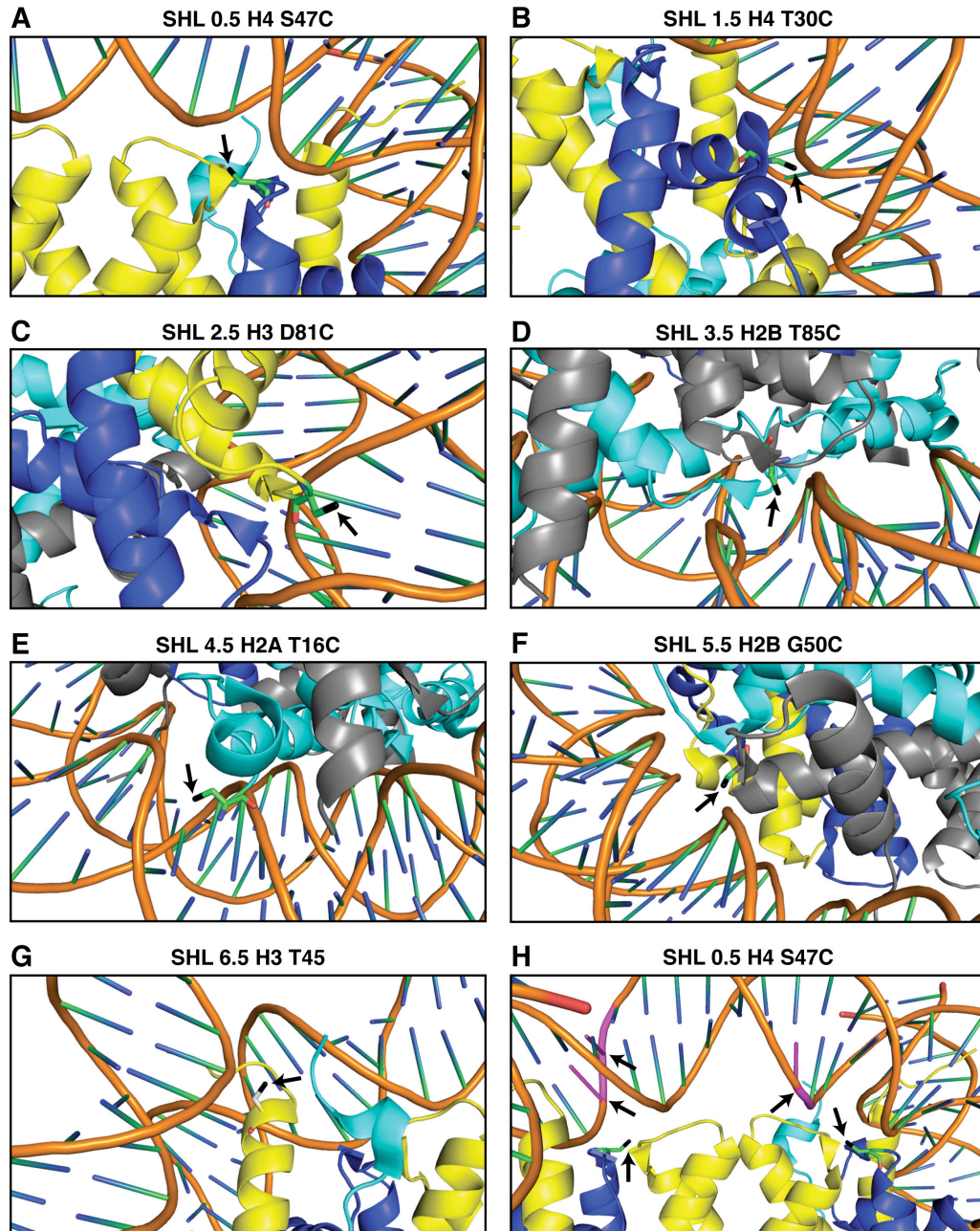


Figure 3.2 Enlarged view of the seven super helical location mapping sites. Panels A-G show a close-up view of the seven SHL mapping positions from SHL 0.5–6.5 respectively. The arrows point to the black sulphur of the mutated cysteine to which the mapping reagent is attached at each location. Panel H shows the original EDTA/Fe²⁺ mapping site and the locations of the primary and secondary cleavage that occur at 2 bases upstream and at 5 and 6 bases downstream of the dyad respectively, coloured magenta.

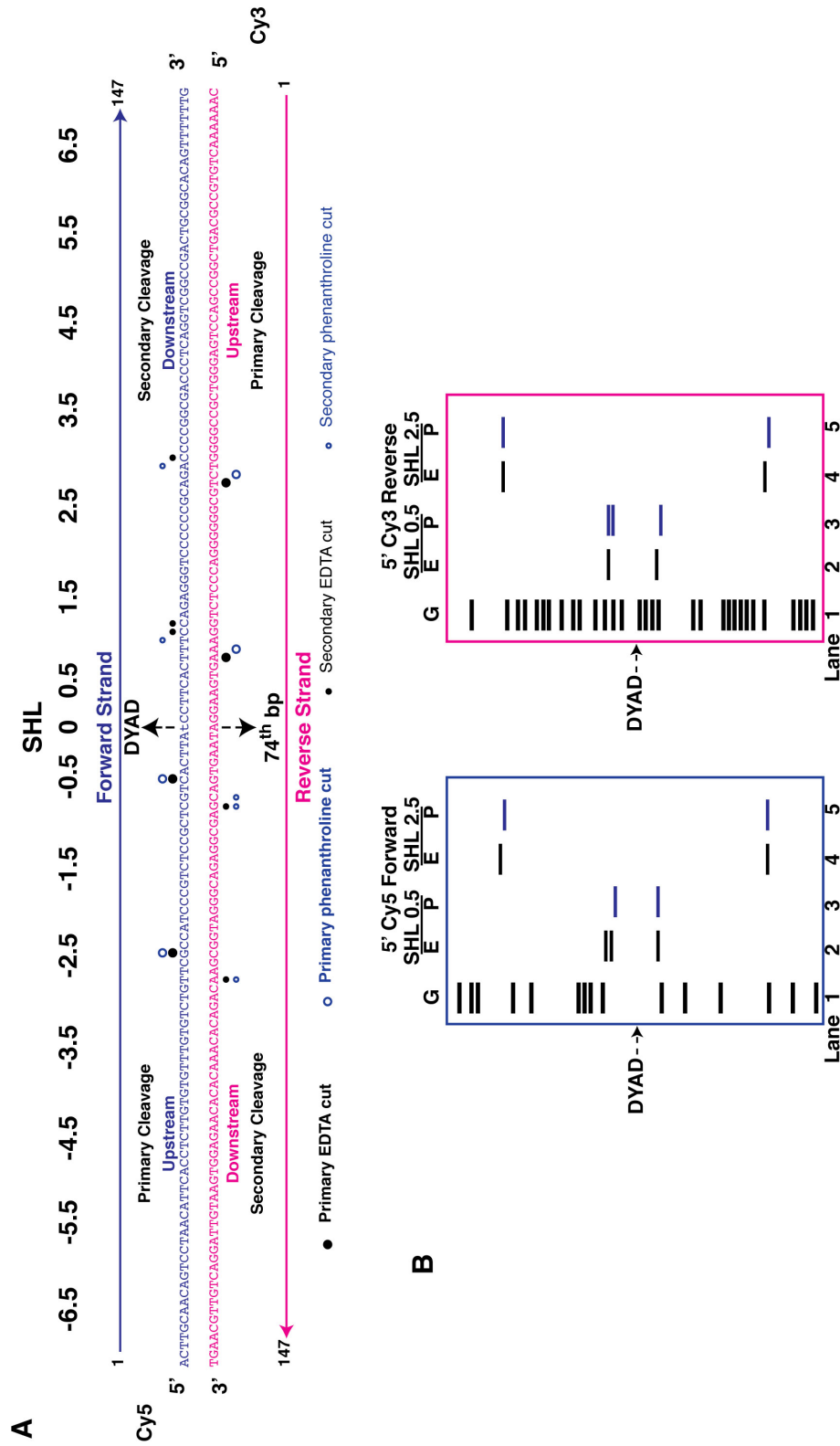


Figure 3.3 Positional terminology of nucleosomal DNA mapping with denaturing PAGE band migration. A. Positional terminology for nucleosomal DNA mapping locations at approximately SHL ± 0.5 and SHL ± 2.5 . Black solid large and small circles represent primary and secondary EDTA mapping sites respectively. Blue open large and small circles represent primary and secondary phenanthroline mapping respectively. **B.** Schematic illustration of nucleosome mapping at approximately SHL ± 0.5 and SHL ± 2.5 for EDTA (E) and phenanthroline (P) on denaturing PAGE. Blue gel represents 5'Cy5 labelled forward strand and the magenta gel represents the 5'Cy3 labelled reverse strand.

3.2 Comparison of Cu^{2+} and Fe^{2+} on nucleosome mapping

In the original EDTA mapping Fe^{2+} was used as the electron donor in the production of hydroxyl radicals (Flaus et al., 1996). However, phenanthroline mapping traditionally has used Cu^{2+} (Brogaard et al., 2012). To test for differences between the two we compared their mapping side by side.

3.2.1 Observations

No differences were observed between the migration distances of nucleosomes with either EDTA or phenanthroline attached in native PAGE, Figure 3.4 A. Mapping results show that Cu^{2+} bound to the EDTA reagent does not induce any significant cutting signal above background level, Figure 3.4 B lane 1 and 3-7. Cu^{2+} bound to the phenanthroline reagent does give a signal (Figure 3.4 B lane 8 and 10-14), although there is no correlation between Cu^{2+} concentration and mapping activity at the concentrations tested.

Phenanthroline with Fe^{2+} maps as efficiently as phenanthroline combined with Cu^{2+} (Figure 3.4 B lanes 9 and 12) and EDTA with Fe^{2+} shows similar mapping activity as phenanthroline with Fe^{2+} , Figure 3.4 lanes 2 and 9. For both metals in conjunction with EDTA and phenanthroline the primary cut site is 2 bp upstream of the dyad at 72 bp as previously observed (Flaus et al., 1996). However, for EDTA/ Fe^{2+} the secondary cuts are observed at 5 and 6 bases downstream of the dyad at bases 79 and 80, whereas with both metals in conjunction with phenanthroline the secondary cuts are observed at 4 and 5 bases downstream of the dyad at bases 78 and 79 respectively, Figure 3.4 B lanes 9-14.

3.2.2 Interpretation

The fact that no obvious differences were observed between the migration distance of either nucleosome in the native PAGE would suggest that these nucleosomes are structurally equivalent. EDTA in conjunction with Cu^{2+} shows little or no mapping activity above background levels compared to the high mapping activity of EDTA in conjunction with Fe^{2+} . This would suggest that Cu^{2+} and Fe^{2+} do not have the same chemical properties when combined with EDTA.

Phenanthroline mapping activity seems to be consistent irrespective of the whether Cu^{2+} or Fe^{2+} is used. The fact that the primary cuts of both EDTA and phenanthroline map to the same position would suggest that both reagents have their reaction center orientated in a similar direction, while mapping results from the secondary cuts would suggest that the reaction center of phenanthroline is orientated slightly back towards the dyad due to the shorter distance of mapping downstream of the dyad. A schematic representation of the cutting sites of each reagent mapped at SHL 0.5 is illustrated in Figure 3.4 C.

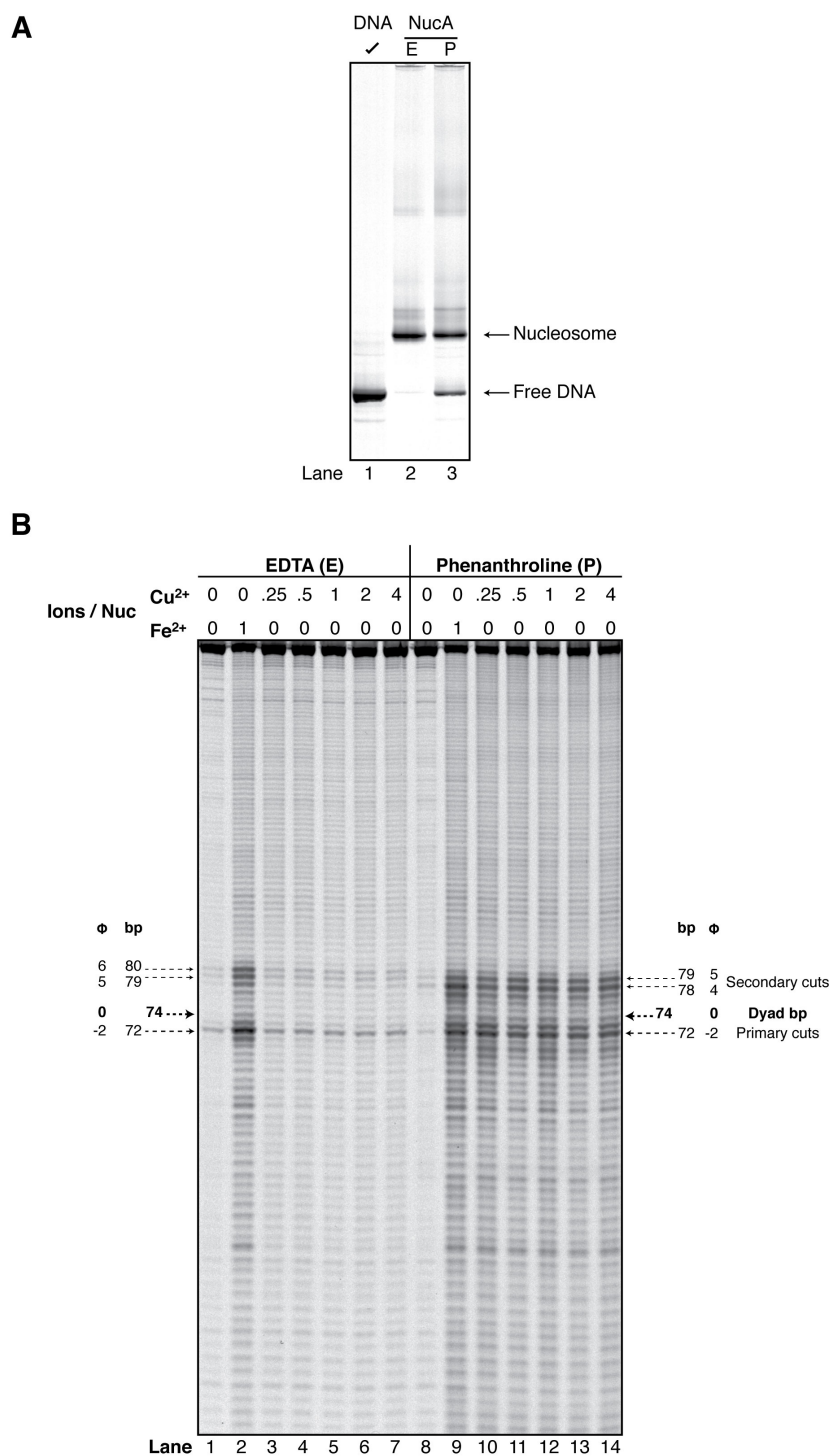
SHL 0.5 H4 S47C mapping using Cu^{2+} and Fe^{2+} 

Figure 3.4 Comparison of Cu^{2+} and Fe^{2+} on nucleosome mapping with EDTA and phenanthroline reagents. **A.** Native PAGE containing free NucA DNA and NucA nucleosomes tethered with EDTA (E) or phenanthroline (P) as mapping reagents. **B.** Denaturing PAGE of the same nucleosomes mapped with titrated concentrations of the divalent metals. Numbers represent molar equivalents of ions / nucleosome. Fragment sizes are shown as full length (bp) and as distance from the dyad (ϕ). Gels A and B were visualised using the Cy5 parameters on the Fuji phosphor-imager FLA-5100.

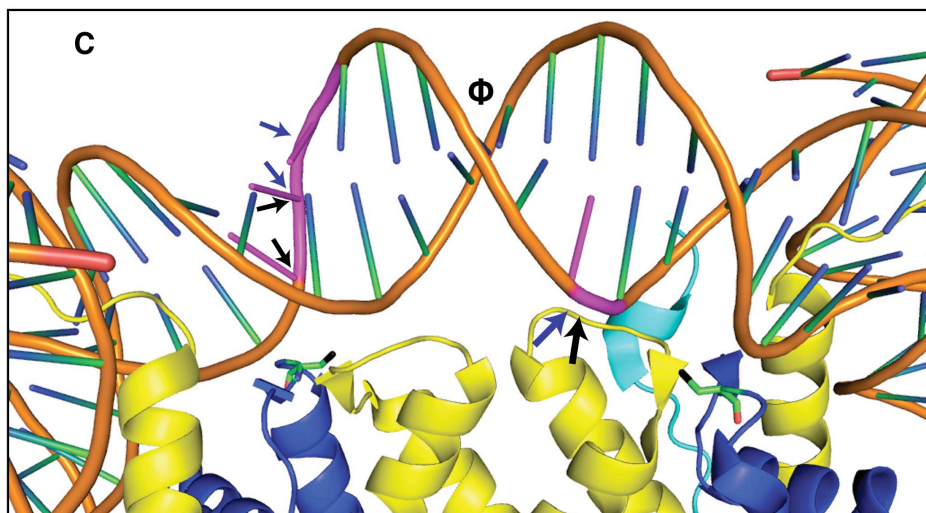


Figure 3.4 Comparison of Cu^{2+} and Fe^{2+} on nucleosome mapping with EDTA and phenanthroline reagents. C. Close-up view of site-directed mapping at SHL 0.5 S47 using EDTA and phenanthroline. Large and small black arrows represent the primary and secondary EDTA cleavage sites respectively. Large and small blue arrows represent the primary and secondary phenanthroline cleavage sites. Both primary cleavage sites for EDTA and phenanthroline occur at 2 bases upstream of the dyad. Secondary cleavage with EDTA occurs at 5-6 bases downstream of the dyad while the secondary phenanthroline cleavage occurs at 4-5 bases downstream of the dyad.

3.3 Nucleosome mapping at SHL 0.5

NucA, 601 and 601.2 nucleosomes were mapped at SHL 0.5 H4 S47C with EDTA and phenanthroline using Fe^{2+} to generate hydroxyl radicals. This replicates previous studies with the NucA sequence and extends it to the 601 sequences.

3.3.1 Observations

Primary cleavage of the forward strand at SHL 0.5 occurs at base 72 or 2 bases upstream of the dyad base. This cleavage pattern is consistent for the three DNA sequences using both EDTA and phenanthroline derivatives, Figure 3.5 B and D lanes 8-13.

The secondary cuts on the same strand occur 5 and 6 bases downstream of the dyad for EDTA (Figure 3.5 B and D lanes 8, 10 and 12), but the secondary cleavage with phenanthroline only cuts at 4 bases downstream of the central dyad base (Figure 3.5 B and D lanes 9, 11 and 13). These secondary cleavage patterns are consistent for the 3 DNA sequences, Figure 3.5 B and D.

Primary cleavage on the reverse strand occurs 2 bases upstream of the dyad on the NucA sequence using both EDTA and phenanthroline reagents, similar to the forward strand. Likewise for both 601 sequences the primary cleavage occurs 2 bases upstream of the dyad axis at base 72, this is consistent with both reagents, Figure 3.5 C and E lanes 8-13.

The secondary cuts occur on the reverse strand of NucA predominantly at 5 bases downstream of the dyad for the EDTA derivative while occurring at 4 and 5 bases downstream of the dyad at bases 78 and 79 with phenanthroline, Figure 3.5 C and E lanes 8-9. Secondary cleavage on both 601 reverse strand sequences occur 5 and 6 bases downstream at bases 79 and 80 using EDTA while occurring at 4 and 5 bases downstream at bases 78 and 79 with phenanthroline, Figure 3.5 C and E lanes 10-13.

Comparing lanes 8-9 with 10-13 in Figure 3.5 C a slight offset is observed between the cutting on NucA and both 601 sequences of the reverse strand, this is not observed on the forward strand, Figure 3.5 B lanes 8-9 and 10-13. Figure 3.5 G

and H shows a G-track marker for the forward and reverse strands of NucA, 601 and 601.2 respectively. The G-track maker is a known DNA sequence that is chemically cleaved at every guanine nucleotide. In this case a G-track was made for the three DNA nucleosome positioning sequences NucA, 601 and 601.2 to compare their migration. G-track markers can also be used as DNA ladders to determine the size of unknown fragment lengths.

Observations from the G-tracks of the forward strands indicate that equivalent bases from all three sequences migrate together. However, observations from the reverse strand would indicate that both 601 sequences migrate 1 base ahead of the NucA sequence.

The primary and secondary EDTA and phenanthroline mapping sites for NucA, 601 and 601.2 DNA at SHL 0.5 are indicated in Figure 3.5 F.

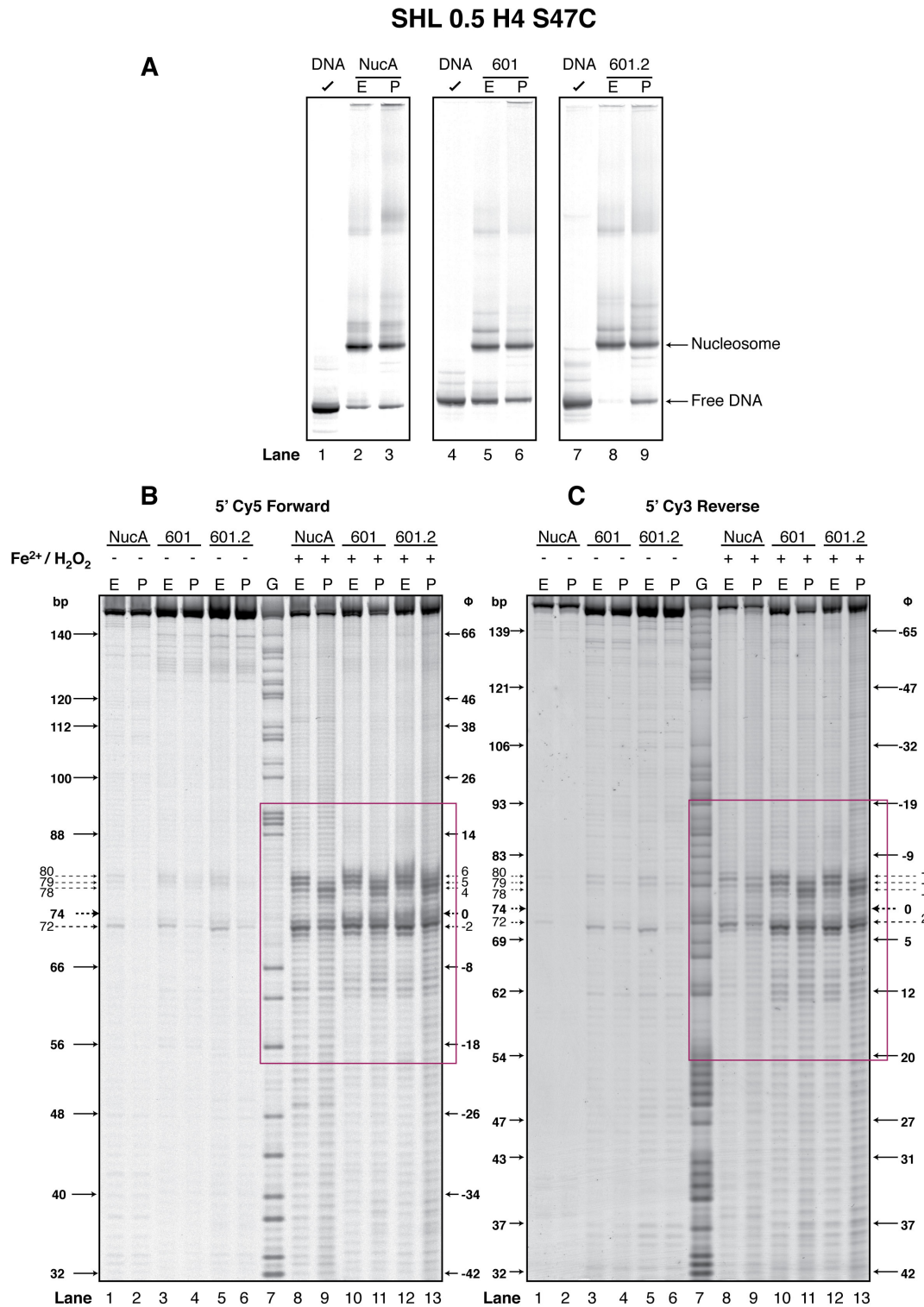


Figure 3.5 Nucleosome mapping at SHL 0.5 with EDTA and phenanthroline on NucA, 601 and 601.2. **A.** Native gels showing MMTV Nucleosome A (NucA), 601 and 601.2 nucleosomes with either EDTA (E) or phenanthroline (P) reagents attached to H4 S47C at SHL 0.5. Lanes 1, 4, and 7 show the free DNA without nucleosomes of NucA, 601 and 601.2 respectively. **B.** Denaturing PAGE showing the DNA forward strand mapping results for the 3 nucleosomes. **C.** Denaturing PAGE showing the reverse strand results for the 3 nucleosomes. (–) and (+) signs represent the respective absence and presence of Fe²⁺ at 1 ion/nucleosome and H₂O₂ in the mapping assays. Magenta boxes represent the region of the profile analysed in Figure 3.5 D and E. The G-track marker (G) represents the NucA sequence cleaved at every guanine nucleotide. Fragment sizes are shown as full length (bp) and as distance from the dyad (φ). Gels were visualised using the Fuji phosphor-imager FLA-5100.

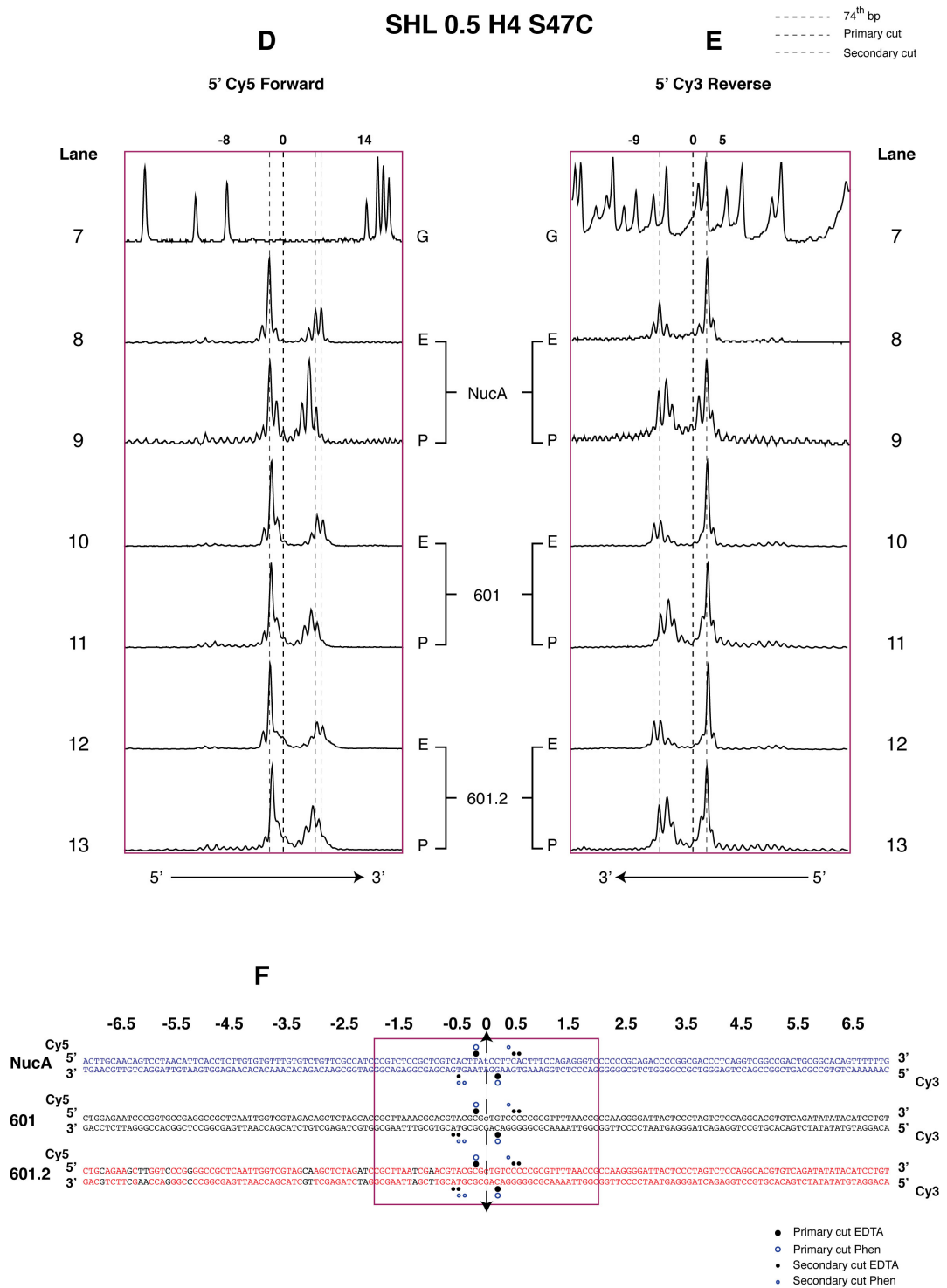


Figure 3.5 Nucleosome mapping at SHL 0.5 with EDTA and phenanthroline on NucA, 601 and 601.2. **D.** Signal profile for the forward strands of NucA, 601 and 601.2 from Figure 3.5 B bases as indicated. **E.** Signal profile of the reverse strand of NucA, 601 and 601.2 from Figure 3.5 C. **F.** DNA sequences of NucA, 601 and 601.2 showing the cutting sites for EDTA and phenanthroline reagents attached to H4 S47C at SHL 0.5. Black nucleotides in the 601.2 sequence represent the 12 base changes made from the original 601 sequence. EDTA (E) and Phenanthroline (P). The G-track marker (G) represents the NucA sequence cleaved at every guanine nucleotide. Numbers over the G-track peaks represent distances from the dyad in bases. Signal profile data taken from Figure 3.5 B and C using AIDA analysis software.

3.3.2 Interpretation

The primary cleavage positions on the forward strand for the EDTA and phenanthroline mapping show no significant differences between DNA sequences, both of which cut 2 bases upstream of the dyad on all three DNA sequences, NucA, 601 and 601.2. This indicates that both reagents behave similarly and that the three DNA sequences are structurally similar at this cleavage position. However, the secondary cuts on the same strand show a 1 base difference between reagents, with EDTA cutting 5 and 6 bases downstream of the dyad, whereas phenanthroline cuts at 4 bases downstream of the dyad.

The secondary cuts on the reverse strands show a similar pattern as they did for the forward strands, with a single base shift towards the dyad for phenanthroline over EDTA. Cutting the NucA sequence at 5 and 4-5 bases downstream of the dyad for EDTA and phenanthroline respectively. Both 601 sequences cut at 5-6 bases and 4-5 bases downstream of the dyad for EDTA and phenanthroline respectively.

Combined, these data suggest that a DNA strand in close proximity to either reagent will cut in the same position. However, for a DNA strand that is further away from the cutting reagent the hydroxyl radical dispersion of phenanthroline tends to cleave towards the dyad with a difference of 1 base over that of EDTA. This suggests that the phenanthroline reagent is orientated slightly more towards the dyad than that of EDTA.

The primary cuts on the reverse strand show both reagents cut 2 bases upstream of the dyad for all three sequences, NucA, 601 and 601.2. Initially it looked as if the 601 sequences may have cut at 3 bases upstream due to the offset band migration. However, this was ruled out when all three G-tracks were run side by side.

The reason behind the faster migration of the reverse strand of both 601 sequences over that of the NucA sequence is unclear. This observation is absent in the forward strand migration suggesting that some strand specific structural difference is causing the migration anomaly. The purine content for the NucA and 601 reverse strands is 64.6 % and 54.4 % respectively, this could be responsible for the NucA reverse strand sequence running ~ 1 base greater than the 601. However, the forward strand of the 601 sequence also contains ~ 10 % more purines than the corresponding NucA sequence and no difference in migration is observed. A possible

reason for the difference in migration may come from the NucA reverse strand sequence having two homopolymer repeats of 6 adenines and 6 guanines within the first 73 bases. However, the overall purine content for the first 73 bases of the reverse strands only differs by 1.4% between NucA and 601, with the former marginally greater.

No obvious sequence configuration allows for the migration difference between the reverse strands of NucA and both 601 sequences and although empirically observed, the cause is still uncertain.

3.4 Nucleosome mapping at SHL 1.5

NucA, 601 and 601.2 nucleosomes were mapped at SHL 1.5 H4 T30C with EDTA and phenanthroline using Fe^{2+} to generate hydroxyl radicals. The expected DNA cleavage would be ~10 bases further on from the SHL 0.5 sites, making the primary and secondary DNA fragments ~10 bases shorter and ~10 bases longer respectively.

3.4.1 Observations

Primary cuts at 11-12 bases are observed on the forward strand of NucA, 601 and 601.2 using both EDTA and phenanthroline, Figure 3.6 B and D lanes 8-13. Additionally, three prominent cleavage sites are located at 15-17 bases upstream of the dyad using phenanthroline on the NucA sequence, Figure 3.6 B and D lane 9. This extra area of cleavage is not observed using EDTA in any of the sequences. However, there is evidence of similar cleavage in both 601 sequences albeit not as prominent, Figure 3.6 B and D lanes 9,11 and 13.

The secondary cuts on the forward strand occur 15-16 bases downstream of the dyad at bases 89-90 for EDTA on the three DNA sequences. The phenanthroline cuts occur at bases 88-90 and 92 for NucA and at bases 88-89 for the 601 sequences, Figure 3.6 B and D lanes 8-13.

The primary cuts on the reverse strand occur 11-12 bases upstream of the dyad for EDTA and phenanthroline on the NucA sequence. The primary cutting occurs at 12 bases upstream of the dyad for EDTA, and 11 and 12 bases upstream of the dyad for phenanthroline on both 601 sequences, Figure 3.6 C and E lanes 8-13.

The secondary cuts on the reverse strand of NucA occur at 15-16 bases downstream of the dyad for EDTA, and at 14, 15 and 18 bases downstream of the dyad on NucA using phenanthroline. The secondary EDTA cuts on the reverse strand of both 601 sequences map at 15-16 bases downstream of the dyad while the phenanthroline maps at 14-15 bases for 601 and 14, 15 and 18 bases downstream for 601.2, Figure 3.6 C and E lanes 8-13. The primary and secondary EDTA and phenanthroline mapping sites for NucA, 601 and 601.2 DNA at SHL 1.5 are indicated in Figure 3.6 F.

SHL 1.5 H4 T30C

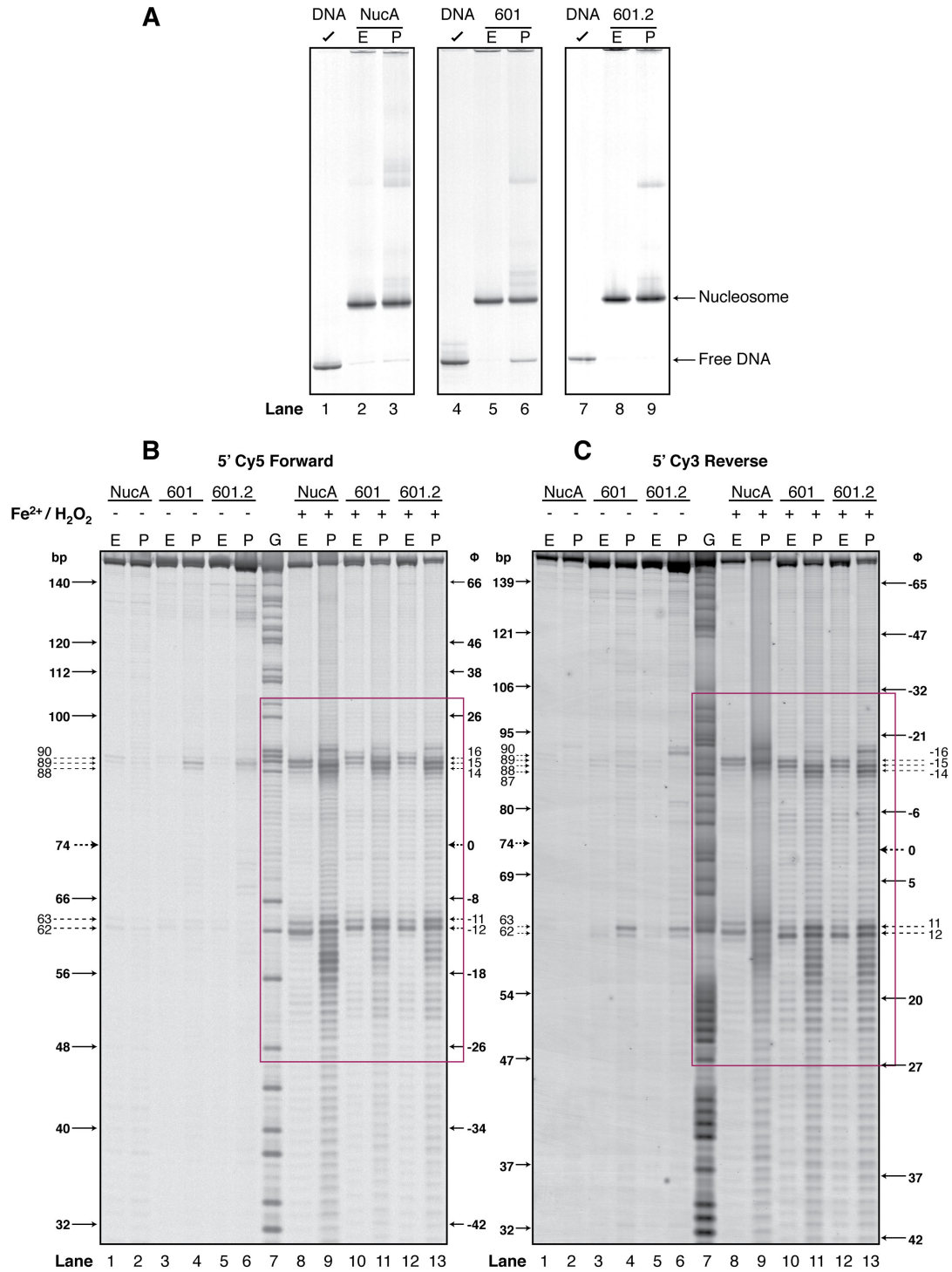


Figure 3.6 Nucleosome mapping at SHL 1.5 with EDTA and phenanthroline on NucA, 601 and 601.2. **A.** NucA, 601 and 601.2 nucleosomes with EDTA and phenanthroline attached to H4 T30C at SHL 1.5 on native PAGE. **B.** Denaturing PAGE showing forward strand mapping results of the same nucleosomes. **C.** Denaturing PAGE showing reverse strand mapping of NucA, 601 and 601.2 nucleosomes at H4 T30C SHL 1.5. (–) and (+) signs represent the respective absence and presence of Fe²⁺ at 1 ion/nucleosome and H₂O₂ in the mapping assays. Magenta boxes represent the region of the profile analysed in Figure 3.6 D and E. The G-track marker (G) represents the NucA sequence cleaved at every guanine nucleotide. Fragment sizes are shown as full length (bp) and as distance from the dyad (φ). Gels were visualised using the Fuji phosphor-imager FLA-5100.

3.4.2 Interpretation

Primary cleavage on both strands of NucA at SHL 1.5 using EDTA and phenanthroline occur at 11-12 bases either side of the central dyad axis, supporting dyad symmetry. Also the SHL 1.5 cleavage sites are 9-10 bases further on from the dyad than the SHL 0.5 sites which would allow for the ~ 10.17 bp per helical turn of nucleosomal DNA. The extra primary phenanthroline cleavage especially prominent on the NucA sequence could be due to dynamics within the DNA at this region, or possibly due to a structural difference between the DNA sequences. It could also be due to phenanthroline occupying different positions within the same minor groove. It is unlikely that this observation is due to phenanthroline-maleimide cross-reaction with a primary amine at an adjacent residue such as a lysine because there is no observed cleavage at the many other locations where lysines are adjacent to DNA.

The primary cleavage on the forward strand of the 601 sequences occur at 11-12 bases upstream of the dyad, consistent with that of the NucA sequence, suggesting structural similarity. The primary cuts on the reverse strands of both 601 sequences also occur at 11-12 bases upstream of the dyad for phenanthroline but only at 12 bases upstream for EDTA. This could further confirm that the phenanthroline sits more orientated towards the dyad over the EDTA reagent. The SHL 1.5 primary cleavage of the 601 sequences are also 9-10 bases further along from the dyad than the SHL 0.5 primary cleavage which allows for the ~ 10.17 bp per helical turn, while also confirming dyad symmetry.

The secondary cuts on the forward strand of all three DNA sequences occur at 15-16 bases downstream of the dyad with EDTA and 14-15 bases with phenanthroline. The location of these cuts is 10-11 bases downstream of the previous 0.5 secondary cuts, as expected for a single helical turn.

An additional secondary cut is noticed on the forward strand of NucA with phenanthroline at 18 bases downstream from the dyad, this cut is equivalent to the additional upstream cuts observed on the same strand. These additional phenanthroline cuts are also noticed on the reverse strand of the NucA sequence, the 601.2 sequence and to a lesser extent the 601. These extra phenanthroline cuts could suggest base pair dynamics within this region, or more likely that phenanthroline itself sits in alternate positions because this is not seen with the EDTA mapping.

3.5 Nucleosome mapping at SHL 2.5

NucA, 601 and 601.2 nucleosomes were mapped at SHL 2.5 H3 D81C with EDTA and phenanthroline using Fe^{2+} to generate hydroxyl radicals.

3.5.1 Observations

EDTA primary cuts at SHL 2.5 on the forward strand occur at 22 bases upstream from the dyad on NucA, 601 and 601.2. The primary phenanthroline cuts on the same strand occur at 22-23 bases upstream of the dyad, which is consistent across the three DNA sequences, Figure 3.7 B and D lanes 8-13.

The secondary EDTA cuts on the forward strand occur at 24-26 bases downstream of the dyad on NucA. The same cuts on both 601 sequences occur at 25-26 bases downstream of the dyad. The secondary phenanthroline cuts on the forward strand occur at 24-25 bases downstream of the dyad in all 3 DNA sequences, Figure 3.7 B and D lanes 8-13.

The primary EDTA cuts on the reverse strands at 22 bases upstream of the dyad on NucA, 601 and 601.2. The primary phenanthroline maps with a double cut at 22-23 bases for all three sequences NucA, 601 and 601.2, Figure 3.7 C and E lanes 8-13.

The secondary EDTA cuts on the reverse strand occur at 25-26 bases downstream of the dyad for NucA, 601 and 601.2. Phenanthroline at the same location maps 24-25 bases downstream of the dyad for all three sequences, Figure 3.7 C and E lanes 8-13.

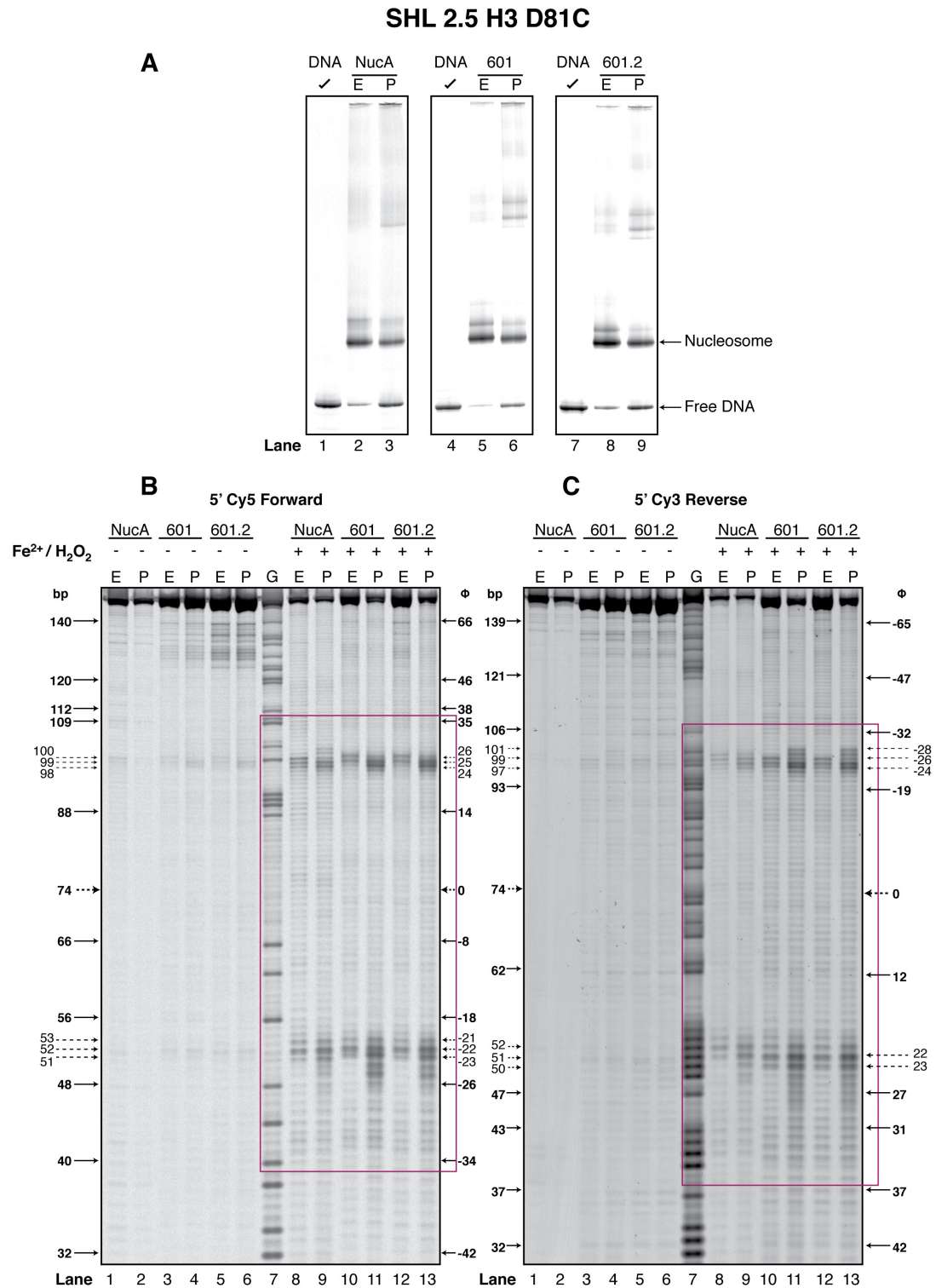
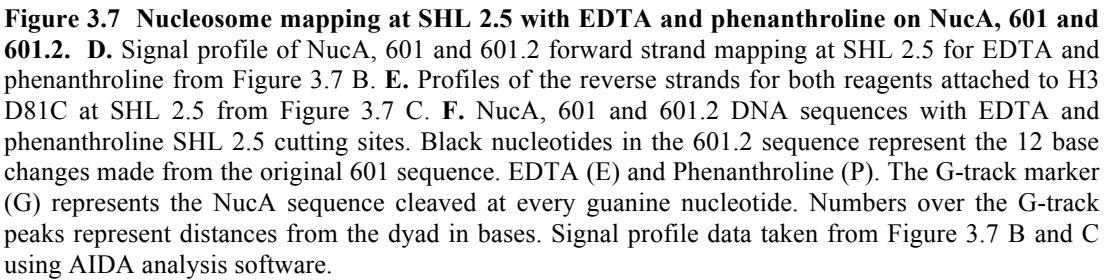


Figure 3.7 Nucleosome mapping at SHL 2.5 with EDTA and phenanthroline on NucA, 601 and 601.2. **A.** Native gels showing NucA, 601 and 601.2 nucleosomes with either EDTA or phenanthroline attached to H3 D81C prior to mapping at SHL 2.5. **B.** Denaturing PAGE showing forward strand mapping with either reagent for the 3 nucleosomes. **C.** Denaturing PAGE showing mapping results on the reverse strand of NucA, 601 and 601.2 nucleosomes at SHL 2.5. (–) and (+) signs represent the respective absence and presence of Fe^{2+} at 1 ion/nucleosome and H_2O_2 in the mapping assays. Magenta boxes represent the region of the profile analysed in Figure 3.7 D and E. The G-track marker (G) represents the NucA sequence cleaved at every guanine nucleotide. Fragment sizes are shown as full length (bp) and as distance from the dyad (ϕ). Gels were visualised using the Fuji phosphor-imager FLA-5100.



3.5.2 Interpretation

The primary cleavage on the forward strand using EDTA is 22 bases upstream of the dyad for the three DNA sequences NucA, 601 and 601.2. The phenanthroline maps at 22-23 bases upstream of the dyad for the 3 sequences. The distance from the SHL 0.5 primary map to the SHL 2.5 primary map is 20-21 bases which would account for 2 helical turns, which in theory cover ~20.4 bp.

The primary cuts on the reverse strand of NucA, 601 and 601.2 are also 22-23 bases upstream of the dyad, as expected by symmetry. These cuts are also 20-21 bases upstream of the SHL 0.5 which is approximately two helical turns as expected

The secondary cuts on the forward strand of the three DNA sequences show almost complete similarity and are again 20-21 bases from the same cuts at 0.5 SHL.

The secondary EDTA cuts on the reverse strand of NucA, 601 and 601.2 cut at 25-26 bases from the dyad, whereas the phenanthroline cuts at 24-25 bases, continuing the pattern of a single base pair shift towards the dyad for the secondary cuts and also continuing the trend of 20-21 bases between 0.5 and 2.5.

3.6 Nucleosome mapping at SHL 3.5

NucA, 601 and 601.2 nucleosomes were mapped at SHL 3.5 H2B T85C with EDTA and phenanthroline using Fe^{2+} to generate hydroxyl radicals.

3.6.1 Observations

The primary mapping on the forward strand of NucA occurs at 33 bases upstream of the dyad for EDTA and phenanthroline. The forward strand primary cuts on both 601 sequences occur at 33-34 bases upstream of the dyad for EDTA and at 33 bases upstream of the dyad for phenanthroline, Figure 3.8 B and D lanes 8-13.

Secondary cuts on the forward strand of NucA occur at 36 and 37 bases downstream of the dyad for phenanthroline and EDTA respectively, Figure 3.8 B and D lanes 8-9. EDTA secondary cuts on the forward strand of the 601 sequences also occur at 37 bases downstream of the dyad, Figure 3.8 B and D lanes 10 and 12.

Secondary cuts on the forward strand using phenanthroline give a double cut at 35-36 bases downstream of the dyad. Extra secondary phenanthroline mapping occurs at 40 bases downstream of the dyad for both 601 sequences, Figure 3.8 B and D Lane 11 and 13.

Primary mapping on the reverse strand of NucA occurs at 33-34 bases upstream from the dyad with EDTA while phenanthroline maps at 34 bases. The 601 sequences also cut at 33-34 bases for EDTA while phenanthroline maps at 33 bases upstream of the dyad, Figure 3.8 C and E lanes 8-13. Phenanthroline also maps with extra cutting on the 601 sequences with the strongest of these occurring at 37 bases upstream of the dyad, Figure 3.8 C and E lanes 11 and 13.

Secondary mapping on the reverse strand cuts at 37 bases downstream of the dyad with EDTA and 35-36 bases downstream with phenanthroline on the NucA sequence, Figure 3.8 C and E lanes 8-9. Likewise for both 601 sequences, EDTA maps at 37 bases and phenanthroline maps at 35-36 bases downstream of the dyad, Figure 3.8 C and E lanes 10-13.

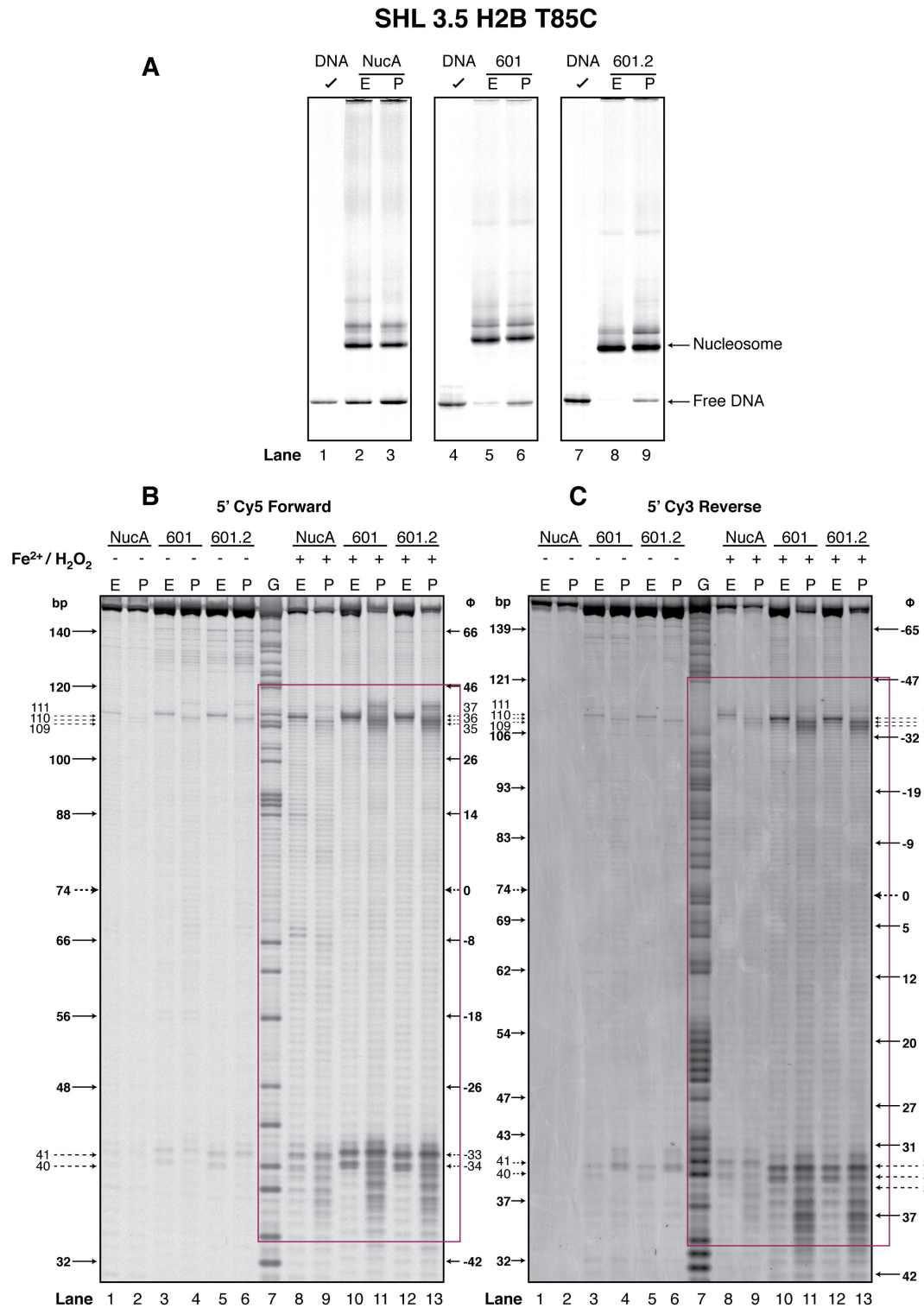


Figure 3.8 Nucleosome mapping at SHL 3.5 with EDTA and phenanthroline on NucA, 601 and 601.2. **A.** Native gels showing NucA, 601 and 601.2 nucleosomes with either EDTA or phenanthroline attached to H2B T85C at SHL 3.5. **B.** Denaturing PAGE with forward strand mapping results for both reagents on the NucA, 601 and 601.2 nucleosomes. **C.** Denaturing PAGE of the reverse strand mapping for EDTA and phenanthroline on the 3 nucleosomes. (–) and (+) signs represent the respective absence and presence of Fe²⁺ at 1 ion/nucleosome and H₂O₂ in the mapping assays. Magenta boxes represent the region of the profile analysed in Figure 3.8 D and E. The G-track marker (G) represents the NucA sequence cleaved at every guanine nucleotide. Fragment sizes are shown as full length (bp) and as distance from the dyad (φ). Gels were visualised using the Fuji phosphor-imager FLA-5100.

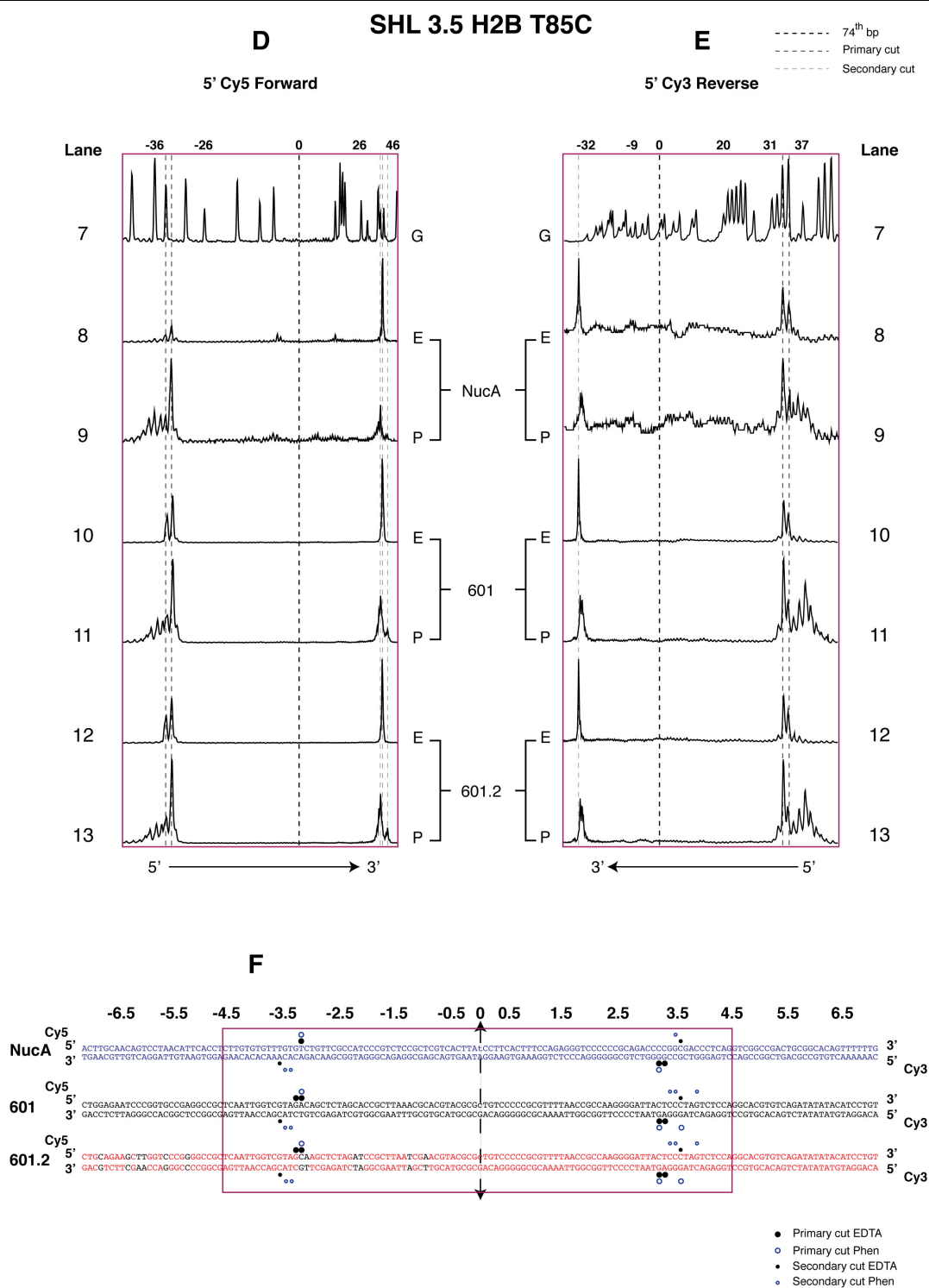


Figure 3.8 Nucleosome mapping at SHL 3.5 with EDTA and phenanthroline on NucA, 601 and 601.2. **D.** Signal profile of the forward strand mapping at SHL 3.5 H2B T85C with EDTA and phenanthroline on NucA, 601 and 601.2 from Figure 3.8 B. **E.** Signal profile of the reverse strand mapping on the 3 nucleosomes from Figure 3.8 C. **F.** NucA, 601 and 601.2 DNA sequences showing the SHL 3.5 cutting sites with EDTA and phenanthroline reagents. Black nucleotides in the 601.2 sequence represent the 12 base changes made from the original 601 sequence. The EDTA derivative is represented by (E) and the phenanthroline derivative by (P). The G-track marker (G) represents the NucA sequence cleaved at every guanine nucleotide. Numbers over the G-track peaks represent distances from the dyad in bases. Signal profile data taken from Figure 3.8 B and C using AIDA analysis software.

3.6.2 Interpretation

Primary cutting on the forward strand of NucA occurs at 33 bases upstream of the dyad for both EDTA and phenanthroline, which is 3 helical turns from SHL 0.5. This is also true for the 601 sequences although an additional cut is noticed at 34 bases from the dyad using EDTA. The primary cleavage on the forward strand of NucA is noticeably weaker than that of the 601 sequences, possibly due to a local DNA structure that hydroxyl radicals cannot reach.

Conversely, the EDTA secondary cut on the forward strand of NucA is stronger than the phenanthroline cut, again suggesting that phenanthroline sits in a slightly different position to EDTA.

Primary cleavage on the reverse strand of NucA is also weak for both reagents as is the secondary phenanthroline cuts of the same strand. But the secondary EDTA on the same strand is also slightly stronger, suggesting that DNA is more in line with the hydroxyl radicals of the EDTA reaction than the phenanthroline reaction in this case.

The 601 sequences show identical cleavage patterns indicating no structural differences between each other at this location. Cutting distances between SHL 0.5 and SHL 3.5 are 31-32 bases consistent with 3 helical turns between the locations.

The extra phenanthroline cleavage observed in the 601 sequences at 37 bp upstream from the dyad on the reverse strand and 40 bases downstream on the forward strand could possibly come from dynamics within the DNA at this location or could be due to the phenanthroline occupying alternate locations.

3.7 Nucleosome mapping at SHL 4.5

NucA, 601 and 601.2 nucleosomes were mapped at SHL 4.5 H2A T16C with EDTA and phenanthroline using Fe^{2+} to generate hydroxyl radicals.

3.7.1 Observations

There is very little evidence of primary cleavage on the forward strand of NucA, 601 and 601.2 using EDTA, Figure 3.9 B and D, lanes 8, 10 and 12. However, phenanthroline does show primary cleavages on the forward strand of NucA at 42 bases upstream of the dyad and for both 601 sequences at 41-43 and 45 bases upstream of the dyad, Figure 3.9 B and D, lanes 9, 11 and 13.

Secondary cleavage on the forward strand of NucA occurs at 46 bases downstream for EDTA and at 44-46 bases downstream of the dyad for phenanthroline. Secondary EDTA cuts both 601 sequences also at 46 bases downstream of the dyad. While secondary phenanthroline cuts are observed at 44-45 bases downstream of the dyad on the forward strand of 601 and at 44-46 bases downstream of the dyad for 601.2, Figure 3.9 F and H lanes 8-13. The secondary mapping data was interpreted from an extra long run gel of the same samples, Figure 3.9 F.

Little or no primary mapping takes place on the reverse strand of NucA using EDTA. However, phenanthroline does map at this location at 42-43 bases upstream of the dyad, Figure 3.9 C and E, lanes 8-9. Similarly, there are no primary EDTA cuts on the reverse strand of the 601 sequences, but phenanthroline does give primary cleavage at 41-43 bases upstream of the dyad for both 601 sequences, Figure 3.9 C and E lanes 10-13.

Secondary cleavage on the NucA reverse strand occurs at 46 bases for EDTA and at 44-46 bases downstream of the dyad for phenanthroline, Figure 3.9 G and I lanes 8-9. The secondary cleavage on the reverse strand for both 601 sequences occurs at 46 bases downstream for EDTA and at 43-45 bases downstream of the dyad for phenanthroline, Figure 3.9 G and I, lanes 10-13.

Bands are also observed between 44-49 bases upstream of the dyad for the 601 reverse strand in both the positive and negative control. These bands are contaminating Cy3 labelled primers that remained after DNA purification.

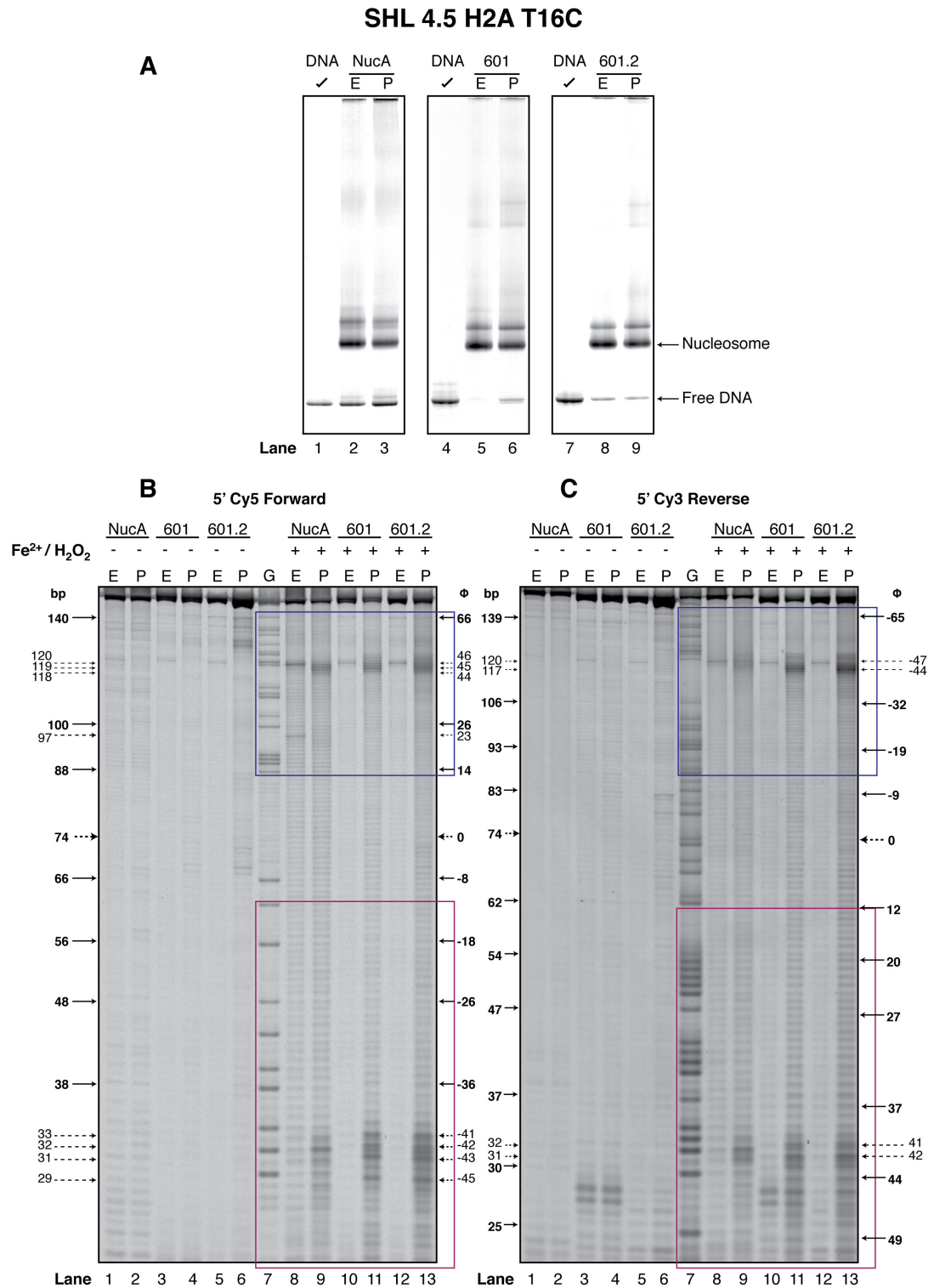


Figure 3.9 Nucleosome mapping at SHL 4.5 with EDTA and phenanthroline on NucA, 601 and 601.2. **A.** Native gels of NucA, 601 and 601.2 nucleosomes with EDTA or phenanthroline attached at SHL 4.5 to H2A T16C. **B.** Denaturing PAGE of the forward strand mapping for the 3 nucleosomes. **C.** Denaturing PAGE showing the reverse strand mapping for EDTA and phenanthroline on NucA, 601 and 601.2 nucleosomes. Magenta boxes represent the region of the profile analysed in Figure 3.9 D and E. Purple boxes represent regions of secondary mapping that required further resolving to accurately determine the fragment size, Figure 3.9 F and G. (–) and (+) signs represent the respective absence and presence of Fe²⁺ at 1 ion/nucleosome and H₂O₂ in the mapping assays. The G-track marker (G) represents the NucA sequence cleaved at every guanine nucleotide. Fragment sizes are shown as full length (bp) and as distance from the dyad (Φ). Gels were visualised using the Fuji phosphor-imager FLA-5100.

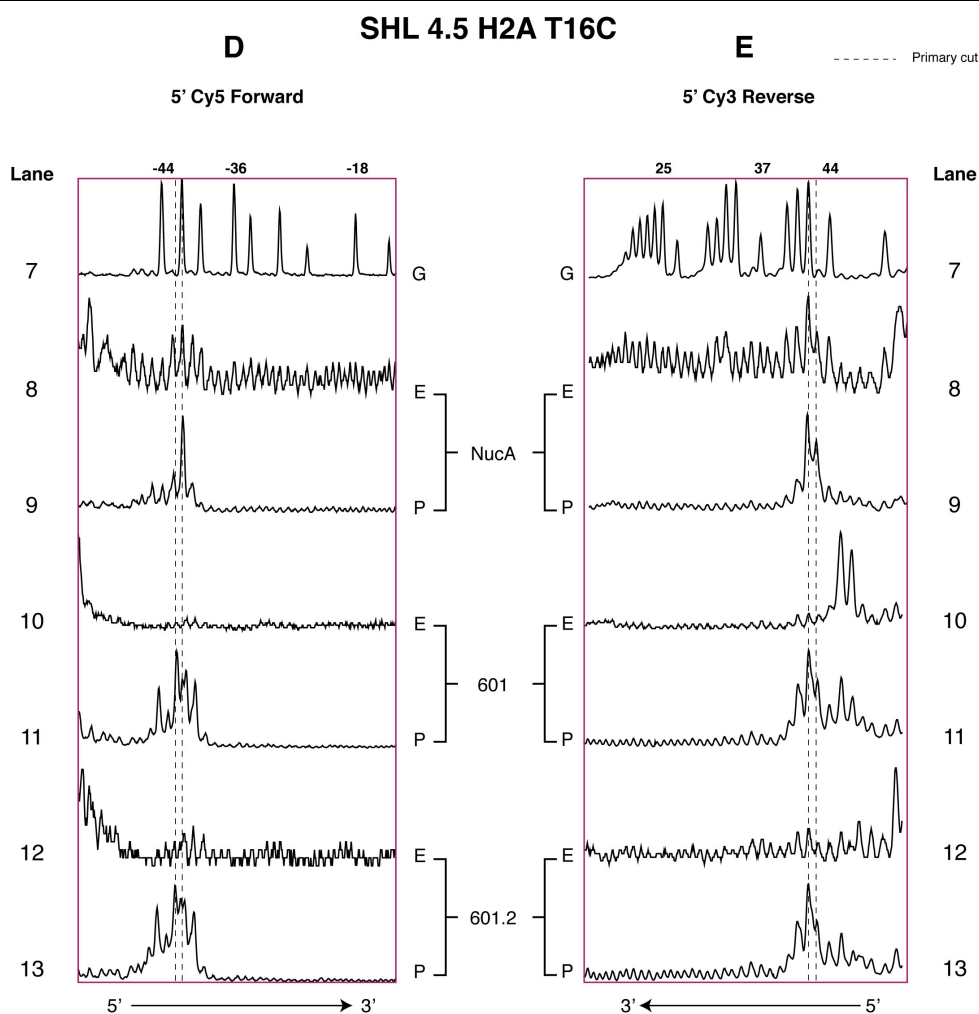


Figure 3.9 Nucleosome mapping at SHL 4.5 with EDTA and phenanthroline on NucA, 601 and 601.2. **D.** Signal profile of the primary mapping on the forward strand at SHL 4.5 H2A T16C for NucA, 601 and 601.2 nucleosomes using EDTA and phenanthroline, from Figure 3.9 B. **E.** Signal profile of the primary mapping on the reverse strand of the 3 nucleosomes for both EDTA and phenanthroline, from Figure 3.9 C. (E) represents the EDTA derivative and (P) the phenanthroline derivative. The G-track marker (G) represents the NucA sequence cleaved at every guanine nucleotide. Numbers over the G-track peaks represent distances from the dyad in bases. Signal profile data taken from the magenta regions of Figure 3.9 B and C using AIDA analysis software.

SHL 4.5 H2A T16C

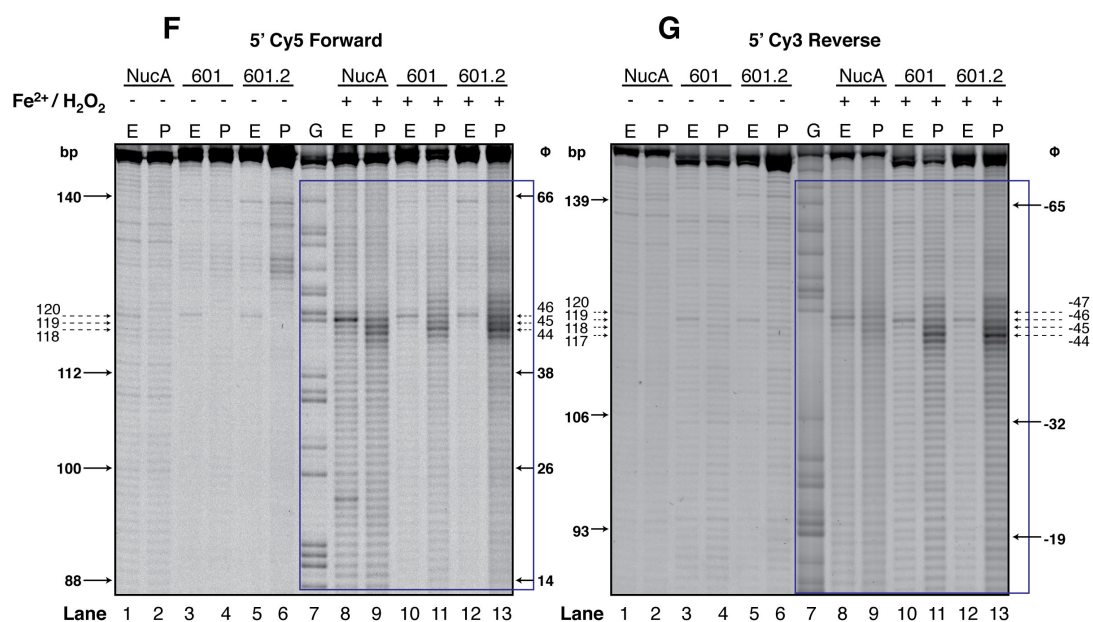


Figure 3.9 Nucleosome mapping at SHL 4.5 with EDTA and phenanthroline on NucA, 601 and 601.2. **F.** Denaturing PAGE of the secondary mapping on the forward strand of NucA, 601 and 601.2 nucleosomes. **G.** Denaturing PAGE of the secondary mapping on the reverse strand at SHL 4.5 H2A T16C of NucA, 601 and 601.2 nucleosomes. These results come from the same samples as Figure 3.9 B and C, however they have been re-run on separate gels for a greater duration to increase resolution. Signal profiles for these gels can be seen in Figure 3.9 H and I. (–) and (+) signs represent the respective absence and presence of Fe²⁺ at 1 ion/nucleosome and H₂O₂ in the mapping assays. The G-track marker (G) represents the NucA sequence cleaved at every guanine nucleotide. Fragment sizes are shown as full length (bp) and as distance from the dyad (φ). Gels were visualised using the Fuji phosphor-imager FLA-5100.

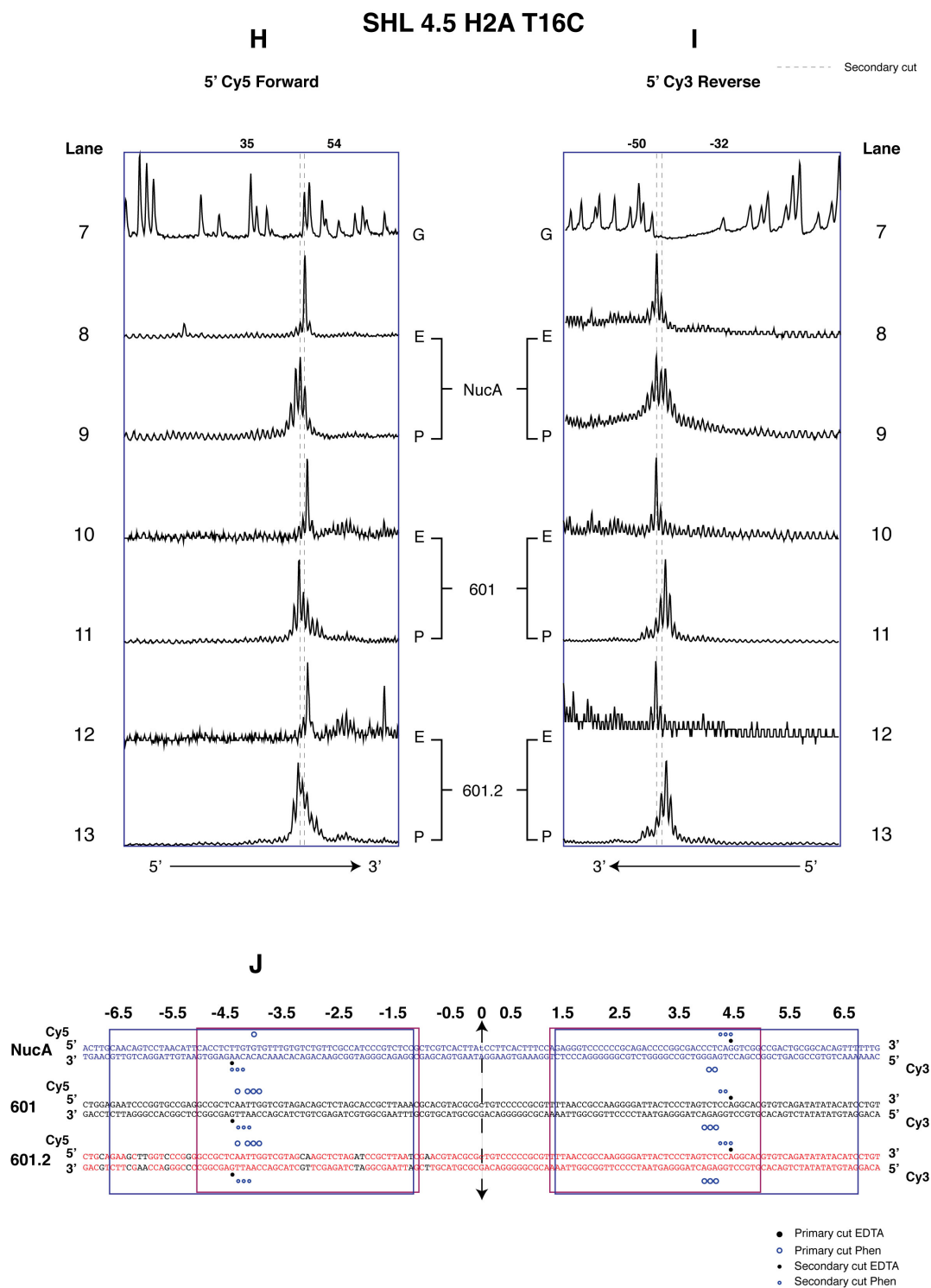


Figure 3.9 Nucleosome mapping at SHL 4.5 with EDTA and phenanthroline on NucA, 601 and 601.2. **H.** Signal profile of the secondary mapping on the forward strand of NucA, 601 and 601.2 from Figure 3.9 F. **I.** Signal profile of the secondary mapping on the reverse strand at SHL 4.5 H2A T16C for NucA, 601 and 601.2 nucleosomes either EDTA or phenanthroline, from Figure 3.9 G. **J.** NucA, 601 and 601.2 sequences with cutting sites for EDTA and phenanthroline. Sequence within the magenta and purple boxes represent the signal profile regions. The EDTA derivative is represented by (E) and the phenanthroline derivative by (P). The G-track marker (G) represents the NucA sequence cleaved at every guanine nucleotide. Numbers over the G-track peaks represent distances from the dyad in bases. Signal profile data obtained using AIDA analysis software.

3.7.2 Interpretation

EDTA gives no primary cuts for any of the three DNA sequences, suggesting that the reagent must lie in a very non-optimal orientation. In contrast, phenanthroline does make a primary cut on the forward strand of NucA at 42 bases upstream of the dyad. This is only 9 bases on from the SHL 3.5 cut at 33 bases, which could suggest a different location of the reagent due to the orientation of the cysteine to which it is attached. Figure 3.9 K shows the actual cut site of 42 bases upstream of the dyad versus the expected cut site of 44 bases upstream. This observation could suggest that the cysteine point mutation and attached reagent is orientated slightly back downstream towards the dyad. It could also indicate a region of stretch between SHL 3.5 and 4.5, although this is less likely.

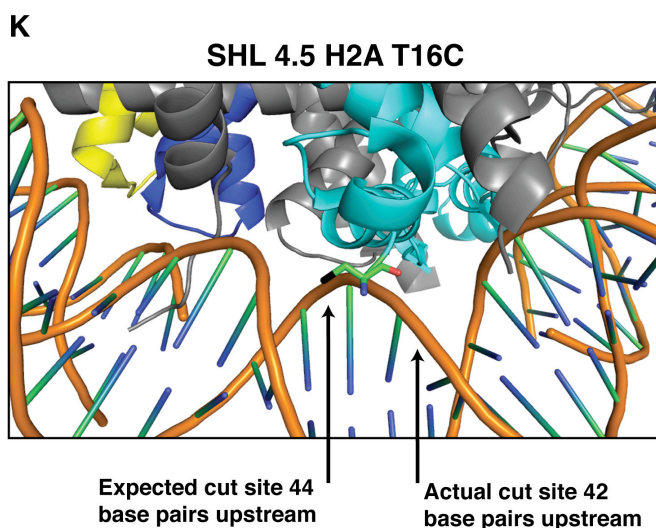


Figure 3.9 Nucleosome mapping at SHL 4.5 with EDTA and phenanthroline on NucA, 601 and 601.2. K. Phenanthroline mapping on NucA at SHL 4.5 H2A T16C demonstrates a shorter mapping distance of 9 bases from the previous mapping site at 3.5. This is due to the mutated cysteine and attached reagent adopting an altered orientation that directs hydroxyl radical cleavage 2 bases back downstream from the expected cut site. Cysteine residue of H2A is shown in green with the thiol group represented in black.

The secondary EDTA cuts on forward strand occur at 46 bases downstream, which is again 9 bases further along from the SHL 3.5 cut of 37 bases. The secondary phenanthroline cuts on the same strand occur at 44-46 bases downstream, which is 8-10 bases further along from the SHL 3.5 phenanthroline cuts.

The primary phenanthroline cuts on the reverse strand of NucA occur at 42-43 bases upstream of the dyad, which is 9-10 bases further along from the same cuts

at the SHL 3.5 position. The secondary EDTA cuts on the same strand occur at 46 bases downstream of the dyad, again 9 bases on from the same SHL 3.5 cuts. The secondary phenanthroline cuts occur at 44-46 bases, which is 10 bases on from the same cuts at SHL 3.5.

Both 601 sequences give an almost identical mapping pattern at the SHL 4.5 position suggesting no structural difference between the two sequences at this location. Primary phenanthroline mapping on both 601 sequences at SHL 4.5 occurs at 40-42 and 44 bases upstream of the dyad, which is 9-10 bases upstream of SHL 3.5 and consistent with the NucA mapping at this location.

The secondary EDTA cut on both 601 forward strands cuts at 46 bases downstream of the dyad, again 9 bases on from the previous SHL 3.5. The secondary phenanthroline cut on the forward strand maps with a double cut at 44-45 bases on the 601 and a triple cut at 44-46 bases on 601.2. However, these cleavage sites are very similar and open to different interpretations due to the difference in cutting intensity. These cuts are also 9 bases further along from the SHL 3.5 mapping sites.

The primary phenanthroline cuts on the reverse strand of the 601 sequences cleave at 41-43 bases upstream of the dyad. The secondary EDTA cuts on the same strands at 46 bases downstream of the dyad and the secondary phenanthroline maps at 43-45 bases downstream. These cleavage patterns also keeps in line with the shorter ~9 base distance between SHL 3.5 and 4.5. However, because the same pattern is seen in all three sequences it would suggest the shorter distance is not structurally significant and explained by the two mapping positions SHL 3.5 and SHL 4.5 being slightly closer together.

3.8 Nucleosome mapping at SHL 5.5

NucA, 601 and 601.2 nucleosomes were mapped at SHL 5.5 H2B G50C with EDTA and phenanthroline using Fe^{2+} to generate hydroxyl radicals.

3.8.1 Observations

Due to primer contamination in the negative controls it is difficult to clarify if any primary mapping occurs on the forward strand of NucA using either EDTA or phenanthroline, Figure 3.10 C, lanes 1-2 and 8-9.

There is also no clear primary mapping on the reverse strand of the NucA sequence due to primer contamination. However, there is evidence of additional cuts upstream of the dyad on the reverse strand of NucA. These additional cuts are located at 29-30 bases upstream of the dyad and are seen with EDTA and phenanthroline, Figure 3.10 D and F, lanes 8-9.

Definite mapping is observed for the secondary cuts on the NucA forward strand. These cuts occur at 56-57 bases downstream of the dyad for EDTA and at 55-56 bases downstream for phenanthroline. Additional cleavage is also noticed at 23-25 bases preceding these secondary cuts at 32-34 bases downstream of the dyad for EDTA and at 31-33 bases downstream of the dyad for phenanthroline, Figure 3.10 G and I, lanes 8-9.

Similar to the forward strand, secondary mapping occurs on the reverse strand of NucA at 56-57 bases downstream of the dyad for EDTA and at 54-56 bases downstream for phenanthroline, Figure 3.10 H and J, lane 8-9.

Possible EDTA primary cuts may occur on the forward strand of the 601 sequences at approximately 51-52 bases upstream, but these bands are hard to interpret due to primer contamination in the negative control. Phenanthroline does show primary mapping at 50-52 bases upstream on the forward strand of both 601 sequences, Figure 3.10 C and E, lane 10-13.

Secondary EDTA cuts are located at 55-57 bases downstream of the dyad on the forward strand of 601, while phenanthroline maps at 54-55 bases downstream of the dyad on the forward strand of 601, Figure 3.10 C and E, lanes 10-11.

The secondary cuts on the forward strand of 601.2 are located at 55-56 bases from the dyad for EDTA, while the phenanthroline cuts are located at 54-55 bases downstream of the dyad, Figure 3.10 C and E, lanes 12-13.

Possible primary EDTA cuts may occur on the reverse strands of both 601 sequences at 52 bases upstream, Figure 3.10 D and F, lanes 10 and 12. However, once again primary EDTA cutting is difficult to interpret due to the primer contamination in the negative control. Phenanthroline shows more evidence of primary cutting at 52 bases upstream of the dyad on the reverse strand for both 601 sequences, Figure 3.10 D and F, lanes 11 and 13.

The secondary cuts on the reverse strands of both 601 sequences are similar, occurring at 56-57 bases downstream of the dyad for EDTA and at 54-56 bases downstream of the dyad for phenanthroline, Figure 3.10 D and F, lanes 10-13.

Figure 3.10 A shows native gels of six nucleosomes: NucA, 601 and 601.2 with either EDTA or phenanthroline attached. DNA wrapping of the EDTA tethered octamer at SHL 5.5 H2B G50 seems to be perturbed. Figure 3.10 B shows four nucleosomes: wildtype, H2B G50C, tethered EDTA and tethered phenanthroline. Nucleosome formation with the wildtype and untethered mutant display greater DNA wrapping than the phenanthroline tethered mutant, which displays greater DNA wrapping than the EDTA tethered mutant.

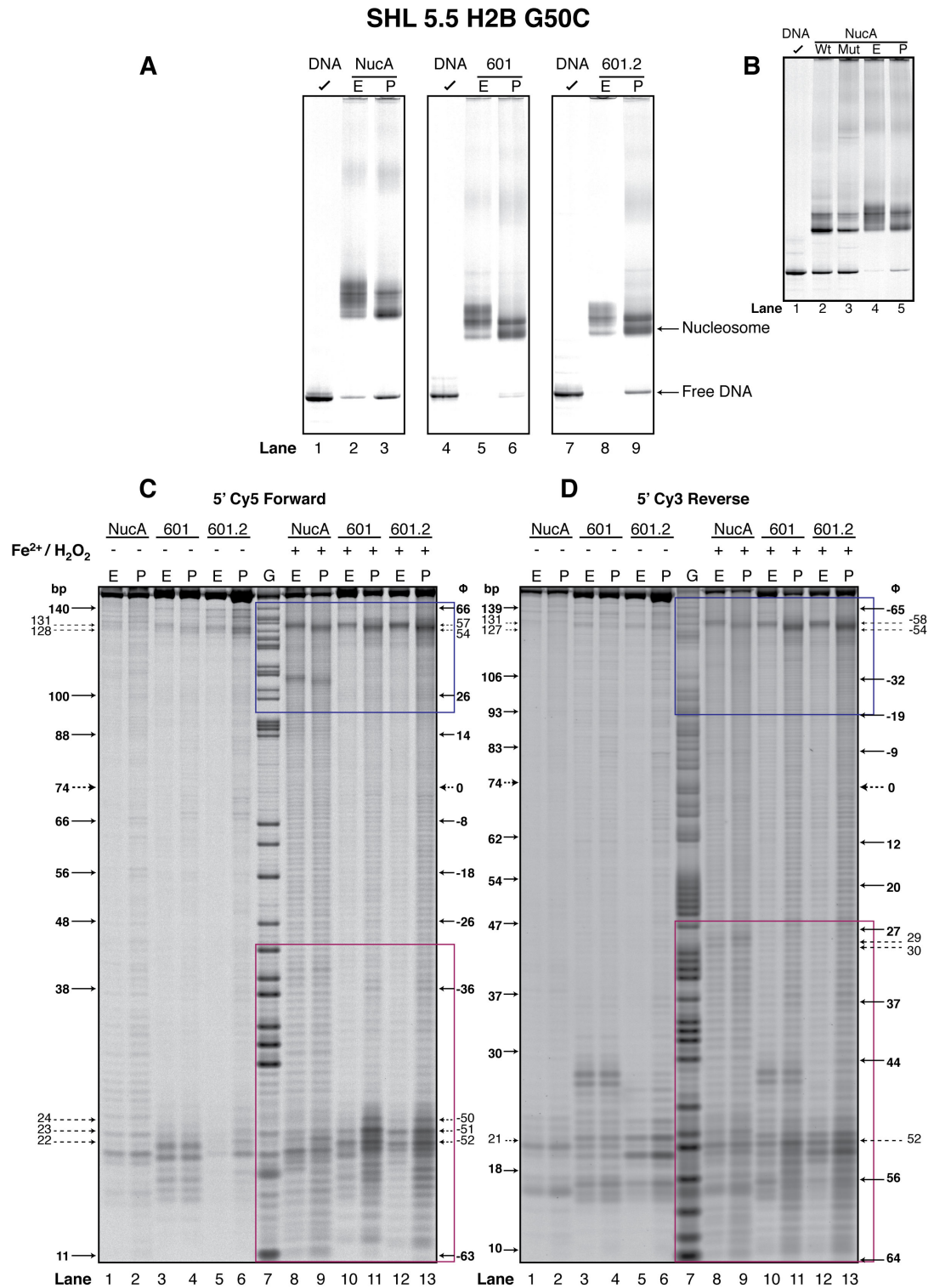


Figure 3.10 Nucleosome mapping at SHL 5.5 with EDTA and phenanthroline on NucA, 601 and 601.2. **A.** Native gels showing NucA, 601 and 601.2 nucleosomes with either EDTA or phenanthroline reagents attached. **B.** Native gel of 4 NucA nucleosomes, *Xenopus* wildtype (Wt), Untethered G50C (Mut), Tethered EDTA (E) and tethered phenanthroline (P). **C.** Denaturing PAGE of SHL 5.5 H2B G50C mapping on the forward strand of NucA, 601 and 601.2. **D.** Denaturing PAGE of mapping on the reverse strand of NucA, 601 and 601.2 nucleosomes. Magenta and purple boxes represent the respective regions of primary and secondary mapping analysed by signal quantification in Figure 3.10 E, F, I and J. (–) and (+) signs represent the respective absence and presence of Fe²⁺ at 1 ion/nucleosome and H₂O₂ in the mapping assays. The G-track marker (G) represents the NucA sequence cleaved at every guanine nucleotide. Fragment sizes are shown as full length (bp) and as distance from the dyad (Φ). Gels were visualised using the Fuji phosphor-imager FLA-5100.

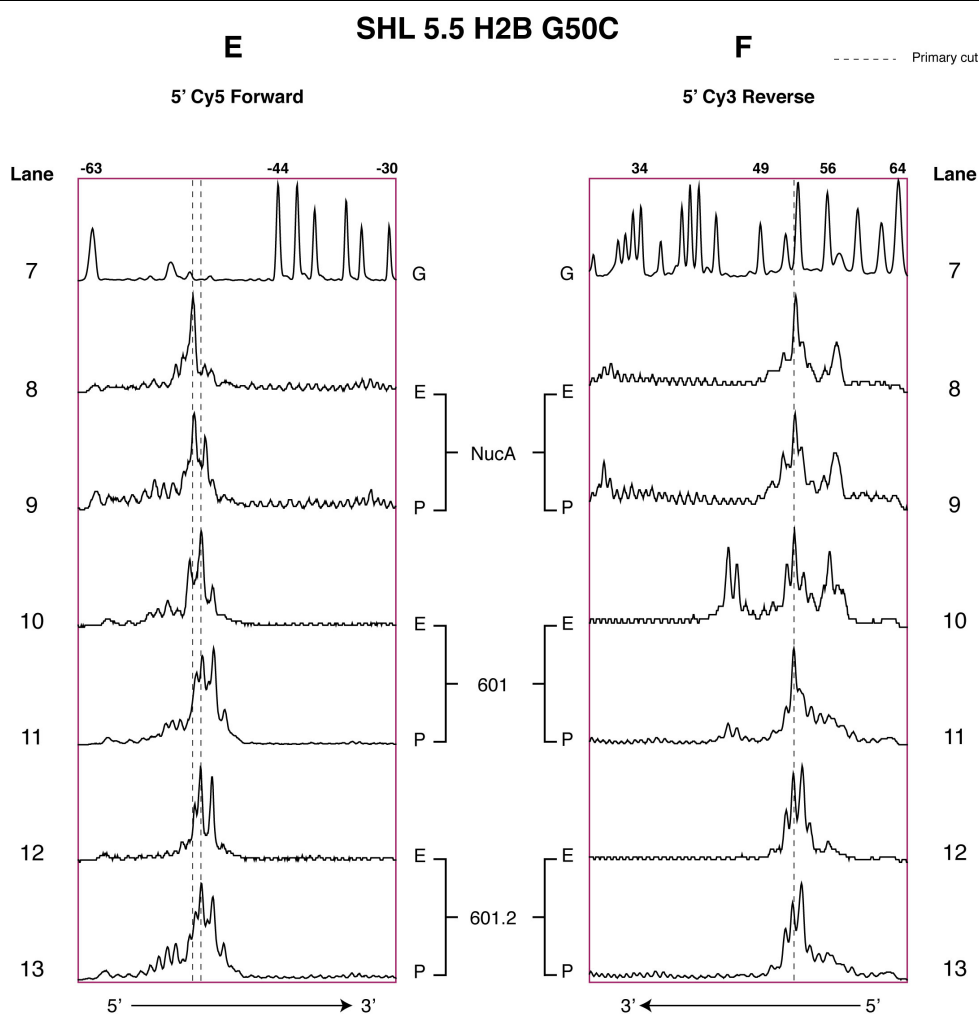


Figure 3.10 Nucleosome mapping at SHL 5.5 with EDTA and phenanthroline on NucA, 601 and 601.2. **E.** Signal profile of the primary mapping on the forward strand of NucA, 601 and 601.2 from Figure 3.10 C. **F.** Signal profile of the primary mapping on the reverse strand of the 3 DNA sequences at SHL 5.5 H2B G50C from Figure 3.10 D. (E) represents the EDTA derivative and (P) the phenanthroline derivative. The G-track marker (G) represents the NucA sequence cleaved at every guanine nucleotide. Numbers over the G-track peaks represent distances from the dyad in bases. Signal profile data taken from the magenta regions of Figure 3.10 C and D using AIDA analysis software.

SHL 5.5 H2B G50C

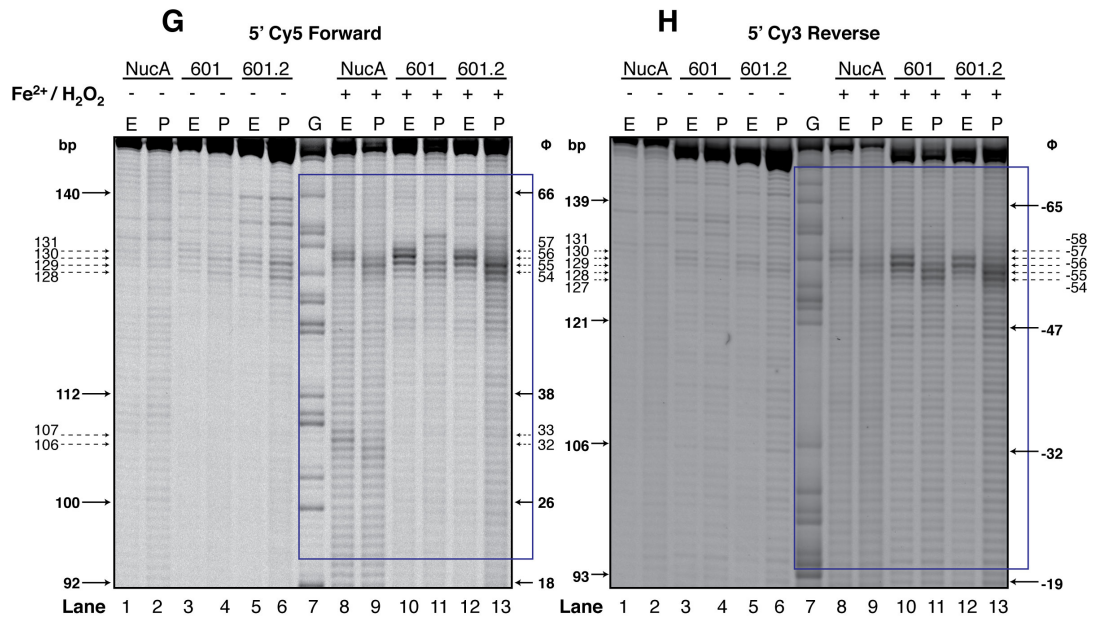
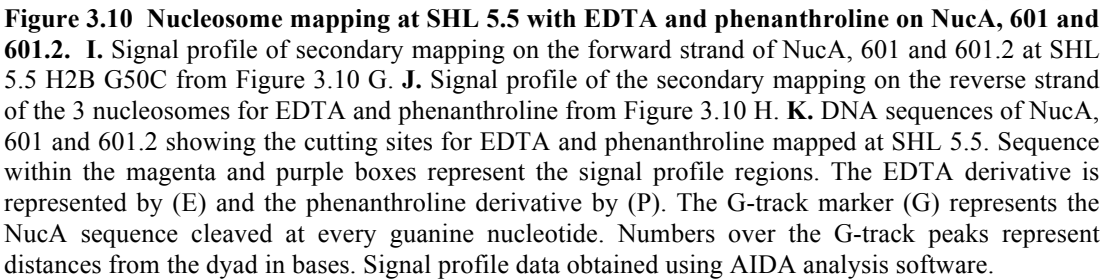


Figure 3.10 Nucleosome mapping at SHL 5.5 with EDTA and phenanthroline on NucA, 601 and 601.2. **G.** Denaturing PAGE of the secondary mapping on the forward strand of the 3 DNA sequences. **H.** Denaturing PAGE of the secondary mapping on the reverse strand of NucA, 601 and 601.2 nucleosomes at SHL 5.5 H2B G50C for EDTA (E) and phenanthroline (P). Purple boxes represent the region of signal quantification in Figure 3.10 I and J. (–) and (+) signs represent the respective absence and presence of Fe²⁺ at 1 ion/nucleosome and H₂O₂ in the mapping assays. The G-track marker (G) represents the NucA sequence cleaved at every guanine nucleotide. Fragment sizes are shown as full length (bp) and as distance from the dyad (φ). Gels were visualised using the Fuji phosphor-imager FLA-5100.



3.8.2 Interpretation

Primary mapping on the forward strand of NucA is difficult to interpret due to the primer contamination. Primer contamination probably occurs due to poor quality DNA purification and/or from the product of unligated primers to the DNA strand itself, which would only become evident after nucleosome mapping. It does seem that the primary EDTA gives little or no mapping and that the phenanthroline may produce some mapping at the primary site. However, due to the uncertainty it was decided to leave this position on NucA unmapped with no entry in Figure 3.10 K.

The secondary cuts on the forward strand show very obvious mapping, at 56-57 bases downstream for EDTA and at 55-56 bases downstream for phenanthroline. These sites are ~10 bases downstream from the SHL 4.5 mapping, indicating that the helical turn length has been restored. It possibly also shows that the SHL 4.5 mapping site was not effectively closer to the SHL 3.5 site due to the fact that there is not a greater distance than ~10 bases between SHL 4.5 and SHL 5.5. However, the distance between the secondary EDTA cuts of SHL 0.5 and SHL 5.5 is 51 bases, which is $(51/5)$ or 10.2 bp per helical repeat. This is very close to the accepted value of 10.17 bp per helical repeat, possibly ruling out the idea of a short helical repeat within this region.

As with the forward strand, primary cutting on the reverse strand of NucA is again difficult to interpret due to the primer contamination of the DNA. But it again appears that there is little or no primary mapping at this location. The secondary cuts on the reverse strand of NucA occur at 56-57 bases for EDTA and at 54-56 bases downstream of the dyad for phenanthroline. These cuts are approximately the same as the secondary cuts on the forward strand of NucA at SHL 5.5. They retain the same positional characteristics, and are in line with the dyad symmetry of that location.

No primary EDTA cleavage at SHL 5.5 on the forward strand of either 601 sequence is clear, again due to the DNA contamination at this location. Primary phenanthroline cleavage can be interpreted due to the intensity of the bands and these are located at 50-52 bases upstream of the dyad on the forward strands of both 601 sequences. At most, this is only 50 bases upstream of SHL 0.5 possibly suggesting

that the 601 sequences can tolerate shorter helical turns averaging 10 bp. However, the high background makes it difficult to draw a strong conclusion.

Secondary EDTA cuts on the forward strand of 601 occur at 55-57 bases downstream of the dyad. The secondary phenanthroline cuts on the same strand occur at 54-55 bases. This is 10 bases on from the previous SHL 4.5 site and 51 bases on from the SHL 0.5 position. Again, very close to the accepted value of 10.17 bp per helical repeat, possibly ruling out the idea of a short helical repeat within this region.

The secondary cuts on the forward strand of the 601.2 sequence occur at 55-56 bases for EDTA and at 54-55 bases downstream of the dyad for phenanthroline. This would imply 601.2 has the same structural characteristics at this location to 601, as expected.

Mapping patterns on the reverse strand of both 601 sequences are identical. No primary EDTA cleavage is observed, while the primary phenanthroline maps at 52 bases upstream of the dyad. Secondary cuts on the reverse strand of both 601 sequences occur at 56-57 bases downstream of the dyad for EDTA and at 53-55 bases downstream of the dyad for phenanthroline. This is 51 bases on from SHL 0.5 which gives an average helical repeat of 10.2 bp supporting the actual accepted value of 10.17 bp per helical turn.

The additional cuts observed ~23 bp upstream from the SHL 5.5 cuts are indicative of a NucA sub-population. It is possible this sub-population of NucA is more prominent due to the inferior wrapping displayed by the reagent tethered H2B G50C mutant.

3.9 Nucleosome mapping at SHL 6.5

NucA, 601 and 601.2 nucleosomes were mapped at SHL 6.5 H3 T45C with EDTA and phenanthroline using Fe^{2+} to generate hydroxyl radicals.

3.9.1 Observations

No primary or secondary cuts were observed on either strand of NucA using the EDTA reagent, Figure 3.11 B-G, lane 8. Faint mapping can be observed on the forward strand of NucA using phenanthroline, the primary cut occurring at 62-63 bases upstream of the dyad, with possible secondary occurred at ~70 bases downstream of the dyad, Figure 3.11 B and F, lane 9. Due to uncertainty at this secondary site, it is not recorded on the NucA sequence mapping, Figure 3.11 J and Figure 3.12.

Primary phenanthroline cuts on the reverse strand of NucA may occur at ~64 bases upstream of the dyad, but these are also very faint and are not registered as mapping sites on the NucA sequence, Figure 3.11 C lane 9. Secondary phenanthroline cuts on the reverse strand of NucA are clearly observed at 69-71 bases downstream of the dyad, Figure 3.11 C and G, lane 9.

No difference was observed in the mapping between 601 and 601.2 at SHL 6.5. The primary EDTA cleavage mapped at 62 bases and primary phenanthroline mapped at 61-63 bases upstream of the dyad on the forward strand. The secondary cuts on the forward strand occur at 68-69 bases for EDTA and at 70 bases downstream of the dyad for phenanthroline, Figure 3.11 B and F, Lane 10-13.

No obvious primary mapping occurred for EDTA on the reverse strand of either 601 sequence. Primary mapping was observed at 58-60 bases upstream of the dyad on the reverse strands using phenanthroline. Secondary cuts on the reverse strands occurred at 68-70 bases for EDTA and between 68-71 bases downstream of the dyad for phenanthroline, Figure, 3.11 C and G, lane 10-13.

Additional cleavage sites were observed at 37 bases downstream of the dyad on the forward strand of both 601 sequences using EDTA, Figure 3.11 B and F, lanes 10 and 12.

There were also additional cuts near the dyad of all three DNA sequences from this SHL 6.5 map. These cuts occurred at 6-7 bases upstream of the dyad on both forward and reverse strands of NucA with phenanthroline, Figure 3.11 B and C, lane 8. They also occurred at 5-6 bases and 6-7 bases upstream of the dyad on the forward strand of both 601 sequences for EDTA and phenanthroline respectively. On the reverse strand of both 601 sequences they also occurred at 5-6 bases and 6-7 bases upstream of the dyad for EDTA and phenanthroline respectively, Figure 3.11 B and C, lane 10-13.

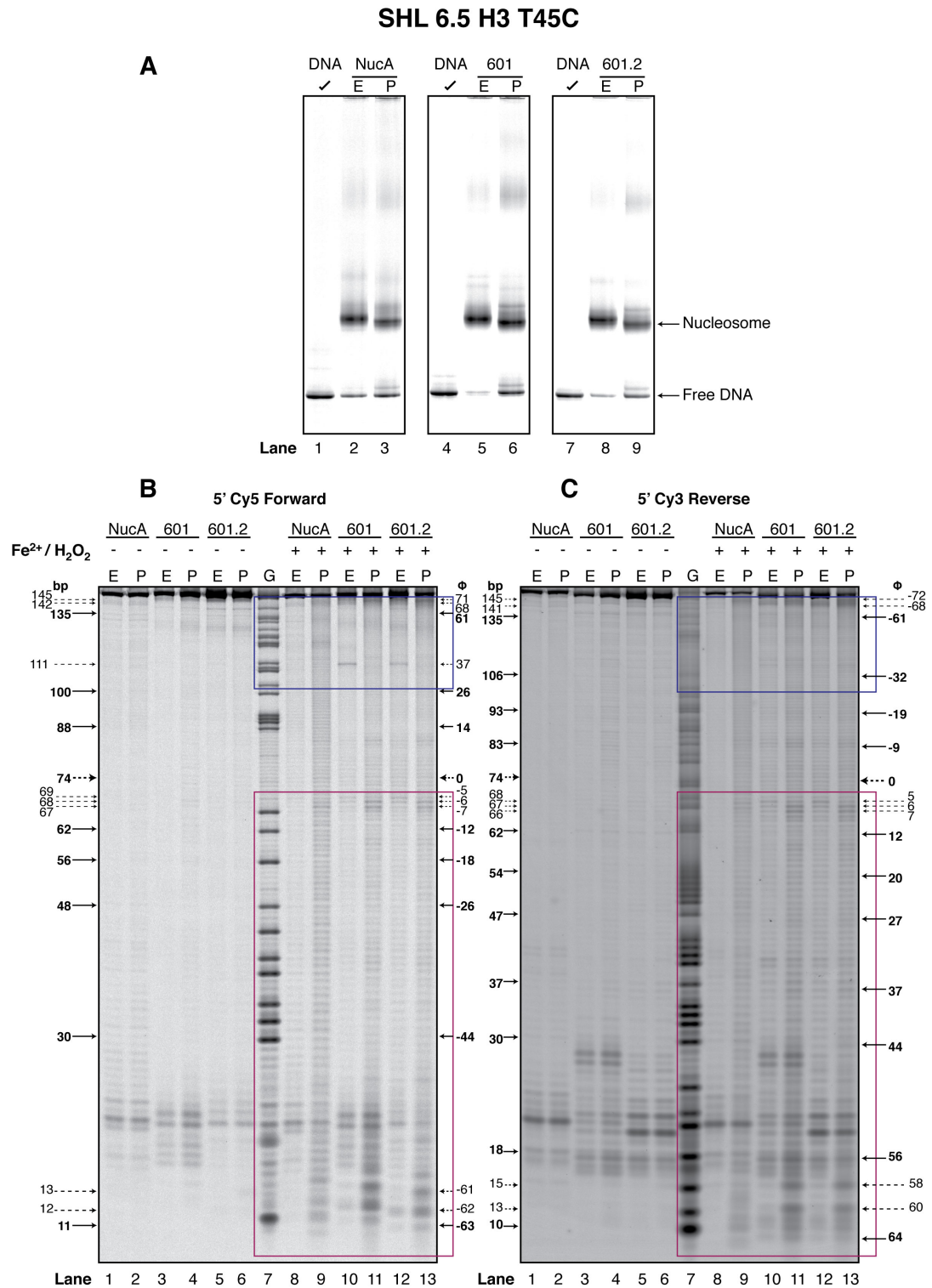


Figure 3.11 Nucleosome mapping at SHL 6.5 with EDTA and phenanthroline on NucA, 601 and 601.2. **A.** Native gels showing NucA, 601 and 601.2 nucleosomes with either EDTA or phenanthroline reagents attached. **B.** Denaturing gel showing forward strand mapping of the 3 nucleosomes at SHL 6.5 H3 T45C. **C.** Denaturing gel showing mapping on the reverse strand of NucA, 601 and 601.2 with EDTA and phenanthroline. Signal profiles for the magenta region are shown in Figure 3.11 D and E. The purple regions are further analysed in Figure 3.11 F, G H and I. (–) and (+) signs represent the respective absence and presence of Fe²⁺ at 1 ion/nucleosome and H₂O₂ in the mapping assays. The G-track marker (G) represents the NucA sequence cleaved at every guanine nucleotide. Fragment sizes are shown as full length (bp) and as distance from the dyad (ϕ). Gels were visualised using the Fuji phosphor-imager FLA-5100.

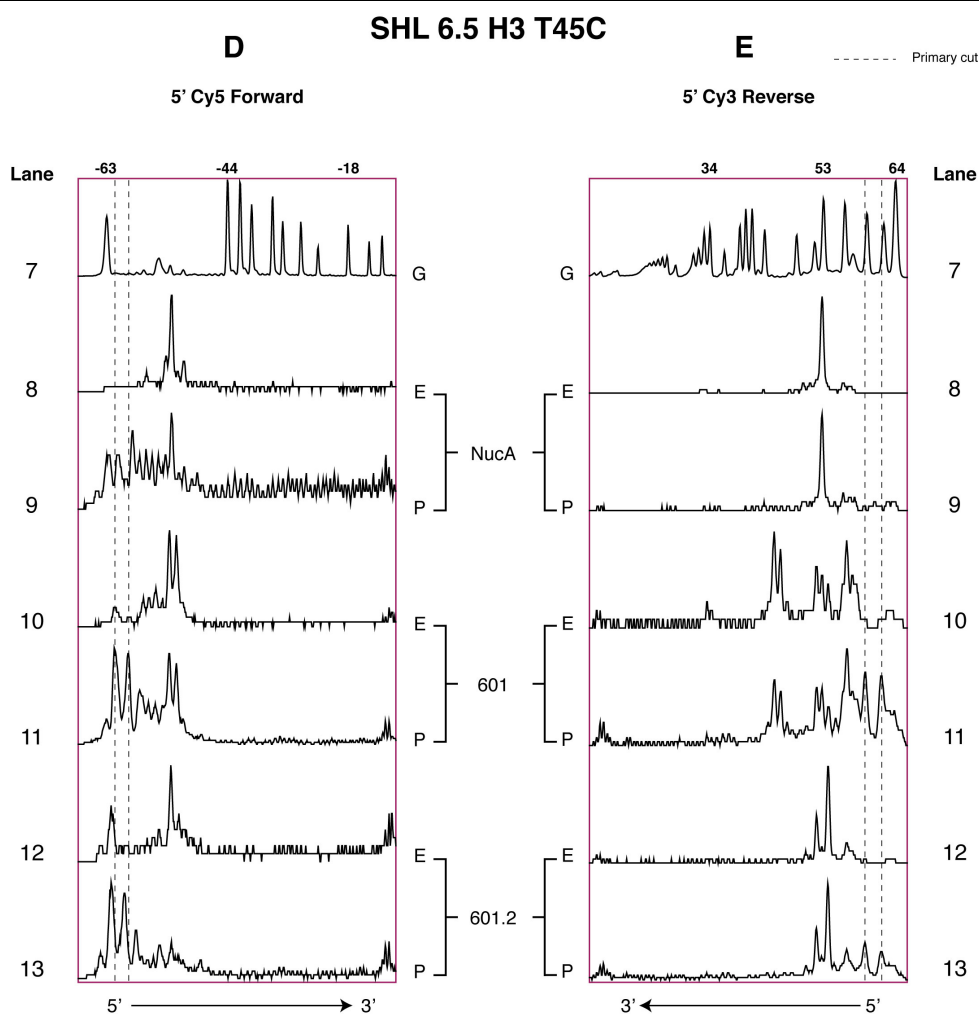


Figure 3.11 Nucleosome mapping at SHL 6.5 with EDTA and phenanthroline on NucA, 601 and 601.2. **D.** Signal profile of the primary mapping on the forward strand of NucA, 601 and 601.2 at SHL 6.5 H3 T45C for EDTA (E) and phenanthroline (P) from Figure 3.11 B. **E.** Signal profile of the primary mapping on the reverse strands of NucA, 601 and 601.2 nucleosomes at SHL 6.5 from Figure 3.11 C. The G-track marker (G) represents the NucA sequence cleaved at every guanine nucleotide. Numbers over the G-track peaks represent distances from the dyad in bases. Signal profile data taken from the magenta regions of Figure 3.11 B and C using AIDA analysis software.

SHL 6.5 H3 T45C

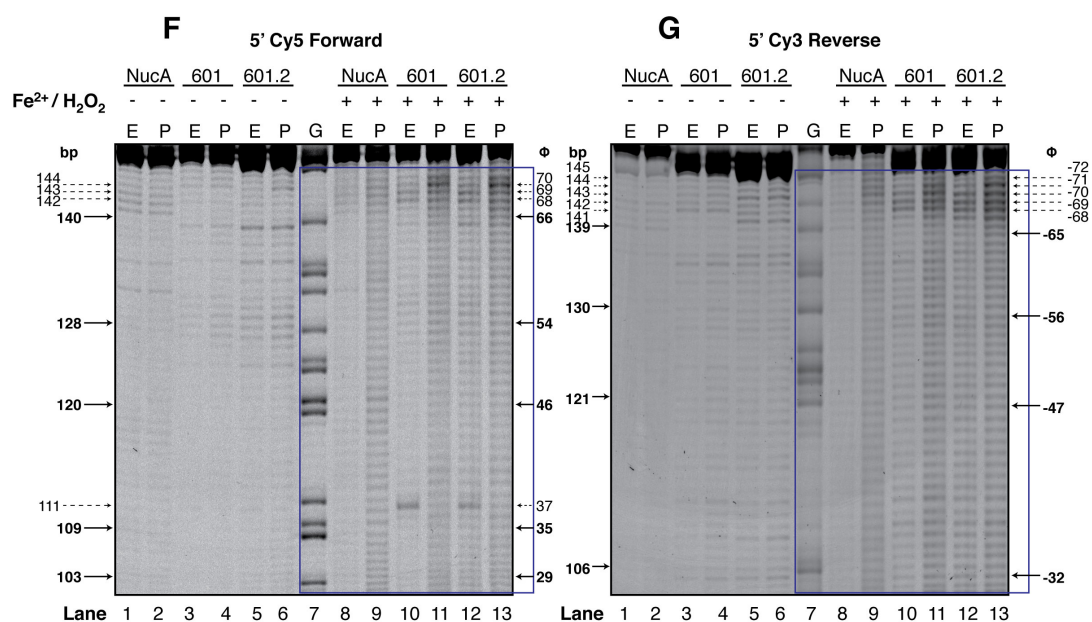


Figure 3.11 Nucleosome mapping at SHL 6.5 with EDTA and phenanthroline on NucA, 601 and 601.2. **F.** Denaturing PAGE showing the secondary mapping on the forward strand of NucA, 601 and 601.2 nucleosomes for EDTA and phenanthroline. **G.** Denaturing PAGE showing the secondary cuts on the reverse strands of the 3 DNA sequences at SHL 6.5 H3 T45. Signal profiles are represented in Figure 3.11 H and I. (-) and (+) signs represent the respective absence and presence of Fe^{2+} at 1 ion/nucleosome and H_2O_2 in the mapping assays. The G-track marker (G) represents the NucA sequence cleaved at every guanine nucleotide. Fragment sizes are shown as full length (bp) and as distance from the dyad (ϕ). Gels were visualised using the Fuji phosphor-imager FLA-5100.

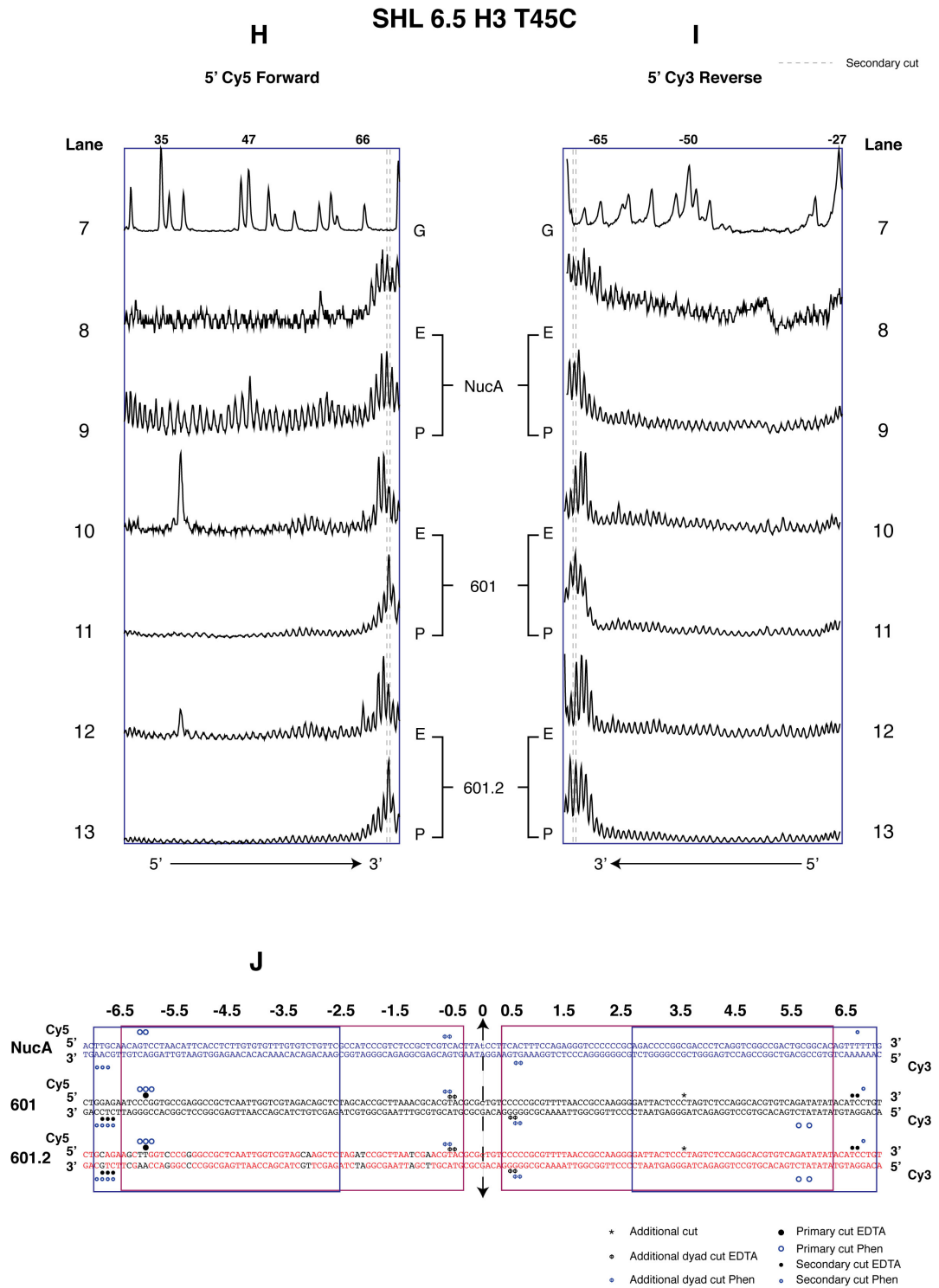


Figure 3.11 Nucleosome mapping at SHL 6.5 with EDTA and phenanthroline on NucA, 601 and 601.2. **H.** Signal profile of the secondary mapping on the forward strand of NucA, 601 and 601.2 from Figure 3.11 F. **I.** Signal profile of the secondary mapping on the reverse strand of NucA, 601 and 601.2 at H3 T45C with EDTA (E) and phenanthroline (P) from Figure 3.11 G. **J.** DNA sequences of NucA, 601 and 601.2 showing the SHL 6.5 cutting sites for EDTA and phenanthroline reagents tethered to H3 T45C. The G-track marker (G) represents the NucA sequence cleaved at every guanine nucleotide. Numbers over the G-track peaks represent distances from the dyad in bases. Signal profile data obtained using AIDA analysis software.

3.9.2 Interpretation

No mapping was observed on the NucA sequence using EDTA at SHL 6.5. This is potentially due to the NucA entry/exit DNA not being tightly wrapped to the octamer structure at this location.

The faint DNA cleavage seen at 62-63 bases upstream of the dyad using phenanthroline is probably due to phenanthroline having a more vigorous cleavage reaction compared to EDTA. The position of this cutting is only 60-61 bases upstream of the SHL 0.5 cut which is slightly less than 6 DNA helical turns. The sites are 20-21 bases upstream of the SHL 4.5 cleavage site, which would support the expected mapping at this location, at base pair resolution.

The secondary phenanthroline cleavage at this location occurs at 70 bases downstream of the dyad. This is 14 bases further on from the previous site and 66 bases on from SHL 0.5. This coordinate may be more accurate because it is read from a region of the gel with low background and where bands are clearly defined, although the mapping is very weak.

If mapping on the reverse strand of NucA using phenanthroline occurs at 64 bases upstream of the dyad, this is 21-22 bases on from SHL 4.5 and 62 bases on from SHL 0.5 which would be consistent with the helical turns of nucleosomal DNA. However, this mapping was also hard to interpret due to the low mapping efficiency and is not recorded on the NucA sequence cutting site summary, Figure 3.11 J and Figure 3.12.

The secondary phenanthroline cleavage on the reverse strand of NucA occurs between 69-71 bases. This is 14 bases on from the previous position, similar to the secondary cleavage on the forward strand. However, it is too large for a single helical turn between SHL 5.5 and SHL 6.5. This larger distance of 13-14 bp is probably due to the mapping site being closer to the N-terminal of the α -N helix of H3 than the exact centre of SHL 6.5.

The fact that no noticeable difference was observed in the mapping results between the 601 and 601.2 sequences suggests that the 4 base-pair changes at this location do not cause any significant structural differences in DNA wrapping.

Primary EDTA mapping on the forward strand of both 601 sequences occurs at 62 bases upstream of the dyad this is 28-29 bases upstream from the same cuts at SHL 3.5. This would suggest that 3 helical turns are covered by 28-29 bp, which seems too short. The same phenanthroline cuts cover 28-30 bp, working out similar to the EDTA result.

The secondary EDTA cuts on the forward strand of the 601 sequences occur at 68-69 bases, this is 31-32 bp further on from SHL 3.5. It is also 12-13 bp on from the same cuts at SHL 5.5. This greater distance comes from the position of the SHL 6.5 mapping location, which is probably a few residues further from the centre of the SHL 6.5 point of contact.

The secondary phenanthroline mapping on the forward strand of the 601 sequences occurs at 70 bases downstream of the dyad. This is 15-16 bp on from the previous phenanthroline cut at SHL 5.5. This larger, unexpected distance comes from phenanthroline mapping to the outside of the EDTA cuts at this location, whereas the majority of all other secondary phenanthroline cuts mapped to the inside (dyad side) of EDTA, Figure 3.12.

No significant primary mapping occurred on the reverse strands of either 601 sequence using EDTA, possibly due to EDTA not being orientated directly toward the reverse strand at this location.

Primary phenanthroline mapping on the reverse strands seem to occur at 58 bases and 60 bases upstream of the dyad. This is only 25-27 bases upstream of SHL 3.5, which again seems too short to cover 3 helical turns. The primary mapping at SHL 6.5 persistently displays coordinates that would suggest the data is interpreted incorrectly. The reason for this is because primary mapping at SHL 6.5 produces very short DNA fragment that do not resolve accurately and are difficult to interpret especially with the high background levels occurring in the denaturing gel. Therefore the primary mapping coordinates at SHL 6.5 do not appear in Figure 3.12.

The secondary cuts on the reverse strand of both 601 sequences occur at 68-70 bases for EDTA and at 68-71 bases downstream of the dyad for phenanthroline. This is positionally similar to the same cuts on the forward strand. However, the mapping at this position incorporates more base pairs, with 1 extra EDTA cut and 3

extra phenanthroline cuts registered. This could suggest DNA dynamics such as breathing or twisting within the DNA at this location.

The additional EDTA cleavage sites on the forward strand of both 601 sequences occur at 37 bases downstream of the dyad at approximately SHL 3.5 and 31-32 bases from the actually SHL 6.5 mapping site. This raises the interesting possibility that dynamics within α N helix of H3 are possible. The additional cuts seen near the SHL 0.5 are consistent with the H3 α N helix positioning itself between the DNA at the entry/exit and center of the nucleosome.

3.10 Compiled Data from SHL 0.5 to SHL 6.5

NucA, 601 and 601.2 nucleosomes were mapped at seven helical turns SHL 0.5 to SHL 6.5 with EDTA and phenanthroline using Fe^{2+} to generate hydroxyl radicals. The resulting data was compiled into a complete mapping profile of the three nucleosomes, Figure 3.12.

3.10.1 Results

The NucA nucleosome is observed from over 80 mapping locations using both EDTA and phenanthroline. This value does not include 14 additional or unexpected cuts that occurred throughout the nucleosome at various locations. The 80 mapping sites occurred on 59 separate bases and include 11 primary and 20 secondary cuts using EDTA, and 18 primary and 31 secondary cuts using phenanthroline. The forward and the reverse strands of NucA were cut at 28 and 31 separate locations respectively, Figure 3.12.

The 601 nucleosome is observed from over 92 locations using both EDTA and phenanthroline. This value excludes the 9 additional or unexpected cuts that occurred throughout the nucleosome. The 92 mapping sites occurred at 73 separate bases and include 11 primary and 26 secondary cuts using EDTA, and 24 primary and 31 secondary using phenanthroline. The forward and the reverse strands of 601 were cut at 37 and 36 separate locations respectively, Figure 3.12.

The 601.2 nucleosome is observed from over 93 locations using both EDTA and phenanthroline, excluding the 9 additional or expected cut sites that occurred throughout the 601.2 nucleosome. The 93 mapping sites occurred at 73 separate bases and include 11 primary and 25 secondary cuts using EDTA, and 24 primary and 33 secondary cuts using phenanthroline. The forward and reverse strands of 601.2 were cut at 36 and 37 separate locations respectively, Figure 3.12.



3.11 Discussion

The overall aim of this work was to obtain a complete mapping profile of NucA, 601 and 601.2 nucleosomes in solution using hydroxyl radicals from EDTA and phenanthroline mapping reagents. The complete mapping profile of the in solution nucleosomes can then be compared against each other and also against the static nucleosome crystal structures.

For this chapter on complete nucleosome mapping each nucleosome was mapped from each super helical location (SHL) at least two times, except for five of the six SHL 6.5 mapped nucleosomes and the 601 nucleosome at SHL 0.5. Table 3.1 shows the number of times each nucleosome was mapped for each mapping reagent and positioning sequence.

Nucleosome mapping repetitions			
SHL	Reagent	Nucleosome	Mapped
0.5 H4 S47C	EDTA	NucA	>3
		601	1
		601.2	2
	Phenanthroline	NucA	2
		601	1
		601.2	2
1.5 H4 T30C	EDTA	NucA	>3
		601	2
		601.2	2
	Phenanthroline	NucA	2
		601	2
		601.2	2
2.5 H3 D81C	EDTA	NucA	>3
		601	2
		601.2	2
	Phenanthroline	NucA	2
		601	2
		601.2	2
3.5 H2B T85C	EDTA	NucA	>3
		601	2
		601.2	2
	Phenanthroline	NucA	2
		601	2
		601.2	2
4.5 H2A T16C	EDTA	NucA	>3
		601	2
		601.2	2
	Phenanthroline	NucA	2
		601	2
		601.2	2
5.5 H2B G50C	EDTA	NucA	>3
		601	2
		601.2	2
	Phenanthroline	NucA	2
		601	2
		601.2	2
6.5 H3 T45C	EDTA	NucA	2
		601	1
		601.2	1
	Phenanthroline	NucA	1
		601	1
		601.2	1

Table 3.1 Number of times mapping was performed for each nucleosome

3.11.1 Reagents and DNA cutting

The single base pair difference observed in secondary mapping between the two reagents was unexpected, as were the similarities Cu^{2+} and Fe^{2+} showed when used in conjunction with phenanthroline, Figure 3.4 B.

Cu^{2+} had no significant DNA cleavage when used in conjunction with the EDTA reagent, Figure 3.4 B. These differences would suggest that both EDTA and phenanthroline cleave DNA through different chemical pathways. The chemical structure of the EDTA and phenanthroline reagent are shown in Figure 3.13.

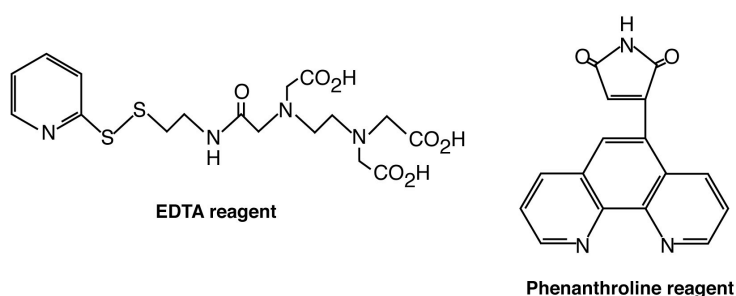


Figure 3.13 Chemical structure of mapping reagents. N-[S-(2-pyridylthio)cysteaminy] ethylene diamine - N,N,N',N'-tetraacetic acid, (EDTA reagent) and 1,10 phenanthroline-5-maleimide, (phenanthroline reagent).

DNA cleavage using EDTA/ Fe^{2+} occurs via the Fenton reaction. EDTA/ Fe^{2+} with H_2O_2 produces the highly reactive hydroxyl radical ($\cdot\text{OH}$), which abstracts the hydrogen from the most accessible deoxyribose carbon leading to DNA backbone cleavage. Diffusible $\cdot\text{OH}$ preferentially cleaves the DNA backbone at the 5' and 4' deoxyribose carbons over that of the 3', 2' and 1' deoxyribose carbons, which are buried in the minor groove (Pogozelski and Tullius, 1998).

The proposed mechanism for DNA cleavage by phenanthroline in conjunction with copper is abstraction of the hydrogen from 1' deoxyribose carbon resulting in DNA backbone cleavage. The identity of the oxidising species is uncertain. Hydroxyl radicals are possible but it is more likely to be a copper bound oxidant such as $[\text{CuO}]^{2+}$ or CuO_2H . Cleavage at the 1' deoxyribose carbon is due to phenanthrolines preference for positioning itself in the DNA minor groove (Pogozelski and Tullius, 1998).

Little is known about the chemistry of DNA cleavage for phenanthroline in conjunction with Fe^{2+} . However, the mechanism of cleavage is probably diffusible hydroxyl radical abstraction of the hydrogen at the 3', 2' or 1' deoxyribose via the Fenton reaction. This produces the same cleavage pattern as Phen/ Cu^{2+} seemingly due to the deoxyribose carbons' impartial preference for either a hydroxyl radical or copper bound oxidant.

The different chemistry and mapping patterns displayed by the EDTA and phenanthroline reagents could become quite significant when designing mapping experiments whether *in vitro* or endogenous in nature. For example, due to endogenous levels of Cu^{2+} and Fe^{2+} it may be more beneficial to use EDTA for *in vivo* mapping due to the lack of DNA cleavage associated with EDTA/ Cu^{2+} . Also the higher efficiency displayed by phenanthroline mapping over that of the EDTA mapping makes phenanthroline mapping a more attractive tool. However, phenanthroline sometimes displays two regions of cutting within a single minor groove, which could hinder the interpretation of data, Figures 3.6-3.8.

3.11.2 NucA sequence nucleosome mapping

Mapping data from the NucA nucleosome suggests that it is dyad symmetric due to the regularity in mapping positioning at either side of the dyad, Figure 3.12. This result was expected and is consistent with the static crystal structures (Luger et al., 1997; Vasudevan et al., 2010).

The quantity of DNA cleavage towards the outer regions of the NucA nucleosome has a decreasing trend, Figure 3.12. As this observation was not as pronounced in both 601 sequences it is possible that this is a consequence of nucleosome breathing.

Short ~9 bp helical turns are observed between SHL 3.5 and SHL 4.5 on both sides of the NucA nucleosome, Figure 3.12. This could possibly indicate a stretch region at this location. However, crystal structures to date have only shown stretch regions at SHL ± 2 and SHL ± 5 (Tan and Davey, 2011). This may suggest that our SHL 4.5 mapping site was chosen too close to the SHL 3.5 site, although the helical pitch from SHL 4.5 to SHL 5.5 is only 10-11 bp, Figure 3.12.

The additional cutting observed between SHL 2.5 and SHL 3.5 on the NucA nucleosome when mapped from SHL 5.5 demonstrates a second nucleosome population, Figure 3.10 C and G, lane 8 and 9. This sub-population is centered 23 bp further upstream from the major NucA position. This second population was also observed in Chapter 4, Figures 4.2 and 4.18 centered at 156 and 105 respectively.

The additional cuts observed around the dyad from the mapping at SHL 6.5 H3 T45 on the α N-helix would suggest that the entry/exit DNA, the H3 α N-helix and center of the nucleosome are in close proximity, Figure 3.11.

3.11.3 601 sequences nucleosome mapping

Both 601 and 601.2 sequences are almost identical in their observed mapping, Figure 3.12. This indicates that the 12 base changes made to the 601.2 sequence does not significantly change its overall nucleosome structure.

As for the NucA nucleosome, both 601 and 601.2 sequences also show complete dyad symmetry, Figure 3.12. This is consistent with the 601 crystal structure (Vasudevan et al., 2010).

A greater number of mapping sites are observed on the outer parts of the 601 and 601.2 nucleosomes compared to NucA, Figure 3.12. This would indicate that the 601 and 601.2 nucleosomes are less dynamic than the NucA nucleosome.

As with NucA mapping, a stretch region was observed between SHL 3.5 and SHL 4.5 during the *in vitro* mapping of both 601 and 601.2 sequences. This ~9 bp span between minor groove contact points is at least 1 bp shorter than typical helical pitches, Figure 3.2. The stretch region in the 601 crystal structure is located between SHL 4.5 and SHL 5.5 (Vasudevan et al., 2010). Therefore this result could possibly indicate that the cysteine mutation at SHL 4.5 is too close to the SHL 3.5 site, deeming this observation insignificant.

3.11.4 NucA versus 601

Only minor differences were observed between the NucA and both 601 and 601.2 nucleosomes. All nucleosomes demonstrated dyad symmetry and there were no indications of any configurational differences between nucleosomes, Figure 3.12.

Differences that were observed between the mapped nucleosomes come mainly from the outer locations at SHL 5.5 and SHL 6.5. These locations demonstrate less cleavage intensity for the NucA nucleosome over that of either 601 sequence. This would suggest that dynamics at the extremities of the NucA are greater than that of either 601 sequence.

Another difference between NucA and 601 nucleosomes is the additional mapping that occurs at SHL 5.5 and SHL 6.5. These are observed 23 bases upstream of the SHL 5.5 site on the NucA nucleosome but are absent in both 601 nucleosomes. These cuts are explained by a second nucleosome population that exists on the NucA 147 bp sequence possibly caused by a slight reduction in the NucA positioning due to the reagent attachment.

Also, additional cutting is observed ~31 bp upstream of the actual SHL 6.5 site on the forward strand of both 601 sequences using EDTA, which are not observed in the NucA sequence. These additional sites could be caused by dynamics of the α N helix of H3, although it is uncertain why these do not occur for the NucA nucleosome.

3.11.5 In solution nucleosomes versus crystal structures

No conformational differences were observed between the in solution mapping of NucA, 601 and 601.2, Figure 3.12. However, it is possible and likely that differences exist between the structures that are beyond the scope of resolution of what site-directed mapping can offer and that can only be determined by crystal structures. Also, it is probable that slight conformation differences exist between nucleosomes in solution and static nucleosome crystal structures. However, taken together our data suggests structural consistency between nucleosomes in solution and nucleosome crystal structures.

Chapter 4 Nucleosome Sliding

4.1 Introduction

Nucleosome sliding is a process whereby nucleosomes mobilise along a length of DNA from one position to another without dissociation. This process can be achieved actively with ATP dependent remodelers or passively at elevated ionic strength and/or temperature. The exact mechanism behind nucleosome sliding is poorly understood and two main explanations have been proposed: twist defect diffusion and loop defect diffusion.

To investigate the mechanism(s) behind nucleosome sliding we thermally slid a range of different nucleosomes at various temperatures and mapped them using the site-directed mapping technique with EDTA reagent attached at SHL 0.5-6.5. If mapping patterns were observed that demonstrated nucleosome populations were separated by multiples of ~10 bp this would support the loop defect diffusion mechanism of sliding. However, if single base pair steps were observed between nucleosome populations this would provide support for a twist defect mechanism of nucleosome sliding.

Mapping the sliding nucleosome from SHL 0.5-6.5 would give a better understanding of the dynamics associated to each location of the nucleosome during sliding. For example, if no mapping was observed from the outer positions of the nucleosome this would indicate that less than 147 bp are attached to the nucleosome during sliding. Also if no mapping was observed from positions SHL 3.5-5.5 this could indicate loosening of the H2A/H2B dimer during sliding. Furthermore, nucleosomal dyad symmetry enables the observation of sliding dynamics from both sides of the nucleosome.

Due to changes in the DNA fragment length products from mapping at SHL 0.5-6.5 nucleosome populations will be identified based on their position relative to the nucleosome dyad and not on the size of the DNA product after mapping. For example a nucleosome with its dyad base pair at the 151st bp along a positioning sequence is known as a 151-centered nucleosome. This 151-centered population

produces different length DNA fragments when mapped at each of the SHL sites although the nucleosome has not shifted from the 151-centered position.

As with the nucleosome mapping in the previous chapter distances between primary and secondary mapping for consecutive SHL positions will increase by approximately 20 bp. This is due to the relationship between the nucleosome dyad symmetry and the helical repeat length of DNA/octamer binding.

4.2 Nucleosome sliding on 601.2

To investigate nucleosome sliding on the 601.2 positioning sequence we incubated nucleosomes containing the 219 bp 54(601.2)18 DNA fragment at 0-60 °C for 60 minutes. These nucleosomes were then mapped using EDTA at SHL 0.5 H4 S47C.

The 5' Cy5 labelled 219 bp fragment contains the 147 bp 601.2 nucleosome positioning sequence that is flanked upstream and downstream by 54 and 18 bp respectively. From the initially positioned nucleosome, the expected DNA fragment sizes from mapping from SHL 0.5 would be 2 bp upstream and 5-6 bp downstream of the dyad for the primary and secondary cutting respectively. Therefore the DNA fragments should be $(54+74-2)=126$ bp, $(54+74+5)=133$ bp and $(54+74+6)=134$ bp.

To keep consistent numbering from SHL 0.5 to 6.5 nucleosome positions are described in relation to the dyad base pair at that particular position and not in relation to the size of DNA fragments produced. So before sliding the 54(601.2)18 nucleosome population is centered at $(54+74)$ 128 bp.

4.2.1 Observations

Relatively little sliding was observed on the 601.2 nucleosome after incubation at 0-60 °C for 60 minutes. From the native PAGE in Figure 4.1 A, two nucleosome populations can be identified at 0 °C while three populations are observed at higher temperatures. This additional band noticed at the higher temperatures suggests nucleosome sliding has occurred although this was not profound.

The denaturing gel in Figure 4.1 B shows the mapping positions at SHL 0.5 for the nucleosome populations incubated between 0-60 °C for 60 minutes. The main cut on this gel is at 126 bases, which is 2 bases upstream from the expected dyad position at 128 bp. Faint bands on this gel suggest a second minor population of nucleosomes that are centered at 119 bp and this population is observed in all mapped samples. Another minor population of nucleosomes are observed centered at 148 bp although this population is only visible at the higher temperatures.

4.2.2 Interpretation

Two populations of nucleosomes observed at all temperatures indicate that the 54(601.2)18 DNA fragment is capable of forming separate nucleosome populations at low temperature and ionic strength. The dominant population as expected is centered on the 601.2 sequence at 128 bp, a second minor population is centered 9 bp upstream of the main population at 119 bp.

A third population appearing after incubation at high temperatures (45-60°C) could suggest that a small portion of either of the two initially positioned nucleosomes are capable of sliding. Figure 4.1 C shows that the abundance of nucleosome sliding from either the 128 or 119 to the 148 population is extremely low. Also the minor populations centered 9 bases upstream and 20 bases downstream are approximately shifted 1 and 2 helical turns from the dominant 128 population respectively.

The 601.2 nucleosome is not ideal for looking at the mechanism of thermal mobilisation of nucleosomes due to the high temperatures needed and difficulty in observing low occupancy intermediates on what is already a short range and inefficient sliding reaction.

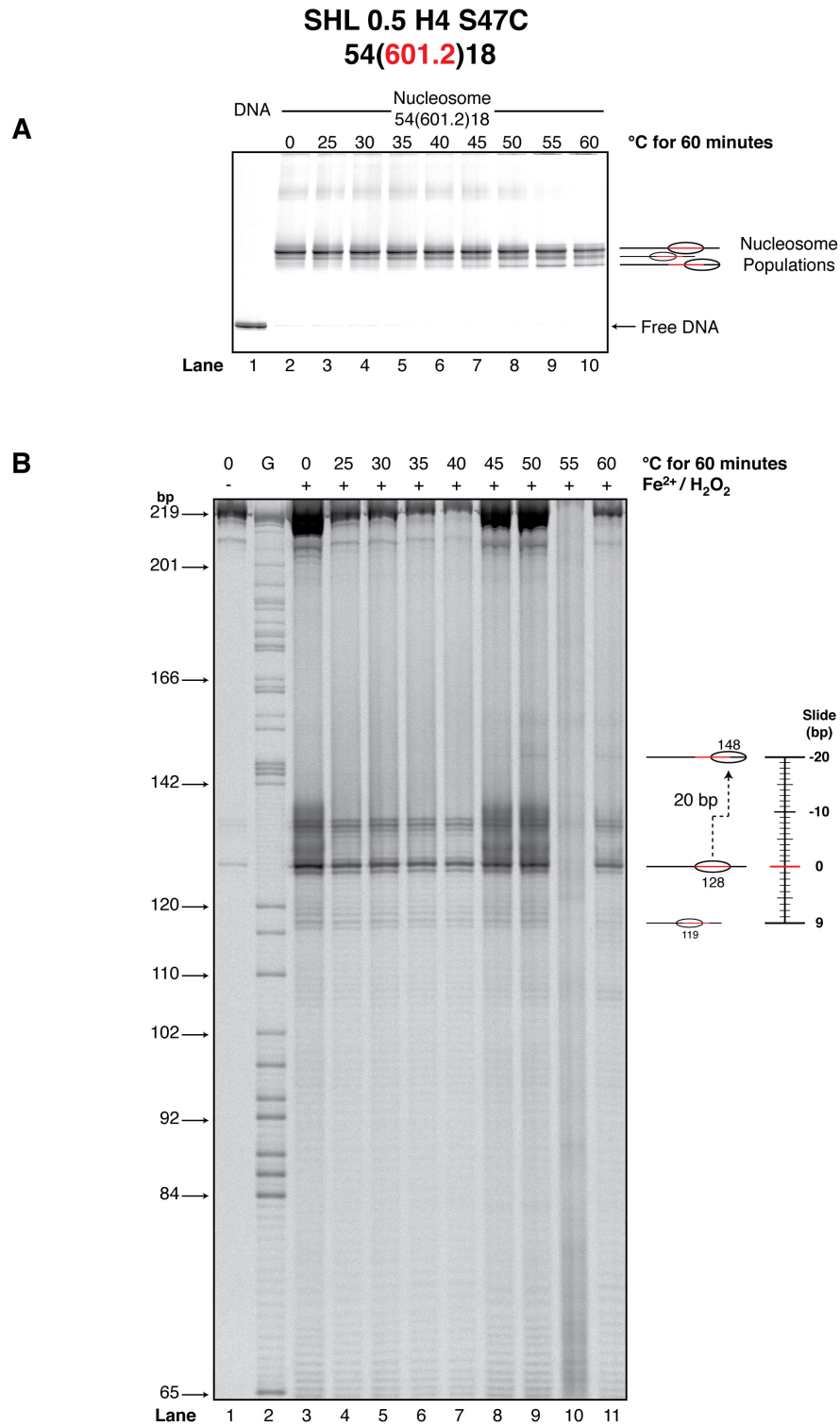


Figure 4.1 Thermal sliding of the 601.2 nucleosome mapped at SHL 0.5. **A.** Native PAGE of nucleosomes containing the 601.2 sequence incubated at 0-60 °C for 60 minutes. **B.** Denaturing PAGE of 54(601.2)18 nucleosomes incubated at 0-60 °C for 60 minutes and mapped at SHL 0.5 with EDTA reagent. (–) and (+) signs represent the respective absence and presence of Fe²⁺ at 1 ion/nucleosome and H₂O₂ in the mapping assays. The G-track marker (G) represents the 105(NucA)-31 DNA sequence cleaved at every guanine nucleotide, fragment size is given in base pairs (bp). Nucleosome positions are given in relation to the central dyad base pair. Gels were visualised using the Fuji phosphor-imager FLA-5100.

SHL 0.5 H4 S47C
54(601.2)18

C

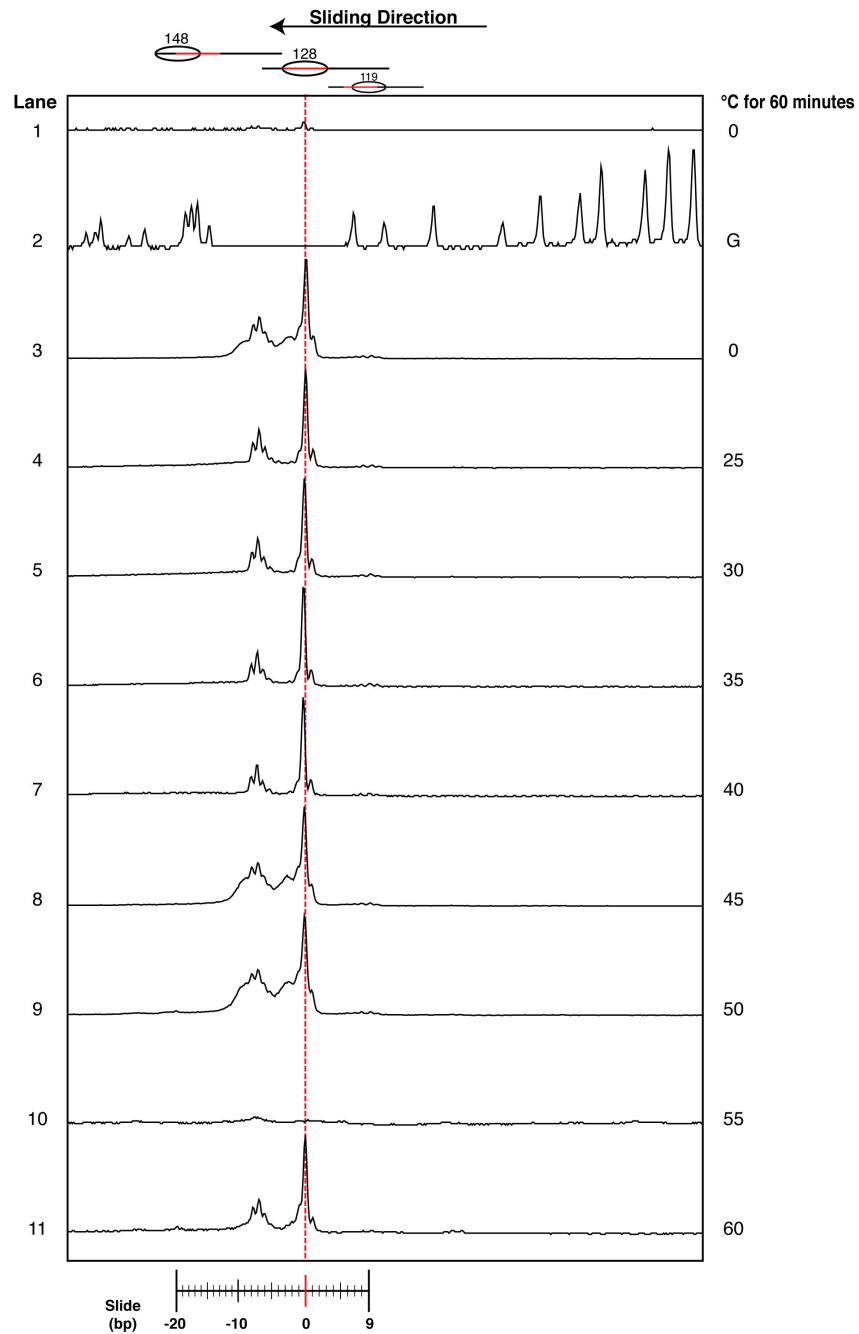


Figure 4.1 Thermal sliding of the 601.2 nucleosome mapped at SHL 0.5. C. Signal profile of 54(601.2)18 nucleosomes incubated at 0-60 °C for 60 minutes and mapped at SHL 0.5 using EDTA. The red broken line indicates the initial position of the 601.2 nucleosome centered at 128 bp. Signal profile data taken from Figure 4.1 B using AIDA analysis software.

4.3 Nucleosome sliding on NucA

To investigate nucleosome sliding on the NucA positioning sequence we incubated nucleosomes containing the 252 bp 105(NucA)0 DNA fragment at 0-60°C for 60 minutes. These nucleosomes were then mapped at SHL 0.5 H4 S47C using the EDTA reagent. Initially the DNA fragment used was 54(NucA)18 but this produced little intermediate positioning so it was not ideal for looking at nucleosome positioning. Initial nucleosome populations on the DNA fragment 105(NucA)0 are centered at $(105+74)=179$ bp.

4.3.1 Observations

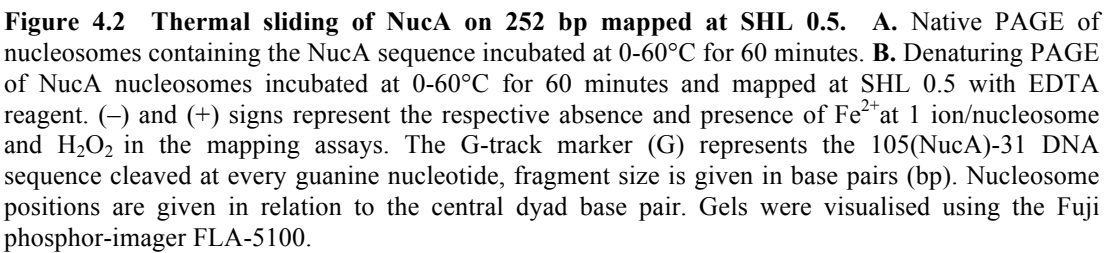
The main nucleosome population was centered at 179 bp as expected. However, other minor populations are also present including 156 bp, 131 bp, 93 bp and 85 bp centered nucleosomes, Figure 4.2. The main 179 bp centered nucleosome persists up to ~40°C. At higher temperatures the majority of this population slides 94 bp to have a nucleosome center at 85 bp. Some intermediate positioning is observed between 156 and 131, these include positions at 151, 148 and 136. The native PAGE in Figure 4.2 A shows a nucleosome population that migrates higher on the gel than the major populations at 179 and 85. This population is observed in all nucleosome samples of the native PAGE but is not observed in the denaturing gel.

4.3.2 Interpretation

The fact that the NucA positioned nucleosome only begins to slide at temperatures $\geq 40^\circ\text{C}$ (Figure 4.2 A) makes it a relatively stable nucleosome that requires high thermal energy to activate sliding. The relatively few intermediate populations between the major initial population 179 and end population 85 would suggest that the activating energy is too high for substantial intermediate populations to exist. Therefore using one of the less stable intermediate positions on this DNA fragment as the initial nucleosome position would give rise to a nucleosome population requiring less thermal energy to initiate nucleosome sliding. This would then lead to an increase in the number of intermediate positions occupied by

nucleosomes over the sliding region. An increase in intermediate positioning should therefore allow greater insight into the path nucleosomes take during sliding.

The high migrating nucleosome population observed in the native gel is probably due to the binding of additional histone complexes to the free linker DNA. However, from the denaturing gel there is no obvious signs of this additional complex producing any DNA cleavage due to hydroxyl radical cleavage from the EDTA/Fe²⁺ at H4 S47C, suggesting that the additional complex could be a H2A/H2B dimer.



SHL 0.5 H4 S47C
105(NucA)0

C

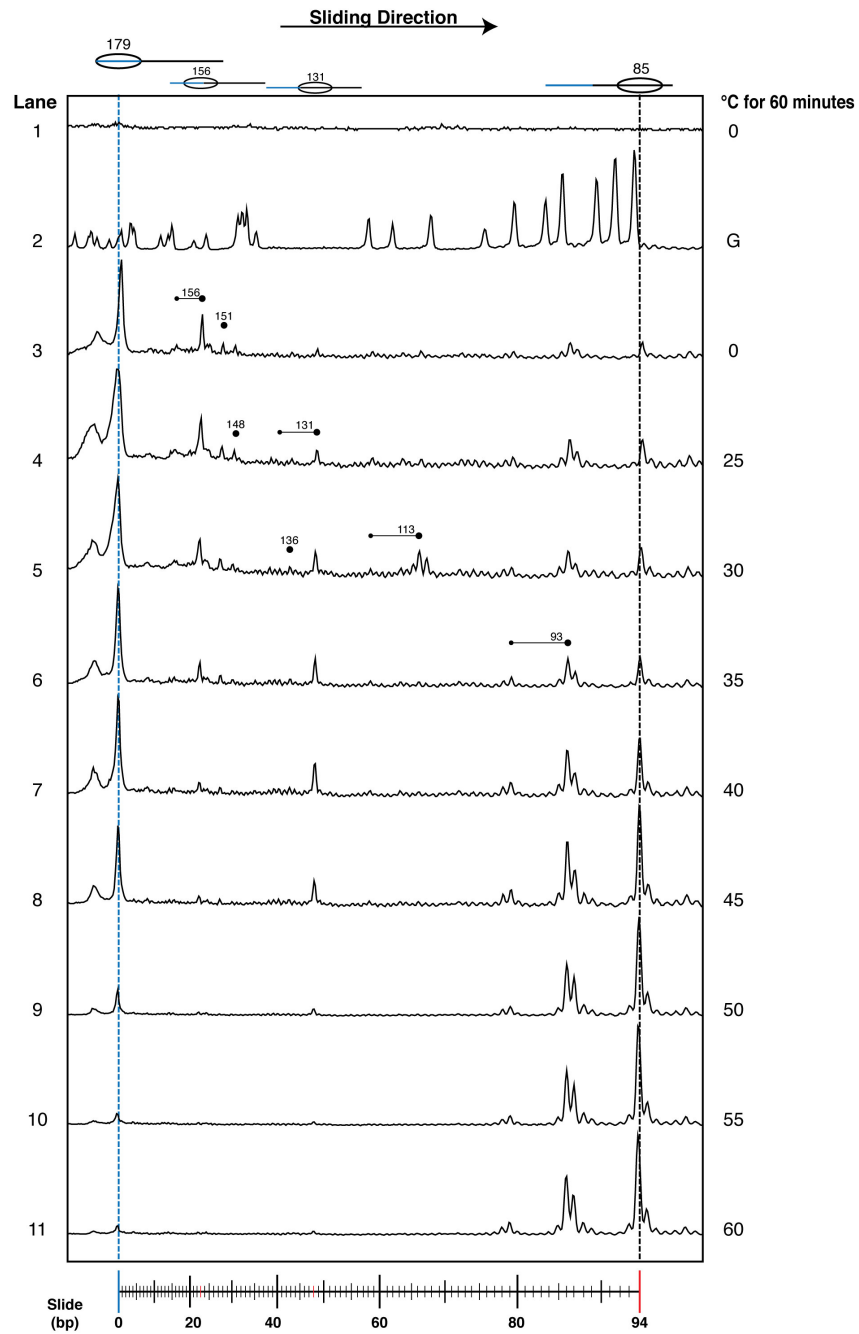


Figure 4.2 Thermal sliding of NucA on 252 bp mapped at SHL 0.5. C. Signal profile of 105(NucA)0 nucleosomes incubated at 0-60°C for 60 minutes and mapped at SHL 0.5 using EDTA. The blue broken line indicates the initial position of the 105(NucA)0 nucleosome. The black broken line represents the terminal nucleosome position. Large and small black circles represent the primary and secondary mapping of a population respectively. Signal profile data taken from Figure 4.2 B using AIDA analysis software.

4.4 Nucleosome sliding on NucA-31

To reposition the NucA nucleosome to a less stable position for allowing greater observation of intermediate positioning, we truncated the 3' end of NucA by 31 bp creating the 221 bp 105(NucA)-31 DNA fragment. To look at nucleosome sliding on this truncated NucA-31 positioning sequence we incubated nucleosomes containing the 221 bp fragment at 0-60°C for 60 minutes. These nucleosomes were then mapped at SHL 0.5 H4 S47C using EDTA reagent and Fe^{2+} .

4.4.1 Observations

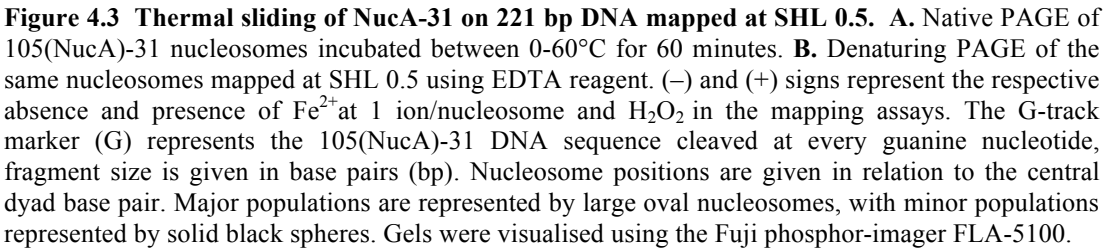
The truncated NucA-31 fragment forms a nucleosome that centers at 151 bp. This nucleosome population showed thermal sliding as low as 30°C and the majority of this population shifted by 40°C, Figure 4.3 A and B. As with the 105(NucA)0 nucleosome, the terminal position of sliding is centered at 85 bp with a relatively stable intermediate population centered at 131 bp, Figure 4.3 B, C. There are also less stable intermediate populations observed between the 151 bp and 131 bp populations, Figure 4.3 B. These intermediate populations centre at 148 bp, 140 bp, and 136 bp. Intermediate populations are also observed between 131 bp and 85 bp centers, these occur at 121 bp, 100 bp and 93 bp. Once again this larger histone/DNA complex is observed on the native gel but produces no obvious signs of mapping on the denaturing gel Figure 4.3 A and B.

4.4.2 Interpretation

The 31 bp truncation of the 105(NucA)0 sequence repositions the nucleosome to centre 28 bp upstream at 151 bp. This new initial position which was also present as a minor position in the 105(NucA)0 has reduced thermal stability and as a consequence the 105(NucA)-31 nucleosome slides from as low as 30°C. Due to the lower thermal energy input required to initiate nucleosome sliding an increased number of intermediate positions are formed, which allows for a greater interpretation of nucleosome sliding compared to the 601.2 or NucA positioning sequences. This makes the 105(NucA)-31 positioning sequence more suitable for

probing intermediates of nucleosome sliding so it was the sequence chosen for further analysis.

The high migrating nucleosome population observed in the native gel is probably due to additional histone complexes such as H2A/H2B dimers binding to the free linker DNA. This higher migrating band was observed for the 252 bp 105(NucA)⁰ and the 221 bp 105(NucA)-31 positioning sequences but was not observed for the 219 bp 54(601.2)¹⁸ sequence.



SHL 0.5 H4 S47C
105(NucA)-31

C

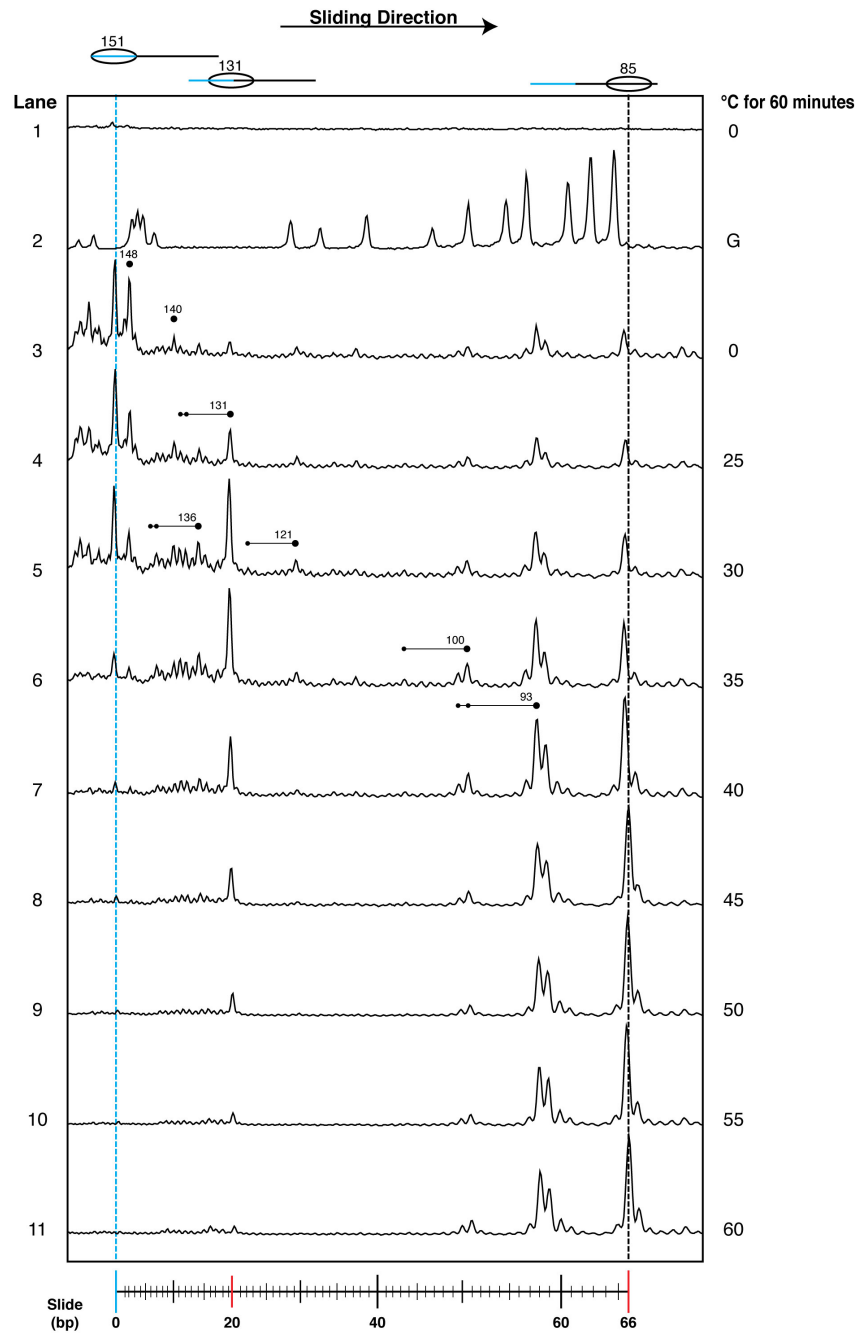


Figure 4.3 Thermal sliding of NucA-31 on 221 bp DNA mapped at SHL 0.5. C. Signal profile of 105(NucA)-31 nucleosomes incubated at 0-60°C for 60 minutes and mapped at SHL 0.5 H4 S47C using EDTA. The cyan broken line indicates the initial position of the 105(NucA)-31 nucleosome and the black broken line represents the terminal position. Large and small black circles represent the primary and secondary mapping of a population respectively. Signal profile data taken from Figure 4.3 B using AIDA analysis software.

4.5 NucA-31 sliding at 37°C mapped at SHL 0.5

To expand the sensitivity of detection of intermediate positions over the first 20 bp slide from positions 151 to 131, the 105(NucA)-31 nucleosome was incubated at a fixed temperature of 37°C for 0-128 minutes prior to mapping at SHL 0.5 H4 S47C.

4.5.1 Observations

The majority of the nucleosomes centered at 151 bp were stable for <8 minutes at 37°C, Figure 4.4 B lanes 3-7. A clearly stable intermediate resulted from a 20 bp slide centering the nucleosome at 131 bp. However, transient intermediate nucleosome positions between the 151 and 131 nucleosomes were observed centered at 140 bp and 136 bp, Figure 4.4 B lanes 4-8. Along with the initial 151 population, there is also a second nucleosome population centered at 148 bp. This 148 population demonstrates less stability than the 151 bp centered nucleosome, sliding from ≥ 2 minutes at 37°C to reposition to the 140, 136 and 131 positions, Figure 4.4 B and C.

Interestingly cleavage above the secondary cuts of the 151 bp centered nucleosome seems to be low compared with DNA cleavage in the sliding regions, but this is probably artefactual.

Once again the higher migrating band is observed in the native PAGE but a corresponding band cannot be observed in the denaturing gel, Figure 4.4 A and B.

4.5.2 Interpretation

At least 5 nucleosome positions occur over the initial 20 bp slide from start to finish, these occur at 151, 148, 140, 136 and 131 bp centers. This would indicate that nucleosomes can slide at increments that are not related to the helical repeat length of nucleosomal DNA of ~10.17 bp.

Throughout the sliding regions single base pair increments in cutting are observed between stable nucleosome populations, consistent with nucleosomes sliding by single base pair increments between regions of higher positional stability.

Such nucleosome sliding at 37°C on a relatively stable positioning sequences would suggest that endogenous mammalian chromatin would be highly dynamic even in the absence of chromatin remodelers.

Some intermediate positioning occurs between the 131 and 85 populations. These occur at 121, 113, 100 and 93 bp centers, but the temperature/time parameters are not suitable to allow good probing due to the relative stability of 131 at 37°C, Figure 4.4 B and C lane 11.

The higher migrating band in the native PAGE that continuously occurs with 105(NucA)0 and 105(NucA)-31 sequences is probably due to additional sub-octamer complexes such as H2A/H2B dimers or H3/H4 tetramers binding to nucleosomal free DNA.

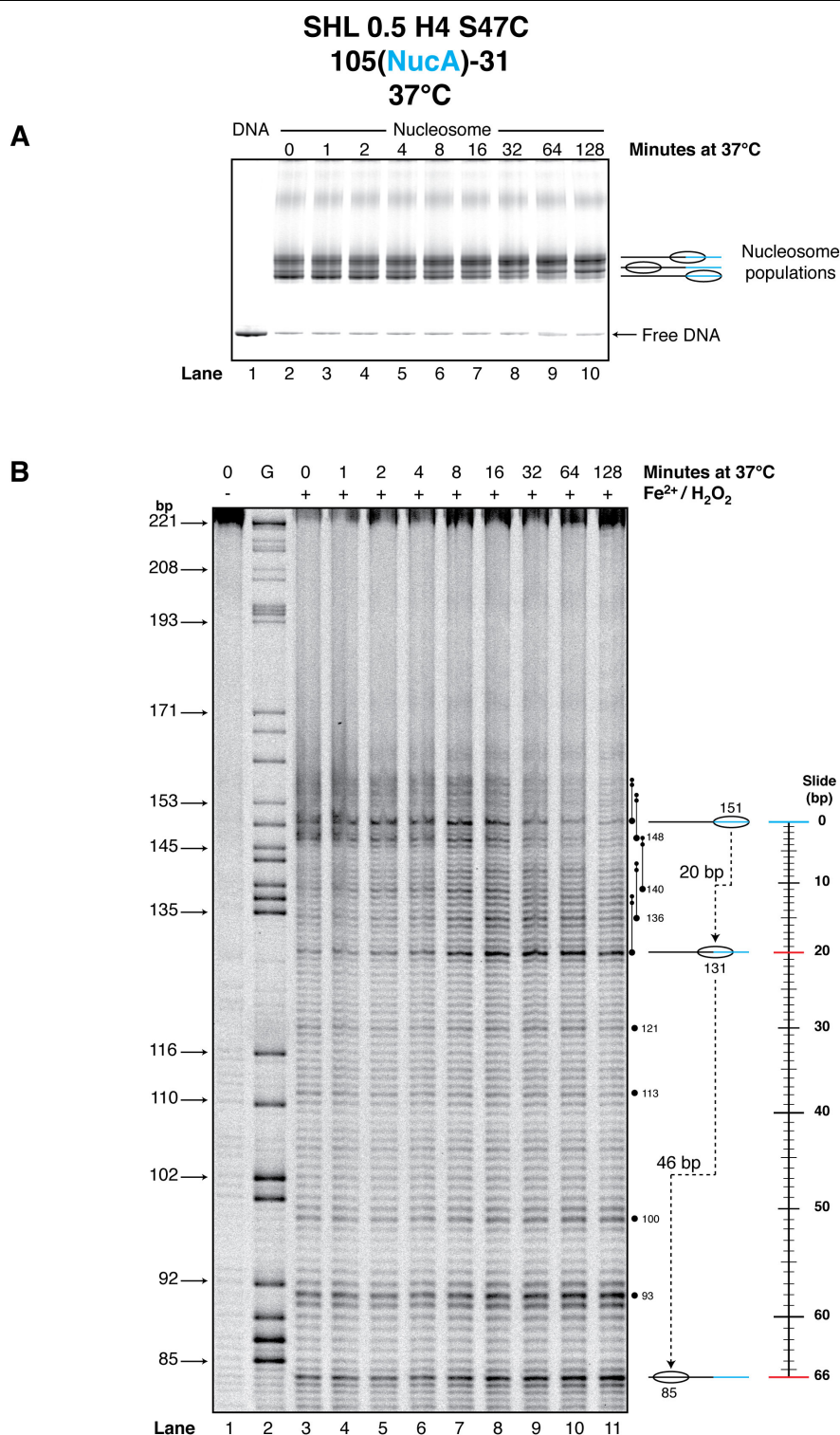


Figure 4.4 Thermal sliding of 105(NucA)-31 mapped at SHL 0.5. **A.** Native PAGE of 105(NucA)-31 nucleosomes incubated at 37°C for 0-128 minutes. **B.** Denaturing PAGE of 105(NucA)-31 incubated at 37°C for 0-128 minutes and mapped at SHL 0.5 with EDTA reagent. Signal profiles are shown in Figure 4.4 C. Large black circles represent primary cutting and small black circles represent secondary cutting. (–) and (+) signs represent the respective absence and presence of Fe²⁺ at 1 ion/nucleosome and H₂O₂ in the mapping assays. The G-track marker (G) represents the 105(NucA)-31 DNA sequence cleaved at every guanine nucleotide, fragment size is given in base pairs (bp). Nucleosome positions are given in relation to the central dyad base pair. Gels were visualised using the Fuji phosphor-imager FLA-5100.

SHL 0.5 H4 S47C
105(NucA)-31
37°C

C

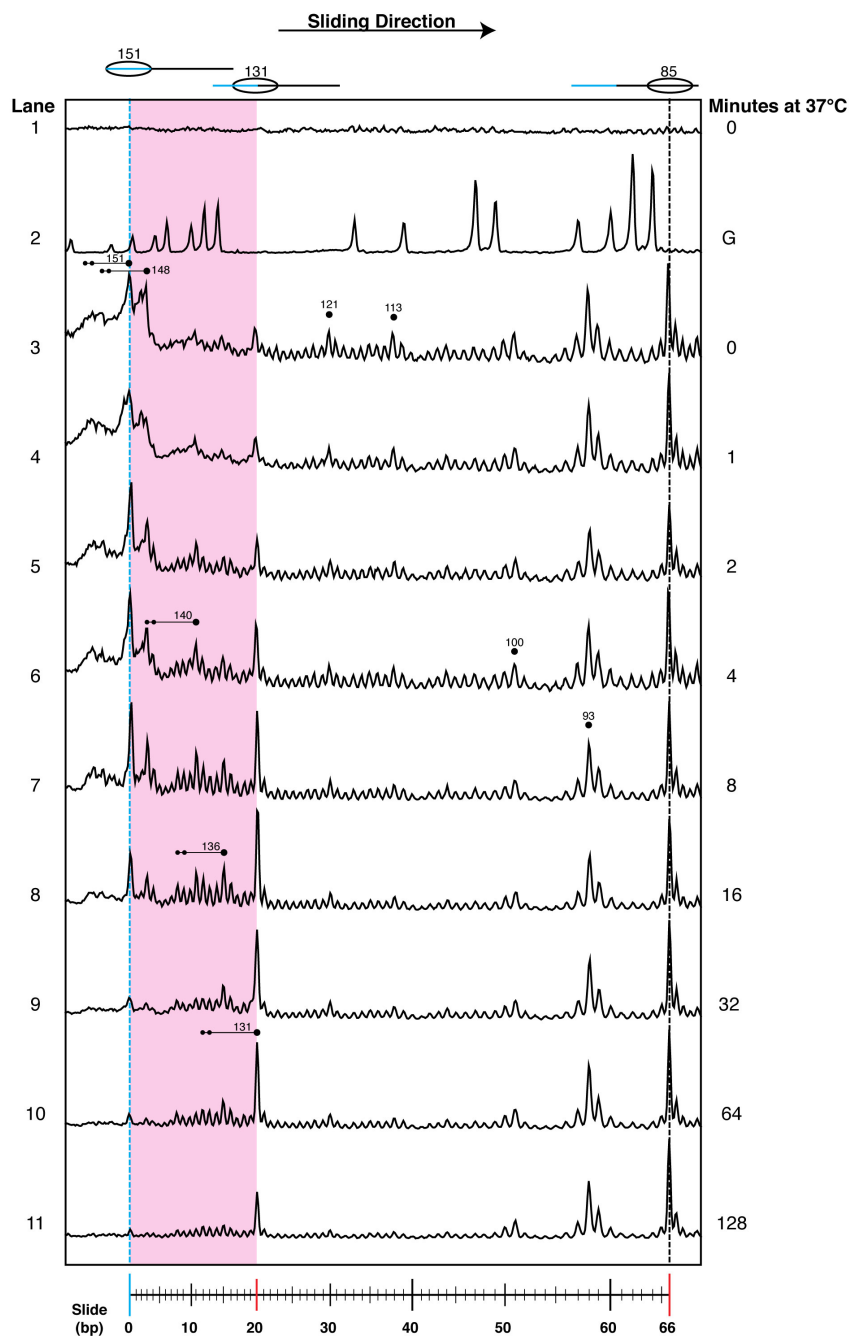


Figure 4.4 Thermal sliding of 105(NucA)-31 mapped at SHL 0.5. C. Signal profile of 105(NucA)-31 nucleosomes incubated at 37°C for 0-128 minutes and mapped at SHL 0.5 with EDTA, from Figure 4.4 B. The cyan lines represent the initial position of the dyad and the magenta region highlights the sliding over the first 20 bp. Large and small black circles represent the primary and secondary mapping of a population respectively. Signal profile data taken from Figure 4.4 B using AIDA analysis software.

4.6 NucA-31 sliding at 45°C mapped at SHL 0.5

To expand the level of sensitivity for later intermediate positions between the 131 bp and 85 bp centered nucleosomes on the 105(NucA)-31 sequence, nucleosomes were incubated at 45°C for 0-128 minutes prior to mapping at SHL 0.5 H4 S47C using the EDTA reagent.

4.6.1 Observations

The larger kinetic energy of the reaction means sliding over the first 20 bp at 45°C occurs rapidly with the majority of the 151 population shifted to 131 bp after 4 minutes of incubation. There is a clear reduction in the 151 bp nucleosome population and passage through the 131 position to the terminal 85 bp centered nucleosome population, Figure 4.5.

From the start of the second sliding phase at least 4 different nucleosome positions are observed over the 46 bp shift from 131 to 85. These populations are separated by distances from 7-13 bp and occur at 121, 113, 100 and 93 bp centers. After the 128 minute incubation at 45°C the vast majority of nucleosomes are centered at the terminal 85 bp, Figure 4.5 B and C.

4.6.2 Interpretation

Providing necessary energy to exit the 131 position at a reasonable rate requires higher temperatures. This makes it more difficult to detect transitory intermediates. However, four populations of nucleosomes are detected over the 46 bp sliding phase. As with the initial 20 bp sliding phase, no cleavage pattern was observed that would indicate absolute 10 bp increments synonymous with loop defect diffusion, although steps of between 7-13 bp are observed.

Single base pair steps between intermediate populations could be interpreted, although this could be little more than background within the samples. Everything considered, there is little evidence supporting any particular mechanism of sliding from mapping this nucleosome at SHL 0.5 at 37°C and 45°C.

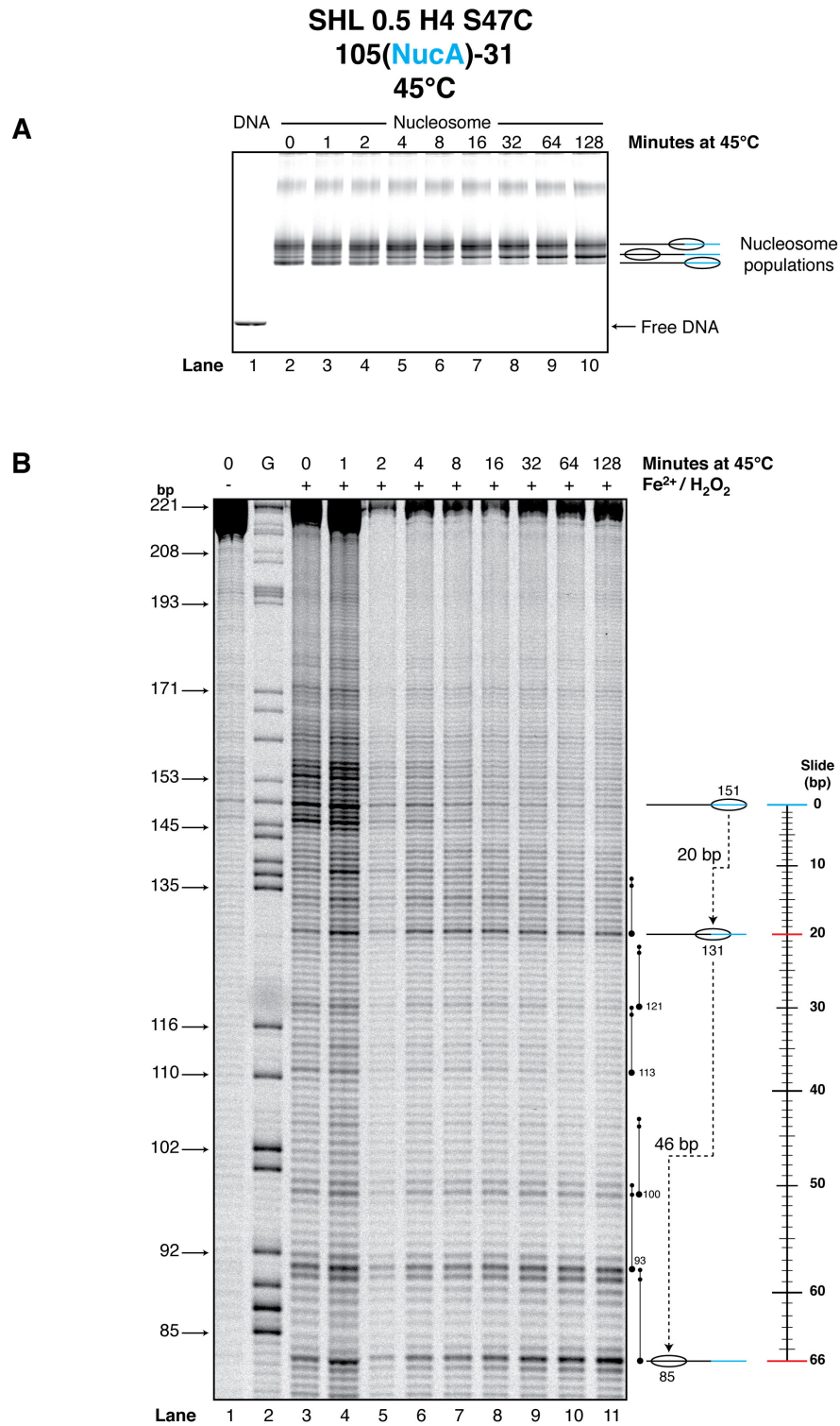


Figure 4.5 Thermal sliding of 105(NucA)-31 nucleosomes mapped at SHL 0.5. **A.** Native PAGE of 105(NucA)-31 nucleosomes incubated at 45°C for 0-128 minutes. **B.** Denaturing PAGE of 105(NucA)-31 nucleosomes incubated at 45°C for 0-128 minutes and mapped at SHL 0.5 using EDTA reagent. Large black circles represent primary cutting and small black circles represent secondary cutting. (–) and (+) signs represent the respective absence and presence of Fe²⁺ at 1 ion/nucleosome and H₂O₂ in the mapping assays. The G-track marker (G) represents the 105(NucA)-31 DNA sequence cleaved at every guanine nucleotide, fragment size is given in base pairs (bp). Nucleosome positions are given in relation to the central dyad base pair. Gels were visualised using the Fuji phosphor-imager FLA-5100. Signal profiles are shown in Figure 4.5 C.

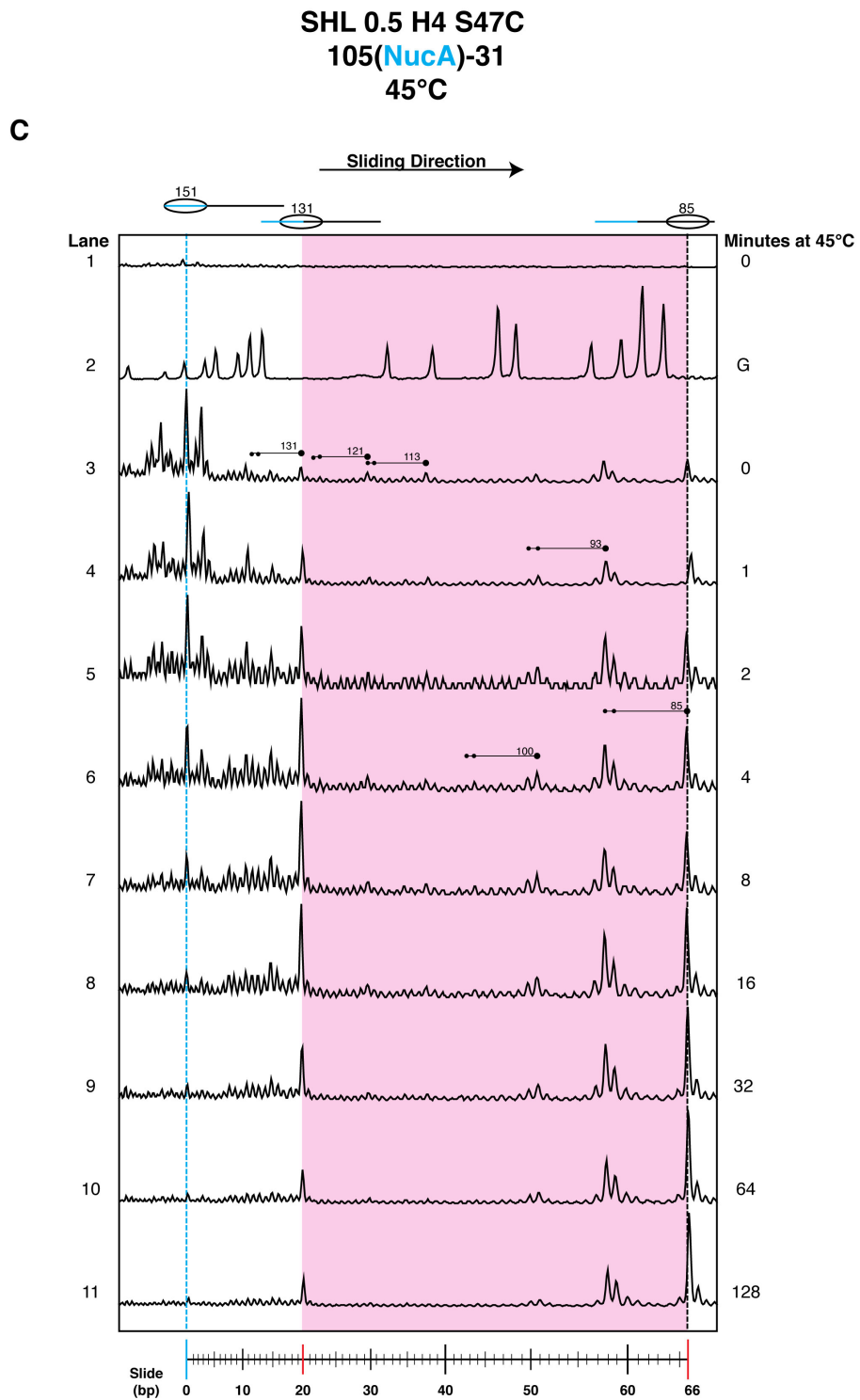


Figure 4.5 Thermal sliding of 105(NucA)-31 nucleosomes mapped at SHL 0.5. C. Signal profile for 105(NucA)-31 nucleosomes incubated at 45°C for 0-128 minutes and mapped at SHL 0.5 using EDTA, from Figure 4.5 B. The cyan lines represent the initial position of the dyad and the magenta region highlights a second stage of sliding that covers 46 bp. Signal profile data taken from Figure 4.5 B using AIDA analysis software.

4.7 NucA-31 sliding at 37°C mapped at SHL 1.5

NucA-31 nucleosomes were incubated at 37°C for 0-128 minutes. After incubation the nucleosomes were mapped at SHL 1.5 H4 T30C using EDTA reagent. The distance between primary and secondary cutting when mapping at SHL 1.5 is 27/28 bp.

4.7.1 Observations

SHL 1.5 mapping for NucA-31 nucleosome sliding follows a slightly different path than for the SHL 0.5 mapping over the first 20 bp phase. For instance there is less of the minor nucleosome position 148 and a new minor position at 133 bp that was not obvious at the SHL 0.5 mapping.

The 151 centered nucleosome slides 11 bp to centre at the 140 bp position. Further incubation sees the 140 centered nucleosome slide to the 131 centered position via two less stable positions at 136 and 133, Figure 4.6 B and C.

A contaminating band labeled X seen in the undigested negative control of lane 1 is found in all samples and is probably a DNA fragment picked up during the purification of nucleosomal DNA, Figure 4.6 B and C.

4.7.2 Interpretation

NucA-31 nucleosome mapped at SHL 1.5 and mobilised over 20 bp produces almost the same pattern as the NucA-31 nucleosome mapped at SHL 0.5 with three differences. There is a reduction in the quantity of the minor 148 centered nucleosome. This could be due to a small influence of the cysteine with reagent at H4 residue 30 having less affinity for the 148 position than the equivalent structure at SHL 0.5.

Secondly, there is a stronger mapping signal at 140 compared to the observation at SHL 0.5. This is due to a combination of primary cuts from the 140 nucleosome and secondary cuts from the 113 positioned nucleosome which is 27/28 bp further upstream.

Thirdly, there is an additional minor position apparent at 133, which is not observed in cutting at SHL 0.5. This position between 136 and 131 underlines the base-pair stepwise nature of sliding.

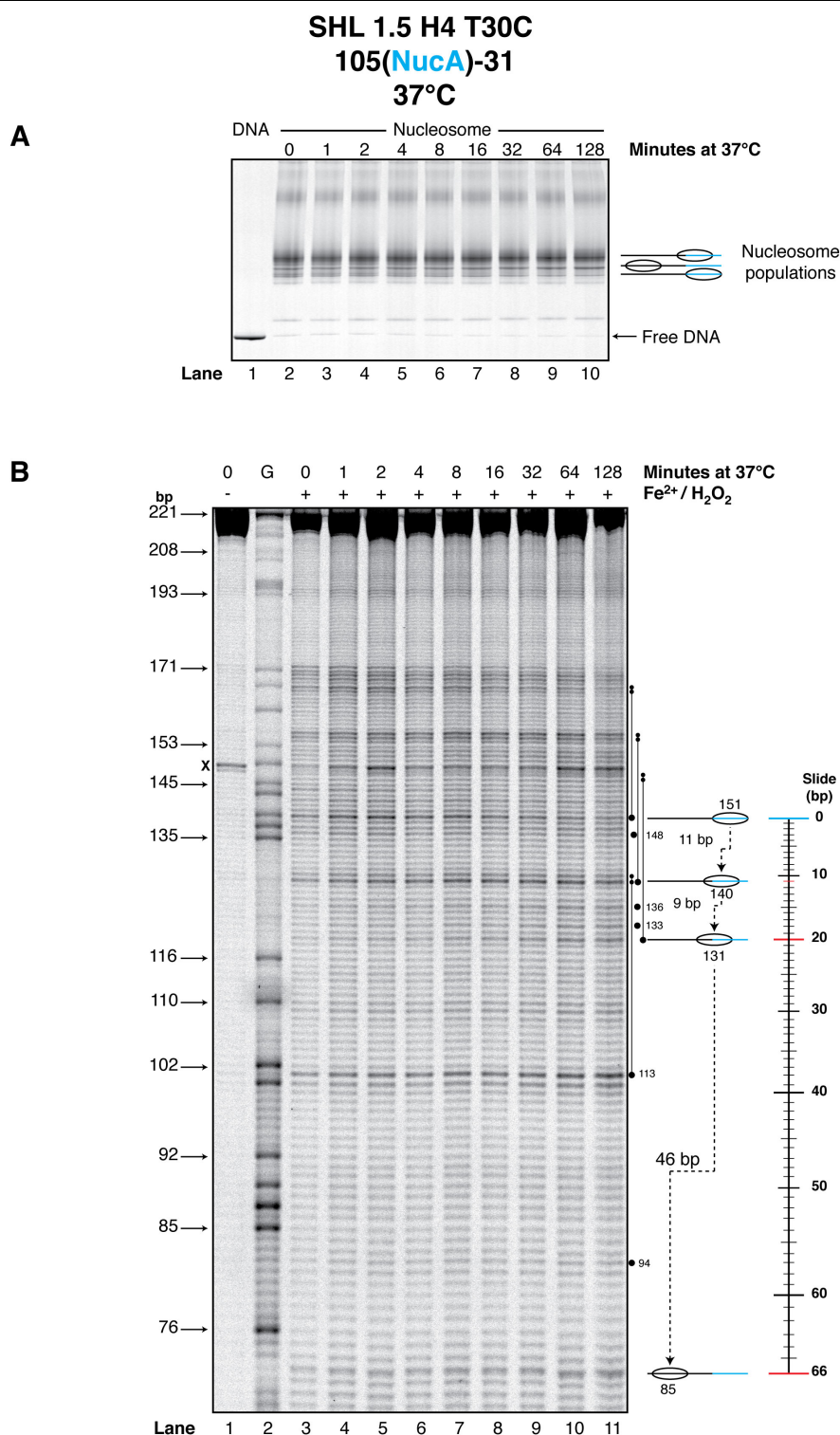


Figure 4.6 Thermal sliding of 105(NucA)-31 nucleosomes mapped at SHL 1.5. **A.** Native PAGE of 105(NucA)-31 nucleosomes incubated at 37°C for 0-128 minutes. **B.** Denaturing PAGE of 105(NucA)-31 nucleosomes incubated at 37°C for 0-128 minutes and mapped at SHL 1.5 using EDTA reagent. Signal profiles are shown in Figure 4.6 C. Band X found in all samples is contaminant DNA. Large black circles represent primary cutting and small black circles represent secondary cutting. (–) and (+) signs represent the respective absence and presence of Fe²⁺ at 1 ion/nucleosome and H₂O₂ in the mapping assays. The G-track marker (G) represents the 105(NucA)-31 DNA sequence cleaved at every guanine nucleotide, fragment size is given in base pairs (bp). Nucleosome positions are given in relation to the central dyad base pair. Gels were visualised using the Fuji phosphor-imager FLA-5100.

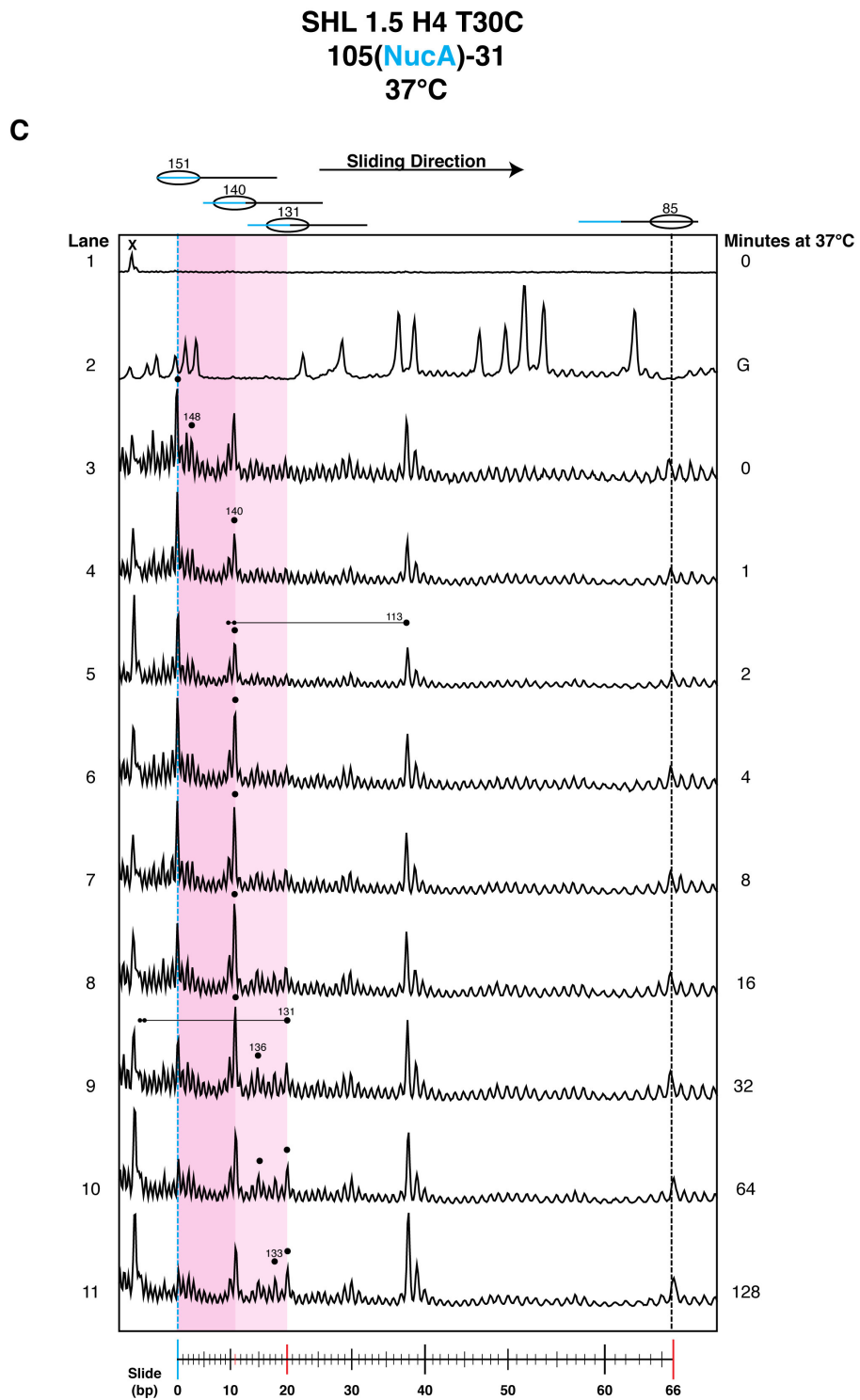


Figure 4.6 Thermal sliding of 105(NucA)-31 nucleosomes mapped at SHL 1.5. C. Signal profile for 105(NucA)-31 nucleosomes incubated at 37 °C for 0-128 minutes and mapped at SHL 1.5 using EDTA, from Figure 4.6 B. The cyan lines represent the initial position of the dyad while the magenta regions represent the sliding over the first 20 bp. Large black spheres represent primary mapping with small black spheres representing secondary mapping. Signal profiles obtained using AIDA analysis software.

4.8 NucA-31 sliding at 45°C mapped at SHL 1.5

NucA-31 nucleosomes were incubated at 45°C for 0-128 minutes to probe the number of intermediate positions between the 131 bp and 85 bp centered nucleosomes. After incubation the nucleosomes were mapped at SHL 1.5 H4 T30C using EDTA reagent.

4.8.1 Observations

Mapping results for these samples were quite poor, although some data can be interpreted. Most of the 151 population of nucleosomes have slid from their initial position after 4 minutes of incubation. However, pauses for relatively few of these sliding nucleosomes can be observed at 140 or 131. There is some mapping consistent with intermediates at 98 and possibly 94, Figure 4.7 C. There is high signal from position 113, although this probably comes from the secondary mapping of position 85. Incubation times >16 minutes sees most nucleosomes centered at 85 bp.

4.8.2 Interpretation

Sliding over this 46 bp region is difficult to interpret but close positional similarities exist between the mapping at SHL 1.5 and SHL 0.5 as expected. For example the 131 and terminal 85 bp centered positions are observed in the mapping at both locations. This would suggest that the DNA dynamics at both of these locations are similar, as would be expected due to both mapping locations being on the same histone protein.

Once again sliding over this 46 bp region does not display the ~10 bp steps associated with loop defect diffusion. Single base pair steps associated with twist defect diffusion possibly could be occurring although this cannot be verified due to the high level of background signal between intermediate positioning.

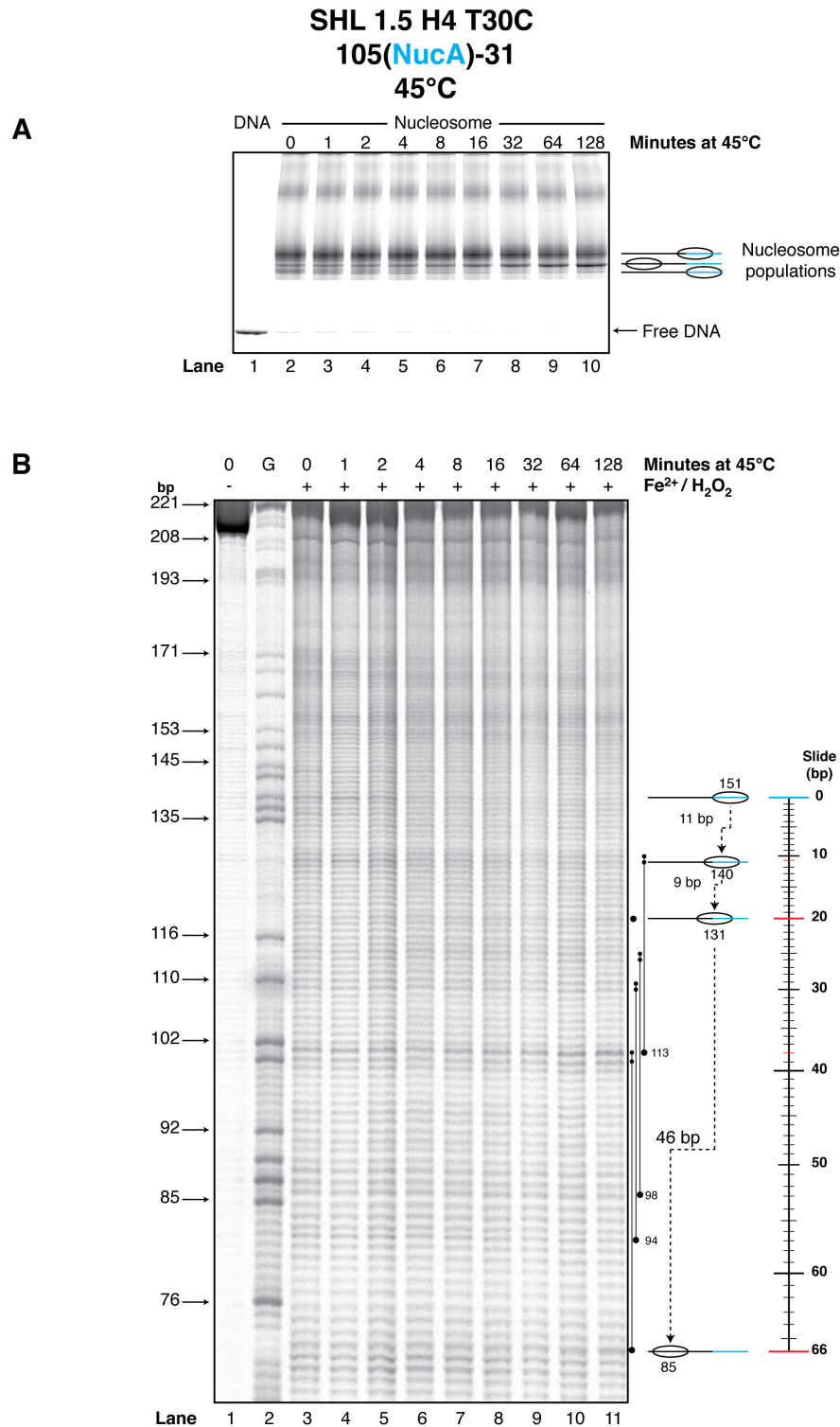


Figure 4.7 Thermal sliding of 105(NucA)-31 mapped at SHL 1.5. **A.** Native PAGE of 105(NucA)-31 nucleosomes incubated at 45°C for 0-128 minutes. **B.** Denaturing PAGE of 105(NucA)-31 nucleosomes incubated at 45°C for 0-128 minutes and mapped at SHL 1.5. Signal profiles shown in Figure 4.7 C. Large black circles represent primary cutting and small black circles represent secondary cutting. (–) and (+) signs represent the respective absence and presence of Fe²⁺ at 1 ion/nucleosome and H₂O₂ in the mapping assays. The G-track marker (G) represents the 105(NucA)-31 DNA sequence cleaved at every guanine nucleotide, fragment size is given in base pairs (bp). Nucleosome positions are given in relation to the central dyad base pair. Gels were visualised using the Fuji phosphor-imager FLA-5100.

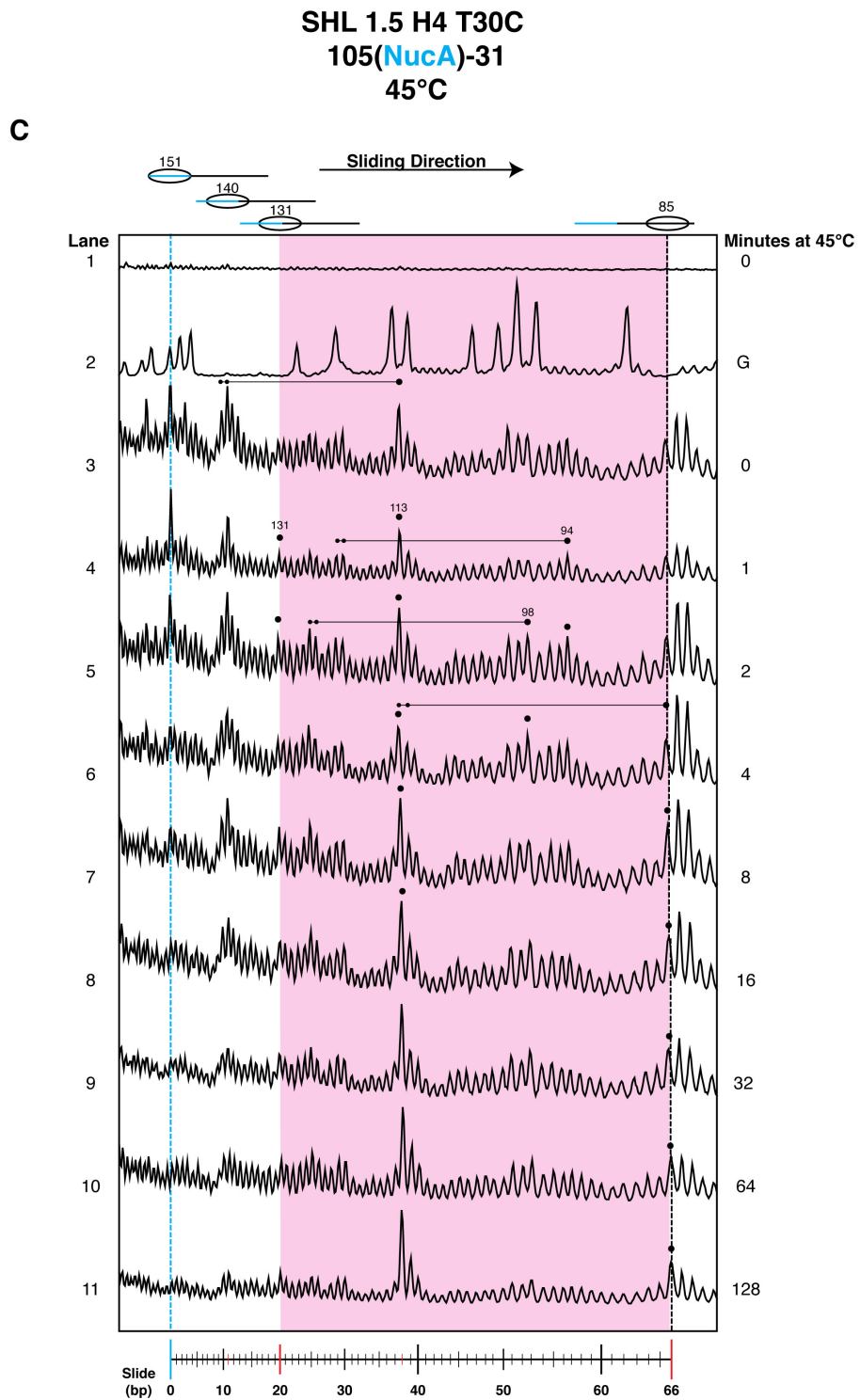


Figure 4.7 Thermal sliding of 105(NucA)-31 mapped at SHL 1.5. C. Signal profile of 105(NucA)-31 nucleosomes incubated at 45°C for 0-128 minutes and mapped at SHL 1.5 using EDTA reagent, from Figure 4.7 B. The magenta region represents the second stage of sliding over 46 bp from positions 131 to 85. Large black circles represent primary cutting and small black circles represent secondary cutting. Signal profiles obtained using AIDA analysis software.

4.9 NucA-31 sliding at 37°C mapped at SHL 2.5

NucA-31 nucleosomes were incubated at 37°C for 0-128 minutes to expand intermediate positioning between the 151 and 131 nucleosome populations. After incubation the nucleosomes were mapped at SHL 2.5 H3 D81C. The distance between primary and secondary cutting for SHL 2.5 increases to 47/48 bp.

4.9.1 Observations

The native gel clearly shows sliding over the 128 minute incubation. Some of the 151 centered nucleosome population seems to persist throughout the incubation, although the majority of this population has slid by 32 minutes, Figure 4.8 A.

Positions taken up on leaving the 151 position and over the first 20 bp sliding phase include the previously observed 140, 136 and 131 bp centered nucleosomes, Figure 4.8 B and C.

Further incubation sees nucleosomes centre 38 and 46 bp upstream at nucleosome centers 93 and 85 respectively. Initial sliding of the 151 nucleosome takes it 11 and 20 bp to centre at position 140 and 131 bp respectively. Incubation >8 minutes sees the 140 population slide to centre at 136, Figure 4.8 C lanes 7 and 8. Incubation >32 minutes destabilises the 136 population for positions at 131, 93 and 85.

4.9.2 Interpretation

The same nucleosome populations are observed yet again at the 151, 140, 136 and 131 centered nucleosomes, demonstrating consistency between the 3 mapping location SHL 0.5-2.5. Possible single base pair steps are observed between stable positions, suggesting there could be nucleosomes centered at every base pair along the sliding region. If so this would be indicative of a twist defect mechanism.

The high signal double peaks occurring in the initial 20 bp sliding regions after the 16 and 32 minute incubations and identified in Figure 4.8 C, lane 8 and 9 come from the secondary cleavage of nucleosomes centered further upstream.

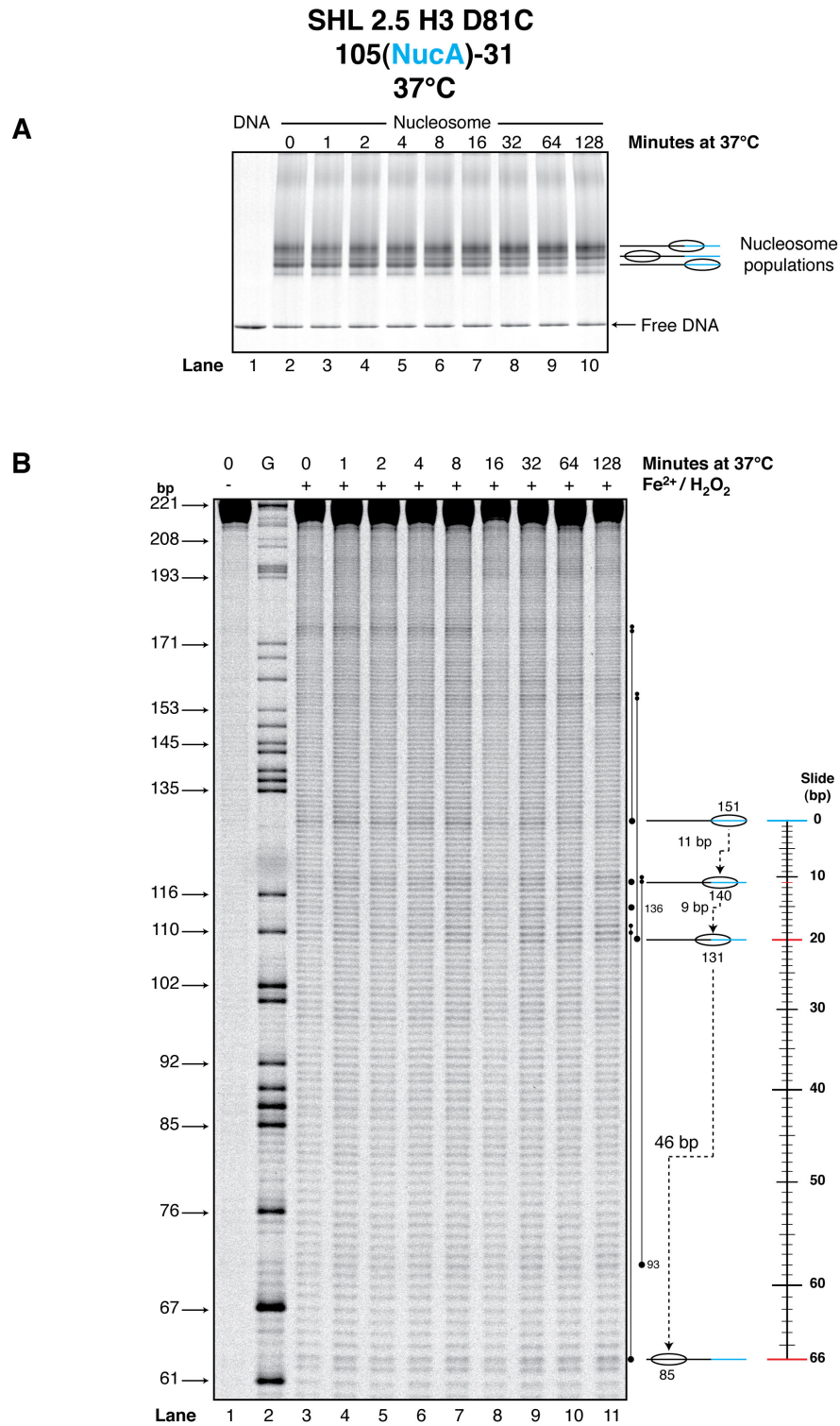


Figure 4.8 Thermal sliding of 105(NucA)-31 mapped at SHL 2.5. **A.** Native PAGE of 105(NucA)-31 nucleosomes incubated at 37°C for 0-128 minutes. **B.** Denaturing PAGE of 105(NucA)-31 nucleosomes incubated at 37°C for 0-128 minutes and mapped at SHL 2.5 H3 D81C with EDTA reagent. Signal profile shown in Figure 4.8 C. Large black circles represent primary cutting and small black circles represent secondary cutting. (–) and (+) signs represent the respective absence and presence of Fe²⁺ at 1 ion/nucleosome and H₂O₂ in the mapping assays. The G-track marker (G) represents the 105(NucA)-31 DNA sequence cleaved at every guanine nucleotide, fragment size is given in base pairs (bp). Nucleosome positions are given in relation to the central dyad base pair. Gels were visualised using the Fuji phosphor-imager FLA-5100.

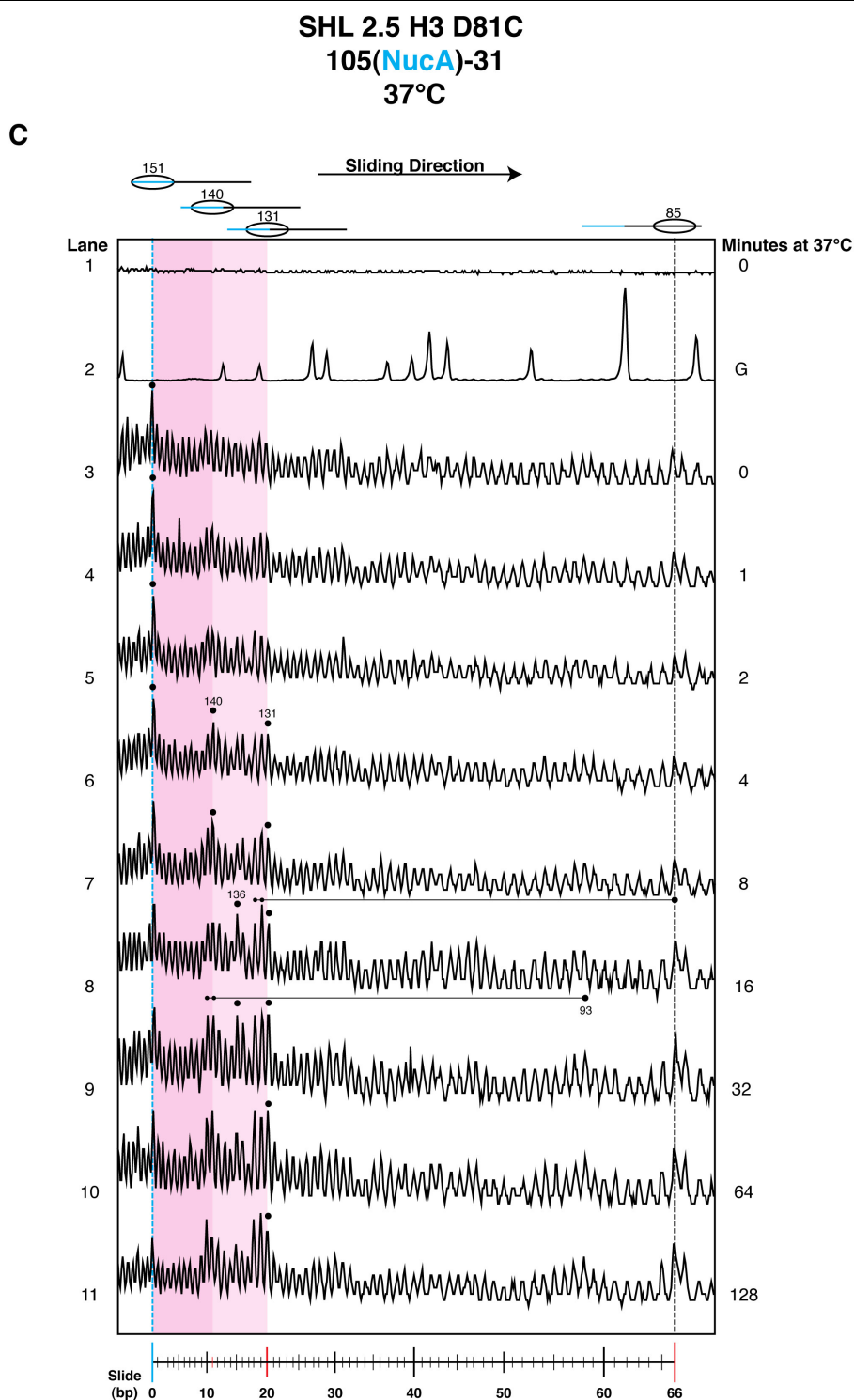


Figure 4.8 Thermal sliding of 105(NucA)-31 mapped at SHL 2.5. C. Signal profile of 105(NucA)-31 nucleosomes incubated at 37°C for 0-128 minutes and mapped at SHL 2.5 with EDTA, from Figure 4.8 B. Magenta regions represent the primary mapping over the initial 20 bp sliding region. Large black spheres represent primary mapping with small black spheres representing secondary mapping. Distances between primary and secondary mapping at SHL 2.5 is 47-48 bp. Signal profiles obtained using AIDA analysis software.

4.10 NucA-31 sliding at 45°C mapped at SHL 2.5

NucA-31 nucleosomes were incubated at 45°C for 0-128 minutes to expand intermediate positioning between the 131 and 85 bp centered nucleosome populations. After incubation the nucleosomes were mapped at SHL 2.5 H3 D81C. For SHL 2.5 mapping the distance between primary and secondary cuts increases to 47/48 bp.

4.10.1 Observations

From the native and denaturing gel it can be seen that before incubation the majority of nucleosomes are again centered at 151 bp, as expected. As incubation increases the 151 population destabilises and slides to centre at 131 as before.

Further incubation sees a 120 population appear then destabilize to take up position at either 131 or 85 bp centres, Figure 4.9 B and C. Incubation times >16 minutes destabilise the 131 bp centered population for positions at 93 and 85 bp centres.

After 64 minutes at 45°C the 93 bp centered nucleosome is destabilised and most nucleosomes have slid to take up position at 85 bp, making this terminal position the destination of the vast majority of nucleosomes after 128 minutes at 45°C, Figure 4.9 C.

4.10.2 Interpretation

This 46 bp sliding region mapped at SHL 2.5 demonstrates 4 nucleosome positions from start to finish, at 131, 120, 93 and 85 bp centres. Sliding between these positions shows no real pattern that would be synonymous with the single base-pair steps of twist defect diffusion or the ~10 bp steps of loop defect diffusion.

Mapping at SHL 2.5 does not seem to produce any obvious significant differences between the mapping at either SHL 0.5 or SHL 1.5, probably due to the mapping locations all occurring on the highly stable H3-H4 tetramer.

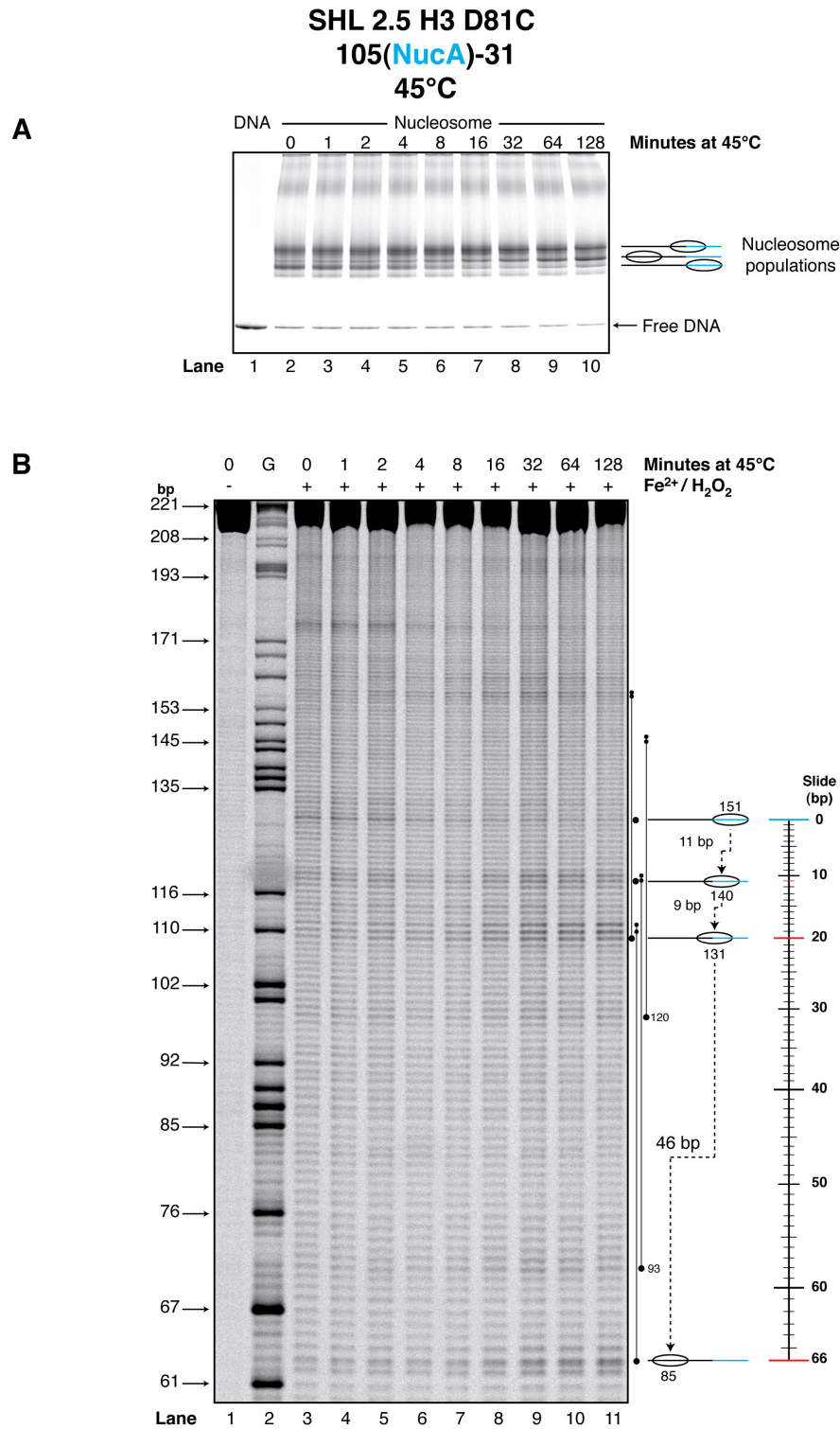


Figure 4.9 Thermal sliding of 105(NucA)-31 mapped at SHL 2.5. **A.** Native PAGE of 105(NucA)-31 nucleosomes incubated at 45°C for 0-128 minutes. **B.** Denaturing PAGE of 105(NucA)-31 nucleosomes incubated at 45°C for between 0-128 minutes and mapped at SHL 2.5 D81C. Signal profile shown in Figure 4.9 C. Large black circles represent primary cutting and small black circles represent secondary cutting. (–) and (+) signs represent the respective absence and presence of Fe^{2+} at 1 ion/nucleosome and H_2O_2 in the mapping assays. The G-track marker (G) represents the 105(NucA)-31 DNA sequence cleaved at every guanine nucleotide, fragment size is given in base pairs (bp). Nucleosome positions are given in relation to the central dyad base pair. Gels were visualised using the Fuji phosphor-imager FLA-5100.

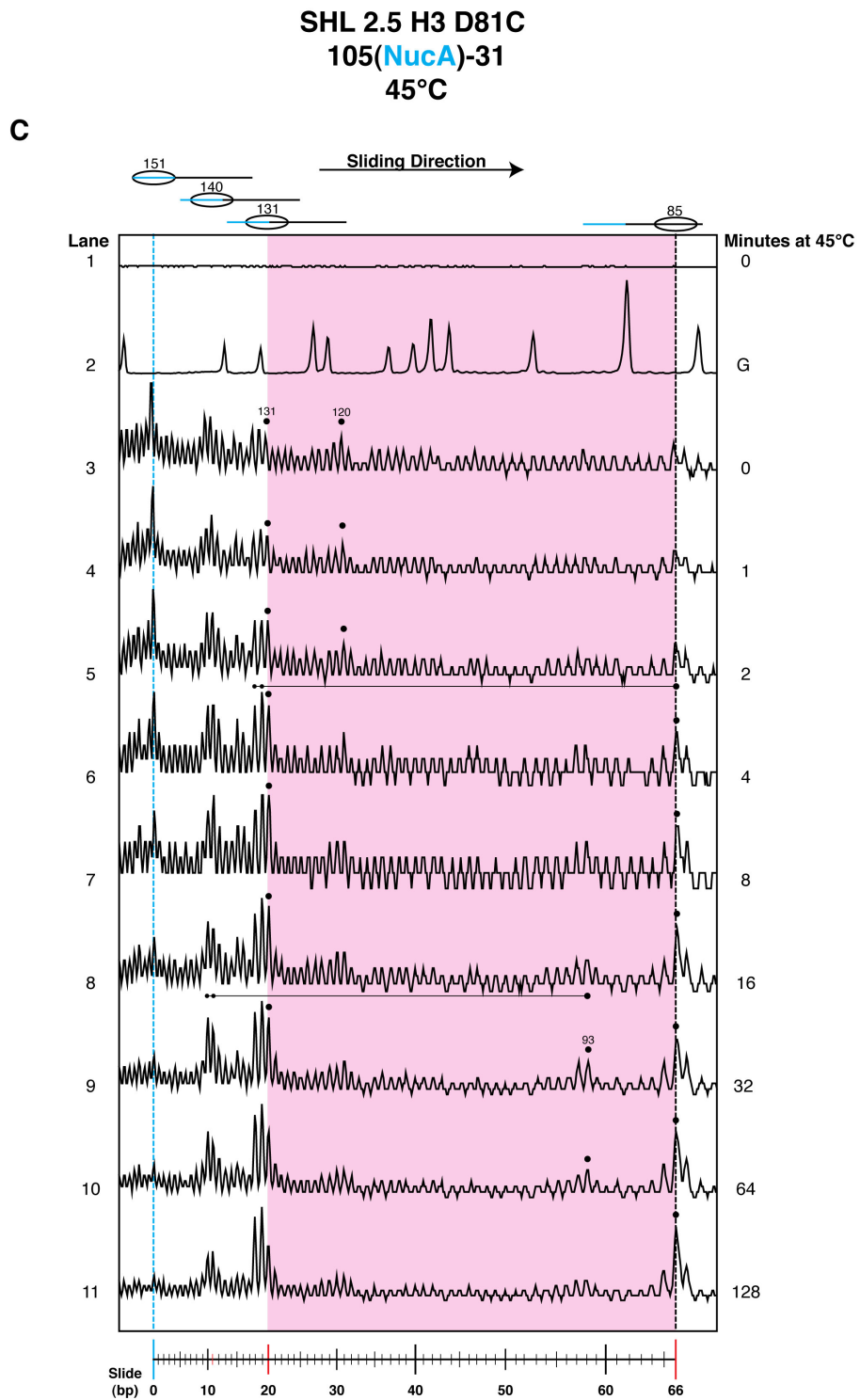


Figure 4.9 Thermal sliding of 105(NucA)-31 mapped at SHL 2.5. C. Signal profile of 105(NucA)-31 nucleosomes incubated at 45°C for 0-128 minutes and mapped at SHL 2.5 using EDTA, from Figure 4.9 B. Magenta region represents primary cutting over the 46 bp second stage of sliding. Large black spheres represent primary mapping with small black spheres representing secondary mapping. Distances between primary and secondary mapping at SHL 2.5 is 47-48 bp. Signal profiles obtained using AIDA analysis software.

4.11 NucA-31 sliding at 37°C mapped at SHL 3.5

NucA-31 nucleosomes were incubated at 37°C for 0-128 minutes to expand intermediate positioning over the first ~20 bp sliding phase. After incubation the nucleosomes were mapped at SHL 3.5 H2B T85C. For SHL 3.5 the mapping distance between primary and secondary cuts increases to ~70 bp.

4.11.1 Observations

Positioning was calculated from the secondary mapping at SHL 3.5 due to the cleavage efficiency being stronger for the secondary cutting. Also, from the native gel it can be seen that distinct nucleosome population are not visible as in previous gels, Figure 4.10 A and B.

Starting from the secondary mapping site of the 151 bp centered nucleosome and increasing the incubation time at 37°C the nucleosome seems to shift 14 bp to center at ~137, Figure 4.10 B and C. The same distance of 14 bp was also observed between the same primary mapping sites. This is compared to an 11 bp shift with the previous sites.

Further incubation sees a rise in a population of nucleosomes centered at 133 bp coming from the destabilisation of the 151 bp centered nucleosome. However this position is not as obvious when mapped from the primary location.

4.11.2 Interpretation

Greater mapping efficiency observed from the secondary sites would indicate that the EDTA reagent is more in proximity to the DNA at the secondary location than at the primary location. It could also indicate that the nucleosomal DNA towards the outer parts of the nucleosome has less affinity for the octamer due to the cysteine mutation and EDTA reagent. This could also explain the reduced quantity of distinct populations on the native gel.

The reason for the aberrant sliding behaviour over the first sliding phase compared with the same sliding phase at SHL 0.5 to SHL 2.5 is probably again due

to the cysteine mutation. However, the initial 151 position demonstrates some consistency probably due to its stronger translational affinity for the octamer.

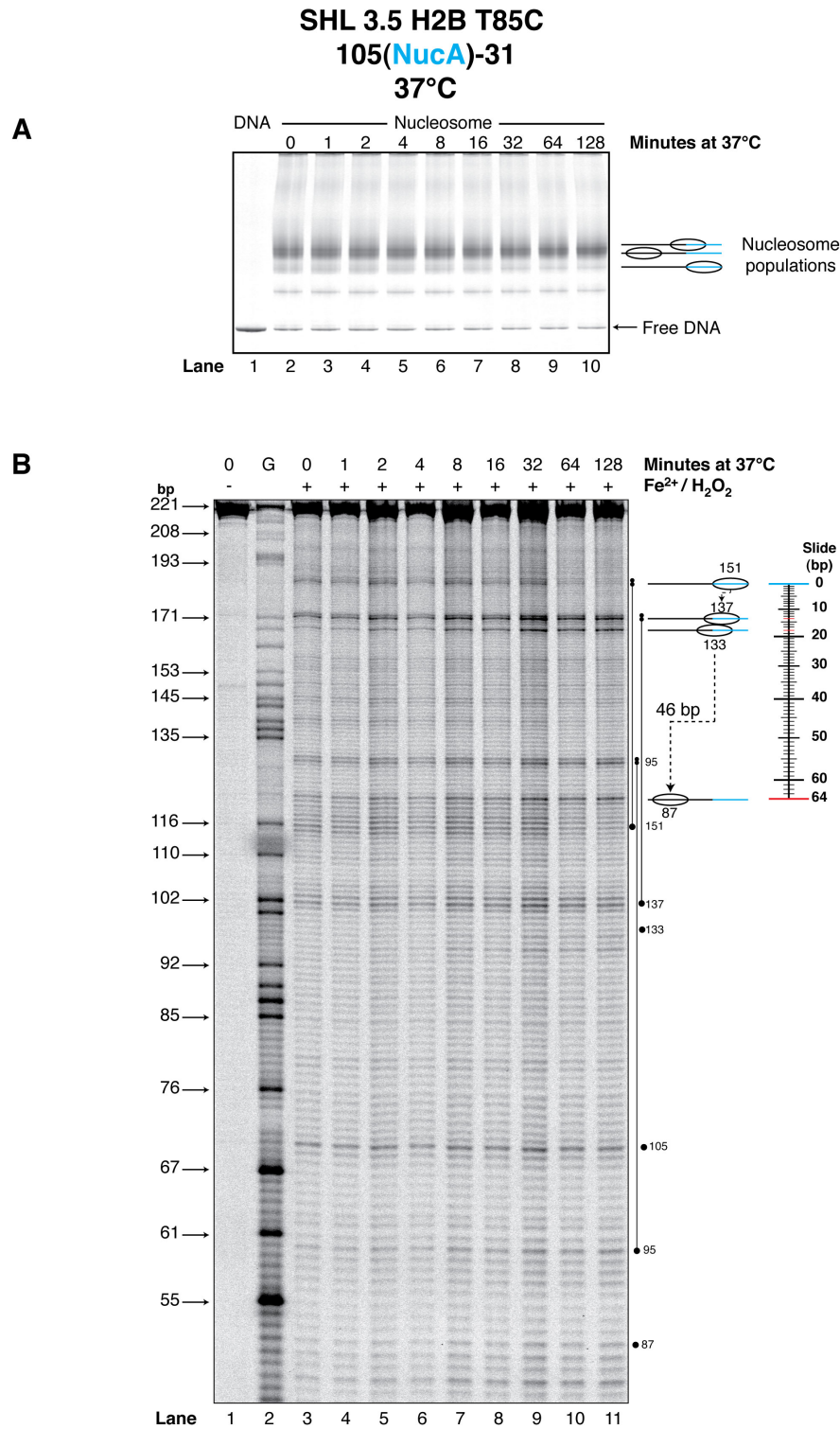


Figure 4.10 Thermal sliding of 105(NucA)-31 mapped at SHL 3.5. **A.** Native PAGE of 105(NucA)-31 nucleosomes incubated at 37°C for 0-128 minutes. **B.** Denaturing PAGE of 105(NucA)-31 nucleosomes incubated at 37°C for 0-128 minutes and mapped at SHL 3.5 using EDTA reagent. Signal profiles shown in Figure 4.10 C. Large black circles represent primary cutting and small black circles represent secondary cutting. (–) and (+) signs represent the respective absence and presence of Fe²⁺ at 1 ion/nucleosome and H₂O₂ in the mapping assays. The G-track marker (G) represents the 105(NucA)-31 DNA sequence cleaved at every guanine nucleotide, fragment size is given in base pairs (bp). Nucleosome positions are given in relation to the central dyad base pair. Gels were visualised using the Fuji phosphor-imager FLA-5100.

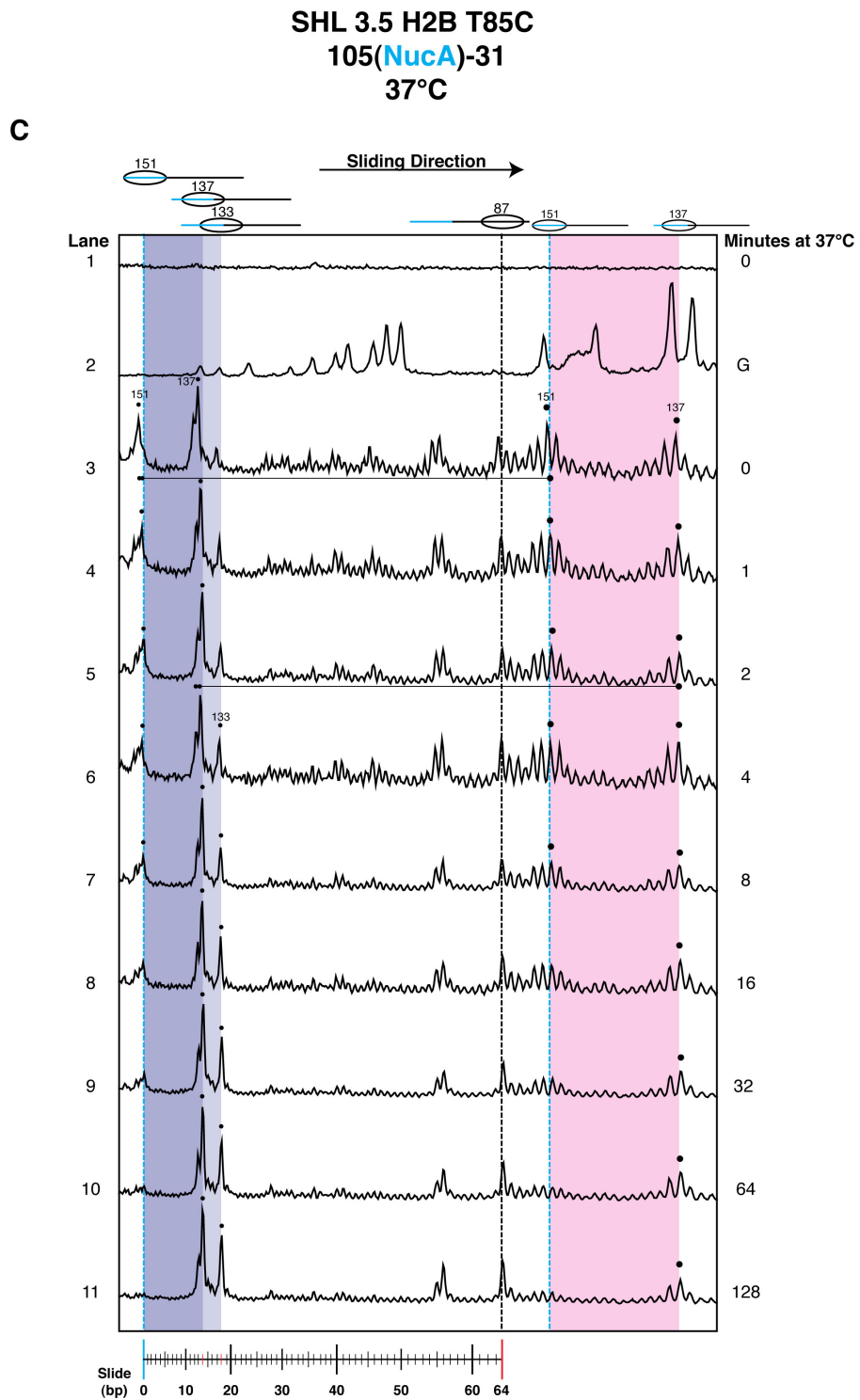


Figure 4.10 Thermal sliding of 105(NucA)-31 mapped at SHL 3.5. C. Signal profile of 105(NucA)-31 nucleosomes incubated at 37°C for 0-128 minutes and mapped at SHL 3.5 using EDTA, from Figure 4.10 B. Purple and magenta regions represent the respective secondary and primary mapping for the first stage of sliding. Large black spheres represent primary mapping and small black circles represent secondary mapping. Signal profiles obtained using AIDA analysis software.

4.12 NucA-31 sliding at 45°C mapped at SHL 3.5

NucA-31 nucleosomes were incubated at 45°C for 0-128 minutes to expand intermediate positioning between the 133 and 87 bp centered nucleosome populations. After incubation the nucleosomes were mapped from the H2A-H2B dimer at SHL 3.5 H2B T85C. For SHL 3.5 mapping, the distance between primary and secondary cuts is ~70 bp.

4.12.1 Observations

Initially the 133 nucleosome population is small compared to the 151 and 137 populations. However after 1 minute of incubation at 45°C an increase is observed in the 133 population along with possible positioning at ~111 and 105 bp, Figure 4.11 B.

Further incubation sees an increase in the 133 population along with an increase in populations centered at 95 and 87. Incubation times >16 minutes reduce the 133 population and sees an increase in the 95 and 87 centered populations, Figure 4.11 B and C.

After 128 minutes of incubation the main populations remaining are centered at 137, 95 and 87 bp. Interestingly the primary mapping intensity of the 137 bp nucleosome is inversely correlated to incubation time, this was not observed within the secondary mapping of the same population, Figure 4.11 C.

Interestingly, the 87 bp centered population does not seem to follow the expected dyad symmetry as other populations have. This can be seen where the theoretical primary cut at 87 is 3 bases above the strongest signal, Figure 4.11 B. This was also observed with the SHL 3.5 37 °C incubation, Figure 4.10 B.

4.12.2 Interpretation

At least 3 nucleosome populations are observed during sliding over the 46 bp phase from 133 to 87, these include 111, 105, and 95 bp centered nucleosomes. No

obvious pattern of sliding is observed between these intermediate positions that would indicate a twist defect or loop defect mechanism of sliding.

The reduction in intensity of the primary mapping with increased incubation time at SHL 3.5, which was not observed in the secondary mapping, could indicate that during sliding DNA peels back from the outer part of the nucleosome enabling the nucleosome to slide along this free DNA. Or it could suggest that the H2A-H2B dimer disengages the nucleosome to allow sliding in the direction of the resulting free DNA.

The 3 bp deviation from dyad symmetry observed with the primary cut at position 87 could indicate that extra base-pairs were located at SHL 3.5 during the mapping of this population. If this is the case it could suggest a mechanism of sliding that involved short steps of 1-3 bp.

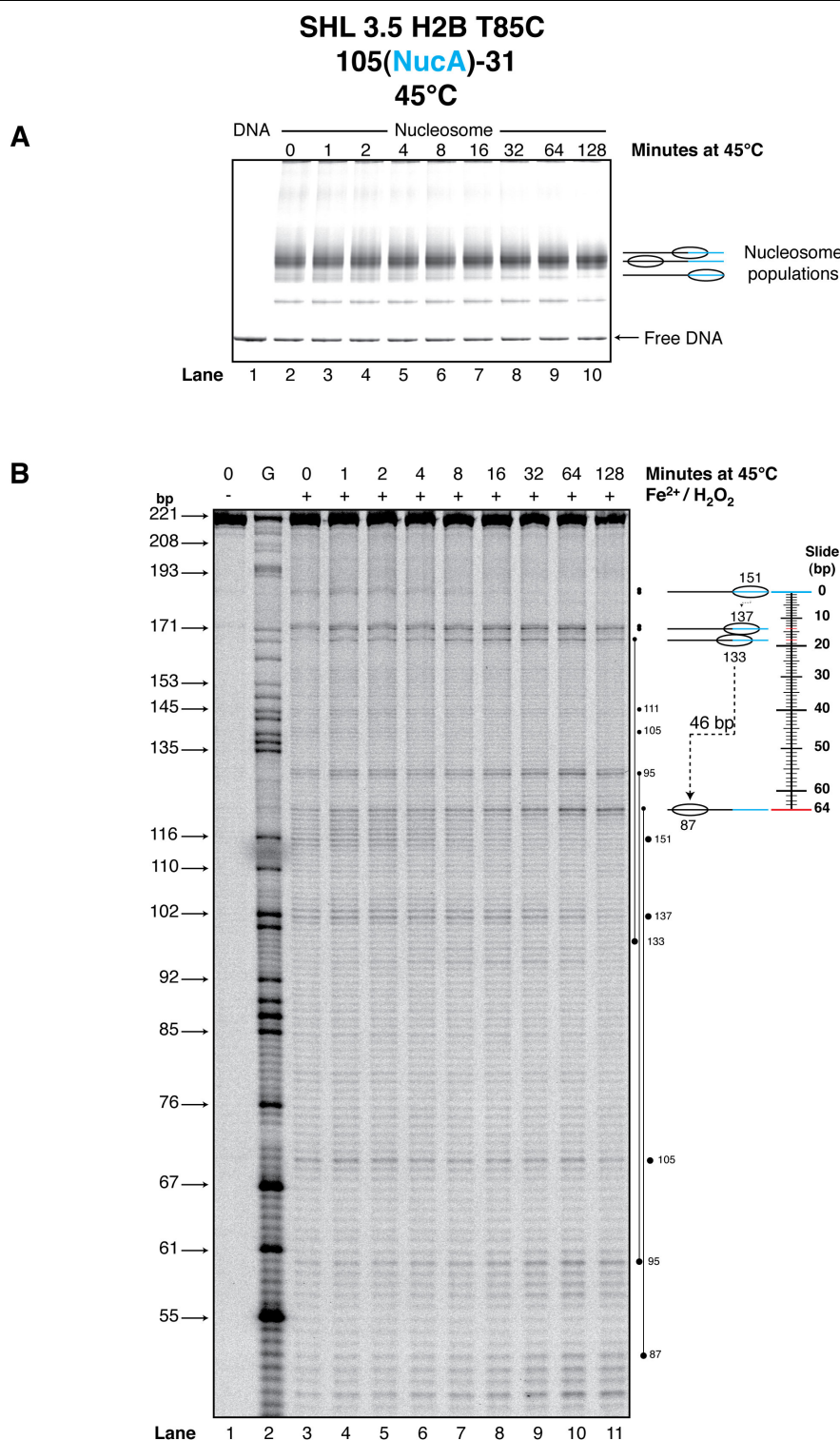


Figure 4.11 Thermal sliding of 105(NucA)-31 mapped at SHL 3.5. **A.** Native PAGE of 105(NucA)-31 nucleosomes incubated at 45°C for 0-128 minutes. **B.** Denaturing PAGE of 105(NucA)-31 nucleosomes incubated at 45°C for 0-128 minutes and mapped at SHL 3.5 using EDTA reagent. Signal profiles shown in Figure 4.11 C. Large black circles represent primary cutting and small black circles represent secondary cutting. (–) and (+) signs represent the respective absence and presence of Fe²⁺ at 1 ion/nucleosome and H₂O₂ in the mapping assays. The G-track marker (G) represents the 105(NucA)-31 DNA sequence cleaved at every guanine nucleotide, fragment size is given in base pairs (bp). Nucleosome positions are given in relation to the central dyad base pair. Gels were visualised using the Fuji phosphor-imager FLA-5100.

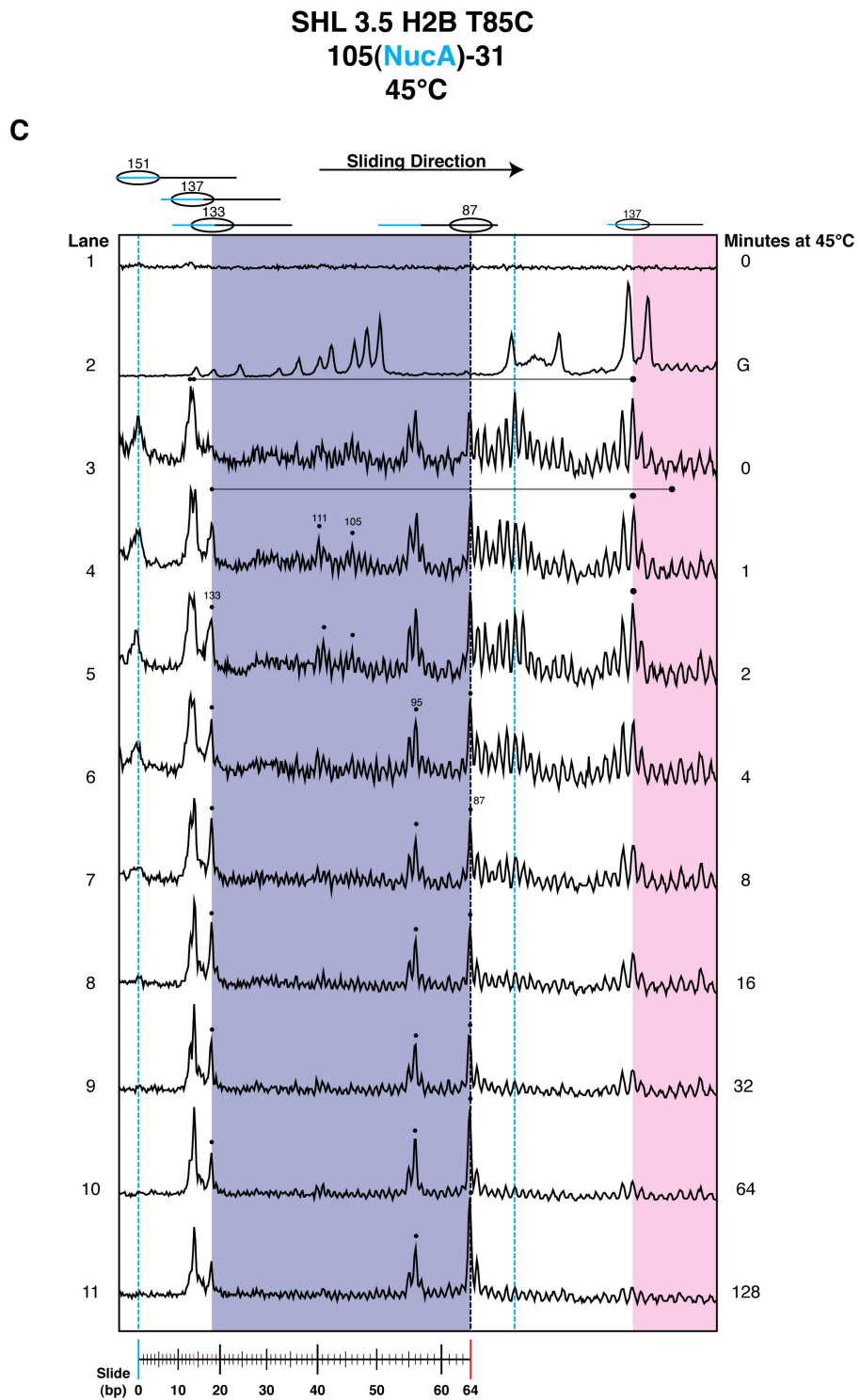


Figure 4.11 Thermal sliding of 105(NucA)-31 mapped at SHL 3.5. C. Signal profile of 105(NucA)-31 nucleosomes incubated at 45°C for 0-128 minutes and mapped at SHL 3.5 using EDTA, from Figure 4.11 B. Purple and magenta regions represent the respective secondary and primary mapping for the second stage of sliding over 46 bp. Large black spheres represent primary mapping and small black circles represent secondary mapping. Signal profiles obtained using AIDA analysis software.

4.13 NucA-31 sliding at 37°C mapped at SHL 4.5

NucA-31 nucleosomes were incubated at 37°C for 0-128 minutes to probe intermediate positioning between the 151 and 131 centered nucleosomes. After incubation the nucleosomes were mapped from the H2A-H2B dimer at SHL 4.5 H2A T16C. For SHL 4.5 mapping, the distance between primary and secondary cuts increases to ~89 bp.

4.13.1 Observations

The nucleosome positioning and stability for the first 20 bp is very similar for SHL 4.5 H2A T16C as observed with SHL 0.5-2.5. Five main populations have been observed over the 20 bp phase, starting at 151 and moving through 140, 135, 133 and 131 centered nucleosomes.

Initially some of the 151 nucleosome slides to the 140 position after 1-2 minutes of incubation. After ≥ 8 minutes of incubation the 140 nucleosome position destabilises and along with the 151 nucleosome slide to take up position at 135, 133 and 131. These positions stay relatively stable for up to 64 minutes whereby further incubation at 37°C sees these populations progressively reduced ultimately sliding to the terminal 85 position, Figure 4.12 B and C.

The primary mapping at SHL 4.5 is relatively poor as can be seen from the full length gel in Figure 4.12 B making it difficult to determine a possible dimer disengagement. Low cutting efficiency was also observed at the primary site using EDTA for mapping the 147 bp NucA sequence, Figure 3.9 B lane 8.

Band resolution on the native gel was difficult to interpret due to fuzziness within the populations possibly caused by DNA unpeeling at the nucleosome extremities.

4.13.2 Interpretation

Restoration back to the original positions that were altered for SHL 3.5 would suggest that the mutation T85C of H2B causes some interference and destabilisation

in the DNA binding at some of the positions, although the initial position 151 showed consistency throughout.

Of the five positions observed within the initial 20 bp slide four of these positions have been consistently observed, these are 151, 140, 133 and 131. The position 135 is similar to another previously mapped position of 136 indicating uniformity throughout the mapping.

The inefficient primary mapping at SHL 4.5 would not confirm or reject a dimer disengagement mechanism for nucleosome sliding as this was also observed during the nucleosome mapping in Chapter 3. However, because the secondary mapping at SHL 4.5 on the dimer is observed and that it has a similar mapping pattern to the tetramer would indicate that at least one dimer is present during sliding.

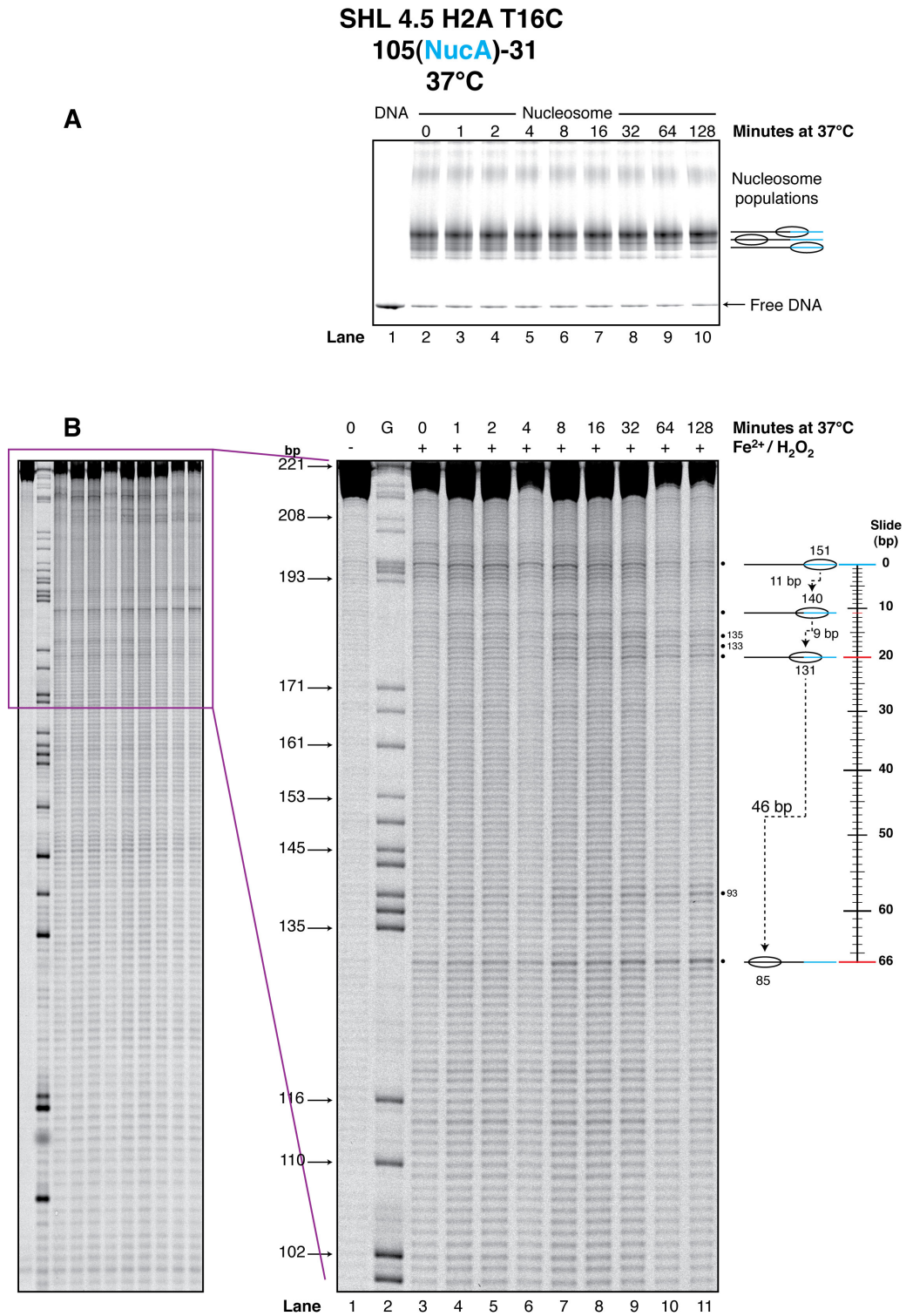


Figure 4.12 Thermal sliding of 105(NucA)-31 mapped at SHL 4.5. **A.** Native PAGE of 105(NucA)-31 nucleosomes incubated at 37°C for 0-128 minutes. **B.** Long and short duration denaturing PAGE of 105(NucA)-31 nucleosomes incubated at 37°C for 0-128 minutes and mapped at SHL 4.5 H2B T85C using EDTA reagent. Signal profiles of long duration PAGE shown in Figure 4.12 C. (–) and (+) signs represent the respective absence and presence of Fe²⁺ at 1 ion/nucleosome and H₂O₂ in the mapping assays. The G-track marker (G) represents the 105(NucA)-31 DNA sequence cleaved at every guanine nucleotide, fragment size is given in base pairs (bp). Nucleosome positions are given in relation to the central dyad base pair. Gels were visualised using the Fuji phosphor-imager FLA-5100.

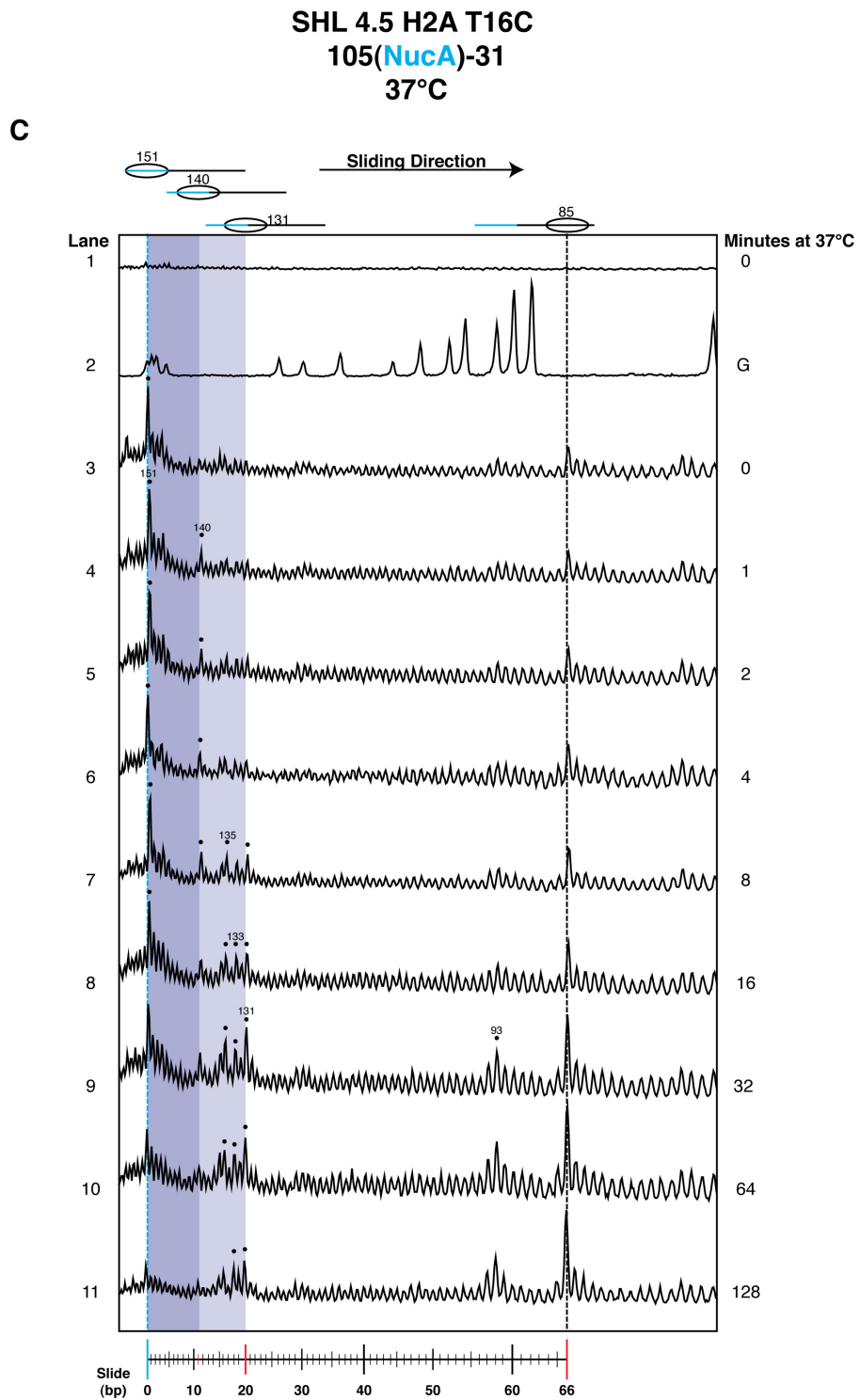


Figure 4.12 Thermal sliding of 105(NucA)-31 mapped at SHL 4.5. C. Signal profile of 105(NucA)-31 nucleosomes incubated at 37°C for 0-128 minutes and mapped at SHL 4.5 using EDTA, from Figure 4.12 B, long duration PAGE. Purple region represents secondary mapping over the initial 20 bp slide. The cyan broken line represents the initial 151 position with the black broken line representing the terminal position. Small black spheres represent secondary mapped populations. Signal profiles obtained from AIDA analysis software.

4.14 NucA-31 sliding at 45°C mapped at SHL 4.5

NucA-31 nucleosomes were incubated at 45°C for 0-128 minutes to probe the intermediate positioning between the 131 and 85 centered nucleosomes. After incubation the nucleosomes were mapped from the H2A-H2B dimer at SHL 4.5 H2A T16C using the EDTA reagent.

4.14.1 Observations

Due to poor mapping efficiency within these samples only one intermediate position is observed over the 46 bp sliding phase between the 131 and 85 positions. This is at the previously observed 93 bp position, Figure 4.13 B and C.

After 2 minutes of incubation at 45°C the quantity of the 85 bp centered nucleosome population seems to have increased due to sliding from the 131 position, Figure 4.13 B and C.

After 8 minutes of incubation the 131, 93 and 85 populations have increased due to transition in the positioning past the initial 20 bp phase from 151 to 131. After 32 minutes the 131 population had destabilised to take up position with 93 and 85 bp centers. Incubation times >64 minutes destabilises the 93 population for positioning at the 85 bp centered nucleosome, Figure 4.13 B and C.

4.14.2 Interpretation

The secondary mapping in these samples is quite poor but sliding can still be observed over the 46 bp region from 131 to 85. Once again no obvious pattern of sliding is observed that would indicate either a twist defect or loop defect mechanism of sliding.

The primary mapping over this region produced little clear cutting. This is consistent throughout as there is little primary cutting observed using the EDTA reagent at SHL 4.5 for the mapping of non-sliding NucA, 601 and 601.2 nucleosomes discussed in Chapter 3.

The poor band resolution in the earlier incubation times of the native gel would indicate that DNA wrapping at the entry/exit is loose and/or that numerous populations exist relatively close together.

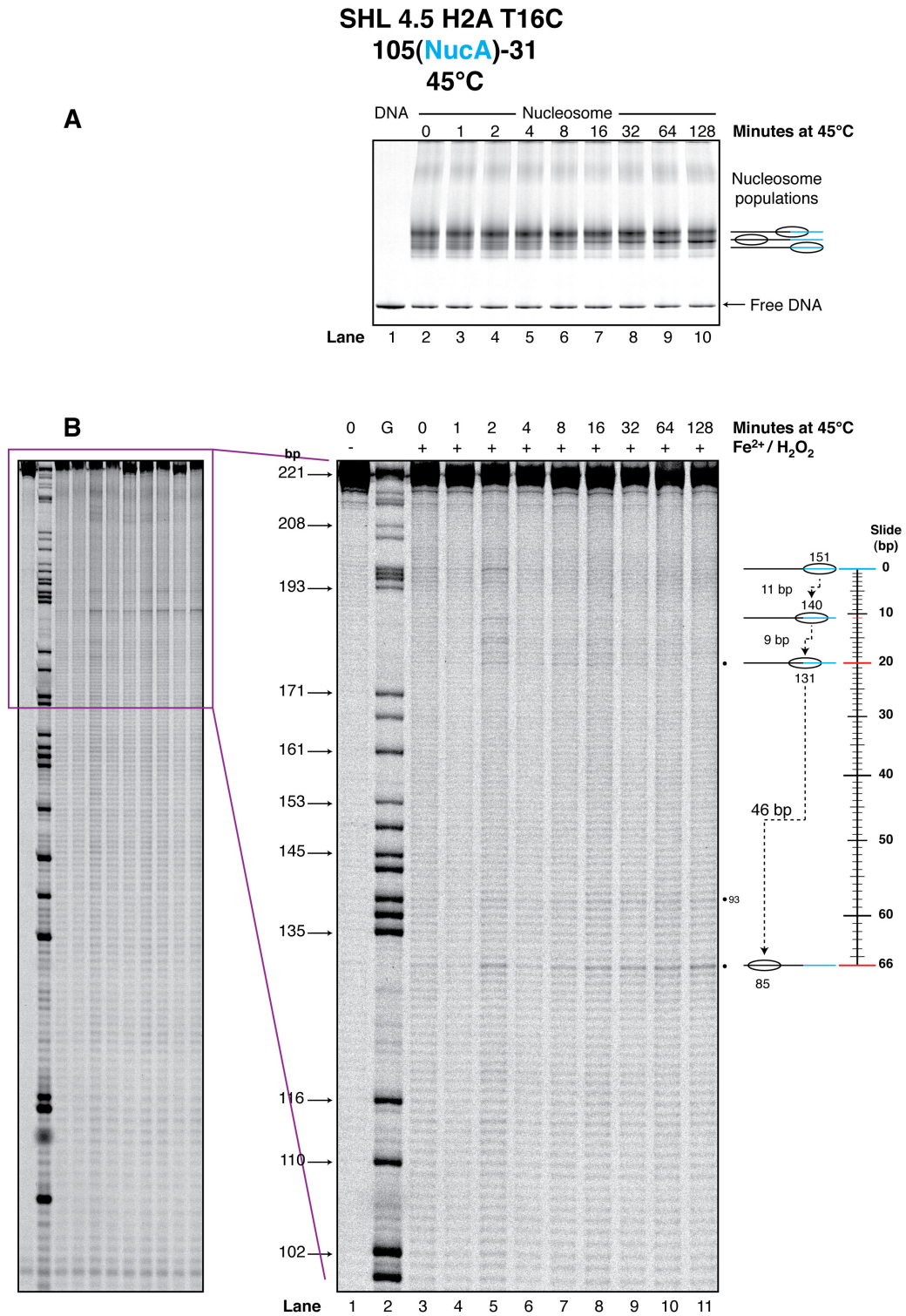


Figure 4.13 Thermal sliding of 105(NucA)-31 mapped at SHL 4.5. **A.** Native PAGE of 105(NucA)-31 nucleosomes incubated at 45°C for 0-128 minutes. **B.** Long and short duration denaturing PAGE of 105(NucA)-31 nucleosomes incubated at 45°C for 0-128 minutes and mapped at SHL 4.5 using EDTA reagent. Signal profile of long duration PAGE shown in Figure 4.13 C. (–) and (+) signs represent the respective absence and presence of Fe^{2+} at 1 ion/nucleosome and H_2O_2 in the mapping assays. The G-track marker (G) represents the 105(NucA)-31 DNA sequence cleaved at every guanine nucleotide, fragment size is given in base pairs (bp). Nucleosome positions are given in relation to the central dyad base pair. Gels were visualised using the Fuji phosphor-imager FLA-5100.

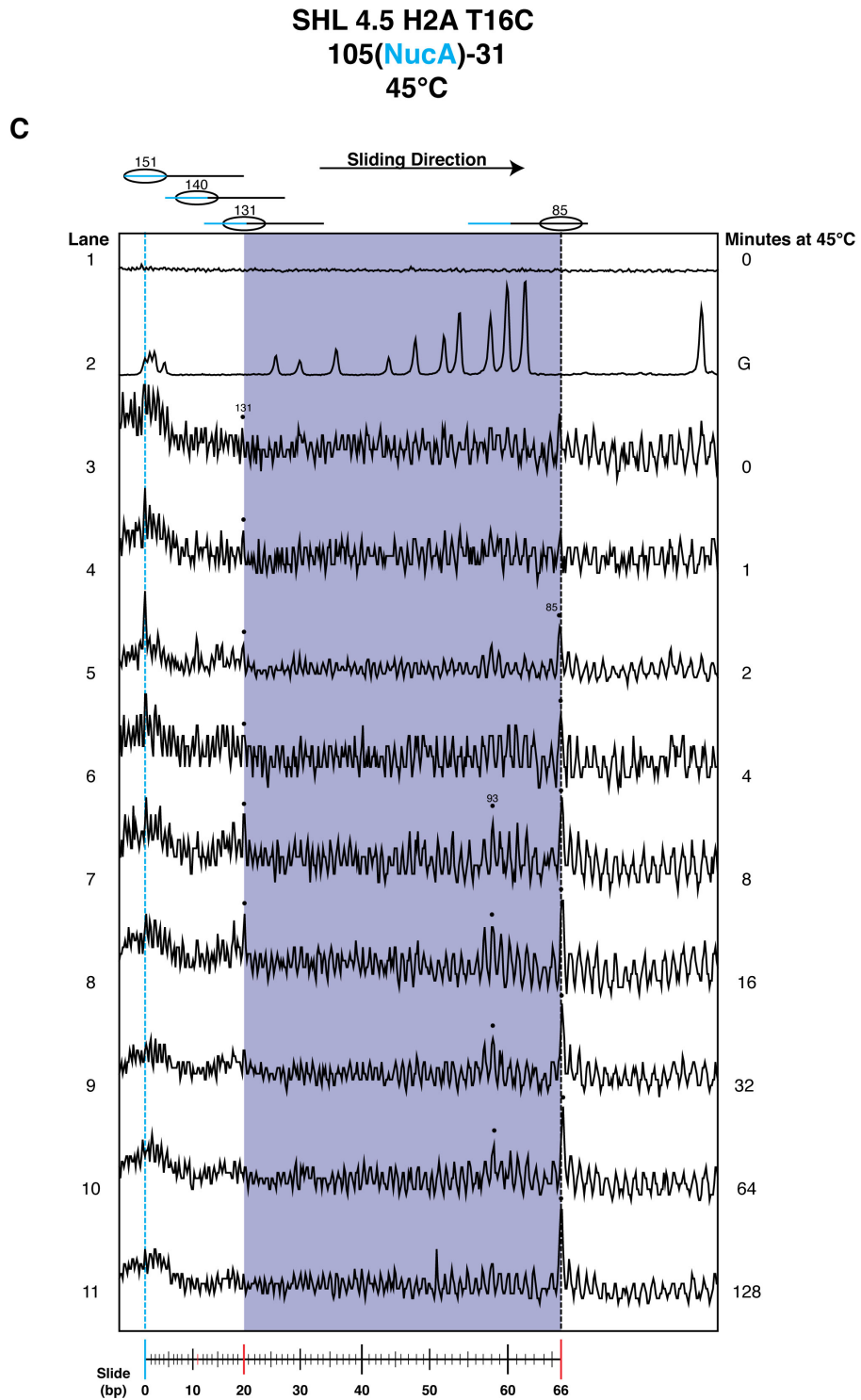


Figure 4.13 Thermal sliding of 105(NucA)-31 mapped at SHL 4.5. C. Signal profile of 105(NucA)-31 nucleosomes incubated at 45°C for 0-128 minutes and mapped at SHL 4.5 using EDTA reagent, from Figure 4.13 B, long duration PAGE. Purple region represents secondary mapping over the 46 bp second stage of sliding. Small black spheres represent secondary mapped populations. Signal profiles obtained from AIDA analysis software.

4.15 NucA-31 sliding at 37°C mapped at SHL 5.5

NucA-31 nucleosomes were incubated at 37°C for 0-128 minutes to probe the intermediate positioning between the 151 and 131 centered nucleosomes. After incubation the nucleosomes were mapped from the H2A-H2B dimer at SHL 5.5 H2B G50C using the EDTA reagent. Distances between primary and secondary mapping sites at SHL 5.5 are approximately 108 bp.

4.15.1 Observations

Mapping at SHL 5.5 is relatively weak but previously observed populations can be determined. After nucleosome assembly the main nucleosome population is the 151 centered nucleosome as expected. Some of this population is destabilised after 2 minutes and moves to 140 bp, Figure 4.14 B and C.

Further incubation at 37°C causes the 140 population to then slide 4 bp to reposition at 136. After 32 minutes the 151 population has further reduced with the 131 population clearly increasing, Figure 4.14 B and C.

Incubation up to 128 minutes sees the 151 and 140 population almost completely depleted while the 136 and 131 populations have greatly reduced. The destabilisation of the 4 populations within this 20 bp region ultimately leads to an increase in the 94 and 85 bp centered populations, Figure 4.14 B and C.

Primary mapping on the H2A-H2B dimer has been observed from this location as seen in the full length gel, Figure 4.14 B. In the earlier incubation times of the native gel (lanes 1-7) multiple populations are observed. This is interpreted by the fuzziness of the banding pattern. Incubation times of ≥ 32 minutes sees a more defined band representing the 93 and 85 populations, Figure 4.14, A.

4.15.2 Interpretation

Both primary and secondary mapping is observed at SHL 5.5, which would suggest that the outer nucleosomal DNA on both sides of the nucleosome is bound to the H2A-H2B dimer during sliding. Similar mapping patterns have been observed for

the first 20 bp sliding phase for nucleosomes mapped at SHL 0.5, 1.5, 2.5, 4.5 and 5.5, with SHL 3.5 the only position to deviate from the general sliding trend. However, it would seem that as the distance from the mapping location to the nucleosomal dyad increases, affinity for intermediate positioning tends to decrease. This is demonstrated by the fact that less intermediate positioning seems to be observed at mapping SHL 4.5 and 5.5 than were observed over the initial 20 bp sliding phase at SHL 0.5 and 1.5. This could be explained by the cysteine mutation and EDTA reagent slightly interfering with the affinity that DNA and octamer have for each other.

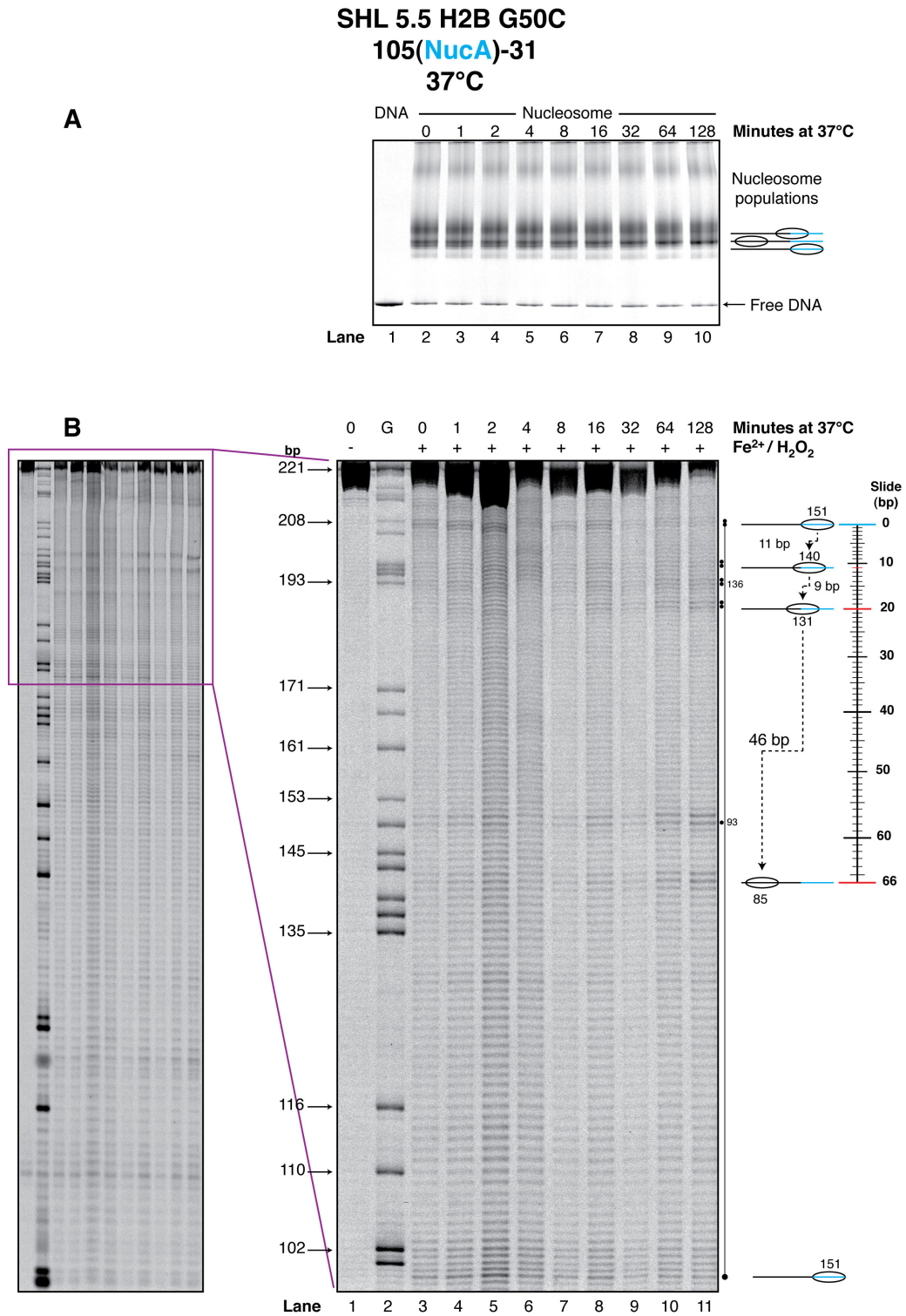


Figure 4.14 Thermal sliding of 105(NucA)-31 mapped at SHL 4.5. **A.** Native PAGE of 105(NucA)-31 nucleosomes incubated at 37°C for 0-128 minutes. **B.** Long and short duration denaturing PAGE of 105(NucA)-31 nucleosomes incubated at 37°C for 0-128 minutes and mapped at SHL 5.5 H2B G50C using EDTA reagent. Signal profile of long duration PAGE shown in Figure 4.14 C. (–) and (+) signs represent the respective absence and presence of Fe²⁺ at 1 ion/nucleosome and H₂O₂ in the mapping assays. The G-track marker (G) represents the 105(NucA)-31 DNA sequence cleaved at every guanine nucleotide, fragment size is given in base pairs (bp). Nucleosome positions are given in relation to the central dyad base pair. Gels were visualised using the Fuji phosphor-imager FLA-5100.

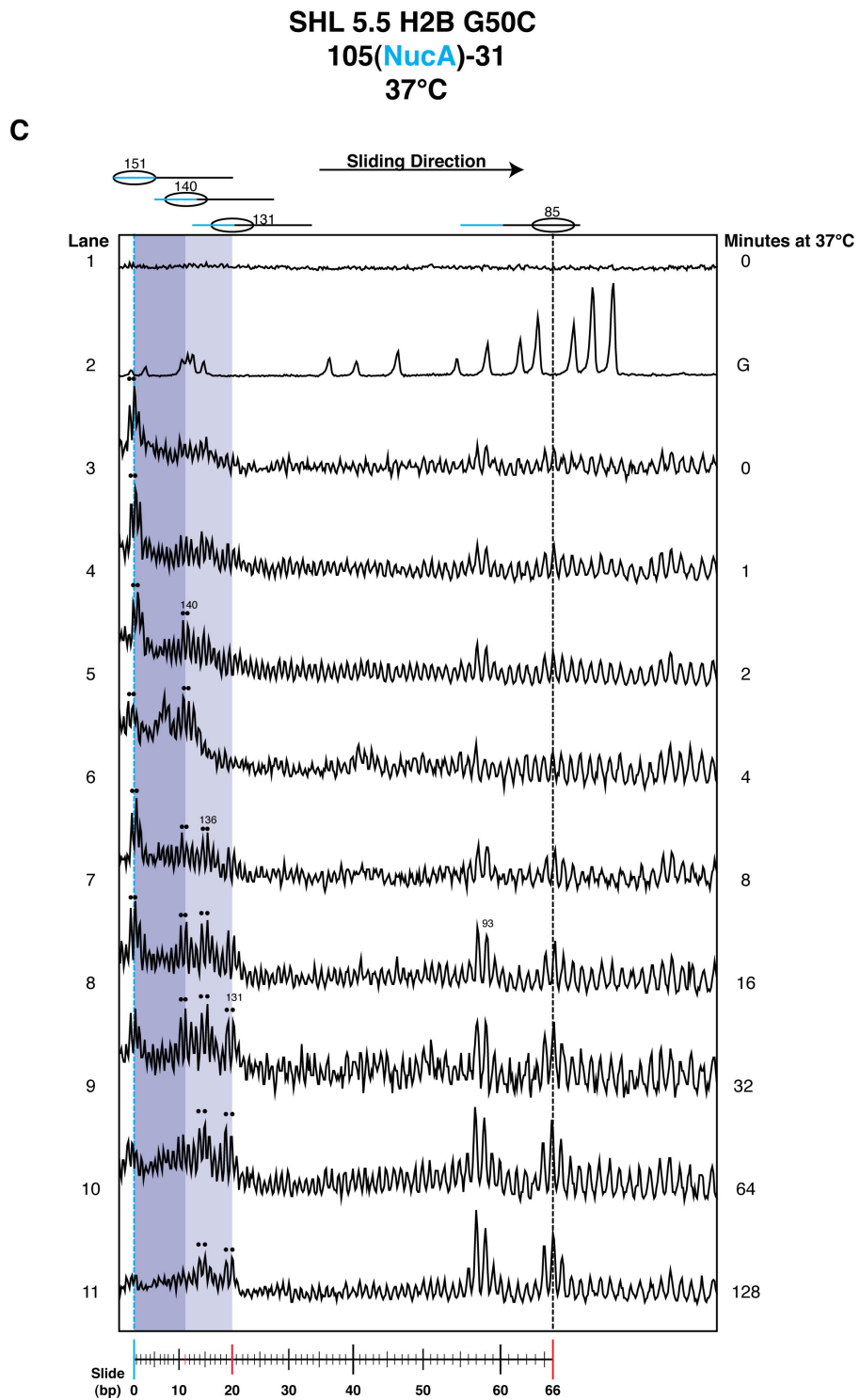


Figure 4.14 Thermal sliding of 105(NucA)-31 mapped at SHL 5.5. C. Signal profile of 105(NucA)-31 nucleosomes incubated at 37°C for 0-128 minutes and mapped at SHL 5.5 using EDTA reagent, from Figure 4.14 B, long duration PAGE. Purple regions represent secondary mapping over the initial 20 bp slide. Small black spheres represent secondary mapped populations. Signal profiles obtained using AIDA analysis software.

4.16 NucA-31 sliding at 45°C mapped at SHL 5.5

NucA-31 nucleosomes were incubated at 45°C for 0-128 minutes to probe the intermediate positioning between the 131 and 85 centered nucleosomes. After incubation the nucleosomes were mapped from the H2A-H2B dimer at SHL 5.5 H2B G50C using the EDTA reagent.

4.16.1 Observations

Nucleosomes assemble predominantly at the expected 151 position. After just 1-2 minutes of incubation at 45°C an increase is observed in the number of nucleosomes at positions 140 and 136, followed by an accumulation at 131 by 4 minutes, Figure 4.15 B and C.

Further incubation up to 8 minutes or more sees a gradual increase in the 94 population and the 85 population. After 32 minutes the repositioning to 94 and 85 centres is almost complete, Figure 4.15 B and C.

Some other small populations exist at 122, 109 and 102 bp centres. However, an obvious pattern of sliding between the positioned nucleosome is not observed and again primary and secondary mapping is observed as for the 37 °C incubation at the same site, Figure 4.15 B and C.

The native gel shows nucleosome sliding, with the earlier incubations showing mixed population relatively close together and the later incubations (lanes 8-10) showing a defined band which represents nucleosomes 94 and 85, Figure 4.15 A.

4.16.2 Interpretation

The same positioning trend is seen over the 46 bp sliding region as observed at previous mapping sites, suggesting uniform mapping between the various SHL sites. The evidence of primary and secondary DNA cleavage indicates DNA contact for both sides of the nucleosome, which would not support any major form of alternative conformation within the nucleosome structure during sliding.

The lack of any obvious DNA cleavage at intervals equivalent to helical turn lengths would suggest the loop defect mechanism of nucleosome sliding is not occurring. However, there are also no obvious single base pair steps between positioned nucleosomes above background level that could indicate a twist defect diffusion mechanism of sliding.

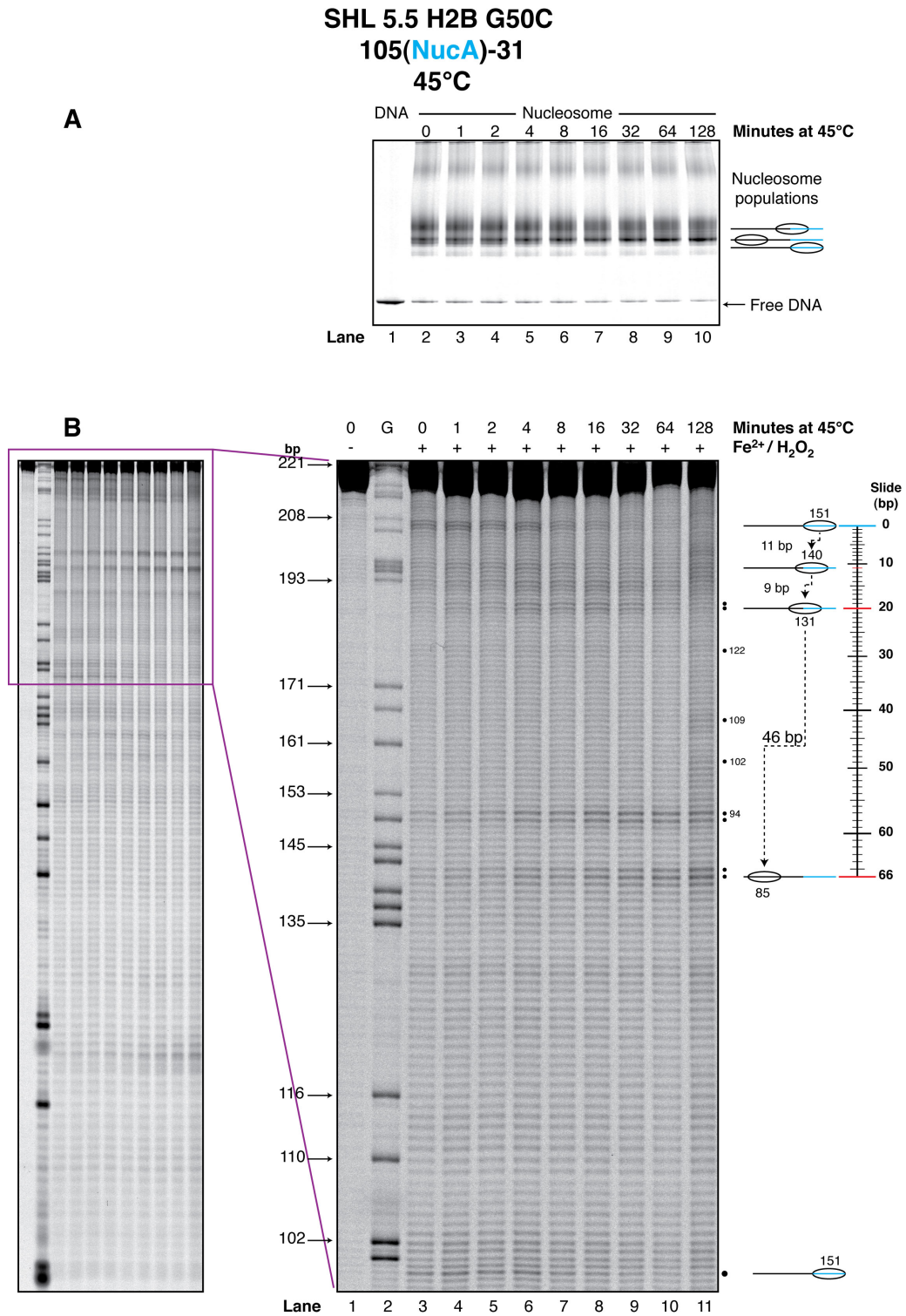


Figure 4.15 Thermal sliding of 105(NucA)-31 mapped at SHL 5.5. **A.** Native PAGE of 105(NucA)-31 nucleosomes incubated at 45°C for 0-128 minutes. **B.** Long and short duration denaturing PAGE of 105(NucA)-31 nucleosomes incubated at 45°C for 0-128 minutes and mapped at SHL 5.5 using EDTA reagent. Signal profile of long duration PAGE shown in Figure 4.15 C. (–) and (+) signs represent the respective absence and presence of Fe²⁺ at 1 ion/nucleosome and H₂O₂ in the mapping assays. The G-track marker (G) represents the 105(NucA)-31 DNA sequence cleaved at every guanine nucleotide, fragment size is given in base pairs (bp). Nucleosome positions are given in relation to the central dyad base pair. Gels were visualised using the Fuji phosphor-imager FLA-5100.

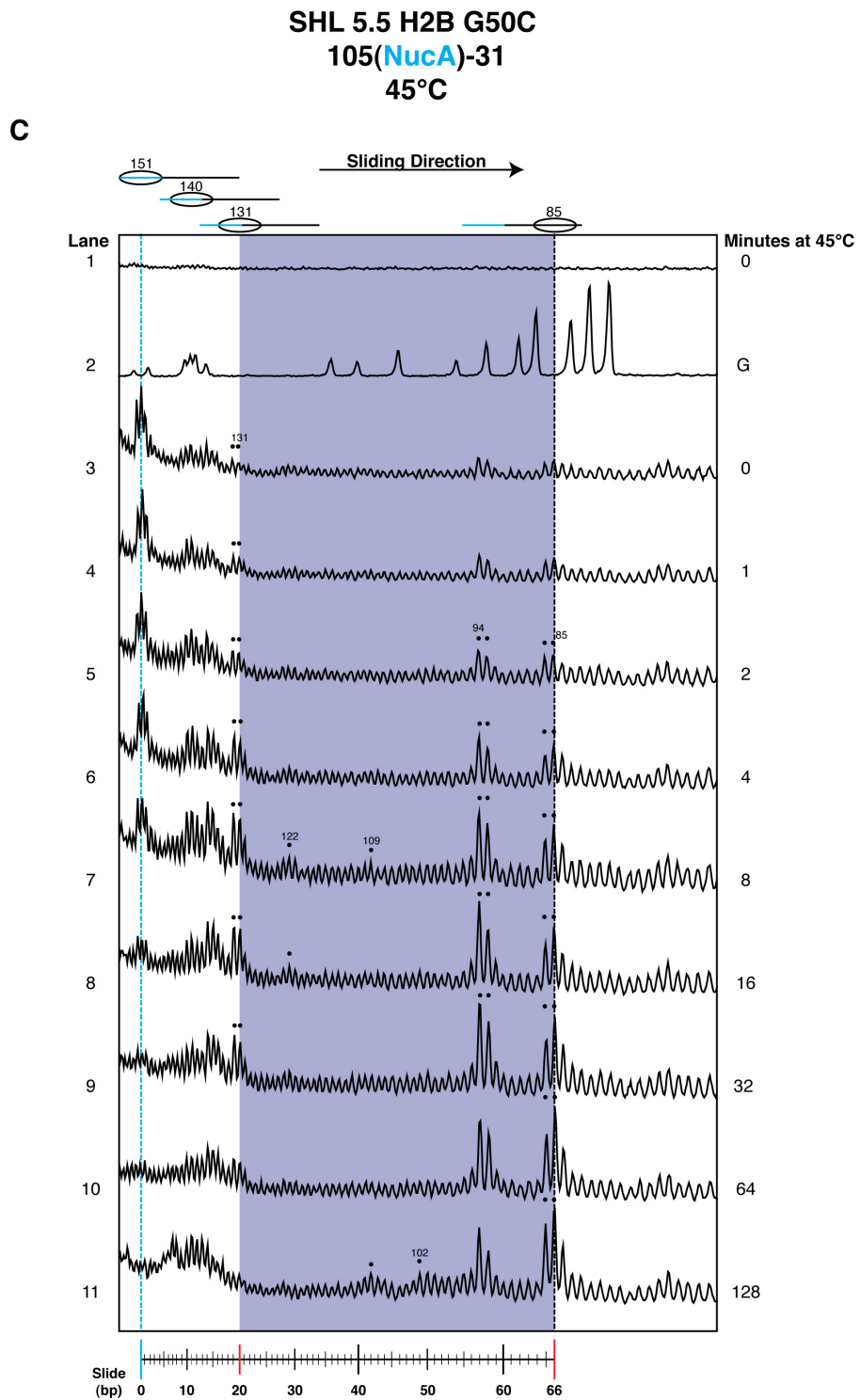


Figure 4.15 Thermal sliding of 105(NucA)-31 mapped at SHL 5.5. C. Signal profile of 105(NucA)-31 nucleosomes incubated at 45°C for 0-128 minutes and mapped at SHL 5.5 using EDTA reagent, from Figure 4.15 B, long duration PAGE. The purple region represents secondary mapping over the 46 bp region. Small black spheres represent secondary mapped populations. Signal profiles obtained using AIDA analysis software.

4.17 NucA-31 sliding at 37°C mapped at SHL 6.5

NucA-31 nucleosomes were incubated at 37°C for 0-128 minutes to probe the intermediate positioning between the 151 and 131 centered nucleosomes. After incubation the nucleosomes were mapped from the α N-helix at SHL 6.5 H3 T45C using the EDTA reagent. Distances between the primary and secondary mapping for SHL 6.5 are approximately 130 bp.

4.17.1 Observations

No obvious primary mapping is occurring. Secondary mapping is observed although the 131 population is the only intermediate position that successfully mapped over the initial 20 bp sliding phase, Figure 4.16 B.

Increased incubation time at 37°C sees an increase in the 131 population, which reaches a peak at 32 minutes. Further incubation sees repositioning of the 131 population over the second sliding phase and these are observed at 93 and 85 bp centers, Figure 4.16 B and C. There is also some evidence of weak mapping at positions between 131 and 93 at positions 103 and 99.

The contaminating DNA fragment band X is observed again throughout all samples. Its relative concentration throughout appears constant with loading suggesting there is no cross contamination within the sliding phase under analysis.

4.17.2 Interpretation

No secondary mapping at 151 could be detected due to the level of full length DNA in the samples. However due to secondary mapping side of the nucleosome containing only 70 bp of DNA it is possible no mapping occurred. This is because the dyad of the 151 population is centered at 151 bp, which leaves 70 bp spanning the secondary mapped side of the nucleosome on a DNA fragment of 221 bp.

The difficulty of mapping nucleosomes at SHL 6.5 is not necessarily unexpected giving the dynamics at this position and the challenges observed in

mapping this region using the NucA, 601 and 601.2 positioning sequences in conjunction with 2 different mapping reagents, Figure 3.11.

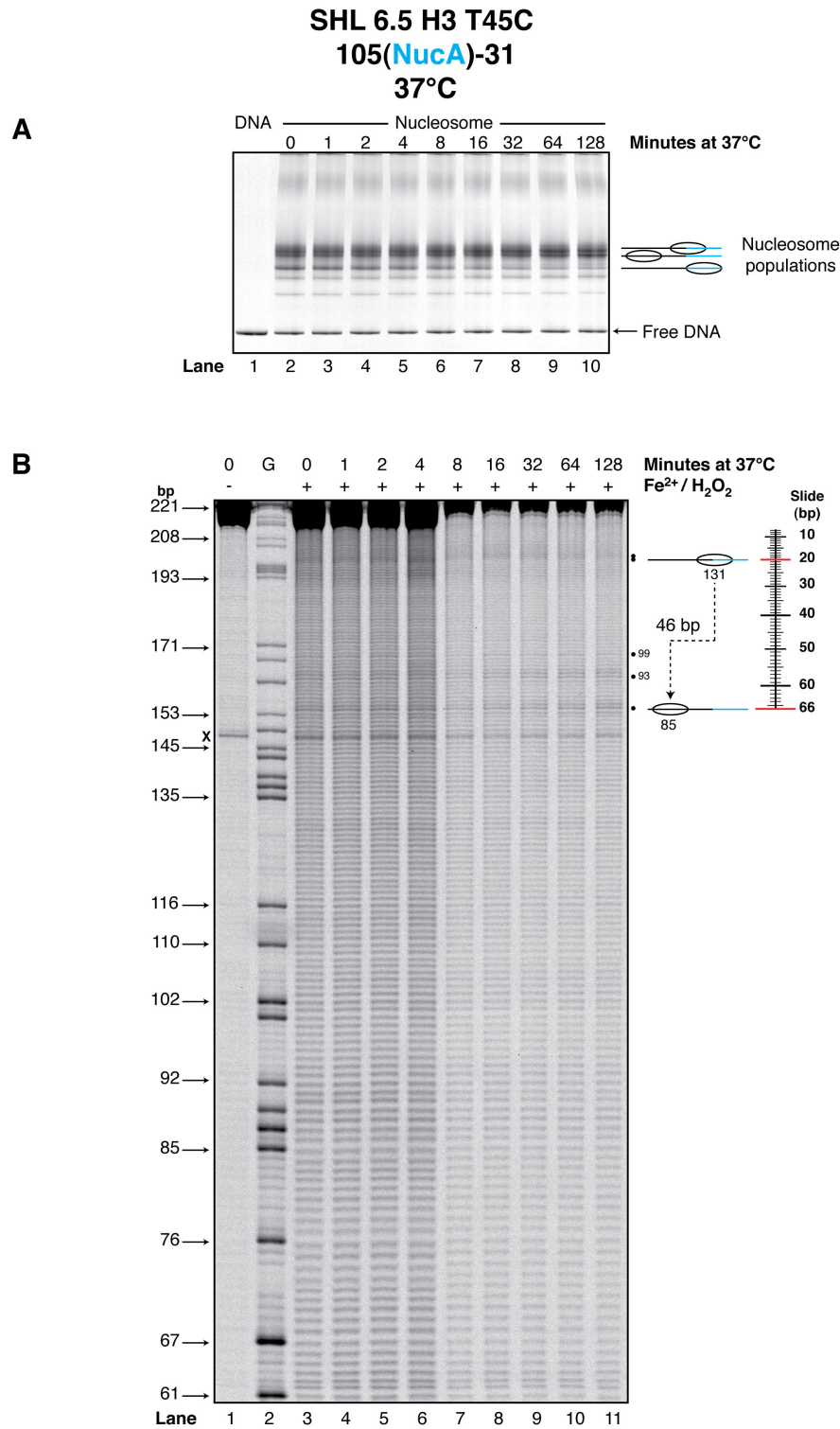


Figure 4.16 Thermal sliding of 105(NucA)-31 mapped at SHL 6.5. **A.** Native PAGE of 105(NucA)-31 nucleosomes incubated at 37°C for 0-128 minutes. **B.** Denaturing PAGE of 105(NucA)-31 nucleosomes incubated at 37°C for 0-128 minutes and mapped at SHL 6.5 H3 T45C using EDTA reagent. Signal profile shown in Figure 4.16 C. Band X is a DNA contamination found in all samples. (–) and (+) signs represent the respective absence and presence of Fe²⁺ at 1 ion/nucleosome and H₂O₂ in the mapping assays. The G-track marker (G) represents the 105(NucA)-31 DNA sequence cleaved at every guanine nucleotide, fragment size is given in base pairs (bp). Nucleosome positions are given in relation to the central dyad base pair. Gels were visualised using the Fuji phosphor-imager FLA-5100.

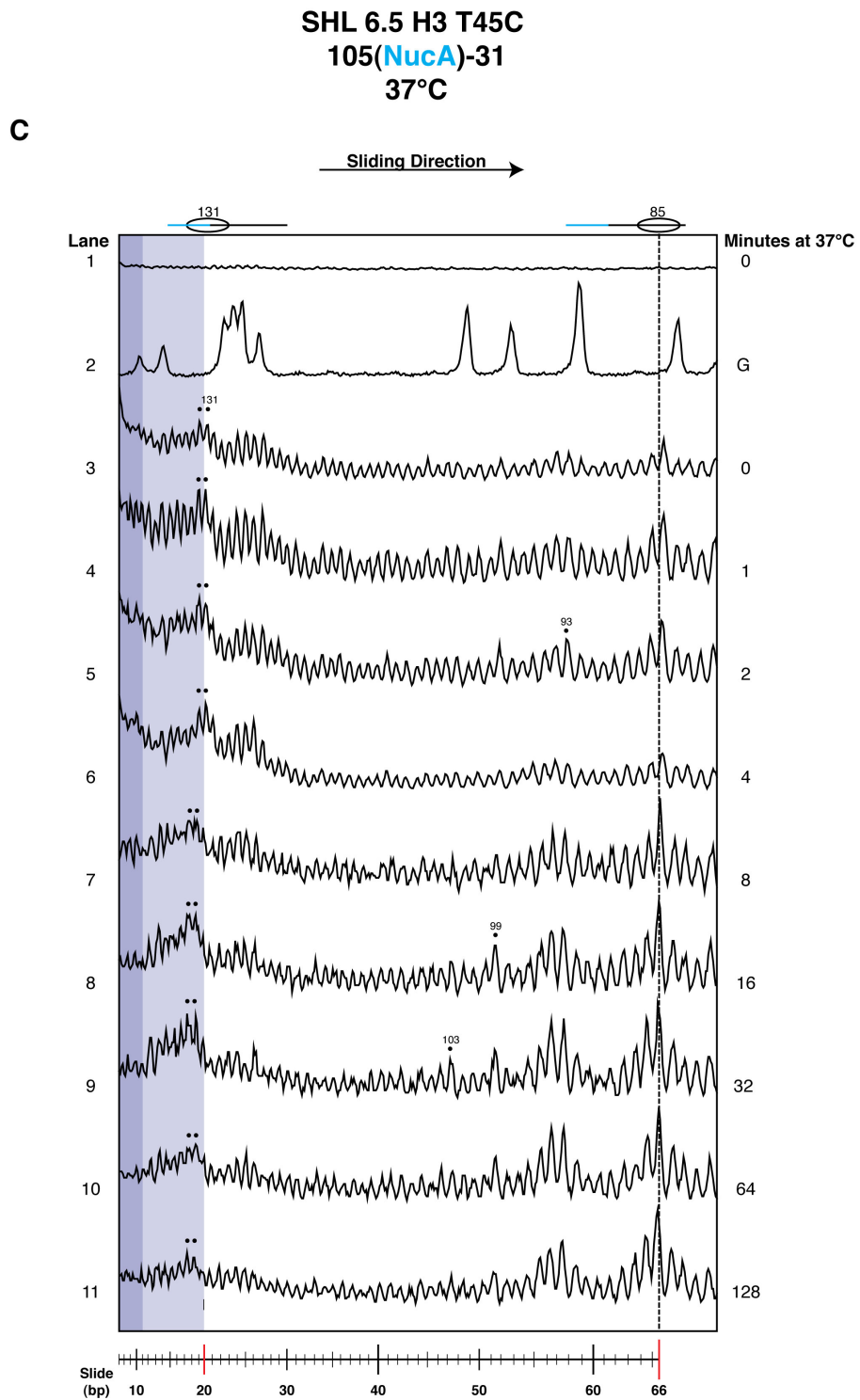


Figure 4.16 Thermal sliding of 105(NucA)-31 mapped at SHL 6.5. C. Signal profile of 105(NucA)-31 nucleosomes incubated at 37°C for 0-128 minutes and mapped at SHL 6.5 using EDTA reagent, from Figure 4.16 B. The purple region represents the secondary mapping up to the 131 positioned nucleosome. Small black spheres represent secondary mapped populations. Signal profiles obtained using AIDA analysis software.

4.18 NucA-31 sliding at 45°C mapped at SHL 6.5

NucA-31 nucleosomes were incubated at 45°C for 0-128 minutes to probe the intermediate positioning between the 131 and 85 centered nucleosomes. After incubation the nucleosomes were mapped from the α N-helix at SHL 6.5 H3 T45C using the EDTA reagent.

4.18.1 Observations

Initially some nucleosome populations are observed between 131 and 85, although these populations at 124, 103, 99 and 93 are only just above background levels, Figure 4.17 C.

After 2 minutes the 131 population has increased while the 103 population has depleted to background level, Figure 4.17 C.

After 16 minutes the main populations remaining are 93 and 85 and with further incubation of up to 128 minutes the 93 bp population is destabilised and repositions to centre at 85 bp. No obvious pattern of nucleosome sliding is observed between positioned nucleosomes, also no primary mapping for the initial 151 nucleosome position was observed, Figure 4.17.

4.18.2 Interpretation

The 46 bp sliding region from 131 to 85 has 4 intermediately positioned nucleosomes above background signal at 124, 103, 99 and 93, demonstrating that the entry/exit DNA has remained associated with the nucleosome in moderately stable transitory nucleosome positions. It would also suggest that DNA looping off the outer parts of the nucleosome, or that of a dimer disengagement event are unlikely to occur frequently to nucleosomes while sliding, at least for one half of the nucleosome.

Once again no mapping patterns were observed that would indicate a loop defect diffusion mechanism of sliding or obvious patterns that would indicate a twist defect mechanism for sliding.

The contamination band X is also observed throughout these samples although it does not interfere with the interpretation of the secondary mapping due to its shorter length.

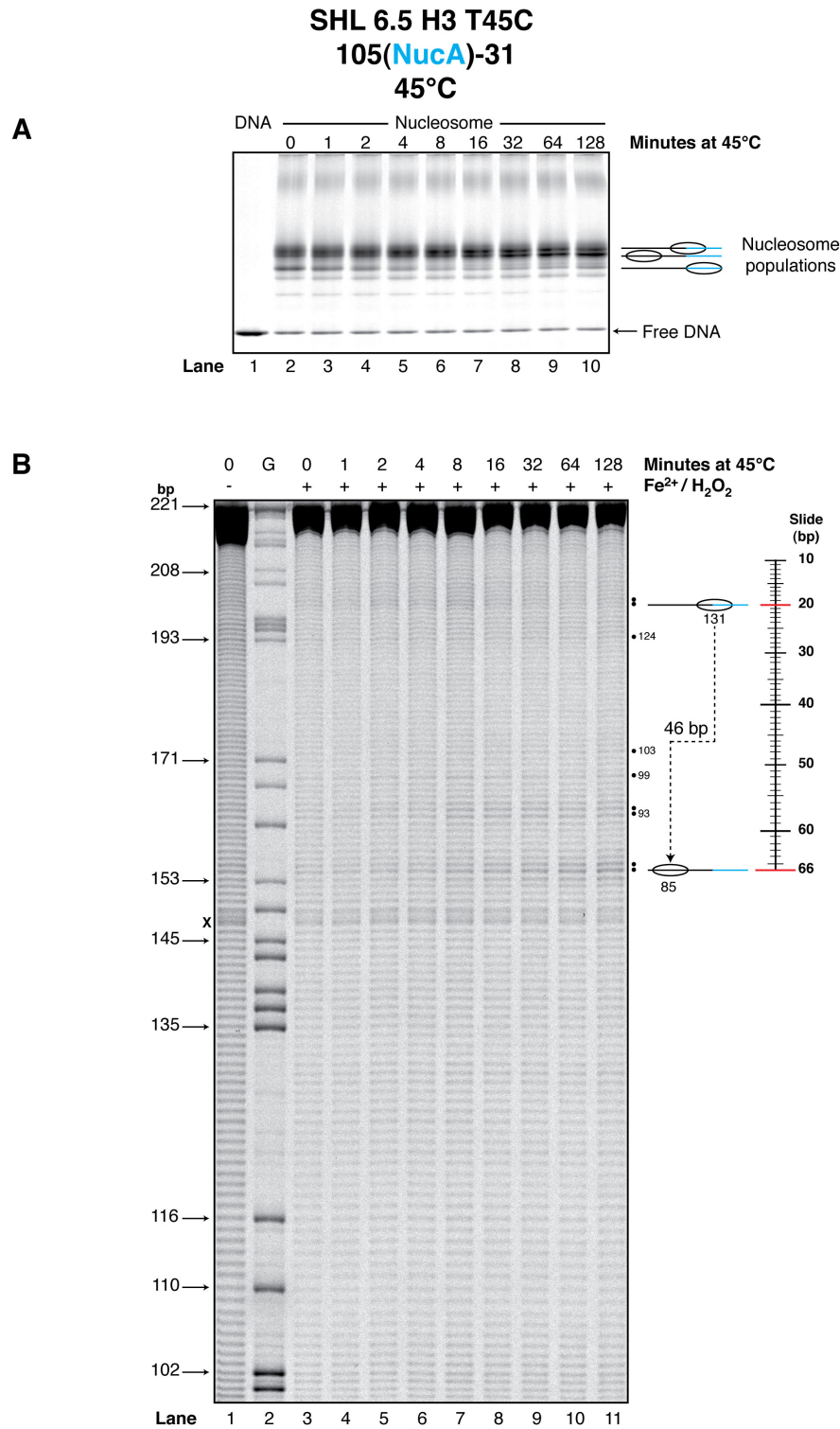


Figure 4.17 Thermal sliding of 105(NucA)-31 mapped at SHL 6.5. **A.** Native PAGE of 105(NucA)-31 nucleosomes incubated at 45°C for 0-128 minutes. **B.** Denaturing PAGE of 105(NucA)-31 nucleosomes incubated at 45°C for 0-128 minutes and mapped at SHL 6.5 using EDTA reagent. Signal profile shown in Figure 4.17. Band X is a DNA contamination found in all samples. (–) and (+) signs represent the respective absence and presence of Fe²⁺ at 1 ion/nucleosome and H₂O₂ in the mapping assays. The G-track marker (G) represents the 105(NucA)-31 DNA sequence cleaved at every guanine nucleotide, fragment size is given in base pairs (bp). Nucleosome positions are given in relation to the central dyad base pair. Gels were visualised using the Fuji phosphor-imager FLA-5100.

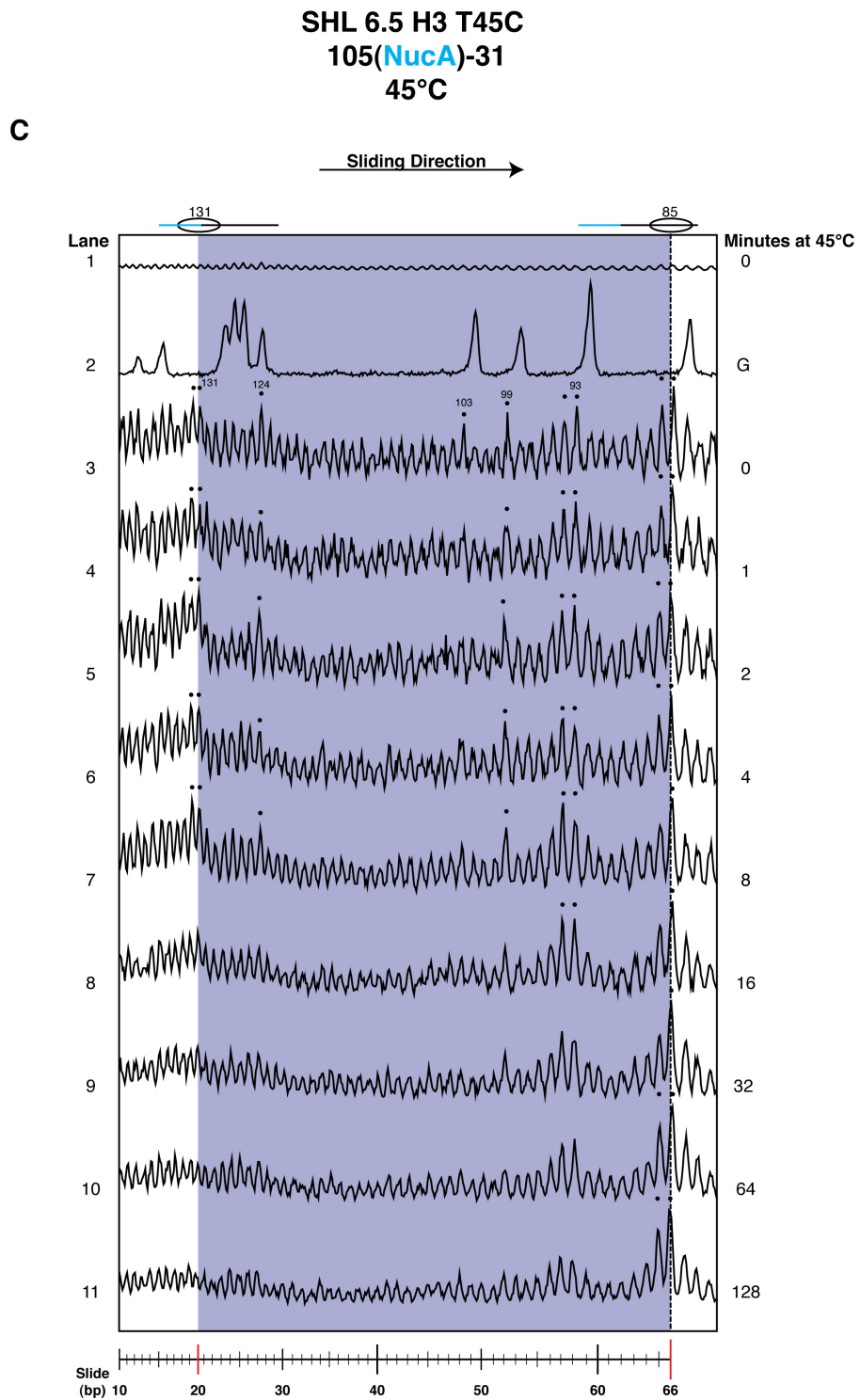


Figure 4.17 Thermal sliding of 105(NucA)-31 mapped at SHL 6.5. C. Signal profile of 105(NucA)-31 nucleosome incubated at 45°C for 0-128 minutes and mapped at SHL 6.5 using EDTA reagent, from Figure 4.17 B. The purple region represents the secondary mapping over the 46 bp second stage of sliding. Small black spheres represent secondary mapped populations. Signal profiles obtained using AIDA analysis software.

4.19 Sliding of variant nucleosomes mapped at SHL 0.5

Xenopus canonical nucleosomes, human canonical nucleosomes and human nucleosomes containing the H2A variant hH2AX were all made using the 54(NucA)18 positioning sequence. They were then incubated at 35-55°C for 60 minutes before being mapped at SHL 0.5 S47C using EDTA reagent.

The C96 of human H3 was not mutated to alanine due to the preliminary stage of this investigation however C96 is non-adjacent to DNA on the α 2-helix of H3 and therefore should not interfere with mapping.

4.19.1 Observations

Migration on native PAGE would indicate that *Xenopus* nucleosomes slide at lower temperatures (40°C) than that of human (40-50°C) or human with H2AX (50-55 °C). Tight migration can be observed with *Xenopus* and human canonical but less so with the hH2AX containing nucleosome, and the migration distance of the *Xenopus* and human canonical nucleosomes is greater than that of the hH2AX containing nucleosome, Figure 4.18 A.

The mapping results indicate that the majority of the *Xenopus* and human nucleosome have slid by 40-45°C whereas the proportion of hH2AX nucleosomes slid at 45°C does not seem as high, Figure 4.18 B. The majority of positions occupied by the 3 nucleosomes after sliding are the same although the abundance of each position varies between *Xenopus* and the two human types. After the 60 minute incubation the majority of *Xenopus* nucleosomes occupy positions 85, 80, and 74, while the majority of the two human type occupy 7 positions spread over 31 bp, Figure 4.18 B.

The *Xenopus* nucleosome at the higher temperatures also shows evidence of downstream sliding with positioning observed at ~174 and ~185 bp, but this was not observed in the human and hH2AX nucleosomes, Figure 4.18 B.

4.19.2 Interpretation

The difference in the level of sliding between nucleosomes suggest that *Xenopus* is less stable than a canonical human nucleosome while the hH2AX containing nucleosome is more stable in terms of sliding on the MMTV NucA sequence. The tight migration of *Xenopus* nucleosomes indicate that most of the nucleosomes are restricted to only a few distinct populations, whereas the hH2AX and to a lesser extent the human nucleosome migration suggest that their populations can exist at many positions relatively close together. This is also consistent with the mapping results.

In the native PAGE the hH2AX nucleosome migrates noticeably slower than either *Xenopus* or the human canonical nucleosome. This is probably due to a combination of the greater molecular weight of the hH2AX histone protein over the H2A and the longer hH2AX tail having an effect on the DNA flexibility of the entry/exit DNA near the dyad.

The greater number of populations observed within the human and hH2AX nucleosomes after assembly but before sliding suggests that these nucleosomes are less directed by the MMTV NucA positioning sequence than the *Xenopus* nucleosome.

The downstream positioning at ~174 and ~185 bp observed with *Xenopus* suggest a bi-directional sliding. This was not obvious within the human nucleosomes using this 54(NucA)18 positional sequence.

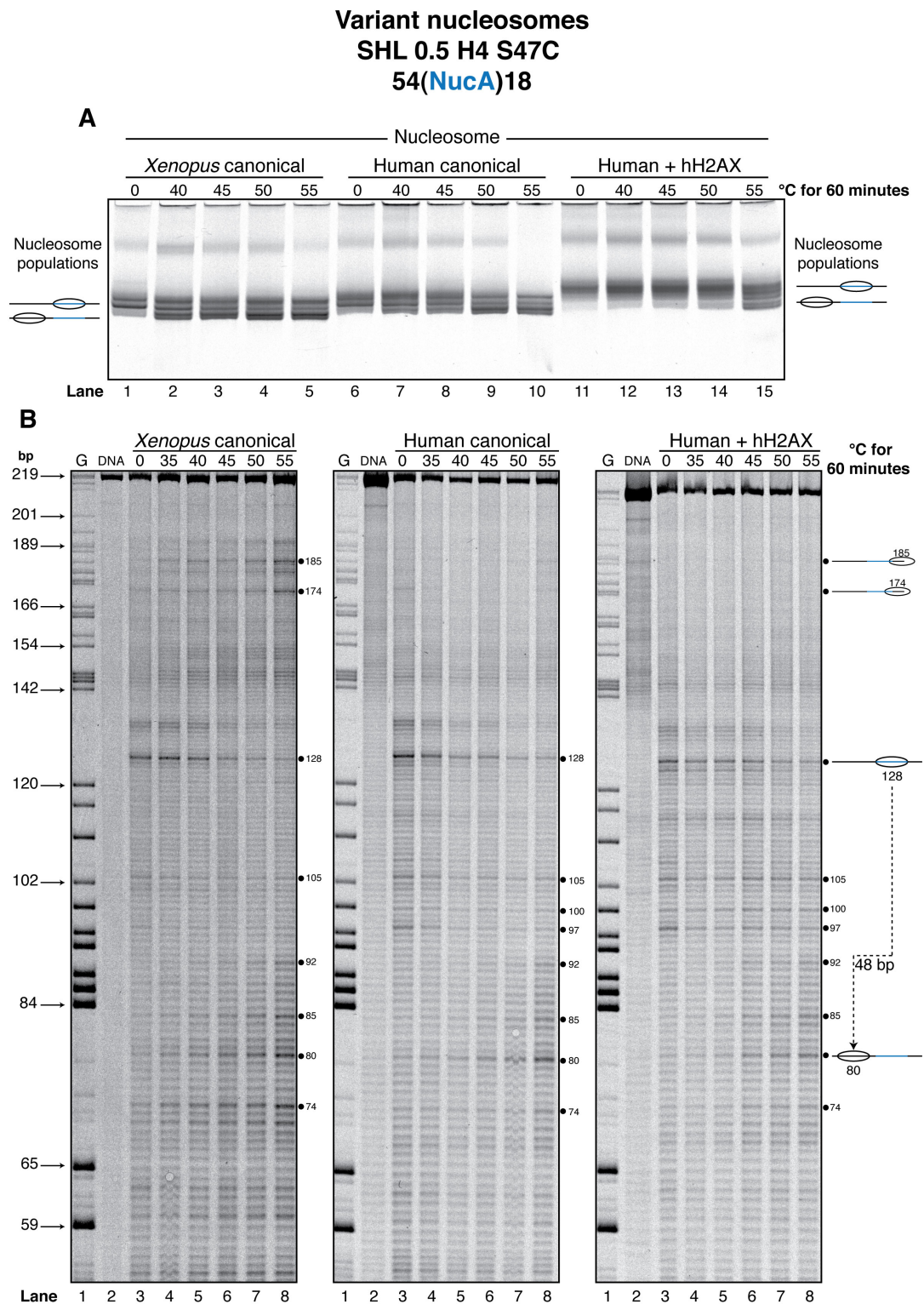


Figure 4.18 Thermal sliding of variant nucleosomes mapped at SHL 0.5. **A.** Native PAGE of *Xenopus*, human and human with hH2AX nucleosomes on 54(NucA)18 incubated at 0-55°C for 60 minutes. **B.** Denaturing PAGE of *Xenopus*, human and human with hH2AX nucleosomes on 54(NucA)18 incubated at 0-55°C for 60 minutes and mapped at SHL 0.5 H4 S47C. The G-track marker (G) is the sequence 54(NucA)18 chemically cleaved at every guanine nucleotide. Full length 54(NucA)18 (DNA) added as negative control. Black spheres represent primary mapped nucleosome populations. (Preliminary data).

4.20 Discussion

The overall aim of this work was to obtain a complete positional representation of nucleosomal DNA for all points of mapping during thermally induced nucleosome sliding using site specific hydroxyl radical DNA cleavage. Using the resulting data it is possible to compare the potential mechanisms for nucleosome sliding.

Each experiment performed in this chapter was carried out at least two times for all SHL mapping sites and incubations except for SHL 5.5 at 45°C and SHL 6.5 at 37°C and 45°C, which were each performed once. Table 4.1 shows the number of times each experiment in this chapter was carried out.

Nucleosome sliding repetitions			
SHL	Nucleosome sequence	Sliding incubation (°C)	Mapping performed
0.5 H4 S47C	54(601.2)18	0-60	2
	105(NucA)0	0-60	2
	105(NucA)-31	0-60	2
		37	2
		45	2
1.5 H4 T30C	105(NucA)-31	37	2
		45	2
2.5 H3 D81C	105(NucA)-31	37	2
		45	2
3.5 H2B T85C	105(NucA)-31	37	2
		45	2
4.5 H2A T16C	105(NucA)-31	37	2
		45	2
5.5 H2B G50C	105(NucA)-31	37	2
		45	1
6.5 H3 T45C	105(NucA)-31	37	1
		45	1

Table 4.1 Number of times the nucleosome sliding assay was performed per SHL

4.20.1 Thermally induced nucleosome sliding

In the first observations of thermally induced nucleosome sliding we compared sliding on 601.2, NucA and NucA-31 sequences. This demonstrated that strong nucleosome positioning sequences are unsuitable for observing the mechanisms of nucleosome sliding due to the high thermal input required to initiate

sliding and the lack of resulting intermediate positioning. Therefore the moderately stable truncated NucA-31 nucleosome was chosen for further analysis.

Mapping the NucA-31 nucleosome adjacent to all minor groove contact points at 37°C and 45°C showed nucleosomes sliding through intermediates to a more favourable upstream position. Analysis of this 66 bp sliding movement demonstrated that the NucA-31 nucleosomes slide from initial position 151 to the near terminal position 85 via three relatively stable intermediate positions at 140, 131 and 93, Table 4.2.

Nucleosome sliding mapping observations

Nucleosome position	SHL						
	0.5	1.5	2.5	3.5	4.5	5.5	6.5
151	✓	✓	✓	✓	✓	✓	✗
140	✓	✓	✓	✗	✓	✓	✗
131	✓	✓	✓	✗	✓	✓	✓
Additional intermediates	148	148					
	136	136	136	137	135	136	-
		133		133	133		
131	✓	✓	✓	✗	✓	✓	✓
93	✓	✗	✓	✗	✓	✗	✓
85	✓	✓	✓	✗	✓	✓	✓
Additional intermediates	121		120			122	124
	113	113		111		109	
	100	98		105	-	102	103
		94		95		94	
				87			
Estimated $t_{1/2}$ for first phase at 37 °C (min)	8	64	32	4	64	32	-
Estimated $t_{1/2}$ for two phases at 45 °C (min)	4	4	8	0	4	8	-

Table 4.2 Summary of sliding observations from SHL 0.5 to SHL 6.5. Summary of intermediate positioning during thermally induced nucleosome sliding mapped from SHL 0.5 to SHL 6.5. First phase positioning is represented in blue and second phase positioning is represented in magenta. Estimated times taken for quantity of initial population to equal quantity of pause population (first phase) or quantity of terminal population (two phases) are also shown.

Nucleosomes sliding from 151 to 131 (phase 1) requires relatively moderate levels of thermal input. However, 131 requires a higher level of thermal input to slide to the terminal 85 position (phase 2).

A number of marginally stable transient positions were also observed in the mapping although these were more variable in strength depending on the SHL mapping mutant, cutting efficiency and background signal. A summary of the intermediate positioning and estimated rates of sliding are shown in Table 4.2.

During the thermal incubation of nucleosomes it would be expected that nucleosomes are not simply sliding through consecutive positions along the DNA sequence until a terminal position is reached. Instead a diffusive mechanism of sliding is more probable where nucleosomes can momentarily leave a position and then return to that same position same position. It would also be expected that nucleosomes can skip regions of stability and do not simply slide to adjacent positions.

4.20.2 Similarities and differences in sliding

Similarities in the sliding pattern are observed between most SHL sites. For example, SHL 0.5 to SHL 5.5 all initially position at 151 and all positions except for SHL 3.5 have their terminal position at 85. Five SHL mapping sites showed common intermediate positions at 140, and positions 136 and 93 each occur for 4 mapping sites. The rates of progression ($t_{1/2}$) through phases were similar for positions SHL 1.5, 2.5, 4.5 and 5.5 suggesting that the cysteine mutant and EDTA reagent had little effect on these locations with regards to DNA wrapping. SHL 3.5 demonstrated the greatest difference with regards to intermediate positioning and sliding rates through the phases. SHL 0.5 also demonstrated that the cysteine mutation and EDTA reagent interfered with stability, although this was only observed for the sliding rates.

The aberrant intermediate positioning displayed by the SHL 3.5 indicates that the cysteine mutant and EDTA reagent at H2B residue 85 somehow destabilise the nucleosome structure. The intermediate positions observed in the first phase of sliding for SHL 3.5 are at 137 and 133. Whereas the other sites demonstrated mapping for the first phase positioned at 140 and 131. The initial reconstitution

position mapped at 151 for SHL 3.5 as it did for SHL 0.5, 1.5, 2.5, 4.5 and 5.5. The mapping at SHL 3.5 on the 147 bp NucA, 601 and 601.2 was also similar to expectation, suggesting that this aberrant behaviour is unique to less stable positioning sequences.

The SHL 3.5 terminal 87 position demonstrates a 2 bp shift from that of the other SHLs, which mapped at the terminal 85. This 2 bp differences is also observed for the final intermediate in the first phase of sliding, which occurs at 131 for all positions except SHL 3.5 which positions at 133. This further demonstrates the aberrant behaviour of SHL 3.5 but at least it shows some consistency between mapping locations.

The mapping at SHL 6.5 did not produce any visible mapping at positions 151 and 140. This maybe due to the poor mapping efficiency observed at SHL 6.5 using EDTA for both primary and secondary cutting. In fact, if secondary mapping did occur at the 151 position it may not be visible due to the size of the resulting DNA fragment which would approach 221 bp and be lost in the uncut DNA at the top of each lane. Also the 221 bp 105(NucA)-31 nucleosome when centered at 151 bp has a DNA length of only 70 bp spanning the secondary mapped half of the nucleosome. This is 3 bp shorter than the regular nucleosome structure, and due to the location of the SHL 6.5 cysteine mutant at residue 45 on H3 being at the extremities of the nucleosome, no cutting may have occurred.

The higher migrating nucleosome population observed throughout in the native PAGE of the 105(NucA)0 and 105(NucA)-31 sequences is probably due to sub-octamer complexes such as H2A/H2B dimers or H3/H4 tetramers binding to the free linker nucleosomal DNA. This higher migration was not observed using the 54(601.2)18 sequence suggesting this anomaly is only observed in linker DNA regions that are greater than 54 bp as with 105(NucA)0 and 105(NucA)-31. As no obvious DNA cleavage was observed during the mapping that corresponds to this population it would possibly suggest random DNA binding of the sub-octamer complexes. Also the fact that no mapping was observed from this population would indicate that results have not been misinterpreted due to additional DNA cleavages.

4.20.3 Nucleosome sliding patterns

The consistency observed throughout the mapping for almost all SHL locations indicates that paused intermediates have the same nucleosome structure. The fact that primary and secondary mapping has been observed at SHL locations anchored on tetramer and dimer proteins suggests that the nucleosome is intact at each stage of sliding and that no large-scale metastable alternative structures are involved.

Eighteen intermediate positions were observed in the various mappings that were relatively minor in strength of mapping compared to the five clear positions that consistently occurred at 151, 140, 131, 93 and 85. These minor positions were located at 148, 137, 135, 133, 124, 122, 121, 113, 111, 109, 105, 103, 102, 100, 98, 95, 94 and 87. These 23 positions occur in the 67 bp sliding region passed through. The maximum gap between these positions is 8 bp and the smallest is 1 bp. For nucleosomes mapped from SHL 1.5, clear intermediate positions are observed at 136, 133, 131. Taken together, this pattern of nucleosome sliding could also be interpreted as evidence towards near single base-pair steps indicative of a twist defect diffusion mechanism of nucleosome sliding.

Ten base pair periodicity from the different positions spread over 67 bp sliding region is also clear. For example, mapping from SHL 0.5 produced positioning at 151, 140, 131, 121, 113, 100, 93 and 85, and SHL 5.5 demonstrated positioning at 151, 140, 131, 122, 109, 102, 94 and 85. Although this could be interpreted to suggest a loop defect mechanism of nucleosome sliding the other minor positions located between these nucleosomes break the helical relationship. The helical relationship is most likely due to static or anisotropic bending giving stability to wrapping a particular DNA face.

It is also probable that some of the single base-pair steps observed during sliding could be explained by a combination of twist and loop diffusion. For example consecutive loops of 9 bp, 10 bp and 11 bp would give rise to populations that are separated by single base-pair steps. This could be interpreted as a twist defect mechanism of nucleosome sliding when in fact it would be a combination of both mechanisms. However, as the helical pitch of nucleosomal DNA can only tolerate ± 1

bp this mechanism of sliding would still not explain all the nucleosome positions that are not helically related.

4.20.4 Nucleosome sliding conclusions

In summary, nucleosome sliding occurs in a progressive manor along DNA occupying a series of intermediates with a variety of stabilities. The intermediately positioned nucleosomes have a distribution of spacing with conserved mapping for all positions and SHLs, suggesting a conserved nucleosome structure. Combined these data would support a thermal sliding mechanism that proceeds in near single base-pair steps without any large-scale metastable alternative structure.

4.20.5 *Xenopus*, human and human containing H2AX nucleosome sliding

Preliminary work with *Xenopus*, human and human containing hH2AX nucleosomes positioned on NucA indicates that the hH2AX nucleosome is more stable than that of either human or *Xenopus* nucleosomes. This is indicated by the higher incubation temperatures required to slide the hH2AX nucleosome.

It also seems that the human and human containing the hH2AX nucleosome is less well-directed by the NucA positioning sequence compared to that of *Xenopus*, which forms tight bands indicative of well-positioned reconstituted nucleosomes.

Finally, the mapping pattern of the *Xenopus* nucleosome demonstrates that sliding is towards both DNA termini in a bi-directional sliding manner. This interesting observation was not entirely obvious with the human type nucleosomes suggesting they may have a preference for unidirectional sliding.

Chapter 5 Conclusion

5.1 Site-directed nucleosome mapping

As previously demonstrated, EDTA/Fe²⁺ produces effective site-directed mapping. EDTA/Cu²⁺ does not produce significant DNA cleavage, while 1,10-phenanthroline in conjunction with Cu²⁺ or Fe²⁺ both produce significant DNA cleavage. DNA cleavage patterns also show a 1 bp difference between secondary mapping of EDTA/Fe²⁺ and Phen/Fe²⁺, and that Phen/Fe²⁺ can occupy two sites within a single minor groove to produce two separate cleavage patterns.

Complete mapping analysis indicates that NucA, 601 and 601.2 nucleosomes in solution are pseudo dyad symmetric and show no observable differences with the static crystal structures. It also suggests that 601 and 601.2 nucleosomes are more stable than NucA nucleosomes, at least at the outer parts of the nucleosome. No significant differences between 601 and 601.2 mapping are observed indicating structural identity between the nucleosomes despite their differences in sequence and stability.

The additional DNA cleavages that were observed at various locations throughout the mapping could indicate the presence of nucleosome sub-populations or possible transient rearrangements of nucleosome structure.

5.2 Thermal nucleosome sliding

The results from nucleosome sliding at moderate temperatures show that strong positioning sequences such as the 601.2 and MMTV NucA stable positions are ineffective for probing mechanisms of nucleosome sliding by investigating transient intermediate positions.

The directing of nucleosome assembly indicate that nucleosome sliding proceeds progressively to occupy a series of intermediates with a variety of stabilities, and that the nucleosome structure is conserved throughout sliding with no large-scale metastable alternative structures involved.

Sliding patterns demonstrated near single base-pair steps between intermediate positions. Some of these intermediates were helically related as expected if bendability influences nucleosome stability

Results also suggest that the cysteine mutation and/or mapping reagent can affect nucleosome positioning especially at low stability intermediate positions. The aberrant behaviour displayed by the SHL 3.5 mapping site during sliding would indicate that the cysteine mutation and/or the EDTA reagent affected nucleosome binding at this site. However, this is only observed at low stability intermediate positions as it was not observed with the assembled NucA, 601, 601.2 and NucA-31 nucleosomes.

Taken together, these observations support a mechanism for thermal nucleosome sliding that proceeds in a progressive, near single base-pair step manner, without any large-scale metastable alternative structure involved. This mechanism is consistent with the twist-defect diffusion model of nucleosome sliding. The point mutation and/or the EDTA reagent can also affect nucleosome positioning on less stable intermediate positions.

The results in this thesis will expand the knowledge currently known about nucleosome structure and dynamics and on site directed mapping in general. For example I have expanded the mapping of the nucleosome from one SHL site to all seven SHL sites and shown that the structure of nucleosomes in solution are consistent with the crystal structure. I have shown that the phenanthroline mapping reagent can be used in conjunction with iron as well as copper. Also I have shown that nucleosome sliding occurs in near single base-pair steps, which allows binding proteins access to concealed DNA sequences with the minimum of structural alterations. The aforementioned advances will inform current thinking in the field and will be highly beneficial when designing future experiments.

References

- Allan, J., Fraser, R.M., Owen-Hughes, T., and Keszenman-Pereyra, D. (2012). Micrococcal nuclease does not substantially bias nucleosome mapping. *J Mol Biol* 417, 152–164.
- Alves, G., Seu nez, H.C.N., and Fanning, T. (1994). Alpha satellite DNA in neotropical primates (Platyrrhini). *Chromosoma* 103, 262–267.
- Anderson, J.D., and Widom, J. (2000). Sequence and position-dependence of the equilibrium accessibility of nucleosomal DNA target sites. *J Mol Biol* 296, 979–987.
- Anderson, J.D., Thåström, A., and Widom, J. (2002). Spontaneous access of proteins to buried nucleosomal DNA target sites occurs via a mechanism that is distinct from nucleosome translocation. *Mol. Cell. Biol.* 22, 7147–7157.
- Andrews, A.J., Chen, X., Zevin, A., Stargell, L.A., and Luger, K. (2010). The histone chaperone Nap1 promotes nucleosome assembly by eliminating nonnucleosomal histone DNA interactions. *Mol Cell* 37, 834–842.
- Arents, G., Burlingame, R.W., Wang, B.C., Love, W.E., and Moudrianakis, E.N. (1991). The nucleosomal core histone octamer at 3.1 Å resolution: a tripartite protein assembly and a left-handed superhelix. *Proc Natl Acad Sci U S A* 88, 10148-10152.
- Bannister, A.J., and Kouzarides, T. (2011). Regulation of chromatin by histone modifications. *Cell Res* 21, 381–395.
- Barnham, K.J., Masters, C.L., and Bush, A.I. (2004). Neurodegenerative diseases and oxidative stress. *Nat Rev Drug Discov* 3, 205–214.
- Belikov, S., Gelius, B., and Wrangé, O. (2001). Hormone-induced nucleosome positioning in the MMTV promoter is reversible. *Embo J* 20, 2802–2811.
- Belmont, P., Constant, J.F., and Demeunynck, M. (2000). Nucleic acid conformation diversity: from structure to function and regulation. *Chem Soc Rev* 30, 70-81.
- Blossey, R., and Schiessel, H. (2011). The dynamics of the nucleosome: thermal effects, external forces and ATP. *Febs J* 278, 3619–3632.
- Brogaard, K., Xi, L., Wang, J.-P., and Widom, J. (2012). A map of nucleosome positions in yeast at base-pair resolution. *Nature* 486, 496–501.
- Brown, D.T., Izard, T., and Misteli, T. (2006). Mapping the interaction surface of linker histone H1(0) with the nucleosome of native chromatin in vivo. *Nat Struct Mol Biol* 13, 250–255.
- Buning, R., and van Noort, J. (2010). Single-pair FRET experiments on nucleosome conformational dynamics. *Biochimie* 92, 1729–1740.
- Burgess, R.J., and Zhang, Z. (2013). Histone chaperones in nucleosome assembly and human disease. *Nat Struct Mol Biol* 20, 14–22.
- Bussiek, M., Müller, G., Waldeck, W., and Diekmann, S. (2007). Organisation of nucleosomal arrays reconstituted with repetitive African green monkey α -satellite DNA as analysed by atomic force microscopy. *Eur Biophys J* 37, 81-93.

- Bussiek, M., Tóth, K., Brun, N., and Langowski, J. (2005). DNA-loop Formation on Nucleosomes Shown by in situ Scanning Force Microscopy of Supercoiled DNA. *J Mol Biol* 345, 695–706.
- Campos, E.I., and Reinberg, D. (2009). Histones: annotating chromatin. *Annu Rev Genet* 43, 559–599.
- Cerf, C., Lippens, G., Ramakrishnan, V., Muyldermans, S., Segers, A., Wyns, L., Wodak, S.J., and Hallenga, K. (1994). Homo- and Heteronuclear Two-Dimensional NMR Studies of the Globular Domain of Histone H1: Full Assignment, Tertiary Structure, and Comparison with the Globular Domain of Histone H5. *Biochemistry* 33, 11079–11086.
- Chen, Q., Chen, Y., Bian, C., Fujiki, R., and Yu, X. (2012). TET2 promotes histone O-GlcNAcylation during gene transcription. *Nature* 493, 561–564.
- Chua, E.Y.D., Vasudevan, D., Davey, G.E., Wu, B., and Davey, C.A. (2012). The mechanics behind DNA sequence-dependent properties of the nucleosome. *Nucleic Acids Res* 40, 6338–6352.
- Chung, H.-R., Dunkel, I., Heise, F., Linke, C., Krobitsch, S., Ehrenhofer-Murray, A.E., Sperling, S.R., and Vingron, M. (2010). The effect of micrococcal nuclease digestion on nucleosome positioning data. *PLoS ONE* 5, e15754.
- Clark, D.J. (2010). Nucleosome Positioning, Nucleosome Spacing and the Nucleosome Code. *J Biomol Struct Dyn* 27, 781–793.
- Cowan, J.A. (2001). Chemical nucleases. *Curr Opin Chem Biol* 5, 634–642.
- Davey, C.A., Sargent, D.F., Luger, K., Maeder, A.W., and Richmond, T.J. (2002). Solvent mediated interactions in the structure of the nucleosome core particle at 1.9 Å resolution. *J Mol Biol* 319, 1097–1113.
- Deindl, S., Hwang, W.L., Hota, S.K., Blosser, T.R., Prasad, P., Bartholomew, B., and Zhuang, X. (2013). ISWI Remodelers Slide Nucleosomes with Coordinated Multi-Base-Pair Entry Steps and Single-Base-Pair Exit Steps. *Cell* 152, 442–452.
- Dingwall, C., Lomonosoff, G.P., and Laskey, R.A. (1981). High sequence specificity of micrococcal nuclease. *Nucleic Acids Res* 9, 2659–2674.
- Donehower, L.A., Huang, A.L., and Hager, G.L. (1981). Regulatory and coding potential of the mouse mammary tumor virus long terminal redundancy. *J Virol* 37, 226–238.
- Draker, R., and Cheung, P. (2009). Transcriptional and epigenetic functions of histone variant H2A.Z. *Biochem. Cell Biol* 87, 19–25.
- Drew, H.R., and Travers, A.A. (1985). DNA bending and its relation to nucleosome positioning. *J Mol Biol* 186, 773–790.
- Dumoulin, P., Ebright, R.H., Knegt, R., Kaptein, R., Granger-Schnarr, M., and Schnarr, M. (1996). Structure of the LexA repressor-DNA complex probed by affinity cleavage and affinity photo-cross-linking. *Biochemistry* 35, 4279–4286.
- Edayathumangalam, R.S., Weyermann, P., Dervan, P.B., Gottesfeld, J.M., and Luger, K. (2005). Nucleosomes in solution exist as a mixture of twist-defect states. *J Mol Biol* 345, 103–114.
- Eltsov, M., MacLellan, K.M., Maeshima, K., Frangakis, A.S., and Dubochet, J. (2008).

- Analysis of cryo-electron microscopy images does not support the existence of 30-nm chromatin fibers in mitotic chromosomes in situ. *Proc Natl Acad Sci U S A* *105*, 19732-19737.
- Engelholm, M., de Jager, M., Flaus, A., Brenk, R., van Noort, J., and Owen-Hughes, T. (2009). Nucleosomes can invade DNA territories occupied by their neighbors. *Nat Struct Mol Biol* *16*, 151–158.
- English, C.M., Adkins, M.W., Carson, J.J., Churchill, M.E.A., and Tyler, J.K. (2006). Structural Basis for the Histone Chaperone Activity of Asf1. *Cell* *127*, 495–508.
- Erdel, F., and Rippe, K. (2011). Chromatin remodelling in mammalian cells by ISWI-type complexes – where, when and why? *Febs J* *278*, 3608-3618.
- Felsenfeld, G., and Groudine, M. (2003). Controlling the double helix. *Nature* *421*, 448–453.
- Fenton, H.J.H. (1894). LXXIII.-Oxidation of tartaric acid in presence of iron. *Journal of the Chemical Society, Transactions* *65*, 899-910.
- Finch, J.T., and Klug, A. (1976). Solenoidal model for superstructure in chromatin. *Proc. Natl Acad Sci U S A* *73*, 1897–1901.
- Flaus, A. (2011). Principles and practice of nucleosome positioning in vitro. *Frontiers in Life Science* *5*, 5–27.
- Flaus, A., and Owen-Hughes, T. (2003). Mechanisms for nucleosome mobilization. *Biopolymers* *68*, 563–578.
- Flaus, A., and Owen-Hughes, T. (2011). Mechanisms for ATP-dependent chromatin remodelling: the means to the end. *Febs J* *278*, 3579–3595.
- Flaus, A., and Richmond, T.J. (1998). Positioning and stability of nucleosomes on MMTV 3'LTR sequences. *J Mol Biol* *275*, 427–441.
- Flaus, A., and Richmond, T.J. (1999). Base-pair resolution mapping of nucleosome positions using site-directed hydroxy radicals. *Meth Enzymol* *304*, 251–263.
- Flaus, A., Luger, K., Tan, S., and Richmond, T.J. (1996). Mapping nucleosome position at single base-pair resolution by using site-directed hydroxyl radicals. *Proc Natl Acad Sci U S A* *93*, 1370–1375.
- Fuchs, J., Demidov, D., Houben, A., and Schubert, I. (2006). Chromosomal histone modification patterns-from conservation to diversity. *Trends Plant Sci* *11*, 199-208.
- Gaffney, D.J., McVicker, G., Pai, A.A., Fondufe-Mittendorf, Y.N., Lewellen, N., Michelini, K., Widom, J., Gilad, Y., and Pritchard, J.K. (2012). Controls of nucleosome positioning in the human genome. *PLoS Genet* *8*, e1003036.
- Gangaraju, V.K., and Bartholomew, B. (2007). Mechanisms of ATP dependent chromatin remodeling. *Mutation Research/Fundamental and Molecular Mechanisms of Mutagenesis* *618*, 3–17.
- Gkikopoulos, T., Schofield, P., Singh, V., Pinskaya, M., Mellor, J., Smolle, M., Workman, J.L., Barton, G.J., and Owen-Hughes, T. (2011). A role for Snf2-related nucleosome-spacing enzymes in genome-wide nucleosome organization. *Science* *333*, 1758–1760.
- Hake, S.B., and Allis, C.D. (2006). Histone H3 variants and their potential role in indexing

- mammalian genomes: the "H3 barcode hypothesis". *Proc Natl Acad Sci U S A* *103*, 6428–6435.
- Hansen, J.C. (2012). Human mitotic chromosome structure: what happened to the 30-nm fibre? *Embo J* *31*, 1621–1623.
- Happel, N., and Doenecke, D. (2009). Histone H1 and its isoforms: contribution to chromatin structure and function. *Gene* *431*, 1–12.
- Hayes, J.J., Tullius, T.D., and Wolffe, A.P. (1990). The structure of DNA in a nucleosome. *Proc Natl Acad Sci U S A* *87*, 7405–7409.
- Heilek, G.M., Marusak, R., Meares, C.F., and Noller, H.F. (1995). Directed hydroxyl radical probing of 16S rRNA using Fe(II) tethered to ribosomal protein S4. *Proc Natl Acad Sci U S A* *92*, 1113–1116.
- Ho, L., and Crabtree, G.R. (2010). Chromatin remodelling during development. *Nature* *463*, 474–484.
- Hörz, W., Fittler, F., and Zachau, H.G. (1983). Sequence specific cleavage of African green monkey alpha-satellite DNA by micrococcal nuclease. *Nucleic Acids Res* *11*, 4275–4285.
- Hughes, A.L., Jin, Y., Rando, O.J., and Struhl, K. (2012). A functional evolutionary approach to identify determinants of nucleosome positioning: a unifying model for establishing the genome-wide pattern. *Mol Cell* *48*, 5–15.
- Jiang, Y., Wang, X., Bao, S., Guo, R., Johnson, D.G., Shen, X., and Li, L. (2010). INO80 chromatin remodeling complex promotes the removal of UV lesions by the nucleotide excision repair pathway. *Proc Natl Acad Sci U S A* *107*, 17274–17279.
- Kaplan, N., Moore, I.K., Fondufe-Mittendorf, Y., Gossett, A.J., Tillo, D., Field, Y., LeProust, E.M., Hughes, T.R., Lieb, J.D., Widom, J., et al. (2009). The DNA-encoded nucleosome organization of a eukaryotic genome. *Nature* *458*, 362–366.
- Konev, A.Y., Tribus, M., Park, S.Y., Podhraski, V., Lim, C.Y., Emelyanov, A.V., Vershilova, E., Pirrotta, V., Kadonaga, J.T., Lusser, A., et al. (2007). CHD1 Motor Protein Is Required for Deposition of Histone Variant H3.3 into Chromatin in Vivo. *Science* *317*, 1087–1090.
- Koopmans, W.J.A., Buning, R., Schmidt, T., and van Noort, J. (2009). spFRET using alternating excitation and FCS reveals progressive DNA unwrapping in nucleosomes. *Biophys J* *97*, 195–204.
- Kornberg, R.D., and Stryer, L. (1988). Statistical distributions of nucleosomes: nonrandom locations by a stochastic mechanism. *Nucleic Acids Res* *16*, 6677–6690.
- Li, G., Levitus, M., Bustamante, C., and Widom, J. (2004). Rapid spontaneous accessibility of nucleosomal DNA. *Nat Struct Mol Biol* *12*, 46–53.
- Liu, C., and Wang, L. (2008). DNA hydrolytic cleavage catalyzed by synthetic multinuclear metallonucleases. *Dalton Trans*, 227–239.
- Liu, N., Peterson, C.L., and Hayes, J.J. (2011). SWI/SNF- and RSC-Catalyzed Nucleosome Mobilization Requires Internal DNA Loop Translocation within Nucleosomes. *Mol Cell Biol* *31*, 4165–4175.
- Lowary, P.T., and Widom, J. (1997). Nucleosome packaging and nucleosome positioning of

- genomic DNA. *Proc Natl Acad Sci U S A* *94*, 1183–1188.
- Lowary, P.T., and Widom, J. (1998). New DNA sequence rules for high affinity binding to histone octamer and sequence-directed nucleosome positioning. *J Mol Biol* *276*, 19–42.
- Lowndes, N.F., and Toh, G.W.-L. (2005). DNA repair: the importance of phosphorylating histone H2AX. *Curr Biol* *15*, R99–R102.
- Luger, K. (2006). Dynamic nucleosomes. *Chromosome Res* *14*, 5–16.
- Luger, K., and Richmond, T.J. (1998). DNA binding within the nucleosome core. *Curr Opin Struct Biol* *8*, 33–40.
- Luger, K., Mäder, A.W., Richmond, R.K., Sargent, D.F., and Richmond, T.J. (1997). Crystal structure of the nucleosome core particle at 2.8 Å resolution. *Nature* *389*, 251–260.
- Makde, R.D., England, J.R., Yennawar, H.P., and Tan, S. (2010). Structure of RCC1 chromatin factor bound to the nucleosome core particle. *Nature* *467*, 562–566.
- Marzluff, W.F., Wagner, E.J., and Duronio, R.J. (2008). Metabolism and regulation of canonical histone mRNAs: life without a poly(A) tail. *Nat Rev Genet* *9*, 843–854.
- Matsuzawa, A., Nakano, H., Yoshimoto, T., and Sayama, K. (1995). Biology of mouse mammary tumor virus (MMTV). *Cancer Letters* *90*, 3–11.
- Mazumder, A., Sutton, C.L., and Sigman, D.S. (1993). 1,10-Phenanthroline-linked *Escherichia coli* Trp repressor as a site-specific scission reagent. Metal ion requirement. *Inorg Chem* *32*, 3516–3520.
- McKnight, J.N., Jenkins, K.R., Nodelman, I.M., Escobar, T., and Bowman, G.D. (2011). Extranucleosomal DNA binding directs nucleosome sliding by Chd1. *Mol Cell Biol* *31*, 4746–4759.
- Messner, S., and Hottiger, M.O. (2011). Histone ADP-ribosylation in DNA repair, replication and transcription. *Trends Cell Biol* *21*, 534–542.
- Miyagi, A., Ando, T., and Lyubchenko, Y.L. (2011). Dynamics of nucleosomes assessed with time-lapse high-speed atomic force microscopy. *Biochemistry* *50*, 7901–7908.
- Negri, R., Buttinelli, M., Panetta, G., De Arcangelis, V., Di Mauro, E., and Travers, A. (2001). Sequence dependence of translational positioning of core nucleosomes. *J Mol Biol* *307*, 987–999.
- Nishino, Y., Eltsov, M., Joti, Y., Ito, K., Takata, H., Takahashi, Y., Hihara, S., Frangakis, A.S., Imamoto, N., Ishikawa, T., et al. (2012). Human mitotic chromosomes consist predominantly of irregularly folded nucleosome fibres without a 30-nm chromatin structure. *Embo J* *31*, 1644–1653.
- Noll, M. (1974). Internal structure of the chromatin subunit. *Nucleic Acids Res* *1*, 1573–1578.
- Ong, M.S., Richmond, T.J., and Davey, C.A. (2007). DNA stretching and extreme kinking in the nucleosome core. *J Mol Biol* *368*, 1067–1074.
- Pennings, S., Meersseman, G., and Bradbury, E.M. (1991). Mobility of positioned nucleosomes on 5 S rDNA. *J Mol Biol* *220*, 101–110.

- Peterson, C.L., and Laniel, M.A. (2004). Histones and histone modifications. *Curr Biol* 14, R546-551.
- Pinto, D.M.S., and Flaus, A. (2010). Structure and function of histone H2AX. *Subcell Biochem* 50, 55-78.
- Pogozelski, W.K., and Tullius, T.D. (1998). Oxidative Strand Scission of Nucleic Acids: Routes Initiated by Hydrogen Abstraction from the Sugar Moiety. *Chem Rev* 98, 1089-1108.
- Pointner, J., Persson, J., Prasad, P., Norman-Axelsson, U., Strålfors, A., Khorosjutina, O., Krietenstein, N., Peter Svensson, J., Ekwall, K., and Korber, P. (2012). CHD1 remodelers regulate nucleosome spacing in vitro and align nucleosomal arrays over gene coding regions in *S. pombe*. *Embo J* 31, 4388-4403.
- Polach, K.J., and Widom, J. (1995). Mechanism of protein access to specific DNA sequences in chromatin: a dynamic equilibrium model for gene regulation. *J Mol Biol* 254, 130-149.
- Prunell, A. (1983). Periodicity of exonuclease III digestion of chromatin and the pitch of deoxyribonucleic acid on the nucleosome. *Biochemistry* 22, 4887-4894.
- Richard-Foy, H., and Hager, G.L. (1987). Sequence-specific positioning of nucleosomes over the steroid-inducible MMTV promoter. *Embo J* 6, 2321-2328.
- Richmond, T.J., and Davey, C.A. (2003). The structure of DNA in the nucleosome core. *Nature* 423, 145-150.
- Robinson, P.J.J., Fairall, L., Huynh, V.A.T., and Rhodes, D. (2006). EM measurements define the dimensions of the "30-nm" chromatin fiber: evidence for a compact, interdigitated structure. *Proc Natl Acad Sci U S A* 103, 6506-6511.
- Ronald Morris, N. (1976). Nucleosome structure in *Aspergillus nidulans*. *Cell* 8, 357-363.
- Ross, S.R. (2010). Mouse Mammary Tumor Virus Molecular Biology and Oncogenesis. *Viruses* 2, 2000-2012.
- Ryan, D.P., Sundaramoorthy, R., Martin, D., Singh, V., and Owen-Hughes, T. (2011). The DNA-binding domain of the Chd1 chromatin-remodelling enzyme contains SANT and SLIDE domains. *Embo J* 30, 2596-2609.
- Satchwell, S.C., Drew, H.R., and Travers, A.A. (1986). Sequence periodicities in chicken nucleosome core DNA. *J Mol Biol* 191, 659-675.
- Schalch, T., Duda, S., Sargent, D.F., and Richmond, T.J. (2005). X-ray structure of a tetranucleosome and its implications for the chromatin fibre. *Nature* 436, 138-141.
- Schones, D.E., Cui, K., Cuddapah, S., Roh, T.-Y., Barski, A., Wang, Z., Wei, G., and Zhao, K. (2008). Dynamic regulation of nucleosome positioning in the human genome. *Cell* 132, 887-898.
- Segal, E., Fondufe-Mittendorf, Y., Chen, L., Thåström, A., Field, Y., Moore, I.K., Wang, J.-P.Z., and Widom, J. (2006). A genomic code for nucleosome positioning. *Nature* 442, 772-778.
- Shiio, Y., and Eisenman, R.N. (2003). Histone sumoylation is associated with transcriptional repression. *Proc Natl Acad Sci U S A* 100, 13225-13230.
- Shlyakhtenko, L.S., Lushnikov, A.Y., and Lyubchenko, Y.L. (2009). Dynamics of

- nucleosomes revealed by time-lapse atomic force microscopy. *Biochemistry* **48**, 7842–7848.
- Sigman, D.S. (1990). Chemical nucleases. *Biochemistry* **29**, 9097–9105.
- Simpson, R.T. (1978). Structure of the chromatosome, a chromatin particle containing 160 base pairs of DNA and all the histones. *Biochemistry* **17**, 5524–5531.
- Simpson, R.T., and Stafford, D.W. (1983). Structural features of a phased nucleosome core particle. *Proc Natl Acad Sci U S A* **80**, 51–55.
- Simpson, R.T., Thoma, F., and Brubaker, J.M. (1985). Chromatin reconstituted from tandemly repeated cloned DNA fragments and core histones: A model system for study of higher order structure. *Cell* **42**, 799–808.
- Spicuglia, S., Kumar, S., Chasson, L., Payet-Bornet, D., and Ferrier, P. (2004). Potassium permanganate as a probe to map DNA–protein interactions in vivo. *J Biochem Biophys Methods* **59**, 189–194.
- Stockdale, C., Flaus, A., Ferreira, H., and Owen-Hughes, T. (2006). Analysis of nucleosome repositioning by yeast ISWI and Chd1 chromatin remodeling complexes. *J Biol Chem* **281**, 16279–16288.
- Strohner, R., Wachsmuth, M., Dachauer, K., Mazurkiewicz, J., Hochstatter, J., Rippe, K., and Längst, G. (2005). A “loop recapture” mechanism for ACF-dependent nucleosome remodeling. *Nat Struct Mol Biol* **12**, 683–690.
- Sullivan, K.F. (2001). A solid foundation: functional specialization of centromeric chromatin. *Curr Opin Genet Dev* **11**, 182–188.
- Talbert, P.B., and Henikoff, S. (2010). Histone variants — ancient wrap artists of the epigenome. *Nat Rev Mol Cell Biol* **11**, 264–275.
- Tan, S., and Davey, C.A. (2011). Nucleosome structural studies. *Curr Opin Struct Biol* **21**, 128–136.
- Travers, A.A., and Klug, A. (1987). The bending of DNA in nucleosomes and its wider implications. *Philos Trans R Soc Lond B Biol Sci* **317**, 537–561.
- Udugama, M., Sabri, A., and Bartholomew, B. (2011). The INO80 ATP-dependent chromatin remodeling complex is a nucleosome spacing factor. *Mol Cell Biol* **31**, 662–673.
- van Attikum, H., Fritsch, O., Hohn, B., and Gasser, S.M. (2004). Recruitment of the INO80 complex by H2A phosphorylation links ATP-dependent chromatin remodeling with DNA double-strand break repair. *Cell* **119**, 777–788.
- Vasudevan, D., Chua, E.Y.D., and Davey, C.A. (2010). Crystal structures of nucleosome core particles containing the “601” strong positioning sequence. *J. Mol. Biol.* **403**, 1–10.
- Vogler, C., Huber, C., Waldmann, T., Ettig, R., Braun, L., Izzo, A., Daujat, S., Chassignet, I., Lopez-Contreras, A.J., Fernandez-Capetillo, O., et al. (2010). Histone H2A C-terminus regulates chromatin dynamics, remodeling, and histone H1 binding. *PLoS Genet* **6**, e1001234.
- Widom, J. (1998). Chromatin structure: Linking structure to function with histone H1. *Curr Biol* **8**, R788–791.
- Wilson, K.S., and Noller, H.F. (1998). Mapping the Position of Translational Elongation

- Factor EF-G in the Ribosome by Directed Hydroxyl Radical Probing. *Cell* 92, 131–139.
- Winterbourn, C.C. (1995). Toxicity of iron and hydrogen peroxide: the Fenton reaction. *Toxicol Lett* 82-83, 969–974.
- Wondrak, G.T., Cervantes-Laurean, D., Jacobson, E.L., and Jacobson, M.K. (2000). Histone carbonylation in vivo and in vitro. *Biochem J* 351 Pt 3, 769–777.
- Wood, C.M., Nicholson, J.M., Lambert, S.J., Chantalat, L., Reynolds, C.D., and Baldwin, J.P. (2005). High-resolution structure of the native histone octamer. *Acta Crystallogr Sect F Struct Biol Cryst Commun* 61, 541–545.
- Xiao, B., Freedman, B.S., Miller, K.E., Heald, R., and Marko, J.F. (2012). Histone H1 compacts DNA under force and during chromatin assembly. *Mol Biol Cell* 23, 4864–4871.
- Yuan, G.-C., Liu, Y.-J., Dion, M.F., Slack, M.D., Wu, L.F., Altschuler, S.J., and Rando, O.J. (2005). Genome-scale identification of nucleosome positions in *S. cerevisiae*. *Science* 309, 626–630.
- Zhang, Y., Moqtaderi, Z., Rattner, B.P., Euskirchen, G., Snyder, M., Kadonaga, J.T., Liu, X.S., and Struhl, K. (2009). Intrinsic histone-DNA interactions are not the major determinant of nucleosome positions in vivo. *Nat Struct Mol Biol* 16, 847–852.
- Zhang, Y., Smith, C.L., Saha, A., Grill, S.W., Mihardja, S., Smith, S.B., Cairns, B.R., Peterson, C.L., and Bustamante, C. (2006). DNA translocation and loop formation mechanism of chromatin remodeling by SWI/SNF and RSC. *Mol Cell* 24, 559–568.
- Zhang, Z., Wippo, C.J., Wal, M., Ward, E., Korber, P., and Pugh, B.F. (2011). A Packing Mechanism for Nucleosome Organization Reconstituted Across a Eukaryotic Genome. *Science* 332, 977–980.
- Zofall, M., Fischer, T., Zhang, K., Zhou, M., Cui, B., Veenstra, T.D., and Grewal, S.I.S. (2009). Histone H2A.Z cooperates with RNAi and heterochromatin factors to suppress antisense RNAs. *Nature* 461, 419–422.
- Zofall, M., Persinger, J., Kassabov, S.R., and Bartholomew, B. (2006). Chromatin remodeling by ISW2 and SWI/SNF requires DNA translocation inside the nucleosome. *Nat Struct Mol Biol* 13, 339–346.

Appendix

Nucleosome positioning sequences

MMTV NucA

ACTTGCAACAGTCCTAACATTACCTCTTGTGTGTTTGTGTCTGTTTCGCCATCCCGT
CTCCGCTCGTCACTTA†CCTTCACTTTCCAGAGGGTCCCCCGCAGACCCCGGCGAC
CCTCAGGTCGGCCGACTGCGGCACAGTTTTTTG

601

CTGGAGAATCCCGGTGCCGAGGCCGCTCAATTGGTCGTAGACAGCTCTAGCACCGCT
TAAACGCACGTACGCG†TGTCCCCGCGTTTTAACCGCCAAGGGGATTACTCCCTAG
TCTCCAGGCACGTGTCAGATATATACATCCTGT

601.2

CTGCAGAAAGCTTGGTCCGGGGCCGCTCAATTGGTCGTAGCAAGCTCTAGATCCGCT
TAATCGAACGTACGCG†TGTCCCCGCGTTTTAACCGCCAAGGGGATTACTCCCTAG
TCTCCAGGCACGTGTCAGATATATACATCCTGT

54(601.2)18

GACTCACTATAGGGCGAATTCGAGCTCGGTACCCGGACCCTATACGCGGGCGCACTG
CAGAAGCTTGGTCCCGGGGCCGCTCAATTGGTCGTAGCAAGCTCTAGATCCGCTTAA
TCGAACGTACGCG†TGTCCCCGCGTTTTAACCGCCAAGGGGATTACTCCCTAGTCT
CCAGGCACGTGTCAGATATATACATCCTGTGCATGTAGGGGATTCTCT

105(NucA)0

GAGCTCTGAGTGTTCTATTTTCCTATGTTCTTTTGAATTTATCCAAATCTTATGTA
AATGCTTATGTAAACCAAGATATAAAAGAGTGCTGATTTTTTGGAGTAAACTTGCAAC
AGTCCTAACATTACCTCTTGTGTGTTTGTGTCTGTTTCGCCATCCCGTCTCCGCTCG
TCACTTA†CCTTCACTTTCCAGAGGGTCCCCCGCAGACCCGGCGACCCTCAGGTC
GGCCGACTGCGGCACAGTTTTTTG

105(NucA)-31

GAGCTCTGAGTGTTCTATTTTCCTATGTTCTTTTGAATTTATCCAAATCTTATGTA
AATGCTTATGTAAACCAAGATATAAAAGAGTGCTGATTTTTTGGAGTAAACTTGCAAC
AGTCCTAACATTACCTCTTGTGTGTTTGTGTCTGTT†CGCCATCCCGTCTCCGCTCG
TCACTTATCCTTCACTTTCCAGAGGGTCCCCCGCAGACCCGGCGACCC

PCR primers

Primers	Sequence			
	Label	Forward	Label	Reverse
NucA	Cy5	ACTTGCAACAGTCC TAAC	Cy3	CAAAAACTGTGCCG CAG
601	Cy5	CTGGAGAATCCCGG TGCC	Cy3	ACAGGATGTATATAT CTGACACGTGCC
601.2	Cy5	CTGCAGAAGCTTGG TCCC	Cy3	ACAGGATGTATATAT CTG
54(601.2)18	Cy5	GACTCACTATAGGG CGAATTC	-	AGAGAATCCCCTACA TGC
105(NucA)0	Cy5	GAGCTCTGAGTGTT CTAT	-	CAAAAACTGTGCCG CAG
105(NucA)-31	Cy5	GAGCTCTGAGTGTT CTAT	-	GGGTCGCCGGGGTCT GC
xH4 S47C	-	GGTGGTGTTAAACG TATCTGCGGTCTGA TCTACGAAGAA	-	TCCTCCGTAGATCAG ACCGCAGATACGTTT AACACCACC
xH4T30C	-	CGTGACAACATCCA GGGTATCTGCAAGC CGGCTATCCGTCGT C	-	GACGACGGATAGCCG GCTTGCAGATACCCT GGATGTTGTCACG
xH3D81C	-	GCTCAGGACTTCAA GACCTGCCTGCGCT TCCAGAGCTCG	-	CGAGCTCTGGAAGCG CAGGCAGGTCTTGAA GTCCTGAGC
xH2B T85C	-	CATTACAACAAGCG CTCCTGCATCACCT CCCGGGAGATC	-	GATCTCCCGGGAGGT GATGCAGGAGCGCTT GTTGTAATG
xH2A T16C	-	CGCGCTAAGGCCAA GTGTCGCTCATCTC GGGCTGG	-	CCAGCCCGAGAT GAGCGACACTTG GCCTTAGCGCG
xH2B G50C	-	GTGCACCCCGATAC CTGCATCTCGTCCA AGGCC	-	GGCCTTGGACGAGAT GCAGGTATCGGGGTG CAC
xH3 T45C	-	CGTTACCGGCCCGG CTGCGTCGCTCTCC GCGAGATC	-	GATCTCGCGGAGAGC GACGCAGCCGGGCCG GTAACG
xH3 C110A	-	CTTTGAGGACACCA ACCTGGCCGCCATC CACGCCAAGAGG	-	CCTCTTGGCGTGGAT GGCGGCCAGGTGGT GTCCTCAAAG